STUDYING RELATIONSHIPS BETWEEN LUNAR VOLCANIC FEATURES: REMOTE SPECTROSCOPY FROM VISIBLE TO THERMAL INFRARED WAVELENGTHS

By Lori M. Pigue

A Dissertation

Submitted in Partial Fulfillment

of the Requirements for the Degree of

Doctor of Philosophy

in Astronomy and Planetary Science

Northern Arizona University

August 2023

Approved:

Kristen Bennett, Ph.D., Co-Chair

Christopher Edwards, Ph.D., Co-Chair

Mark Loeffler, Ph.D.

Cristina Thomas, Ph.D.

ABSTRACT

STUDYING RELATIONSHIPS BETWEEN LUNAR VOLCANIC FEATURES:

REMOTE SPECTROSCOPY FROM VISIBLE TO THERMAL INFRARED WAVELENGTHS

LORI M. PIGUE

To better understand the evolution of the lunar surface and subsurface, it is important to characterize the distribution of subsurface volatiles, which can be inferred from trends in volcanism and geologic history. Most volcanism on Earth has both effusive and explosive phases, whereas on the Moon effusive and explosive volcanism are often studied as separate events. I hypothesize that lunar volcanism is just as complex as terrestrial volcanism, where individual eruptions can experience multiple phases and can erupt from the same vent. To address this hypothesis, I employ multiple methodologies by conducting a global, regional, and local investigation, in wavelength ranges that span the visible to thermal infrared.

In a global study, I combine and expand prior inventories of sites of explosive volcanism (called Lunar Pyroclastic Deposits or LPDs) and evaluate the relationship between the locations of LPDs to the lunar crustal structure and potential magma sources. Crustal thickness plays a role in volcanic emplacement, and multiple volcanic features can erupt from a shared magma source; however, I investigate whether these trends are globally true or deposit specific. Next, I focus on compositional relationships between volcanic features in the Montes Apenninus region. I find that co-located LPDs and effusive features (e.g., rilles, mare) can erupt from the same volcanic vent, even at the same time, although generally the stratigraphic and eruptive relationships between these features vary (in the same way that they do on Earth). Diving further into properties of LPDs, I then investigate the thermophysical properties of a subsample of the Montes Apeninnus region called the Mare Vaporum basin. I investigate a wide variety of features in this basin by temperature

and find that we can establish different properties based on their different temperatures, rock abundances, and thermal intertias. These combined methods are used to infer a geologic history of these features, providing a wealth of information about volcanic features on the Moon.

Acknowledgements

I was terrified starting a PhD in a department called "Physics and Astronomy," fearing I would not be smart enough to complete the coursework or that I lacked the skills necessary to do the research. I asked before I even knew what classes I'd be taking, what I could do to fill knowledge and skill gaps. I was told I would be fine and that I'd learn what I needed along the way. That was not the right answer. That was the answer to someone who has generational knowledge of academia, to someone who went to an R1 undergrad, or who was in contact with professors who could guide them in what a PhD student would need to be successful. I tried my best to not let my naiveite show, but masks are imperfect and to those who supported me quietly and didn't make a bigger deal about the gap I was trying to make up, I thank you. The truth is, I didn't come from an R1. Or an R2, or even an R3. I graduated from an M1 and although I had worked for a major scientific research organization in undergrad and built a life as a scientist afterwards, there was an entire world of exposure that I lacked. Ty Robinson and the grant writing seminar/course(s) and Andrew Richardson and the writing class that focused my first manuscript – I'm forever indebted to you, and I wish more resources like those were available for PhD students like me. To the first-generation students out there, you are not alone, and you can do it. To the first-generation students of color, immigrant, non-native speakers, non-majority ethnicities, I can't imagine how difficult this is and the number of insurmountable barriers you face. You can do it, and I hope you do.

To my first Primary Advisor, Moses Milazzo, thank you for teaching me more than the academic things necessary to keep moving forward in my PhD. I'll never forget your compassion and commitment to people in planetary science, and I am immensely grateful for your mentorship, then and continuing. To my first Research Advisor, Lisa Gaddis, thank you for your guidance and the wealth of knowledge you gave me in the short time I was able to spend with you. I'm eternally grateful that we crossed paths and that I was able to learn many very important lessons, academic and otherwise, from you at a critical point of my career.

To my Fairy-God Advisor, Christopher Edwards, thank you for being the level-minded one in all the chaos. I appreciate all the opportunities you've opened for me, especially through all the challenges. Thank you to the rest of the PIXEL Group also for welcoming in this orphan and letting me be involved in things. To my Research Advisor, Kristen Bennett, thank you for being a wonderful advisor. It was truly my fortune that your path crossed into mine at the exact time it needed to, and I couldn't have finished without you and all of these stars aligning. I know you probably didn't want to sign up for so many firsts all at once, but you've been amazing and I'm glad to have you for an ally. Thank you also to Cristina Thomas and Mark Loeffler for your guidance throughout my PhD journey.

To those at the USGS who let me in and treated me like any other USGS employee, your welcoming meant the world to me. Belonging was hard to come by but was a big part of what sustained me. Thanks to Lauren AK for being my partner in crime in the DEIA Council and letting me carry on those works in your stead. Immense thank you to Railyn Moyers for encouraging me to pursue my passions in communication and for helping me through all the strife of my position – you rock! Thanks to Elise Rumpf for being an awesome officemate and humoring me with all my weird questions. Thank you to Lillian Ostrach for office chats and reality checks – I'm glad I wasn't always going crazy. Thank you to Laz Kestay for reviews and guidance in so many aspects, and to Chris Okubo for being an awesome supervisor, I consider that I've been fortunate to have the opportunity to observe and learn from you both. Thanks to Ryan Anderson and Greg Vaughan for continuing to let me work on the PLANETS team and collaborate on outreach and communications. The work that I was able to do with PLANETS, Outreach, and AstroComm, where I felt capable and that I was making a difference, was an escape that I needed during times where I felt I had no competence in my research. To the rest of the PLANETS team (the other multiplicative of Lori^2, Anne, Aradhana, Jöelle, the Partners), I appreciate your support through the years.

I also want to thank my internet friends for keeping me sane during the PhD – the Ray Chen's Violin Discord through the pandemic and TSV for getting me back into violin so I can have that outlet again. I also want to thank the ridiculous members and mods of the Geology Discord Server for random feedback and discussions over the last several years and for being my internet friends. Maybe one day we'll find the frequency of the power of the eruption of that volcano...

To Christian, thank you for being the other lunatic and my close friend through this. Schuyler, I'm so grateful that you came into my life and are constantly challenging me, professionally and personally. Schuyler and Christian, you are both so talented and resilient and I'm so thankful to have crossed paths with you. Your support in dragging me through the toughest times and being my friends means the world to me, and always will. To Sarah, whom I am also grateful to have crossed paths, I'm so happy seeing every achievement that you're awarded and every milestone you crush. To Alissa, I was glad to know you for the time that I did. You deserve to be here too.

To my Mom and Dad, thank you for being patient and supporting me from afar. I know this was difficult, especially through the COVID-19 pandemic, but you know how important this was to me and how determined I am to do things that are important to me. To my Bro Chris, Ralph, and We Eat Sandwiches Together, thanks for your love and support. I know it was difficult for me to communicate my journey and the struggles that I was having. Thank you for understanding when I didn't have the energy to talk or the ability to explain. To Carol, Meagan and Tony, and Chris and Alyssa, thank you so much for your love and words of encouragement. Your constant support was an anchor during some of the hardest times.

The thing that I learned at the end of this is that even though I didn’t go to an R1 and I didn’t come from a college-educated family, I was smart enough. Because it doesn’t take genius to do science, it’s about creativity, Curiosity, and yes, we’ll go with the theme and add Endurance (you thought I, a lunar scientist, was going to say Perseverance?). It was never about being smart enough but being able to identify what we don’t understand and responding by putting together a plan to learn more and using your community to help get you to the end. You can be a natural and get through, you can be gifted and get through, but you can also be determined and get through.

- The Determined One

Table of Contents

List of Tables

List of Figures

Preface

Chapters of this dissertation were written as manuscript articles for submission in selected journals and are in various stages of review. Chapter 3, *Relationship between explosive and effusive volcanism in the Montes Apenninus region of the Moon*, and its data repository, have been reviewed internally by peer reviewers at the U.S. Geological Survey and has been submitted to the Journal of Geophysical Research: Planets for external peer review, awaiting resubmission addressing peer reviewer comments. Chapter 2 and Chapter 4 have both been written with the intent for publication (including grammar and syntax). Chapter 4, *Varied volcanism present in Mare Vaporum revealed by thermophysical properties of surface features*, is being submitted as part of a special issue of the Planetary Science Journal. The anticipated submission date is near the end of 2023.

Chapter 1: Introduction and Motivations

Volcanic processes have been shaping the surface of the Earth since its formation and is a primary contributor to the evolution of the terrestrial interior. Understanding the volcanism of a silicate body can reveal its origins, in addition to its compositional and volatile evolution as eruptive processes separate, reincorporate, expel, and preserve gases and minerals throughout time. Similarly, lunar volcanism provides a window into the composition of the lunar interior and the evolution of interior volatiles. Through the analysis of volcanic features, we can understand how volcanic centers have changed through their lifetime and infer magmatic volatile exchange, compositional differentiation, and volcanic evolution. In this work, I investigate how explosive volcanic deposits on the Moon are related to other lunar volcanic features (i.e., a variety of effusive features and their magma source regions) that are spatially correlated and understand eruption conditions of these volcanic centers. I use remote sensing datasets through visible, near infrared, and thermal infrared wavelength ranges to characterize explosive volcanic features, and various relationships that occur on the lunar surface (i.e., how they are distributed on the surface, how they relate to effusive features, and their relationships within a geologic context). I investigate global pyroclastic deposits and their trends in distribution with respect to latitude, longitude, size, and magma source region. I examine a large region with multiple features (the Montes Apenninus), and then focus on a basin within that region (Mare Vaporum) with a different dataset to enhance the overall investigation of these features. The diversity of information I obtain from these datasets and study areas allow me to identify and map mineralogy and rock and regolith properties in fine detail and broad geologic settings to relate the nature of these materials to their volcanic eruption and emplacement styles.

In terrestrial volcanism, we understand that most volcanoes erupt both explosively and effusively (Popa et al., 2021), sometimes simultaneously (e.g., Wadsworth et al., 2020). On the Moon, we observe both explosive (i.e., pyroclastic) and effusive (e.g., lava flows, mare basalts, sinuous rilles) volcanic features. However, it is common when studying pyroclastic eruptions on the Moon that the focus of a study is on only the explosive processes and eruption styles that create the pyroclastic deposit (e.g., Gaddis et al., 1985; Head and Wilson, 1979; Keske et al., 2020; Trang et al., 2017). This work seeks to connect explosive volcanic eruptions on the Moon to the complex volcanic processes that were likely occurring during the emplacement of the pyroclastic deposits. I first investigate the locations of explosive volcanism (called Lunar Pyroclastic Deposits or LPDs) and identify trends in their distribution on the lunar surface with respect to latitude, longitude, areal extent, and relationship to other volcanic features through their magma source regions. These trends are correlated to known lunar conditions (e.g., crustal thickness, eruption style, and magma source types) to get a more focused look at conditions that influence volcanic eruption. From this global dataset of LPDs (Figure 1 blue boxes, and Chapter 2), I sample a region of the Moon with several diverse types of explosive deposits that each have different effusive volcanic features nearby (e.g., mare flows, sinuous rilles). For these I evaluate their composition to unravel how the explosive deposits may be related to the nearby effusive volcanic features (Figure 1 pink box, and Chapter 3). From this area, I select a smaller subset region with a diverse array of volcanic features to investigate the physical properties of volcanic basin and develop a geologic history (Figure 1 purple box, and Chapter 4). These three analyses combined provide a broad overview into relationships between a variety of types of volcanism, while also creating an in-depth study of one region, using all three analyses.

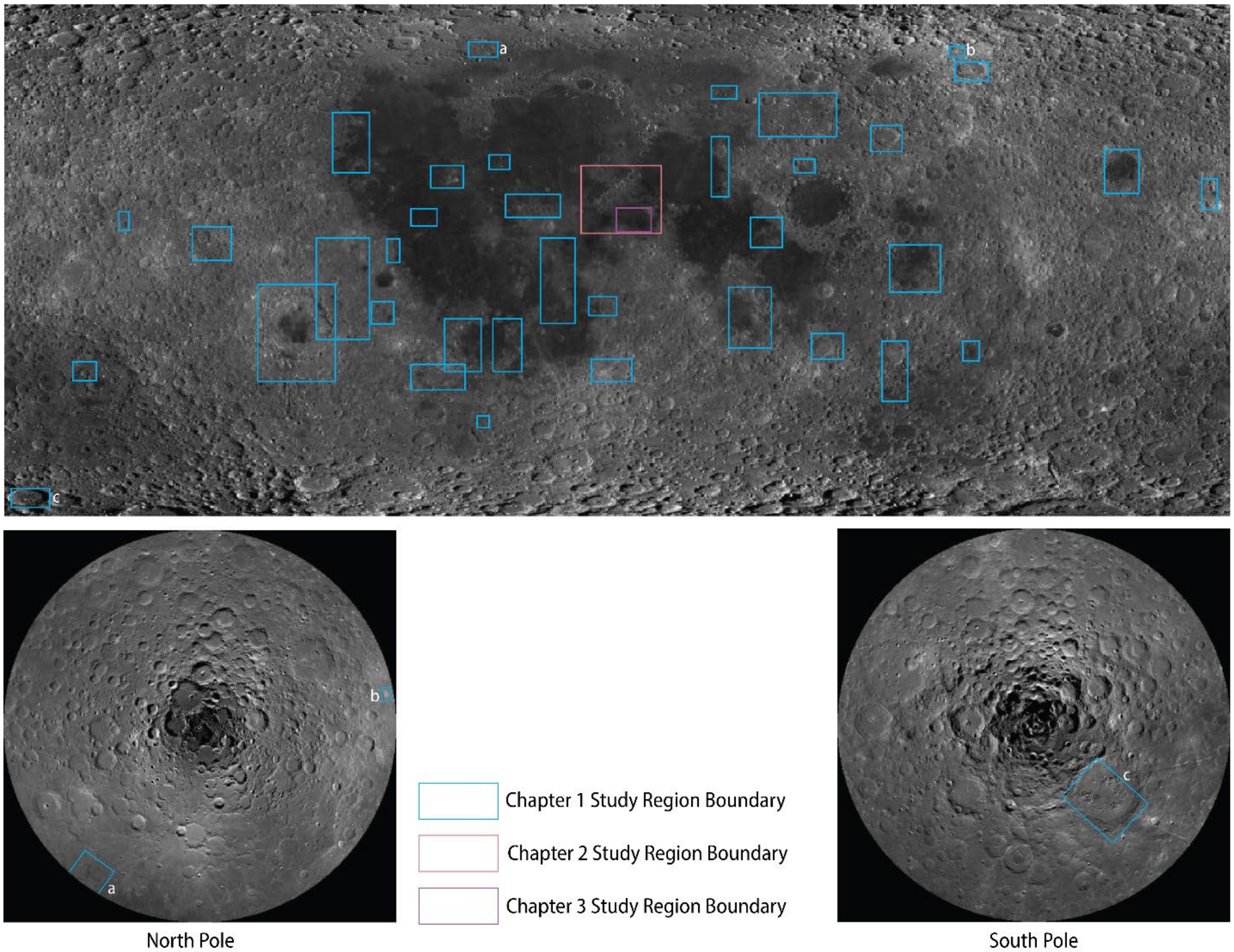

Figure 1: Locations of study regions on the Moon for analysis. Blue boxes are regions processed using M^3 for the global inventory. Pink box is the Montes Apenninus region, processed using M^3 to evaluate compositional relationships between explosive and effusive features. Purple box is the Mare Vaporum region, processed using Diviner to evaluate thermophysical properties of explosive and effusive volcanic features.

Volcanism is a complex process, often involving multiple eruptive phases with a range of volatile conditions and magma compositions (Bennett et al., 2016; Keske et al., 2020; Luo et al., 2023; Popa et al., 2021). Explosive volcanic eruptions on the Moon are responsible for producing deposits known as Lunar Pyroclastic Deposits (LPDs), also referred to as “dark mantling deposits” (Coombs and Hawke, 1991; Gaddis et al., 1985; Head, 1974). Lower-volatile effusive eruptions create lava flows, flood basalt-type mare deposits, and channelized lava features like sinuous rilles. These two types of volcanic features (i.e., explosive and effusive volcanic deposits) are different in their physical, mineralogical, and sometimes compositional properties, owing to their unique magma storage and eruption conditions. Historically these volcanic features are investigated individually as the methods to evaluate their morphology, composition, and physical properties have distinct challenges. Only by investigating co-located effusive and explosive volcanic features together will I be able to elucidate many of the complex relationships that exist in the geologic history of each region.

LPDs are nearly ubiquitous on the lunar surface as they occur in nearly every type of lunar terrain (e.g., mare, highland, and within craters), and have been observed on the nearside and farside and at nearly all latitudes. The largest LPDs are described as being of a "regional" size classification, as those being over 1000 km^2 (Gaddis et al., 1985) or 2500 km^2 (Gaddis et al., 2000) and those below the regional size classification are said to be localized lunar pyroclastic deposits. These size classifications have been used to distinguish LPDs by eruptive product volume flux, which can relate to eruption style and volatile content. Additionally, these size classifications have implications for magma source regions as the correlations between regional LPDs and nearby geologic features (e.g., maria and mare margins) have demonstrated structural controls on large-scale eruptions.

Pyroclastic deposits are sourced from perched magma chambers, magma bodies from the deep interior, or from the lunar mantle. These magma source regions supply a variety of types of volcanic features including the lavas that form sinuous rilles, mare basalts, and general lava flows. Information about the contents of the magma source region (e.g., volatile species, level of evolution, depth to source) can be captured in the composition and mineralogy of the erupting volcanic feature. For example, melt inclusions in glass droplets and olivine grains of returned Apollo samples has revealed the volatile species and volatile content of the magma chamber from which these materials originated (Hauri et al., 2011). The variability between magma source regions is closely tied to the magma's evolution prior to eruption, which can be observed using remote sensing methods. Magmatic volatile content and composition relate to pyroclast distribution and grain size through the analysis of eruption styles and modeling (e.g., Morgan et al., 2021). The composition of a magma body can also vary due to fractional crystallization with increased residency (Luo et al., 2023), which can be observed in the composition and mineralogy of erupted materials. Pyroclastic glasses are thought to originate from deeper in the lunar interior and have been subjected to less fractional crystallization than if they had originated in a perched magma chamber (Shearer and Papike, 1993; Weitz et al., 1998). Pyroclastic glasses are the result of the quenching of magma droplets in the cold lunar environment, resulting from the immediate burst of dissolved volatiles in lunar surface conditions (Delano, 1986a; Wilson and Head, 1981).

This study creates new research conducted in explosive volcanism and uses research conducted in effusive volcanism (e.g., mare formation, eruptive vent formation) to develop enhanced geologic context for lunar volcanism. These two diverging lines of research are combined here and enhanced with new analyses of deposit distribution, composition, and physical properties. Typical studies in explosive and effusive volcanism on the Moon focus on only the explosive or effusive phase or reduce the process to a linear degassing process (i.e., initial degassing explosive phase followed by a low-volatile effusive phase, Head and Wilson, 2017; Wilson and Head, 2017). Work I've conducted suggests that lunar volcanism follows a more familiar terrestrial model, where a single eruption can have multiple eruptive phases or can have multiple eruptive types (i.e., explosive and effusive) erupting from the same vent at potentially even at the same time. This research has a number of research objectives that involve investigating volcanic deposits in multiple wavelength ranges. First, I will create a database of pyroclastic deposits on the Moon and evaluate their distribution using a single remote sensing dataset (Chapter 2). This type of inventory has not been conducted for two decades (Gaddis et al., 2003), despite the discovery of many new LPDs and a greater understanding of the properties of explosive volcanism. Additionally, this updated inventory will be made available to the community as a Geographic Information System (GIS) shapefile, combining these discoveries from multiple sources into a single, accessible location for future use. This inventory evaluates the areal extent of LPDs, their distribution on the surface, and connects these explosive deposits to conduits to subsurface magma bodies. Providing an inventory of LPDs in a single, accessible source can open a path for additional research into LPDs in different geologic settings, size classifications, and regions of exploration. This also provides users with an increased capacity to conduct analyses on LPDs using their own datasets as I created boundaries of each pyroclastic deposit that will be released as a shapefile that can be easily integrated into a user's georeferenced dataset and allow the user to find values for their dataset within the boundaries of each LPD. The methods to generate these boundaries are also included, giving the community the ability to create their own LPD boundary shapefiles based on their own datasets, increasing our understanding of the nature of LPDs in different wavelength ranges, using different instruments, and using different processing tools.

I then conduct a compositional analysis of the Montes Apenninus region (Chapter 3), to characterize relationships between pyroclastic deposits and effusive features within the Montes Apenninus region. I evaluate the differences in mineralogy between pyroclastic deposits within the context of other local eruptive products and features to develop an eruptive relationship between each LPD in the region and nearby effusive features. Using physical and spatial relationships between the effusive and explosive volcanic mineralogy, I evaluate the timing and potential co-occurrence of these eruptions. Focusing on a smaller region within the Montes

Apenninus for Chapter 4, I relate a variety of volcanic features in Mare Vaporum by investigating their thermophysical properties. I find temperatures, rock abundance and H-parameter (a regolith property comparable to thermal inertia) of features in the Mare Vaporum basin to relate the geologic histories of this region.

Eruptions that produce LPDs sample subsurface magma and capture evidence of the conditions of the lunar interior (Delano, 1986; Shearer and Papike, 1993), making them high priority targets for scientific value (Scientific Context for Exploration of the Moon, 2007; Jawin et al., 2019). LPDs also have high exploration value as a potential resource for water, metals, and easily processed regolith (van der Bogert et al., 2021). Water and raw materials like titanium and iron could be necessary future resources for extraction from lunar regolith for sustained exploration activities (e.g., using water or oxygen for rocket fuel, using metals to create or repair parts). Pyroclastic deposits typically have a uniform grain size, making this particular type of regolith easy to acquire and process. This combination of high scientific importance and high resource potential make Lunar Pyroclastic Deposits a focus of many studies as the Artemis Program continues to grow (Committee on the Scientific Context for Exploration of the Moon et al., 2007; Jawin et al., 2019; van der Bogert et al., 2021). In Appendix A, I outline the resource potential of each LPD in the Montes Apenninus region, enhancing this scientific investigation.

1.1: Characteristics of volcanic features

Although somewhat varied in morphology, composition, and surface roughness, Lunar Pyroclastic Deposits (LPDs) have some common characteristics. These deposits have also been referred to in the literature as dark mantling deposits (DMDs; Head, 1974). As the nomenclatures suggests, a DMD describes morphological characteristics of these deposits and an LPD describes a formational origin of explosive volcanic deposits. “Dark mantling deposit” describes a material that is observed to have a relatively low albedo that mantles (i.e., blankets) the underlying stratigraphy, smoothing topographic detail (Gaddis et al., 1985). Although DMDs are often inferred to result from explosive volcanism (Gaddis et al., 1985; Head, 1974), this moniker does not explicitly indicate that DMDs are of explosive volcanic origin. The LPD name is explicit in the formation of the deposit as resulting from explosive volcanism (pyroclastic) and does not describe the morphology or physical properties of the deposit, which becomes important as sites of explosive volcanism have been described with a wide range of albedo and other physical properties. A variety of differences exist between LPDs that allow us to focus on factors that might cause these differences. Some LPDs do not exhibit significantly lower albedo than the surrounding terrain (e.g., SE Nectaris, Figure 2a), and some LPDs exhibit higher albedo than the surrounding terrain (e.g., Compton-Belkovich Volcanic Complex, Figure 2b). This is likely due to composition: silicic volcanism rarely produces iron-bearing glasses and is characterized by high reflectance silica glasses, and some regional deposits contain the green types of pyroclastic glasses, which also rarely produce an albedo lower than typical regolith.

Regardless of the name, these sites of explosive volcanism typically mantle the surface, suppressing underlying topography, and reducing crater retention due to their generally homogenous, fine-grained nature (Lucchitta and Sanchez, 1975). LPDs are sometimes marked by a source vent described as a low, positive relief feature (e.g., Gauss LPD vent in Figure 2c) with a central crater that is non-circular in shape, indicating the source vent of the eruption (e.g., Gaddis et al., 2003; Keske et al., 2020; Trang et al., 2017). Volcanic vents can be the source of both explosive and effusive features and have been observed as being the source for eruptions that produce sinuous rille lavas and pyroclastic deposits from a single vent (see Chapter 3). In the absence of a singular volcanic vent, LPDs are often circular to sub-circular in shape, and those with an arcuate shape can be inferred as once having been circular and having been embayed by later lavas, resulting in their final shape (e.g., Rima Bode LPD in Figure 2d; Gaddis et al., 1985).

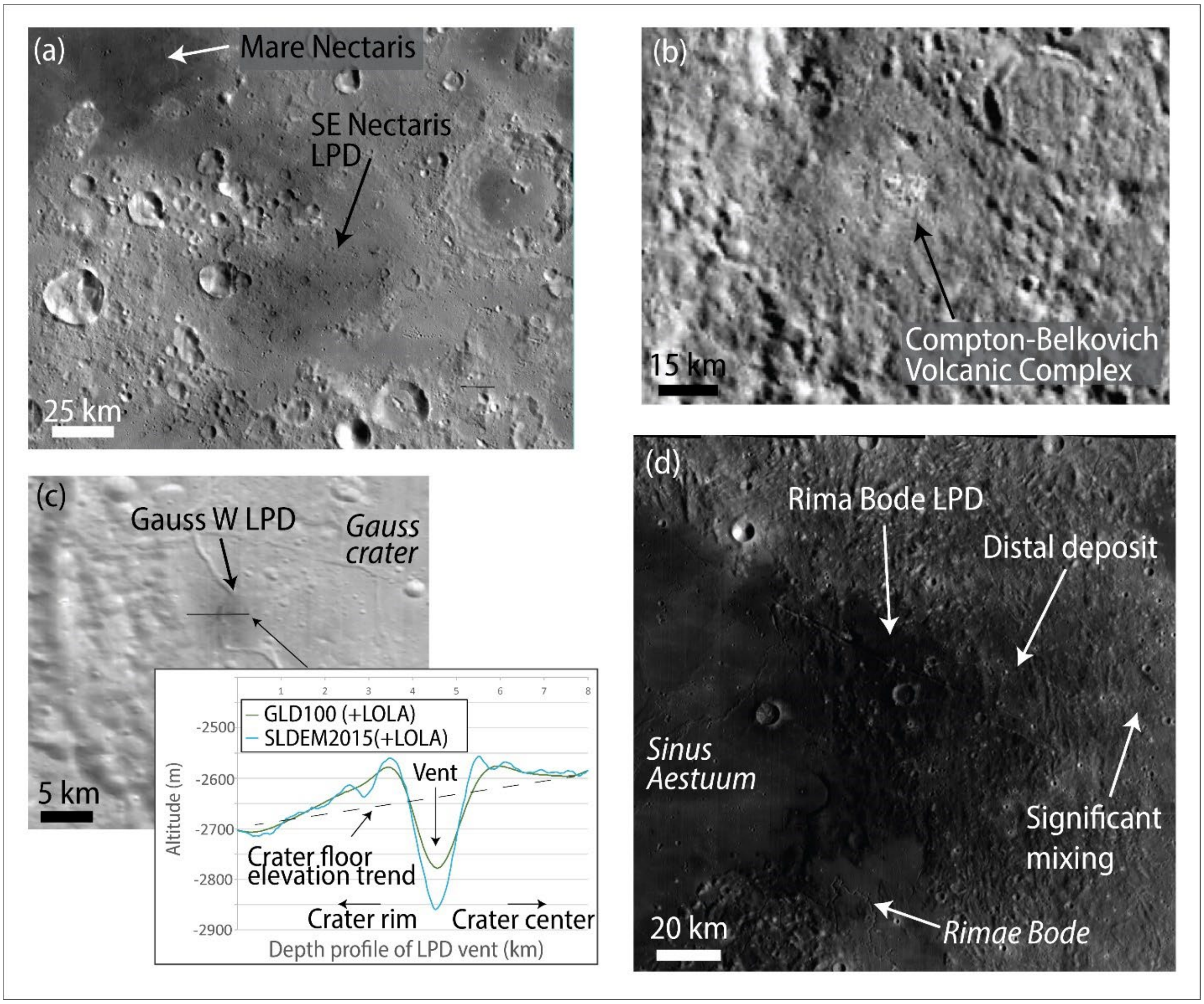

Figure 2: Various surface expressions of lunar pyroclastic deposits. (a) moderate albedo of SE Nectaris LPD – note albedo that is generally similar to nearby Mare Nectaris, and mostly produces dark halo craters. (b) Compton-Belkovich Volcanic Complex, mantled in pyroclastic material that is higher albedo than the surrounding region. (c) Gauss W LPD on fracture of the floor of Gauss Crater. Line indicated crossing Gauss W LPD indicates vent profile shown. (d) Rima Bode LPD, showing arcuate shape of this mare margin LPD.

Extrapolation of lunar conditions to terrestrial lava fountaining events suggest that lava fountain events could disperse pyroclastic materials over elevated highland massifs (e.g., Head, 1974). Detailed observations of LPDs in Alphonsus floor-fractured crater made by Head and

Wilson (1979) calculated the proportion of juvenile material and non-juvenile material based on the morphology of the vents. They proposed that regional LPDs with a large juvenile component were a likely result of Strombolian activity (i.e., the eruption of large bubbles that have coalesced from smaller bubbles in the vent column) and localized LPDs with higher block content and a smaller juvenile component were a likely result of Vulcanian activity (i.e., the eruption from beneath a volcanic plug of country rock). The significant amount of glass and wide dispersal of regional LPDs led later investigators to determine that they were more likely from long-duration lava fountaining events (Gaddis et al., 2003). In this way, it is common to conclude that regional LPDs result from lava fountaining events, whereas localized LPDs may originate from one of many types of eruption styles (Bennett et al., 2016).

Explosive volcanism is driven by volatile exolution and magmatic fragmentation processes. Gases trapped within melt inclusions in pyroclastic minerals from Apollo samples have been analyzed and found to contain water, carbon dioxide and other volcanic gases (Hauri et al., 2011; Saal et al., 2008), which represents magmatic or interior water from the magma body (Trang et al., 2022). LPDs have been shown to have a wide range of juvenile proportions (pyroclasts derived directly from erupting magma) relative to non-juvenile material (erupted fragments derived from the "country rock" that are expelled during eruption and may be of any composition, Keske et al., 2020). As an identifiable source of erupting magma, separate from reworked volcanic material, LPDs represent the best example of the primitive components of the Moon, and would be the best opportunity for characterizing the lunar interior and constraining the origin and evolution of lunar magmatism.

Magma sources generally refer to the subsurface pocket of molten rock that volcanic materials erupt from. Surface volcanic features can mark locations that have tapped these magma sources.

Sinuous rilles are channelized lava flows on the Moon. These are thought to have formed from incision into the surface due to extreme thermal contrast between the lava and the substrate, or from the construction of lava levees on either side of the channel (Hurwitz et al., 2013). Sinuous rilles typically originate from a single vent, often called a "cobra head." Sinuous rilles can be found near mare basins and in craters, flowing through a variety of ages of terrains. A sinuous rille may be linked to subsurface flows or can incise into the subsurface creating lava tubes. Roof collapse of these tubes have revealed pits into subsurface lava caverns that have been left hollow. Floor-fractured craters are another type of magma source region from which volcanic features (particularly pyroclastic deposits) can erupt. These impact craters have concentric fractures in their floors, that are thought to result from either subsurface magmatic inflation or by viscous relaxation (Jozwiak et al., 2012). The presence of a large number of pyroclastic deposits, lava flows, and support the formation of floor-fractured craters by the inflation of a magmatic intrusion under the floor of a crater, and its subsequent eruption onto the crater floor (Jozwiak et al., 2015). This would then further indicate that the volcanic features within the crater floor share the same magma source – the intrusion under the crater.

Mare basins are thought to have formed from large impacts that are later infilled by volcanic basalt (Mackin, 1969). Many mare basins have regional pyroclastic deposits on their margins, between the mare and the surrounding highlands. Some of these deposits have been observed to have been embayed by the mare lavas, indicating that the pyroclastic volcanism occurred during mare emplacement, where the pyroclastic material was erupting in a way to cover parts of the mare, but also be covered by mare during a later event (Chapter 3 and 4). These various relationships between magma source regions and the volcanic features that erupt from them are the topic that I explore. Explosive deposits have been observed to originate from vents or in association with these magma source regions, and often in relationship with effusive features. The stratigraphic relationships between these features can be used to infer complex geologic histories of a region, which relates to the evolution of the subsurface and deep interior.

1.2: Experimental Techniques

Despite being the most-visited planetary surface in the solar system to date, the Moon is still plagued by inaccessibility and knowledge gaps resulting from a paucity of samples and sampled regions. Remote sensing and the analysis of spectra, validated by the returned samples that we do have, is used by planetary scientists to expand the applications of these results, and target future sampling locations to fill gaps. In this work, I use data obtained via orbital remote sensing instruments that span the visible, near infrared, and thermal infrared wavelength ranges to thoroughly characterize explosive volcanic features on the Moon and related effusive features. Analyses of orbitally obtained datasets allow me to identify and map the variability of compositions and physical properties on the surface to relate the distribution of explosive volcanic deposits to other volcanic features. Many of these features have similar analogous features on Earth, like lava flows and small explosive deposits, but some do not (e.g., Irregular Mare Patches). Although field validations to terrestrial analogs is beyond the scope of this work, I make comparisons and inferences to the nature of the relationships between explosive and effusive volcanism based on observations from volcanism on Earth.

I use the Moon Mineralogy Mapper (M^3) hyperspectral imaging spectrometer (Boardman et al., 2011; Pieters et al., 2009) to characterize the visible and near-infrared part of the electromagnetic spectrum. M^3 targets parts of the electromagnetic spectrum useful for evaluating composition, particularly of iron-bearing minerals and glasses (Bennett et al., 2016; Horgan et al., 2014; Mustard et al., 1997). Supplementing the compositional analysis, I also use analyses from the multispectral Diviner Lunar Radiometer Experiment (Diviner) to characterize the thermal infrared part of the electromagnetic spectrum (D. A. Paige et al., 2010; Williams et al., 2017). Products derived from the thermal infrared part of the spectrum reveal thermophysical properties, which can be used to evaluate the physical properties of the surface such as regolith characteristics and rock abundance (Bandfield et al., 2011; Hayne et al., 2017; Powell et al., 2023; Williams et al., 2022, 2017). These two analyses combined provide a comprehensive picture of the nature of volcanic features, as described below.

1.2.1 Research Design

To investigate subsurface magmatic evolution and volcanic eruption dynamics, I evaluate the diversity of volcanic features, and how volatile-rich explosive volcanic features relate to nearby effusive volcanic features. This informs eruption transitions, magmatic volatile evolution, and the geologic history of volcanic features. To conduct this investigation, I first analyze the composition of the Montes Apenninus region of the Moon using M^3. Evaluating the mineralogy and mineral distribution can inform eruption styles, volatility, and multiple phases that an eruption may have gone through. Using knowledge garnered from this research, I apply the methods to a complied global database of pyroclastic deposits and evaluate trends in the distribution of LPDs with potential magma sources (e.g., a magma body under a floor-fractured crater, mare emplacement). Linking LPDs to potential magma sources can open a path to identifying magma storage conditions and evolution through partial differentiation (Luo et al., 2023). I then focus on a sub-region of Montes Apenninus to evaluate the thermophysical properties of explosive and effusive volcanic features to supplement and enhance the compositional analysis. This additional level of detail (both in analysis and in features evaluated closer) provides additional information on volcanic eruption styles and the geologic history of a region and how effusive and explosive volcanic features can be related in space and through time.

1.2.2 Vis-NIR Remote Sensing

I use the M^3 evaluate the composition and mineralogy of explosive and effusive volcanic features on the Moon. The Moon Mineralogy Mapper (M^3) instrument is a hyperspectral imaging spectrometer proposed by Brown University that flew onboard the Indian Space Research Organization's Chandrayaan-1 spacecraft (Boardman et al., 2011; Pieters et al., 2009). M^3 covers a spectral range of 0.35 - 3.0 µm, which includes the visible part of the spectrum, spectral regions targeting iron-bearing minerals and glasses, and the critical water feature for observing surface water content (e.g., Li and Milliken, 2017; Staid et al., 2011). Iron-bearing minerals and glasses are a major component of planetary surfaces, present in a wide variety of geologic features (McCord et al., 1981; Horgan et al., 2014). Specifically, I investigate absorption bands near 1 µm and 2 µm using M^3, which are useful for characterizing mafic mineralogy of LPDs, mapping glass content variability between effusive and explosive volcanism, and identifying other volcanic and non-volcanic spectral diversity in a region (Bennett et al., 2016; Horgan et al., 2014; Chapter 2). These compositional features have specific implications for volcanic processes, as the specific mineralogy and composition can change as a result of magma composition, volatile content, and eruption style (Gaddis et al., 1985; Mustard et al., 1997; Henderson et al., 2021; Scudder et al., 2021). The high spectral resolution (10 nm spectral sampling) and broad wavelength range of M^3 targets the iron absorption features that are characteristic of these critical volcanic minerals and glasses. Using information from these studies, I apply these investigative techniques to a global population of pyroclastic deposits to understand trends in how LPDs are distributed with regards to mineralogy and in their relationship to other volcanic features.

1.2.3 Thermal Remote Sensing

I use the Lunar Reconnaissance Orbiter (LRO) Diviner Lunar Radiometer instrument (Diviner) to map the thermophysical properties of effusive and explosive volcanic features in the Mare Vaporum basin, a sub-area within the Montes Apenninus region. The Diviner instrument is a multispectral thermal infrared instrument with a wavelength range of ~0.3 – 400 μm in 9 spectral channels. I use the Diviner instrument to map the Mare Vaporum region and calculate the effective surface temperature following the methods of Williams et al., (2022, 2017) to produce the surface bolometric brightness temperatures. The bolometric brightness temperature is effectively equal to the temperature of the surface, which we use to evaluate the minimum and maximum temperature of the region and the diurnal temperature curve of each surface material for comparison. I explore the variability of these features within these study areas and use variability observed on the surface to infer relationships between features and the geologic history of the areas.

1.2.4 Data

This study uses publicly-available remote sensing data from standard data sources and produces derived products and information that are made public through the peer review process. M^3 data were obtained and are all publicly available from the Planetary Data System (PDS) as Level-1B and Level-2 products for ingestion into the processing pipeline (Horgan et al., 2014). Diviner data were obtained from the mission archives for ingestion into the processing pipeline (Williams et al., 2022), and are publicly available on the PDS. Data, information, and derived products are made available via manuscript publication with associated datasets being published on USGS-acceptable data repositories.

1.2.5 Analysis

Data downloaded from this study were processed using analysis tools created for the specific purpose of evaluating the lunar surface using these remote sensing instruments. The M^3 analysis pipeline was created by Horgan et al., (2014) for spectral processing (e.g., continuum removal due to space weathering, spectral smoothing, and band parameter analysis) and image mosaicking. The analysis and interpretation of these data follow the methods of Horgan et al., (2014) and Bennett et al., (2016) for understanding explosive volcanism and its relationships to iron-bearing glass and mineralogy. The Diviner analysis pipeline was created by Williams et al., (2022, 2017) for temperature conversion (e.g., radiance to bolometric temperature and brightness temperature), and the production of derived product maps using the methods of others (e.g,, Bandfield et al., 2015; Hayne et al., 2017).

1.3 Applications

Investigating the complexities of lunar volcanism builds our understanding of the origins, evolution, and volatile inventory of the lunar interior. Much of what we know about the lunar interior comes from the analysis of rock samples and in situ analyses conducted by landed missions However, these only provide a small sampling of the diversity of geologic features on the surface and there are a large number of features that have yet to be sampled (e.g., direct sampling of a pyroclastic deposit, lunar swirls, irregular mare patches, red spots). It is therefore clear that as we acknowledge that the evolution of the lunar surface and subsurface is more complex than we once thought, new concepts to describe these complexities must be developed.

In addition to having high scientific importance for understanding the surface and subsurface evolution of the Moon, volcanic deposits have a high value as exploration targets. LPDs are important resource targets as indicated in the Artemis III Science Definition Team Report, (2020).

Generally, LPDs have a generally homogenous and fine-grained distribution within the deposits resulting from the conditions of the explosive eruption of juvenile magmatic material (Gaddis et al., 2003a; van der Bogert et al., 2021). Minerals and metals (e.g., zinc, titanium) found on grain surfaces and as bulk content are generally more concentrated within pyroclastic deposits than typical lunar regolith (Campbell et al., 2008). Finally, as explosive eruptions are driven by volatile processes, these volatiles can get trapped in melt inclusions in mineral and glass grains and brought to the surface during eruption (Hauri et al., 2011). These make LPDs a valuable resource target due to their generally uniform grain size ideal for processing (Hawke et al., 1990), above-average metal oxide content for extraction and volatile entrapment for use as a source of oxygen (Hauri et al., 2011; Saal et al., 2008).

Through the following three chapters, I describe how explosive and effusive volcanic features can be related, and how these relationships can provide information about the subsurface magma sources from which they evolved and erupted. Explosive lunar volcanic features have a wide diversity of eruption styles and many of these eruption styles have a range of relationships with nearby effusive features (including having no relation to nearby effusive features). That is to say, the type of an eruption style of an LPD cannot predict how it will have related to effusive volcanic features at the time of its emplacement. This information can be used to infer changes in the volatile inventory of the magma source as it degassed (i.e., changed from an explosive eruption style to an effusive eruption style) or went through multiple eruption phases (i.e., went from effusive to explosive in multiple phases). Changes in glass content, mineralogy, and composition can also indicate changes in subsurface magma storage conditions, relating to the evolution of lunar magma pockets and the lunar mantle.

Chapter 2: Distribution of Lunar Pyroclastic Deposits using Moon Mineralogy Mapper

Abstract

Earth's moon has a rich history of volcanism and over 100 sites have been identified where characteristics of explosive volcanism are present. Explosive lunar volcanism represents the ascent of volatile-rich magma, often characterized as having volcanic glasses, a mantling of fine-grained lava droplets, and/or a low albedo related to magma compositional variations. To better understand the thermal and structural evolution of the lunar subsurface and deep interior, it is important to understand the distribution of magmatic volatiles, which can be evaluated from the trends in the distribution of these explosive volcanic deposits. We combine and expand prior inventories of these sites of explosive volcanism (called Lunar Pyroclastic Deposits or LPDs) and investigate the complete database of LPDs with a single, high resolution compositional dataset. We create this database to better characterize constraints on explosive volcanism, including crustal thickness and magma source regions. We use the hyperspectral Moon Mineralogy Mapper data to examine the albedo of 179 identified LPDs from historical sources, an updated database, and recent discoveries more than doubling the prior published inventory of pyroclastic deposits. Although pyroclastic deposits are generally ubiquitous on the lunar surface, there is a strong correlation to the location of LPDs with latitude (91% being within 50°N/S) and longitude (83% occurring on the near side). LPDs are also more likely to be found in floor-fractured craters than associated with any other type of volcanic feature (44%).

2.1 Introduction

Lunar Pyroclastic Deposits (LPDs) are low-albedo mantling deposits that are the result of explosive eruptions on the Moon (Gaddis et al., 1985; Gaddis et al., 2003; Keske et al., 2020; Trang et al., 2017). LPDs are often high in glass content as the erupting material is expelled quickly into the cold, near-vacuum conditions above lunar surface and are quenched to glass (Head, 1974; Head & Wilson, 1979; Head & Wilson, 2017; Weitz et al., 1998). Differences in eruption style and composition alter the homogeneity, albedo, and glass content and individual deposits display a range of blockiness, albedo, and crystallinity (Bennett et al., 2016; Pieters et al., 1973; Trang et al., 2022). We evaluate the extents, distribution and relationships to magma source regions of LPDs using Moon Mineralogy Mapper and a database that we updated to be a global inventory of known deposits. This method provides insight into the distribution of pyroclastic materials on the lunar surface, which reveals trends in lunar volcanic origins and evolution. Although this is not meant as a comprehensive or summative work on individual deposits, research into the reported deposit areal extents, locations, and names was conducted. In this work, we introduce (1) an updated inventory of LPDs identified on the lunar surface (2) updated areal extents of LPDs in this database, based on surface albedo from Moon Mineralogy Mapper, (3) an evaluation of the geologic context of LPDs which can be traced to shared or distinct magma sources, (4) the distribution of LPDs by latitude, longitude, and areal extent, and (5) whether this LPD was presented in Gaddis et al., (2003) or if this was a identified elsewhere (and the literature source from which it was identified).

With these research goals, we would expect that LPDs will generally be found in areas with thinner crust; i.e., on the near side, closer to the equator than to the poles, and where the majority of mare basins are located. Further, we predict that where a pyroclastic deposit has been located, there will be other types of volcanic features in the region that may be related to the pyroclastic deposit. Pyroclastic deposits and other volcanic features originate from magma in the deep interior and rise to the surface from conduits through the crust. Thinner crust provides easier eruption pathways for a shorter distance for magma ascent from the source, and these regions of thinner crust are typically found in major mare basins which are on the near side, near the equator and mid-latitudes. Since these volcanic features bring subsurface and deep interior materials to the surface, studying explosive and effusive volcanic features provide the best examples of primitive lunar magma and mantle samples (Gaddis et al., 2003). We create an inventory of pyroclastic deposits to test how the distribution of these volatile-rich eruption centers vary on the lunar surface, evaluating trends specifically in distribution by latitude, longitude, magma source region, and size. We use these trends to connect explosive volcanism to structural controls on the volatile distribution of the lunar interior accounting for crustal thickness and known centers of magma inflation.

Lunar pyroclastic deposits reflect the volatile inventory and subsurface magma plumbing systems of the Moon. This work evaluates the distribution of pyroclastic deposits globally on the Moon, connecting these sites to crustal heterogeneities and potential shared magma sources. These relationships have implications for subsurface magmatic evolution, surface geologic history, and *in situ* resource potential. LPDs have high resource potential as a source for volatiles, homogenous fine-grained material for construction, and oxygen production and this survey and analysis provides a comprehensive evaluation of known pyroclastic deposits. This type of complete, global inventory has not been conducted for two decades (Gaddis et al., 2003), despite the discovery of many new LPDs and a greater understanding of the properties of explosive volcanism. This updated inventory can also be used for other analyses to enable future science. The shapefile of deposit boundaries provided can be used to query data within those polygons, or compare to the distribution of pyroclasts in other datasets (e.g., using other wavelength ranges where the dispersal changes due to differences in penetration depth, sensitivity, or spatial/spectral resolution).

2.2 Characteristics of LPDs

Lunar volcanic features are used to infer subsurface magmatic conditions, bulk composition and compositional evolution, and interior volatile inventory. Pyroclastic deposits represent locations where the ascent of volatile-rich magma has reached the surface, contrasting volatile-poor magma, which results in effusive deposits like lava flows and mare basalts. Understanding the distribution of pyroclastic features on the Moon can reveal the inventory and distribution of volatiles in the deep interior. Concentrations of pyroclastic deposits can indicate regions where a single, volatile-rich magma body was able to reach the surface without significant volatile loss. Although discoveries of new pyroclastic deposits continue to add to our understanding of various properties of explosive volcanism, the total distribution of LPDs and their geospatial relationships on the lunar surface are required to fully understand lunar evolution and volatile inventory of the deep interior. We have therefore compiled a database of known discoveries of pyroclastic deposits on the Moon to understand the distribution of explosive volcanism and the context of LPDs within lunar volcanic history.

To evaluate how LPDs relate to different magma sources, crustal thickness, and eruption styles, we update the inventory of pyroclastic deposits to determine trends in co-located magma source regions, distribution by latitude and longitude, and by areal extent. As prior inventories have a limited scope (e.g., only localized deposits, only a biased selection), we compiled a database of all LPDs from available literature to evaluate total trends, and to provide the community with the same inventory to conduct additional investigations. We specifically investigate how LPDs are related to magma sources as many investigators have studied floor-fractured crater related LPDs (e.g, Bennett et al., Souchon et al., Gaddis et al.,). As floor-fractured craters appear to be a topic of study, we probe how common LPDs are found within these specific class of impact craters.

With the available inventory, we expand this investigation to also include other magma sources (i.e., geologic contexts that may or may not be related to the same magma body from which the LPD erupted), including sinuous rilles, mare margins, and highlands.

Many LPDs in floor-fractured craters are found in regions of thin crust (e.g., SPA Basin), but some LPDs in floor-fractured craters can also be found in regions known to have thick crust (i.e., the lunar farside). We therefore also use the updated inventory to investigate how LPDs correlate to these regions of variable crustal thickness by determining the frequency of eruptive centers by latitude and longitude. The farside is known to have thicker crust than the nearside (with the exception of the SPA Basin), so evaluating the frequency of LPDs by longitude provides a correlation between crustal thickness and magma ascent through thinner crust. The nearside has many major mare basins near the equator, which are regions known to have thinner crust, but the region of the thinnest crust lies near the south pole in the South Pole Aitken Basin. Determining the frequency of LPDs by latitude can reveal similar correlations between crustal thickness and magma ascent through a thin crust.

Lastly, areal extent is used by the lunar community to imply eruption style. The largest, regional LPDs are implied to have erupted from high-volume lava fountain style eruptions and the smaller, localized LPDs are implied to have erupted from a variety of lower-volume eruption styles including Vulcanian, Strombolian, but also lava fountaining styles. With the new, updated inventory, we create new areal extents based on albedo from Moon Mineralogy Mapper to understand how all deposits are distributed by size. We use this new inventory of sizes to investigate whether the existing size classifications for regional and localized LPDs are maintained, or if the size classifications have natural data breaks at locations other than the previously-reported sizes.

2.2.1 Areal Extent

LPDs have been categorized by size as regional (1,000 km^2 or 2,500 km^2 or greater) or localized (999 km^2: Gaddis et al., 1985, or 2,499 km^2 or smaller: Fig. 3d; Gaddis et al., 2000). The areal extent of LPDs has been correlated to the eruption style, with regional LPDs being thought to be a result of long-duration lava fountaining events, and localized LPDs resulting from a greater diversity of eruption styles (Bennett et al., 2016; Gaddis et al., 2003). LPDs are most likely to be of the localized size classification and are far more common than regional LPDs (Gaddis et al., 2003). Because LPDs are created by explosive volcanism, emplacing pyroclasts onto the surface ballistically, deposit boundaries can be diffuse and challenging to map. Additionally, LPDs can have a variety of characteristics and may not consistently present signs of explosive volcanism and for these reasons, comprehensive estimates of all deposit boundaries and their areal extents have not been attempted since Gaddis et al., (2003) These regional and localized size classifications have not been evaluated statistically to understand the distribution of areal extents of LPDs, nor has there been a single database that has been created to define the areal extents of LPDs. Because deposit extent is used to infer important factors relating to the formation and evolution of LPDs and general lunar volcanic evolution, for consistency, we evaluate the boundaries of all deposits using a single dataset (Moon Mineralogy Mapper, M^3). We then compile LPDs by size and evaluate “natural breaks” in the areal extents of LPDs to determine how the data inform the distribution of deposit size, in order to understand whether there is a trend in the different sizes of LPDs and whether these trends correlate to the established size classifications. .

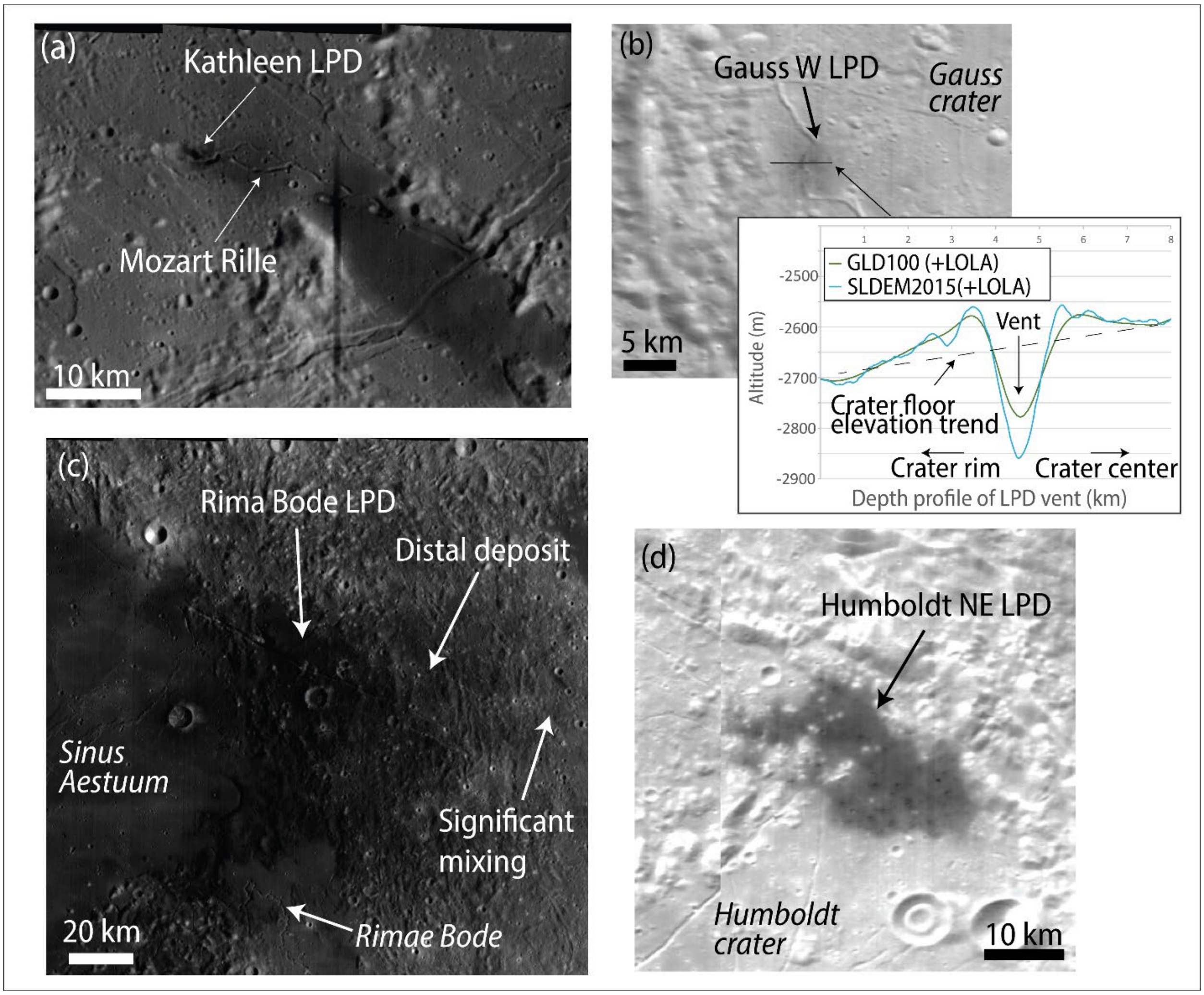

Figure 3: A sample of typical lunar pyroclastic deposits. (a) LPD associated with a sinuous rille: Kathleen LPD is indicated and is apparent as lower albedo around the vent sourcing Mozart rille. (b) Vent profile of Gauss W LPD: the Gauss W LPD erupted from a small vent along a fracture of Gauss crater, a floor-fractured crater. The elevation profile indicates an increase in elevation around the vent, decreasing inside the vent and with distance from the vent. Note that the overall elevation of the crater floor is increasing from the crater rim towards the crater center and is indicated by a black dashed line. (c) Regional LPD Rima Bode. Concentrated area of significantly low albedo shows an arcuate pattern of the overall LPD, increasing in albedo towards the distal parts of the deposit. In the extreme regions of the deposit, significant mixing with the substrate occurs such that it is less clear to differentiate between the LPD and substrate. (d) Localized LPD Humboldt NE.

2.2.2 Magma Source Regions

A pyroclastic eruption is driven by volatiles such as water, carbon monoxide, or H_2 (Fogel and Rutherford, 1995; Gaddis et al., 2003; Lo et al., 2021; Renggli et al., 2017; Wilson and Head, 1981). Differences in mineral composition, albedo, block distribution, deposit size, and glass content can be used to infer variations the magma from which a volcanic feature erupted (e.g., Luo et al., 2023). The albedo of LPDs varies most with composition: so-called "black spot" deposits are associated with high titanium content (Pieters et al., 1973), and some LPDs from silicic eruption centers are actually high in albedo (Clegg-Watkins et al., 2017). Analysis of orange pyroclastic glass beads from Taurus-Littrow indicate that the pyroclastic material in this region is similar in composition to the adjacent mare basalts, with the exception of an enhanced olivine component (Reid et al., 1974). This suggests a shared magma source between the explosive and effusive volcanic deposits in this location, with the potential that the pyroclastic deposit underwent an additional level of partial melting prior to eruption (Green and Ringwood, 1973). This indicates that observations of spatially-associated explosive and effusive volcanic deposits can be used to develop a geologic history of the region, which can be used to infer the compositional and volatile evolution of the magma chamber (Chapter 3).

LPDs are commonly spatially associated with some other type of volcanic feature, including mare basins, sinuous rilles, and floor-fractured craters (FFCs). LPDs within floor-fractured craters are most likely to be of the localized size classification and are far more common than regional LPDs. Regional LPDs are typically found on the margins of mare basins or within mare basins, whereas localized LPDs are more commonly found within floor-fractured craters. Floor-fractured craters are impact craters that have fractures cutting the crater floor (Jozwiak et al., 2012) that may be related to the inflation of a magma body from beneath the surface (Jozwiak et al., 2015). Some pyroclastic deposits are likely to share a magma source by the nature of their location, such as LPDs within a floor-fractured crater sharing the magma body under the crater floor. Vents from which LPDs have erupted are often found along the fractures and fissures in these crater floors.

These fracture pathways likely form conduits for magma to rise more easily from the subsurface magma chamber of an FFC and erupt onto the surface, where observed. Further, past literature on LPDs within floor-fractured craters has revealed that it is common for multiple LPDs to be found within a floor-fractured crater, rather than a single LPD erupting from fractures in the crater floor (e.g., Bennett et al., 2016; Gaddis et al., 2016; Souchon et al., 2013). In this work, we propose that where a magma source can be inferred, multiple volcanic features can be identified that were sourced from this magma body and that these volcanic features will share compositional and mineralogical similarities.

2.2.3 Distribution

LPDs occur in nearly every type of lunar terrain including within mare, on mare margins, in highland terrains, and within floor-fractured and non-fractured craters. LPDs have been observed on the nearside and farside and at most latitudes. The near side of the Moon is distinct from the far side in that it has large mare basins on the near side, resulting in less highland composition coverage and a surface less visibly marred by impact cratering. LPDs are more commonly found on the nearside than the farside, likely owing to the thinner nearside crust and basaltic mare emplacement. More LPDs are found closer to equatorial or mid-latitude regions than at the poles. This relationship, however, is less clear as it is presumed that the thinnest crust is in the South Pole Aitken Basin, a polar far side region that also has mare lavas and complex volcanic features (Wieczorek et al., 2013). Notwithstanding the South Pole Aitken Basin, the crust is thicker on the far side than the near side (Wieczorek et al., 2013), with a variety of hypotheses proposed for this dichotomy (e.g., Garrick-Bethell et al., 2010; Wood, 1973; Zhu et al., 2019). The relationships between LPD distribution and latitude/longitude have yet to be quantified and we hypothesize that, based on structural controls such as crustal thickness and relationships to other magma sources that have been observed, the majority of LPDs are likely to occur on the nearside within ~60° N/S.

2.3 Methods

Remote sensing observations of LPDs often use high iron-bearing glass, low albedo, low radar signal, low crater retention/topographic smoothing, and/or low thermal inertia (i.e., high H-parameter) to identify the location of deposits (Carter et al., 2009; Elder and Hayne, 2017; Gaddis et al., 2003; Souchon et al., 2013; Trang et al., 2017). Databases of features are often useful for identifying trends between features to use to identify new features, and differences in populations within the database of features to characterize their formation, evolution, and interpretation. For our study, we create a new database of Lunar Pyroclastic Deposits and begin evaluating these deposits by determining the deposit boundaries by albedo. To create the database, we start with the original database compiled by Gaddis et al., (2003), which had been maintained through the years as new discoveries were identified in literature. Beginning in 2017, we began a comprehensive literature search for new deposits and references to existing deposits. We compiled this inventory, marking the most recent name of the deposit, latitude/longitude position (of the vent location if known, or approximate deposit centroid if vent location is not known), approximate areal extent if reported, geologic context (e.g., in a floor-fractured crater, on a mare margin, along a sinuous rille), and the reference in which information was found. Table 2 reports the original source in which the LPD was identified and the most recent reference to the LPD (which we use to imply the most updated information about each deposit).

From the latitude/longitude position reported in literature (using the most recent reference), we mapped all LPDs in ArcGIS, noting the distribution of LPDs on the surface for spectral analysis (Figure 4). For image analysis, we use the Moon Mineralogy Mapper (M^3) hyperspectral imaging spectrometer to characterize 179 LPDs in 37 regions. The NASA M^3 instrument flew onboard the Indian Space Research Organization's Chandrayaan-1 spacecraft, providing a near-global hyperspectral dataset (in 82 spectral channels) in the visible-to-near-infrared wavelength range (0.43 - 3.0 µm; Pieters et al., 2009). M^3 has the highest spectral resolution imager to date for the lunar surface, which greatly enhances prior compositional results from Clementine and other imagers. We explored the variability of albedo within pyroclastic deposits identified in our updated database (including contributions from Gaddis et al., 2003; Gustafson et al., 2012; Keske et al., 2020; Trang et al., 2017 and others). To process M^3 images into mosaics for interpretation, we first create regions that have clusters of LPDs to decrease the computing time for each mosaic (Figure 5). Clusters of nearby LPDs are put into localized regions for mosaic processing, instead of processing each LPD as an individual image mosaic. We obtain the relevant images for each mosaic instead of processing M^3 globally where multiple images could be used for each region.

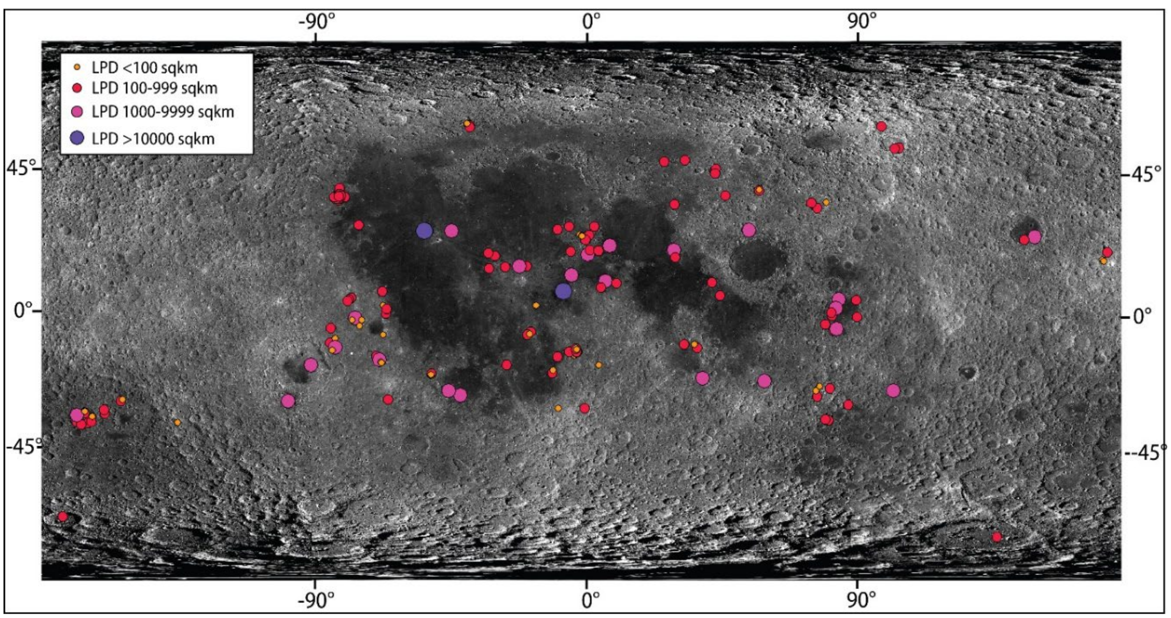

Figure 4: Global map of LPDs on the lunar surface. LPDs are categorized by size, small orange circles are LPDs smaller than 100 km^2, medium-small red circles are LPDs between 100 – 999 km^2, medium-large pink blue circles are LPDs between 1000 – 9999 km^2, and 10000 km^2 LPDs are indicated by large purple circles.

To create the mosaics, we use M^3 data that are available on the Planetary Data System (PDS; see Supplementary Materials for images used for each mosaicked region) and process images to create maps by mosaicking processed images. The image spatial resolution is up to 280 m/pixel as global mode images from both optical periods 1 and 2 were used. Images from optical period 1 were taken from an altitude of 100 km, whereas images from optical period 2 were taken from an altitude of 200 km, reducing the spatial resolution of the images from a nominal resolution of 140 km/pix to a nominal resolution of 280 km/pix. For mosaics where images from both optical periods were used, the higher resolution images were not downsampled to the lower resolution but were mosaicked together. Although this leads to spectral and spatial differences between images in a single mosaic, changes in the surface are still consistent across image boundaries. Spectra and boundaries are not directly compared across optical periods, but variations in albedo and deposit extent can still be derived from images and combined across image boundaries to create a complete picture of the pyroclastic deposit.

2.3.1 Spectral processing

We use PDS-standard corrections for thermal emission, topographic, photometric, and instrumental effects (Boardman et al., 2011; Clark et al., 2011; Green et al., 2011).We process the individual M^3 image cubes following the methods of Horgan et al., (2014) to remove the contribution to the continuum due to space weathering and to smooth the continuum to suppress noise. Both Level 1B and Level 2 data were processed in Interactive Data Language (IDL) Development Environment to create final image cubes for analysis (Bennett et al., 2016; Horgan et al., 2014).

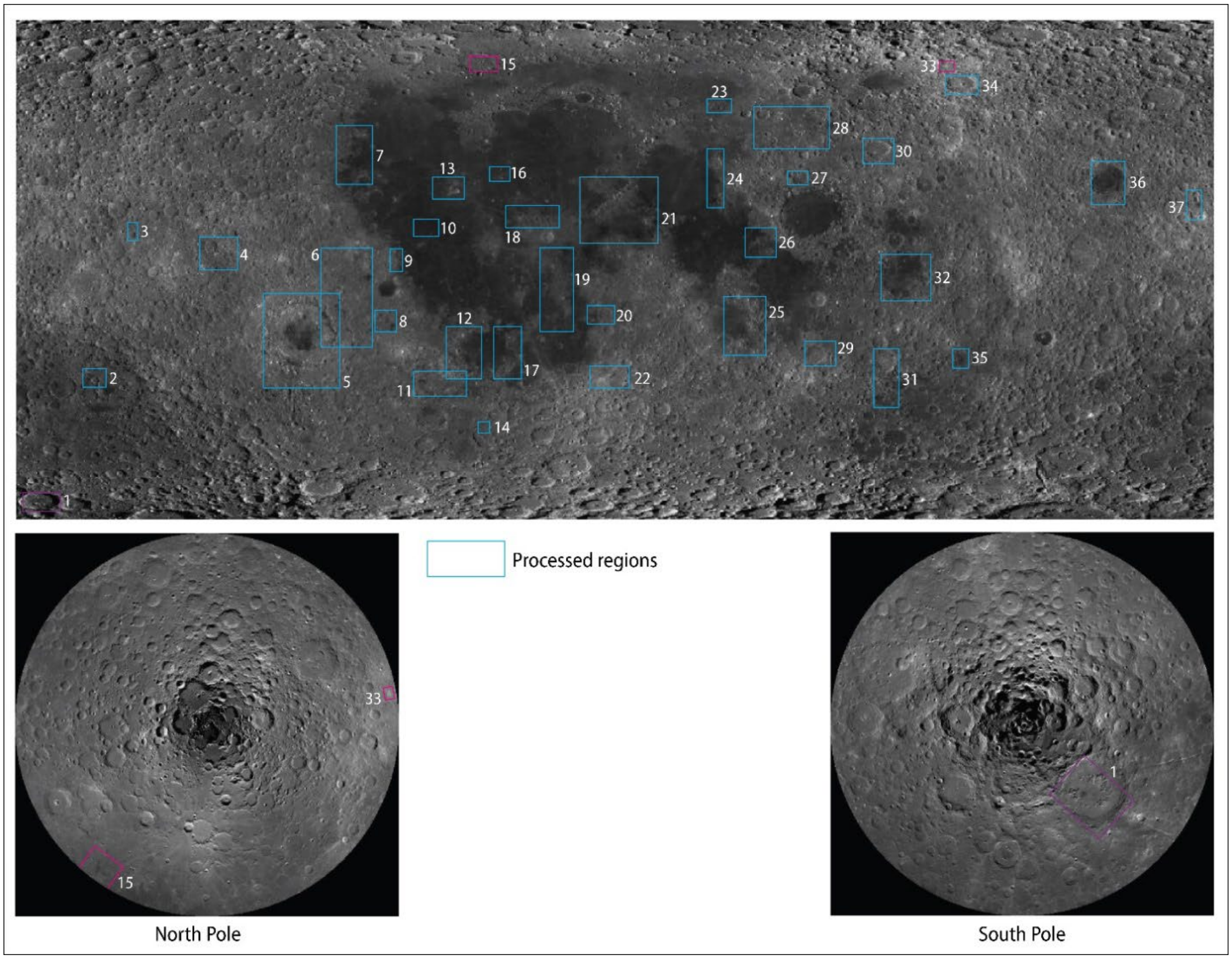

Figure 5: Regions of Interest for LPD analysis. Each blue box is a region that contains at least one LPD. Boxes are numbered from west to east and correspond to LPDs in Table 2, indicating in which region that LPD can be found. Individual M^3 images for these regions were mosaiced for analysis. Top map in cylindrical projection limited to 60°N to 60°S.

To remove the contribution to lunar spectra due to slope reddening, we apply a linear convex hull continuum removal function. This continuum has two segments between 0.6 and 2.6 µm with a floating central tie point near 1.5 µm. The central tie point finds the local maximum for the spectrum of each pixel at a point near 1.5 µm and fixes the left and right continuum segments to that as an endpoint (i.e., the right endpoint for the left segment and the left endpoint for the right segment). The spectra are evaluated relative to these continua to enhance the shape of the spectrum that's been suppressed by space weathering. These spectra are then smoothed using a moving boxcar algorithm to suppress noise from instrument and surface artifacts. The smoothed, continuum-corrected spectra are evaluated reflectance at 2.98 μm. We produce a mosaic of each region using Moon Mineralogy Mapper data to evaluate changes in albedo around each LPD location within that region.

We combine the images for each region into mosaics (Figure 5) and project these onto a cylindrical projection, after which we derive band parameter maps and other products to evaluate the albedo of the region. Deposits nearer to the poles where a cylindrical projection would be inappropriate are projected with a polar projection. We load these maps in the Environment for Visualizing Images (ENVI) to assist with spectral analysis and the evaluation of deposit boundaries. We use the albedo map to evaluate changes in deposit boundaries around each LPD location to understand differences in the emplacement of deposits and dispersal of pyroclasts.

2.3.2 Delineating deposit boundaries

To evaluate the dispersal of pyroclasts, we investigate the variations in albedo (in band 82, 2.98 μm to be consistent with prior analyses using this methodology) of surfaces at the locations in the updated database. Locations of pyroclastic deposits reported in the database typically indicate the latitude/longitude positions of eruptive vents (if a vent is present), deposit centroids (if a vent was not identified), or observable pyroclastic features such as significant albedo changes or surface smoothing (for irregularly-shaped deposits where the centroid is off-deposit). For each pyroclastic deposit, we investigate the histogram of albedo values in the scene (e.g., Figure 6a) and create band thresholds for notable features in the histogram. The first threshold for all images is for anomalously low albedos that identify shadowed areas and areas with no coverage. As each region is a mosaic of images from different orbital periods with varied composition (Figure 5), histograms will have different shapes which describe the frequency of pixels in the scene with that data value. As every region will have unique histogram distributions, each region is evaluated individually rather than having specific ranges for all mosaics. This has the potential to introduce bias in selecting various thresholds for evaluation. For example, the yellow threshold was created from half-max on the increasing side of the first peak to the trough between the first and second peak. Other histograms have such broad first peaks (or have only one peak, which is very broad) that the rising side of the increasing side is split into multiple thresholds. Although this can be subjective, multiple ranges of albedo values are investigated for each deposit (e.g., Figure 6c) showing light green and dark green thresholds) to determine a variety of potential albedo boundaries that most closely align with the observed surface distribution of albedo variation. When the threshold reflects an albedo threshold that is similar to background values in the rest of the image (indicating off-deposit materials) the boundary is outlined (Figure 6d). This boundary is then added to the shapefile that contains the full inventory of deposits (Figure 7).

2.3.3 Evaluating the distribution of deposits

We evaluate the distribution of pyroclastic deposits on the lunar surface in terms of latitude, relationships to magma source regions, and whether they are on the near side or far side. For simplicity, we bin the point shapefile of all LPDs by 10° latitude to evaluate their locations latitudinally. The points indicate deposit vents (i.e., eruption centers) or in the absence of a vent, the deposit centroid which would most likely approximate the location from which the deposit originated (Gaddis et al., 1985). We evaluate the distribution of eruptive centers by latitude rather than the distribution and areal extent of deposits to better connect the subsurface plumbing systems of explosive deposits. In addition to latitude, we also investigate the distribution of LPDs by longitude, binning by 180° (i.e., near side vs. far side). Although the lunar terminator can vary by several degrees due to changes in Earth perspective resulting from lunar libration, we define the near side of the Moon as between 90°W through nearside 0° to 90°E for simplicity.

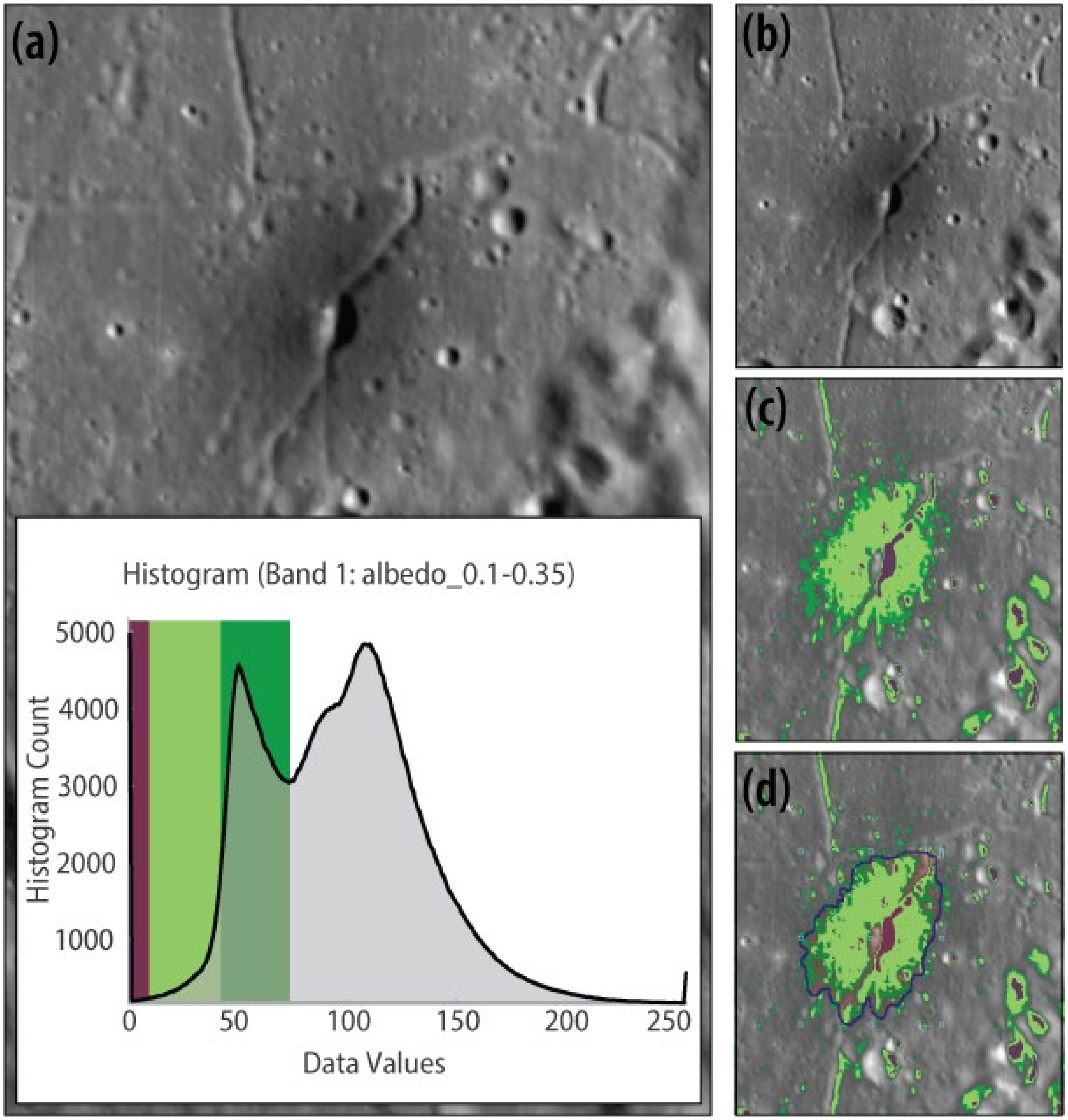

Figure 6: Generation of boundaries in ENVI. (a) Threshold parameters are inspected for value distribution. Band thresholds are created using the distributions within the image. Example given shows two peaks, at 51 and 110, and a valley at 72. Threshold layers are generated for the distribution: shadow, low albedo (highlighted in yellow: half-max of peak 1 to valley), moderate albedo, and high albedo. (b) Example LPD - Alphonsus-R in albedo image. (c) Band thresholds for shadow (purple), low albedo (dark green), and moderate albedo (medium green). (d) Region Of Interest (blue outline) that fully contains and minimizes the thresholded albedo data.

A magma source region is the subsurface magma from which a volcanic feature erupted. This can be identified as a volcanic feature that dominates a region (e.g., a mare basin) or a known, relatively contained magma body (e.g., the magma that inflates under a floor-fractured crater to cause the fractures in the crater floor; Jozwiak et al., 2015). To characterize and map potential magma source regions and connect volcanic features, we rely on previously-compiled databases of volcanic features. For floor-fractured craters, we use a database of floor-fractured crater locations (latitude/longitude positions for the centers of craters) from Jozwiak et al., (2012). We modified this database by creating polygons for each latitude/longitude that approximates the crater rim for each floor-fractured crater. This assists with understanding whether LPDs are within crater rims of floor-fractured craters, and therefore more likely associated with the subsurface magma body. LPDs have been identified along and adjacent to the channel of sinuous rilles, indicating a potential relationship between the sinuous rille lavas and explosive volcanism. We use mapped sinuous rille channel boundaries from Hurwitz et al., (2013). Regional LPDs are often associated with mare margin boundaries, distributing pyroclasts onto the mare and highland borders. Mapping various lava features on the Moon, we use USGS nomenclature to identify each maria, lacus, and sinus that has been mapped previously (International Astronomical Union, n.d.).

2.4 Observations

Updated Inventory of Pyroclastic Deposits on the Moon

NAME	LAT	LON	Areal extent (albedo)	Near/Far	Context	Source
Abel B	-36.4	82.2	41.7	Near	Crater	5
Abel C	-36.1	81.2	65.1	Near	Crater	5
Aestatis	-15.4	-68.5	221	Near	Mare/Highland	2
Airy	-18.1	5.7	130.2	Near	FFC	5
Alphonsus (W)	-13.5	-4.2	122.3	Near	FFC	1
Alphonsus 10	-13.6	-4.1	122.3	Near	FFC	1
Alphonsus 11	-13.7	-4.1	122.3	Near	FFC	1
Alphonsus 5	-13.1	-1.6	9.5	Near	FFC	
Alphonsus 6	-13.5	-1.4	11.7	Near	FFC	
Alphonsus C	-13.7	-3.4	13.9	Near	FFC	1

Alphonsus Exo	-14.9	-2.3	9.7	Near	FFC	5
Alphonsus R	-14.4	-2.0	86.7	Near	FFC	1
Anderson E	17.1	173.6	45.8	Far	FFC	6
Anderson F	16.5	174.1	7	Far	FFC	6
Ann	25.1	0	6.8	Near	Rille	24
Antoniadi	-68.5	-173.0	99*	Far	Other	12
Apollo Basin (E)	-29.5	-15.05	8.28	Far	Highland	5
Apollo Basin (N)	-29.9	-153.0	91.3	Far	Crater	5
Apollo Basin (W)	-30.0	-153.5	2	Far	Highland	5
Aristarchus	26.7	-52.3	49013	Near	Rille/mare	5
Atlas (N)	47.3	44.8	132	Near	FFC	5
Atlas (S)	45.7	44.6	147	Near	FFC	5
Autumni-A	-10.8	-83.9	147.6	Near	Crater	2
Autumni-B	-12.5	-81.8	1746.9	Near	Crater	25
Autumni-B(2)	-13	-83.1	93.4	Near	Crater	25
Barnard	-31.3	89.0	444*	Near	Crater	5
Beer	27.2	-8.2	233.7	Near	Mare/Highland	5
Birt E (N)	-20.4	-10.0	85*	Near	Rille	18
Birt E (S)	-20.7	-9.6	280*	Near	Rille	18
BonplandN	-7.8	-17.3	49.3	Near	Crater	6
BonplandW	-8.1	-16.9	197.6	Near	Crater	25
Briggs A	28.6	-74.2	415	Near	Mare/Highland	5
Buys-Ballot	19.6	175.7	106.5	Far	Mare/Highland	6
Cavalerius	6.4	-66.4	428*	Near	Mare margin	5
CBTA	-99.9	61.4	99*	Near	Other	5
Cleomedes	26.6	54.7	1084	Near	FFC	5
Compton (SC)	54.1	105.1	182*	Far	FFC	5
Compton (SE)	54.0	106.0	45*	Far	FFC	5
Compton (SW)	54.0	104.0	5*	Far	FFC	5
Cruger (W)	-16.7	-66.5	4828	Near	Crater	5
Cruger (S1)	-17.2	-66.7	760	Near	Crater	2
Cruger (S2)	-17.2	-66.8	230	Near	Crater	25
Daguerre	-11.3	34.1	323	Near	Mare	5
Daniell	35.4	31.1	100	Near	FFC	5
Dopplemayer	-28.1	-40.5	2628	Near	Regional	5
Dryden S	-34.3	-158.8	110.1	Far	Crater	15
Dryden T	-33.0	-159.2	245	Far	Crater	15
E Vent	-13.6	-1.6	9.1	Near	FFC	5
E. Mare Frigoris (SE, E)	50.2	34.4	244	Near	Mare/Highland	5
E. Mare Frigoris (SE, W)	49.6	27.5	99*	Near	Mare/Highland	5
Fra Mauro F	-7.1	-16.8	85	Near	Graben - domes	5
Franklin	38.3	47.9	198	Near	FFC	5
Gambart	1.9	-15.1	88	Near	Mare	5
Gassendi	-15	-37.8	250	Near	Highland	19
Gaudibert	-12.3	38.6	400	Near	Crater	5
Gaudibert NW	-11.1	37.7	62	Near	FFC	5
Gauss E	36.0	81.2	70	Near	FFC	5
Gauss S	34.2	78.7	269	Near	FFC	5
Gauss W	35.7	76.0	179	Near	FFC	5
Gay-Lussac N	14.9	-20.7	1400*	Near	Mare margin	6
Gay-Lussac NE	14.8	-18.4	760*	Near	Mare margin	5
Grimaldi	-0.8	-64.8	127	Near	Mare margin	5
Grimaldi F	-7.9	-66.2	90	Near	Mare margin	2
GrimaldiN	0.4	-65.9	120	Near	Mare margin	25
Hadley Cleft	25.2	2.6	898	Near	Rille	5
Haldane	-1.6	83.7	85	Near	FFC	5

Hedin (N)	2.1	-77.0	113	Near	Highland	2
Hedin (NW)	2.2	-77.0	130	Near	Highland	2
Hedin (W)	2.2	-77.1	150	Near	Highland	2
Hell	-32.5	-7.7	57	Near	Crater	5
Hevelius	2.2	-67.5	76	Near	FFC	2
Hohmann Q	-25.7	-95.2	180	Far		5
Humboldt NE	-25.8	82.9	169	Near	FFC	5
Humboldt NW	-25.1	78.9	69	Near	FFC	5
Humboldt SW	-28.5	78.8	277	Near	FFC	5
Humboldt W	-26.6	78.2	94	Near	FFC	5
Hyginus LPD	7.7	6.3	60	Near	IMP	5
Isis	18.9	27.5	100	Near	Mare	21
J. Herschel (C)	62.0	-36.9	120*	Near	FFC	5
J. Herschel (N)	61.7	-36.6	630*	Near	FFC	5
J. Herschel (S)	61.0	-37.0	60*	Near	FFC	5
J. Herschel (NW)	62.4	-35.2	99*	Near	FFC	26
Kathleen	25.3	-0.5	37.3	Near	Rille	5
Kiess	-6.5	84.1	1450	Near	mare crater	5
Kopff	-18.0	-89.8	1100	Near	Regional/FFC	6
Lagrange C	-29.5	-64.4	174	Near	Highland	5
Lassell	-15.4	-7.9	192	Near	Crater	5
Lavoisier F	37.0	-81.0	553	Near	FFC	20
Lavoisier F (N)	37.9	-80.9	330	Near	FFC	27
Lavoisier H	37.9	-78.8	100	Near	FFC	5
Lavoisier - M	38.3	-79.7	5	Near	Mare margin	5
Lavoisier-3	37.8	-80.3	11	Near	FFC	20
Lavoisier-2	38.2	-80.8	568	Near	FFC	20
Lavoisier-4	37.9	-80.7	60	Near	FFC	27
Lavoisier-5	37.5	-81.2	62	Near	FFC	27
Lavoisier-6	37.5	-81.7	23	Near	FFC	27
Lavoisier-7	37.5	-80.7	122	Near	FFC	27
Lavoisier-1	39	-81	250	Near	FFC	27
Lavoisier-8	38.2	-80.9	75	Near	FFC	27
Lavoisier-E1	-40.7	-80.9	47	Near	FFC	5
Lavoisier-E2	-41.7	-80.6	23	Near	FFC	5
Lavoisier-E3	-41.1	-80.9	45	Near	FFC	5
Lavoisier-E4	-41.2	-81.1	30	Near	FFC	5
LavoisierW	38.1	-82.1	390	Near	FFC	20
LavoisierNE	38.8	-80.7	78	Near	FFC	20
LavoisierNE-2	38.4	-80.9	60	Near	FFC	20
LavoisierW-2	38	-82.5	447	Near	FFC	20
Le Monnier	25.8	29.5	322	Near		5
Lubinieszky	-17.1	-24.6	170	Near	Mare/Highland	5
Mare Humorum SW	-26.6	-44.4	1472	Near	Rille	5
Mare Orientale	-24.9	-95.2	1600*	Far		5
Mare Smythii (NNW)	1.1	84.4	5851*	Near	Mare	5
Mare Smythii (SW)	-6.0	85.0	5839*	Near	Crater	5
Mare Smythii (W)	1.0	85.0	245	Near	Mare	5
Mare Smythii (WSW)	-4.5	81.5	355	Near	Mare margin	5
Mare Vaporum	10.0	7.9	4129	Near	Mare	5
McAdie	3.6	91.7	43*	Far	Mare margin	5
Mersenius (NW)	-20.9	-49.9	129	Near	FFC	5
Mersenius (SW)	-21.6	-49.3	91	Near	FFC	2
Mersenius (W)	-21.6	-49.2	76	Near	FFC	2
Mersenius (WNW)	-21.5	-49.2	91	Near	FFC	2
Messala N	40.5	59.3	49	Near	Crater	5

Messala S	40.1	59.3	116	Near	Crater	5
Michael	25	0.2	18.8	Near	Rille	5
Monira	-12.5	-1.7	17.9	Near	FFC	1
Mons Huygens	19.7	-3.5	1365	Near	Mare margin	5
Mons Moro	-11.8	-19.9	65	Near	Mare	5
Montes Carpatus	14.6	-25.4	354	Near	Highland	5
Montes Harbinger	26.6	-43.4	2877	Near	Rille	5
Moscoviense	23.6	147.7	3700	Far	Mare margin	5
Moscoviense SE	24.7	151.2	1022*	Far	FFC	5
Mozart	23.8	1.3	589*	Near	Mare	5
NE Lavoisier (W)	40.9	-80.6	14	Near	FFC	5
NE Vent	-12.4	-2.2	99*	Near	FFC	5
Oppenheimer	-34.0	-165.5	38	Far	FFC	5
Oppenheimer	-37.5	-164.6	25	Far	FFC	5
Oppenheimer	-35.8	-163.3	13	Far	FFC	5
Oppenheimer E	-35.3	-163.2	26	Far	FFC	15
Oppenheimer N	-33.6	-165.5	76	Far	FFC	15
Oppenheimer NW	-34.8	-168.2	1500	Far	FFC	5
Oppenheimer S	-37.9	-166.9	890	Far	FFC	15
Oppenheimer SE	-37.0	-163.4	190	Far	FFC	15
Oppenheimer SSE	-37.1	-134.6	44	Far	FFC	15
Oppenheimer SW	-37.0	-168.3	227	Far	FFC	5
Orientale	-30.3	-97.5	5321	Far	Regional	5
Osiris	18.6	27.6	100	Near	Rille	21
Palmieri	-27.3	-46.6	14	Near	Other	5
Patricia	24	1.1	21	Near	Rille	5
Petavius	-23.5	61.0	1645	Near	FFC	5
Plato	52.6	-5	100	Near	Rille	13
Ravi	-12.5	-1.9	30.5	Near	FFC	1
Riccioli (N)	-2.4	-75.5	1089	Near	FFC	5
Riccioli (S)	-2.6	-75.5	85	Near	FFC	25
Riccioli (W)	-2.4	-83.1	150	Near	FFC	2
Riccioli E	-2.4	-84.1	21	Near	FFC	25
Rima Bode	11.9	-3.4	5040	Near	Mare margin	5
Rima Conon	17.7	2.5	703.2	Near	Rille	23
Rima Fresnel	28.2	4.4	307	Near	Rille	5
S. Sinus Aestuum	6.6	-5.9	10357	Near	Mare margin	5
Schluter	-5.8	-83.5	10	Near	FFC	10
Schluter A	-9.2	-82.2	40	Near	Crater	5
Schrodinger	-75.4	138.6	819	Far	FFC	5
SE of Nectaris	-22.4	40.5	2905	Near	Regional	5
Smythii NW	1.1	84.8	5851	Near	Mare	5
Soraya	-12.9	-1.6	60	Near	FFC	1
Sulpicius Gallus	21.7	9.4	4322	Near	Mare margin	5
Taquet	17.1	17.4	2623	Near	Mare margin	17
Taruntius	5.1	46.2	250	Near	FFC	5
Taruntius NW	9.4	43.6	819*	Near	Mare	5
Tasso S	-2.0	92.0	250*	Far	Mare margin	5
Taurus-Littrow	20.2	30.7	2940	Near	Mare margin	5
Titius	-26.7	103.9	2159	Far	Regional	5
Tobias Mayer N	18.2	-28.8	680	Near	Mare margin	6
Tobias Mayer NW	19.2	-31.1	170	Near	Mare	6
Tobias Mayer SW	14.0	-30.7	370	Near	Mare margin	6
Vitruvius	17.7	31.2	120	Near	Crater	5
Walther A	-33.2	1.4	660	Near	Crater	10

Pyroclastic deposits removed from database				
Alphonsus (E)	*-12.6*	*-1.7*	*10*	*Near*
Alphonsus (E)	*-13.0*	*-1.6*	*48*	*Near*
Alphonsus (W)	*-13.7*	*-4.3*	*79*	*Near*
Alphonsus E	*-14.3*	*-1.9*	*82*	*Near*
Alphonsus NE	*-12.8*	*-1.7*	*97*	*Near*
Alphonsus SE	*-14.3*	*-2.0*	*95*	*Near*
Cruger (W1)	*-16.7*	*-66.7*	*50*	*Near*
Cruger (W2)	*-16.7*	*-66.7*	*50*	*Near*
Riccioli (SE)	*-2.6*	*-82.9*	*20*	*Near*
Riccioli (SW)	*-2.6*	*-83.0*	*50*	*Near*
Riccioli (W)	*-2.5*	*-83.1*	*40*	*Near*
Riccioli (W-SW)	*-2.5*	*-83.0*	*40*	*Near*
Pacificus	*-28.5*	*-99.0*	*1600*	*Far*
Lavoisier(?)	*38.0*	*-80.1*	*18*	*Near*
Lavoisier-9	*38.5*	*-81.9*	*5*	*Near*
Lavoisier-10	*38.9*	*-81.4*	*100*	*Near*
Lavoisier-11	*38.9*	*-81*	*100*	*Near*
Lavoisier-12	*38.8*	*-80.7*	*100*	*Near*
Lavoisier-13	*38.4*	*-80.3*	*100*	*Near*

*Table 1: Inventory of pyroclastic deposits identified on the Moon, comprising deposits compiled from sources listed in the last column. *Areal extent obtained from source, rather than derived from methodology. See discussion for details. Sources: 1: Head and Wilson, 1979; 2: Coombs et al., 1992; 3: Peterson et al., 1995; 4: Yingst & Head, 1998; 5: Gaddis et al., 2003; 6: Gustafson et al., 2012; 7: Gaddis et al., 2013 8: Kramer et al., 2013; 9: Jawin et al., 2014; 10: Besse et al., 2014; 11: Lena & Fitzgerald, 2014; 12: Sruthi &Kumar, 2014; 13: Any LROC blog; 14: Gaddis et al., 2015; 15: Jawin et al., 2015; 16: Kramer et al., 2015; 17: Farrand et al., 2022; 18: Trang et al., 2017; 19: Giguere et al., 2020; 20: Ivey et al., 2022; 21: Weitz & Head, 1999; 22: Head and Wilson, 1993; 23: Fortezzo et al., 2020; 24: Pigue et al., 2023 (Chapter 3); 25: This work; 26: Stopar et al., 2023; 27: Souchon et al., 2015*

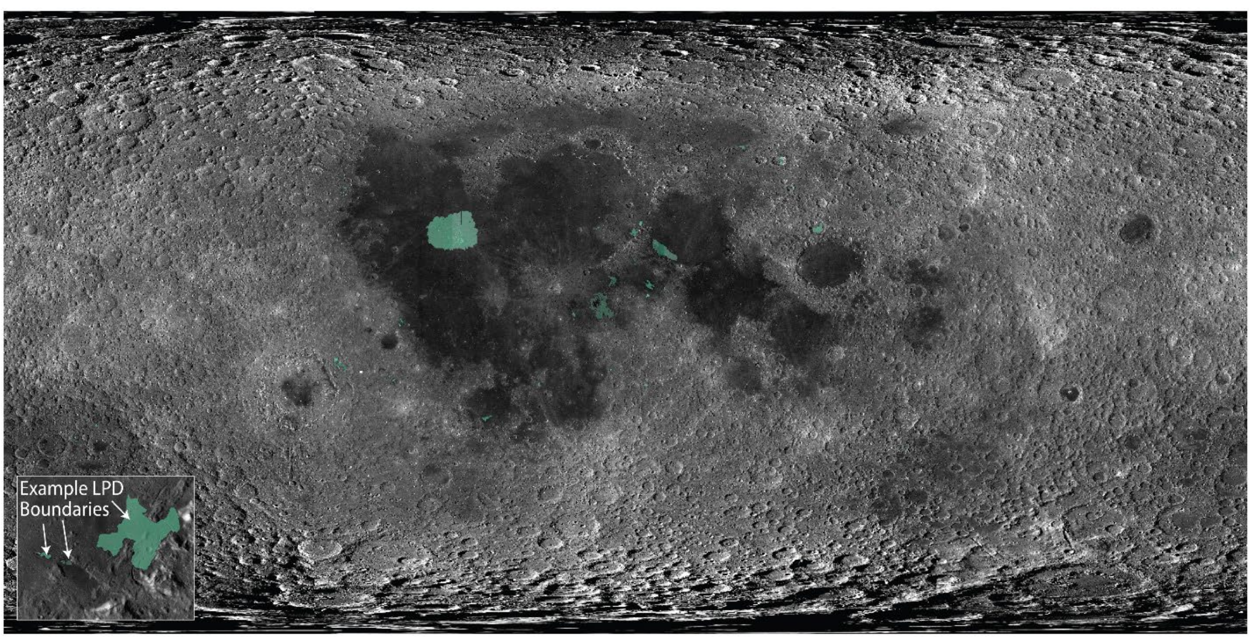

Figure 7: Boundaries of LPDs on the lunar surface based on albedo. Inset (lower left) shows close-up of example areal extent boundaries of a small sample of LPDs.

2.4.1: Trends in areal extent, distribution, and magma source regions

Our updated inventory of lunar pyroclastic deposits has 179 total deposits, more than doubling the number of LPDs evaluated in Gaddis et al., (2003). The largest by areal extent is still Aristarchus at 96,194 km^2. The smallest LPD was previously Apollo W at 2 km^2, but this LPD increased in area to larger than the next-smallest in the new inventory, which is now Lavoisier-M at 4 km^2. Nearly half (~44.1%) of the pyroclastic deposits evaluated in this study were found within FFCs (N=79). Although a significant proportion of the LPDs were identified in FFCs, only 14.2% of FFCs have identified LPDs in their crater floor (N=155). By longitude, ~17.9% pyroclastic deposits were found on the far side, past 90° E/W.

2.4.2 Distribution by size and classifying

LPDs have traditionally been classified by size when discussing populations of pyroclastic eruptions. The largest LPDs are described as being of a "regional" size classification, as those being over 1,000 km^2 (Gaddis et al., 1985) or 2,500 km^2 (Gaddis et al.,) and those below the regional size classification are said to be localized lunar pyroclastic deposits (i.e., 999 km^2 or 2,499 km^2 and below). These size classifications have been used to distinguish LPDs by eruption style with regional LPDs being formed from lava fountaining events and localized LPDs being formed from diverse eruption styles (Bennett et al., 2016; Gaddis et al., 2003; Trang et al., 2017; Wilson and Head, 1981). As eruption style has vast implications for volatile content, composition, and mineralogy, investigating these size classifications is important.

Here we use the clustering method Jenks natural breaks optimization to evaluate the natural breaks in the distribution of the areal extents of LPDs (Jenks, 1967). This method iterates over an increasing number of "breaks" or gaps in an ordered dataset. This removes arbitrary classification and returns a statistical classification, whereby the data demonstrate where the gaps exist and how many gaps are present. We order the areal extents of all deposits (derived from the albedo values) and run through Jenks natural breaks optimization up to 5 breaks.

The Jenks results indicate that large pyroclastic deposits are rare on the lunar surface, which is likely a combination of magma availability and surface reprocessing by later mare emplacement, impact cratering, and space weathering. Very small pyroclastic deposits are very common, with deposits 100 km^2 or smaller comprising 41.9% of all deposits. This is a significant change from Gaddis et al., (2003) however, as previously over 70% of all LPDs were categorized as under 100 km^2. The break in largest LPDs demonstrates that the largest two Aristarcus at 96,194 km^2 and South Sinus Aestuum at 10,357 km^2) are, in practicality, outliers as the next-closest in size is below 6,000 km^2. Omitting these two as a break (i.e., creating a user-introduced break in the Jenks algorithm at the median between 5,851 km^2 and 10,357 km^2), we get the distribution in Figure 8. The break between Regional and Localized LPDs was previously at 1000 km^2, where now there appear to be more clusters in the areal extents of the data. Most LPDs fall below ~500 km^2 where the first break exists, but above 1,200 km^2 there is a jump in size. This indicates that the boundary between Regional and Localized might need to be reevaluated, and LPDs between 1,000 km^2 and 1,200 km^2 considered localized. Further, above 1,200 km^2 are additional breaks in the areal extents, indicating that the sizes of LPDs above 1,000 km^2 is likely more complicated than previously indicated.

As these size classifications are used by the lunar community to infer eruption conditions, further investigation into the clustering of the areal extents and the correlation to LPD physical and compositional properties is required. First, the distributions should be investigated in more detail with such a heavy-tailed distribution of areal extents (i.e., nearly 70% are below the first break at 500 km^2). A specialized clustering method such as the Heads/Tails Breaks (Jiang, 2011) should be conducted to better classify the areal extents, partitioning the sizes into two parts before clustering to find the natural breaks.

After LPDs have been fully evaluated by size in both the smaller size classification and large size classification, the composition, crystallinity, and physical properties of LPDs should be conducted to determine if there are trends within each size classification. Evaluating each size group and characterizing these as a set can reveal whether eruption conditions influence deposit size. Understanding trends within size groups also can be used to characterize magma conditions such as volatile flux (via crystallinity), compositional evolution between deposits, and lunar thermal evolution.

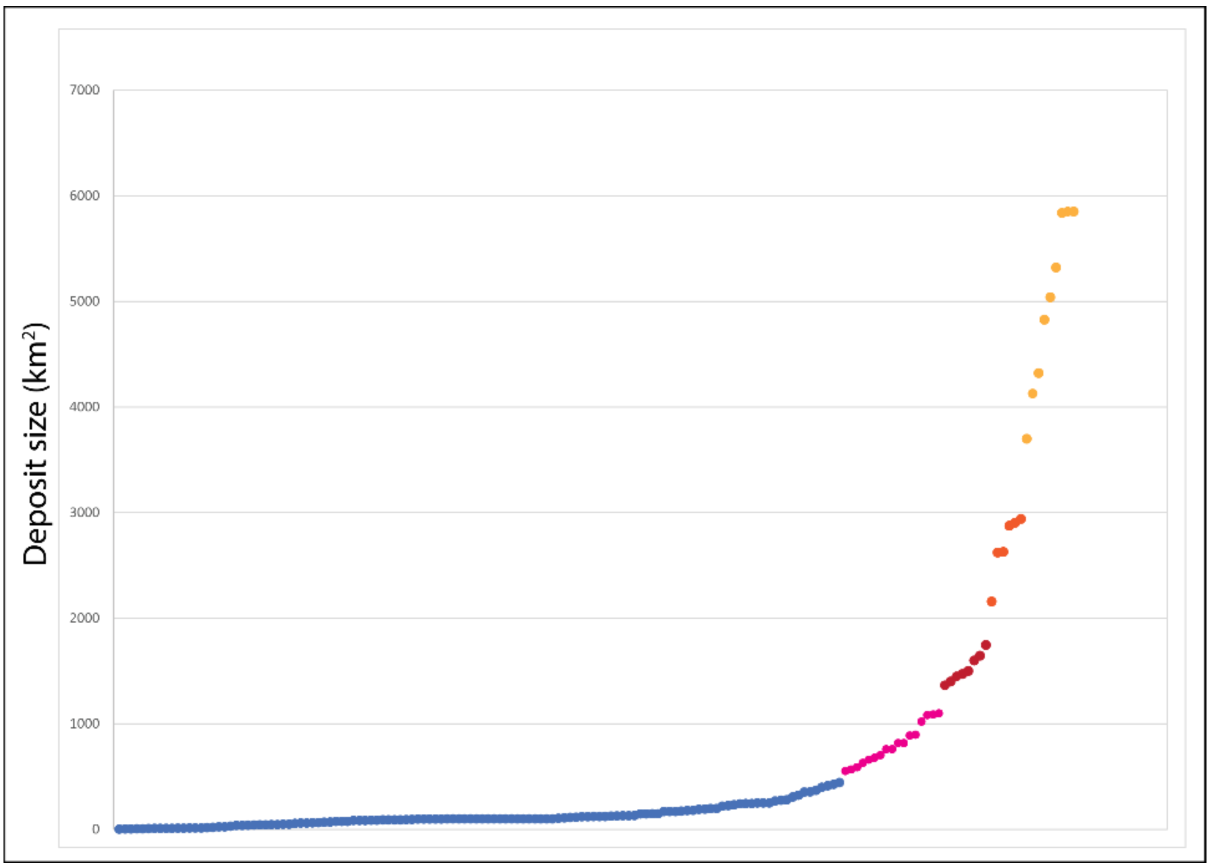

Figure 8: Jenks breaks of the ordered dataset, with clustered areal extents indicated in blue, pink, red, orange, and yellow. X-axis does not plot meaningful data, only the ordered series.

2.5 Discussion

2.5.1 LPDs in FFCs

More LPDs were identified within floor-fractured craters (FFCs) than any other magma source region (~44%). Impact crater floors with concentric, often connected, fractures are known as floor-fractured craters, and are used to infer the location of an inflated magma body in the lunar interior. The fractures in the floor are potentially caused by the inflation of the magma under the crater surface (Jozwiak et al., 2015), or could be caused by viscous relaxation. Many of these pyroclastic deposits within floor-fractured craters (FFCs) were found along fractures and fissures in the impact crater floors (Figure 9). These fracture pathways likely form conduits for magma to rise more easily from the subsurface magma chamber of an FFC and erupt onto the surface, where observed. Although this might suggest that there is a direct relationship between the crater impact and the subsequent rise of magma beneath the surface, many of these craters are shallow and unlikely to significantly affect magma inflation due to overburden pressure release. Additionally, although a significant proportion of the LPDs were identified in FFCs, only 14.2% of FFCs have identified LPDs in their crater floor. As there are more LPDs currently identified on the lunar surface than FFCs (179 in the LPD database compared to 155 in Jozwiak et al., 2012 table of identified floor-fractured craters), this shows that if an LPD is identified in a FFC, there is likely to be more than one LPD in a single FFC. Magma bodies under floor-fractured craters do not appear to be more likely to erupt, given the low percentage of FFCs that have LPDs, but it appears that when a magma body does erupt within a floor-fractured crater, it has a high efficiency of producing multiple conduits to the surface, creating multiple pyroclastic deposits. No LPDs were identified near the outside rim of a crater within approximately 1 crater radius (with floor fractures or otherwise, with the exception of the complex region Laviosier that has multiple floor-fractured craters in close proximity), implying that the lithostatic pressure of the crater wall that keeps the magma within the crater likely also prevents dike propagation to the outside of the crater.

Pyroclastic deposits are not the only forms of volcanic features found within floor-fractured craters. Many floor-fractured craters have also been observed to be infilled with basalt and to have sinuous rilles in the crater floors. Although so few floor-fractured craters have erupted with explosive volcanic features, the combination of volcanic features observed in floor-fractured craters support the hypothesis that floor-fractured craters have formed from magmatic inflation rather than viscous relaxation. Further investigation into these other forms of volcanic features could reveal similar structural controls on the eruption sites of effusive features (i.e., LPDs are typically found near fractures, indicating that these fracture pathways likely form conduits to the surface). Additionally, correlations between floor-fractured craters with observed effusive features and the ages of these craters could reveal information about the volatile inventory of the lunar subsurface. Deep magma bodies with high residence times may have higher rates of degassing prior to eruption, which may be revealed by younger age-dated craters. Further surveys in floor-fractured craters for volcanic features (explosive and non-explosive), particularly along crater floor fractures, may reveal LPDs not previously identified.

2.5.2 Pyroclastic deposits by magma source regions

Many LPDs (7.8%) occur near or within sinuous rilles, which are features that relate to lava channels. The connection between channelized-type lava flows and explosive volcanoes (e.g., fissure eruptions) is a well-known occurrence on Earth, including, for example, the 2018 eruption at Kīlauea in Hawai'i (Neal et al., 2019). Effusive lava flows and explosive lava fountaining events were happening simultaneously during this eruption, and at times from the same vent. On the Moon, pyroclastic deposits have been observed around vents in sinuous rilles. For example, there are vent-type depressions that lie alongside Mozart rille, and spectral analysis of two vent depressions along Mozart rille show that they are spectrally consistent with LPDs (Chapter 3). Each vent identified along Mozart rille has a pyroclastic glass signature on the downstream portion of the depression, demonstrating a structural connection between the erupting pyroclasts and the flow of the rille. These strongly indicate vents alongside a main rille as a fissure eruption with multiple vents with localized lava-fountaining resulting in relatively small deposits. The explosive eruption of these materials concurrently with the emplacement of Mozart rille would be consistent with known eruption mechanisms on Earth (Popa et al., 2021). The three LPDs along a sinuous rille would be consistent with co-eruption of the rille with the pyroclastic eruption, indicating that explosive and effusive eruption was occurring in this location, and therefore that these explosive and effusive features were sharing a magma source.

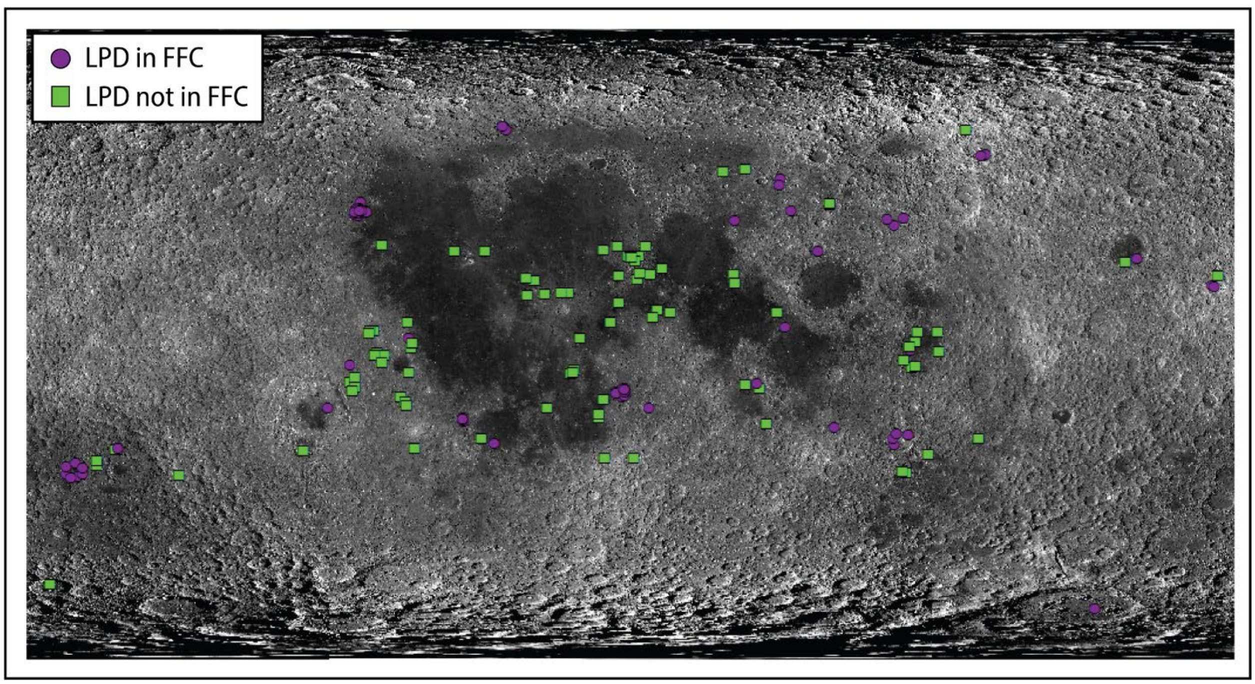

Figure 9: Mapped LPDs, indicating whether they are in a floor-fractured crater or not. Purple circles are LPDs found within floor-fractured craters, green squares are LPDs found in source regions that are not floor-fractured craters.

Mozart rille is one of the many volcanic features within the Montes Apenninus, a highland mountainous terrain that separates two major mare basins on the nearside. The majority of LPDs occur closest to the equator, thinning in population density closer to the poles (Figure 10, right bars). Although not unexpected as the majority of mare basins are centralized around the equator, more LPDs were expected to be found in what is considered the thinnest crust at the Moon – the South Pole Aitken basin (SPA; Wieczorek et al., 2013). This finding implies that thin crust isn't the only requirement for explosive volcanism, but a combination of eruptible magma and a pathway to the surface are required, not just any magma body (e.g., mantle or perched magma) and thinner crust. The crust in mare regions is thinner than at the northern pole, which has the potential to reduce barriers to the surface and allow eruption to occur. The two LPDs nearest the south pole (Schrodinger and Antoniadi) are both in craters, one being an identified floor-fractured crater (Schrodinger; Jozwiak et al., 2012) and the other being a crater that was not previously identified as a floor-fractured crater (Antoniadi), but is in the South Pole Aitken Basin. Some small fractures were observed in the floor of Antoniadi but identifying a crater as a floor-fractured crater was outside of the scope of this work. The pyroclastic deposit in Antoniadi was not found near a visible fracture, but some fractures could potentially be buried. This pyroclastic deposit had been identified by Sruthi and Kumar, (2014) as being near volcanic domes in the floor of Antoniadi crater. Other LPDs not near the south pole, but within the SPA Basin include the ten LPDs within the floor-fractured crater Oppenheimer crater (~35°S), two within Dryden crater (~34°S), and two in a highland composition of the Apollo basin (~30°S). These distinct magma source regions near the south pole indicate that there are a variety of magma pathways in this region, and the structural controls of thinner crust near the SPA basin have little effect on the emplacement of explosive volcanic features. The frequency of LPDs does not increase as the latitude increase. Additionally, LPDs in this region still fit global trends as they relate to magma source regions – most LPDs in SPA are found within floor-fractured craters, followed by craters and highland regions as the next-most common magma source correlations. This indicates that, although the crust is thinner in this part of the Moon, magma ascent is controlled by intrinsic conditions such as volatile content/species, volatile exsolution, and magma fragmentation.

With the exception of the SPA basin, the lunar near side is marked by large mare infilled basins that distinguish it from the lunar farside, which is mostly covered by cratered anorthositic highlands. The crust is thinner under these mare regions than on the thicker farside crust (Wieczorek et al., 2013). This thicker crust on the farside may place limits on the ability for subsurface dikes to reach the surface and erupt onto the service. Of the pyroclastic deposits identified to date as included in this study, ~17.9% were found on the far side (Figure 10, top bars). LPDs identified on the lunar farside were generally found in basaltic infilled craters (e.g., Anderson E and F). While it is unknown whether some of the lava flows cover older LPDs, the observation that some LPDs occur on top of these lava flows in FFCs suggests at least some pyroclastic volcanism occurred after these lava flows. Although having a thinner crust does not necessarily facilitate volcanic activity, a thicker crust could inhibit magma from reaching the surface, and increase the probability that volcanic dikes stall in the subsurface before erupting.

Further investigation into GRAIL crustal thickness maps and the locations of LPDs could reveal correlations between regions of crustal thinning (e.g., mare basin impacts) and eruption centers. Specifically, linking LPDs to regions of thin crust and other regions of basaltic volcanism may enhance the correlations between explosive volcanism and near-side latitude, particularly in regions where multiple mare regions intersect. Many farside LPDs are found within craters with basalt infill, indicating complex volcanism at these sites. As the pyroclastic material can be observed mantling these effusive materials, there may have been multiple eruptions occurring in these regions, in the same way that complex volcanism has been observed in the Montes Apenninus region (Chapter 3). Further investigation into these regions, the compositions of these deposits and the effusive features, and the relationships between the volcanism and the impact cratering processes (e.g., whether these are suspected to have been floor-fractured craters) would be required to more fully develop lunar farside volcanic histories.

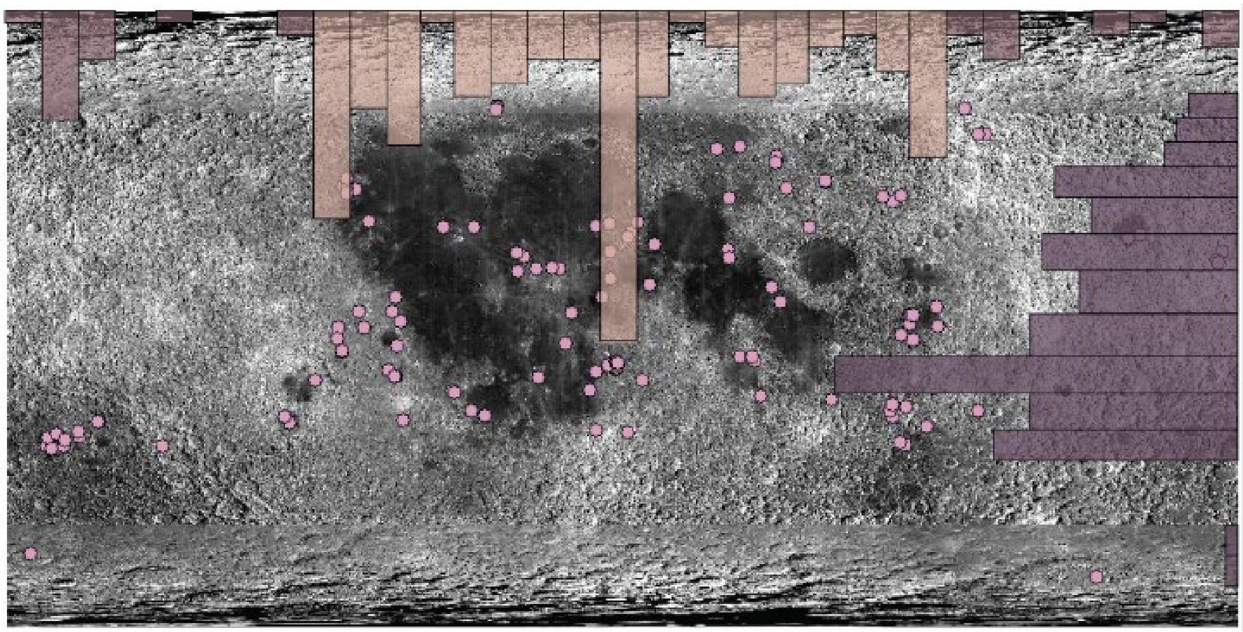

Figure 10: Relative distribution of LPDs by latitude and longitude. Bars along the top indicate the number of LPDs in each bin of 10° longitude. Light pink bars indicate nearside LPDs, dark pink bars indicate farside LPDs. Bars along the right indicate the number of LPDs in each bin of 10° latitude. Bars are scaled in thickness to account for the difference in latitude as a result of projection (i.e., 10° at the equator appears to cover a larger area than 10° at 60°S due to the map projection).

2.5.3: Discussion of added, removed, and modified LPDs

This work analyzed nearly 200 pyroclastic deposits, including many that have been identified from sources that have differences in analysis methods in terms of spatial and spectral resolution, observational constraints, and motivations. This means that some deposits identified in other datasets may not be visible in our dataset, using the methods we employ. Here we detail many of the deposits not identified, their locations, the source where we identified them first, and common observations that indicated that we were not able to confirm these as pyroclastic deposits. For future reference, the deposits identified in the literature that were not confirmed as LPDs by this study are included in a separate table.

An LPD was identified south of Archimedes crater from a signature that might be indicative of pyroclastic volcanism in a Clementine RGB composite, when compared to surrounding highlands and crater materials. The location associated with this region, and mapped in Gaddis et al., (2003) as an LPD, was investigated in detail for signs of pyroclastic volcanism, including glass content, changes in orthopyroxene and clinopyroxene distribution that might indicate volcanism, and the analysis of a variety of RGB composites and multiple datasets (including using the albedo methodology in this work). No vent location was identified in this region or within Archimedes crater and no morphologic signatures were apparent (e.g., low crater retention or topographic smoothing). Albedo signatures were generally homogenous in the region, transitioning from the exterior crater wall of Archimedes crater to the Apennine bench, with no indication that a mantling deposit was present. This previously identified LPD does not appear to be present in the datasets we evaluated, and was put onto the "removed" list.

Bostovich crater has two "mantling deposits" identified in Fortezzo et al., (2020) to the southeast, outside of the crater rim. This area does not exhibit a variation in albedo (either high or low) compared to materials around the rest of the crater, indicating a change in composition or a mantling of different material. This region also did not exhibit any morphological differences from the surrounding region that would indicate a mantling deposit or a change in the physical properties of the surface. Further, this region was investigated in Chapter 4 for its thermal and thermophysical properties and no indications of a change in the thermal inertia, maximum daytime temperatures, minimum nighttime temperatures, or rock abundance from the surrounding regions provided an indication that there was a change in the surface material properties that would indicate a mantling deposit. Deposits identified by geologic mapping but not identified in literature as having been evaluated for their volcanic emplacement were not included in the current database as we were unable to confirm that these were pyroclastic deposits. Investigation into the datasets and observations that informed the original results would be warranted to determine how this deposit was originally mapped. Further, detailed morphological investigation of this deposit and the surrounding region would be needed to determine how this deposit relates to the impact crater it is near, and surrounding region that may or may not be related to its emplacement. This could include detailed geomorphic mapping, compositional analysis using Clementine and Lunar Orbiter results, and/or investigation of radar datasets.

Pacificus was identified in (Coombs and Hawke, 1991) as a pyroclastic deposit near Mare Orientale. The description of the deposit in (Coombs and Hawke, 1991) is characterized as "an unusual dark annulus [that] crosses the outer Montes Rook in the southwestern sector of Orientale Basin (Scott et al., 1977)." The Mare Orientale deposit is also in this location and is described as an annulus, the only other pyroclastic deposit on the Moon described as such. Additionally, as search of the geologic map of Scott et al., (1977) did not reveal a pyroclastic deposit in this region, nor was it described in the Description of Map Units. As these two deposits are listed in the same location and have the same unusual description, we believe that these are the same deposit and removed the Pacificus LPD from the previous database.

Many deposits in Lavoisier crater were excluded as duplicates or unable to be identified by albedo. With the exception of legacy deposits (i.e., those identified in early literature), the numbering convention used in this database follows the numbering system introduced by Souchon et al., (2013) to avoid confusion in using the cardinal directions employed by previous authors. This resulted in some deposits being duplicates (e.g., Lavoisier-1 being re-named as Lavoisier-10). This also resulted in some duplicates that had been added from Souchon et al., (2013) from legacy sources (e.g., LaviosierWNW being Lavoisier-9). For these deposits, a review of the albedo and glass signatures was conducted, in addition to a search for potential fractures and vent structures to ensure that multiple deposits were not located in the same location (e.g., as Alphonsus 10, 11, and W are – three vents so closely spaced that the deposits overlap completely). Combining Lavoisier deposits from all inventories, six were identified as duplicates.

Cruger is an impact crater that previously had three pyroclastic deposits identified: Cruger N, Cruger W1, and Cruger W2. In an examination of the distribution of pixels by albedo in the floor of Cruger crater, the northern and western regions of Cruger crater were fairly homogenous and there was no discernable reduction in albedo between the locations where these three LPDs were mapped. Additionally, there were no discernable fractures or vents that could indicate a source for the pyroclastic deposits. The three previously identified pyroclastic deposits in the floor of Cruger were therefore combined into a single LPD. During the investigation of the Cruger pyroclastics, two regions of lower albedo were identified in the southern region of Cruger. These two locations were separate in concentration and were distinct from the new Cruger W deposit. These two LPDs were then added as Cruger-S1 and Cruger-S2.

2.6 Summary and Conclusions

In this study, we present an updated database of lunar pyroclastic deposits with reported locations, areal extents, and geologic contexts. We evaluated past identified LPDs, verifying pyroclastic and volcanic features in those regions for inclusion in the database. Using the locations of the updated inventory of deposits, we evaluate the albedo of LPDs to estimate the areal extent of each deposit. These areal extents are combined into a single shapefile of deposit boundaries that can be used for future research into the distribution and characterization of pyroclastic deposits and related volcanic features. We find that 19 could not be included in the database as duplicates or unconfirmed LPDs.

This database allows us to connect LPDs with subsurface plumbing systems. Floor-fractured craters had the most LPDs associated with them than any other magma source at ~44.1 LPDs. The fractures in the crater floors above inflating subsurface magma likely form conduits for magma to rise more easily and erupt onto the surface, where observed. Although a significant proportion of the LPDs were identified in FFCs, only 14.2% of FFCs have identified LPDs in their crater floor. As there are more LPDs currently identified on the lunar surface than FFCs (179 in the LPD database compared to 155 in Jozwiak et al., 2012 table of identified floor-fractured craters), this shows that if an LPD is identified in a FFC, there is likely to be more than one LPD in a single FFC.

LPDs have high resource potential as a source for volatiles, homogenous fine-grained material for construction, and oxygen production and this inventory can provide future explorers with locations for this potential resource. This updated database can also be used by others to enable future scientific investigations. The shapefile of deposit boundaries provided can be used to query data within those polygons, or comparing the areal extents with datasets in other wavelength ranges where the dispersal changes due to differences in penetration depth, sensitivity, or spatial/spectral resolution.

Chapter 3: Relationship between explosive and effusive volcanism in the Montes Apenninus region of the Moon

L. M. Pigue (0000-0002-6675-6877)[1,2], K. A. Bennett (0000-0001-8105-7129)[1], B. H. N. Horgan (0000-0001-6314-9724)[3], L. R. Gaddis (0000-0001-9953-5483)[4]

Manuscript Submitted to JGR: Planets and reproduced here

[1] U.S. Geological Survey Astrogeology Science Center. [2] Northern Arizona University Dept of Astronomy & Planetary Science. [3] Purdue University Earth Atmospheric and Planetary Sciences. [4] Lunar and Planetary Institute.

Abstract

Lunar Pyroclastic Deposits (LPDs) are sites of explosive volcanism and often occur in areas of effusive volcanism on the Moon. On Earth, it has been observed that most volcanism has both effusive and explosive phases, whereas on the Moon these two types of volcanism have typically been considered separately. We hypothesize that the relationship between explosive and effusive volcanism on the Moon is like what is observed on the Earth, where individual eruptions can experience multiple phases rather than one type of volcanism always preceding another or occurring separately. We present observations from Moon Mineralogy Mapper detailing compositional relationships between volcanic features in the lunar Montes Apenninus region. We evaluated whether co-located LPDs and effusive features (e.g., rilles, mare) could have erupted from the same volcanic vent or even at the same time based on their compositional similarities and stratigraphic relationships. We find that the LPDs have varied stratigraphic relationships with co-located effusive features. We identified LPDs near sinuous rilles that may be related to the formation to the rille, where explosive and effusive volcanism occurred at the same vent (e.g., Mozart Rille), and LPDs that may be unrelated to the rille (e.g., Rimae Bode and Rima Bode LPD). Our results suggest that lunar volcanism can mirror terrestrial volcanism, with explosive and effusive eruptions demonstrating more complex dynamics and relationships than previously

thought. This variability suggests that the relationship between LPDs and nearby volcanic features cannot be generalized for studies on their resource potential, eruption styles, or deposit volume.

Plain Language Summary

Volcanic eruptions can be explosive or non-explosive (effusive), and sometimes both types of eruptions can be seen at a single volcanic site. This can be interpreted as two types of eruptions happening at the same time from the same vent, happening at the same time from different vents, or happening from the same vent at different times. Having different eruption types is common for volcanoes on Earth and often a volcano will erupt explosively and effusively at the same time. Even though we see signs of explosive and effusive volcanism on the Moon, there is currently no active volcanism to inform how these eruptions are correlated. To study this, we use the Moon Mineralogy Mapper, an instrument that helps identify minerals in the products of explosive volcanism called Lunar Pyroclastic Deposits (LPDs). We also include effusive features around these LPDs to understand whether these features could have erupted at the same time or from the same vent. We found that LPDs are complex – some of the explosive deposits originate from the same vents as effusive features, but some explosive deposits completely cover nearby effusive features, so we could not determine a consistent pattern.

3.1 Introduction

Lunar Pyroclastic Deposits (LPDs) are the surface materials left on the Moon by explosive eruptions, and they are often found near effusive volcanic features. Also known as “dark mantling deposits” or “DMDs” they are typically low albedo and “mantle” or blanket the surface, smoothing underlying topography It has been demonstrated in studies of volcanoes on Earth that most terrestrial volcanoes have both an explosive and effusive eruptive phase (e.g., Popa et al., 2021). For example, effusive lavas and explosive lava fountain eruptions at Kīlauea are both supplied with the same mantle-derived magma that enters the shallow magma plumbing system (Neal et al., 2019). The relationships between eruptive phases as observed on Earth are much better understood compared to volcanic features on the Moon, and detailed relationships between effusive and explosive lunar volcanism remains relatively unexplored. The main difference between effusive and explosive volcanism on the Moon is related to volatile content; explosive volcanism requires a relatively volatile-rich eruption whereas effusive activity is thought to be relatively volatile-poor (Morgan et al., 2021 and references therein). Due to this clear distinction, historically effusive and explosive volcanic deposits have typically been examined separately. However, modeling studies suggest that all effusive eruptions on the Moon may be preceded by explosive eruptions because of gas that builds up at the front of the magma in the conduit (e.g., Wilson & Head, 2018). Here we hypothesize that lunar volcanism should mirror terrestrial volcanism in that individual eruptions may experience different eruptive phases that are not necessarily constrained to only the beginning of the eruption. To investigate this, we evaluate co-located explosive and effusive lunar volcanic deposits and how the two types of volcanism relate stratigraphically.

We selected the Montes Apenninus region for this study because it includes a variety of volcanic features from many different terrains, including eight previously identified LPDs (see Table 1) and several identified effusive features. Many explosive volcanic features in this area are co-located with effusive features including mare margins (the boundaries between the mare basin lavas and highland terrain), rilles (i.e., lava channels), and mare infilled basins. Although most types of volcanic features can tell us about the volcanic history of a region, explosive deposits in particular preserve information about volatile content, compositional evolution, and the structure of the lunar deep interior (Keske et al., 2020; Wilson and Head, 1981). This analysis will help to provide a more comprehensive understanding of lunar volcanic phases, lunar volcanic evolution (deriving compositional data for eight explosive and associated effusive features), and the composition of the lunar surface. Pyroclastic deposits are also important exploration targets for *in situ* resource utilization, and this study provides further constraints on the nature and distribution on LPDs in near-side regions of high scientific and exploration interest to the Artemis Program (Artemis III Science Definition Team, 2020). We investigate the relationship between the different eruption styles to understand the history and evolution of volcanism in the Montes Apenninus region of the Moon.

In this study, we characterize the distribution of minerals and glass for known explosive deposits and co-located effusive features in the Montes Apenninus region of the Moon. We detail each deposit's geologic context and determine the relationship between effusive and volcanic features by (1) characterizing the diversity of the mineralogy of pyroclastic deposits within the Montes Apenninus region, (2) evaluating the differences in mineralogy between pyroclastic deposits within the context of other local eruptive products and features, and (3) using physical and spatial relationships between the effusive and explosive volcanic mineralogy to evaluate the timing and potential co-occurrence of these eruptions. We target spectral absorptions of iron-bearing minerals in the near-infrared that are useful for characterizing mafic mineralogy of LPDs, mapping glass content variability between effusive and explosive volcanism, and identifying other volcanic and non-volcanic spectral diversity in the surrounding terrain. Iron-bearing minerals are a major component of planetary surfaces (McCord et al., 1981; Horgan et al., 2014) and have specific implications for volcanic processes (Gaddis et al., 1985; Henderson et al., 2021; Mustard et al., 1997; Scudder et al., 2021). Viewing compositional information from Moon Mineralogy Mapper (M^3) in a morphologic context as we do in this study gives additional detail on the emplacement of volcanic materials, stratigraphic relationships, and the distribution of minerals and glasses. The Montes Apenninus area has complete M^3 coverage and a wide range of volcanic features and therefore is an ideal diverse testbed for our investigation into the source, spatial distribution, and correlation of LPDs with effusive features on the Moon. M^3 also provides high spectral resolution (hyperspectral) dividing critical parts of the visible and near-infrared spectrum into 82 spectral channels for detailed analyses.

3.2 Background

Compositional, mineralogical, and morphological differences between explosive and effusive volcanism can be used to infer volatile content (e.g., Bennett et al., 2016; Head & Wilson, 1979; Trang et al., 2017) and eruption style of volcanic features Bennett et al., 2016; Gaddis et al., 2003; Head and Wilson, 2017). Mineralogy and glass content, and the distribution of those materials, are closely connected to eruption conditions, eruption style, and type of eruption (Souchon et al., 2013). It is generally thought that explosive volcanism on the Moon ceased approximately 2.8 billion years ago. although effusive mare volcanism may have continued until as recently as ~1 billion years (Hiesinger et al., 2011, 2010). The age of irregular mare patch type features is currently actively debated (Qiao et al., 2017) but includes the hypothesis that they may be even younger than 1 billion years old. More than 100 LPDs have been identified on the Moon (e.g., Gaddis et al., 2003; Gustafson et al., 2012; Keske et al., 2020; Trang et al., 2017) in various types of lunar terrains, although, like the lunar maria, they occur at a higher frequency on the nearside than the farside (Head, 1974). LPDs are found in or near virtually every lunar terrain and at times are associated with other volcanic features, lunar impact craters, or lava-filled crater basins (Adams et al., 1974). The explosive volcanic eruptions that create LPDs will expel the local country rock and/or subsurface magma known as juvenile magma. LPDs are generally basaltic in composition and have often been categorized by size (Heiken et al., 1974; Gaddis et al., 1985;

Gaddis et al., 2003): deposits larger than 1,000 km^2 are labeled regional LPDs and deposits 999 km^2 and smaller are classified as localized LPDs. Glass content and proportion of local country rock present in a pyroclastic deposit can indicate eruption style. Vulcanian and Strombolian eruptions have similar intermittent, modest-sized eruptions, but Vulcanian eruptions eject a significant amount of older, colder, rock and Strombolian eruptions eject mostly new melt. With varying volatile content and composition, different LPDs will exhibit varying levels of glass content due to the rate at which the ejected material was being quenched in the near-vacuum conditions of the lunar surface (Jawin et al., 2015). Increased rates of glassiness indicate that the eruption column was optically thin and that the magma droplets did not have time to crystallize (Besse et al., 2014). Glass-rich deposits are then correlated with lower volatile content (Weitz et al., 1998b). LPDs with high glass content relative to country rock are typically categorized as lava fountain style eruptions (also known as Hawaiian-style eruptions or fire fountain eruptions), where lava droplets were able to quickly quench in an optically thin eruption column and little country rock was expelled during eruption. Regional LPDs are thought to have erupted by more continuous lava-fountaining (also known as fire fountaining or Hawaiian-style; e.g., Wilson and Head, 1981; Gaddis et al., 2003), comprising a majority juvenile component with increased glass content. Localized pyroclastic deposits may have been more likely to be created by intermittent gas-rich (i.e., Vulcanian or Strombolian) eruptions (Wilson and Head, 1981; Bennett et al., 2016). However, detailed analysis of many smaller LPDs has shown that they can also be produced through a local lava fountaining eruption and can more readily transition to an effusive phase. Bennett et al. (2016) found that LPDs in Oppenheimer crater were produced from eruptions of different eruption styles using observations of the abundance of juvenile material, iron content of glasses, and overall mineralogy of the LPDs.

3.3 Description of Study Region

Montes Apenninus is a northeast-southwest trending chain of mountains that are part of the eastern rim of the Imbrium basin on the lunar near side (Lat 5°W – 15°E, Lon 0°N – 35°N, Figure 11). Many locations within this region were targets of the Apollo program and have been observed or sampled during the landed Apollo missions. Apollo 15 landed near Rima Hadley, sampling mare basalts of the Imbrium Basin and several types of volcanic glass, including magnesium-rich green glass. Apollo 17 landed outside of the Montes Apenninus study area but had several low-orbit flyovers of the Sulpicius Gallus area. Pyroclastic glasses and mare basalts were sampled from the area that appeared to have similar characteristics (i.e., color and origin) as those within the Sulpicius Gallus deposit and surrounds (Lucchitta & Schmitt, 1974). The western part of the Montes Apenninus region is the Apennine Bench Formation, a light plains unit that is older than the surrounding Mare Imbrium (Spudis et al., 1988), also targeted for investigation during Apollo 15. There are many rilles in the Montes Apenninus study region (locations are marked in *Figure 12*), including Rima Hadley, Rimae Bode, and various other linear, circular, and sinuous rilles (Hurwitz et al., 2013b). Many rilles have irregular depressions that are unlike the morphology typically observed with impact craters which tend to have circular rims, lie within the rilles or adjacent to the rilles. These are generally interpreted as the locations of vents from which volcanic materials have erupted. Such depressions and rilles may indicate the locations of effusive eruptions that create lava channels and explosive eruptions that create pyroclastic deposits. In the north, the montes are bound to the west by Mare Imbrium and to the east by Mare Serenitatis. To the south, the Montes are bound by Sinus Aestuum to the west and Mare Vaporum to the east. Regional LPDs are commonly found along mare margins, mantling the highland and mare boundaries on the edges of major and minor mare basins.

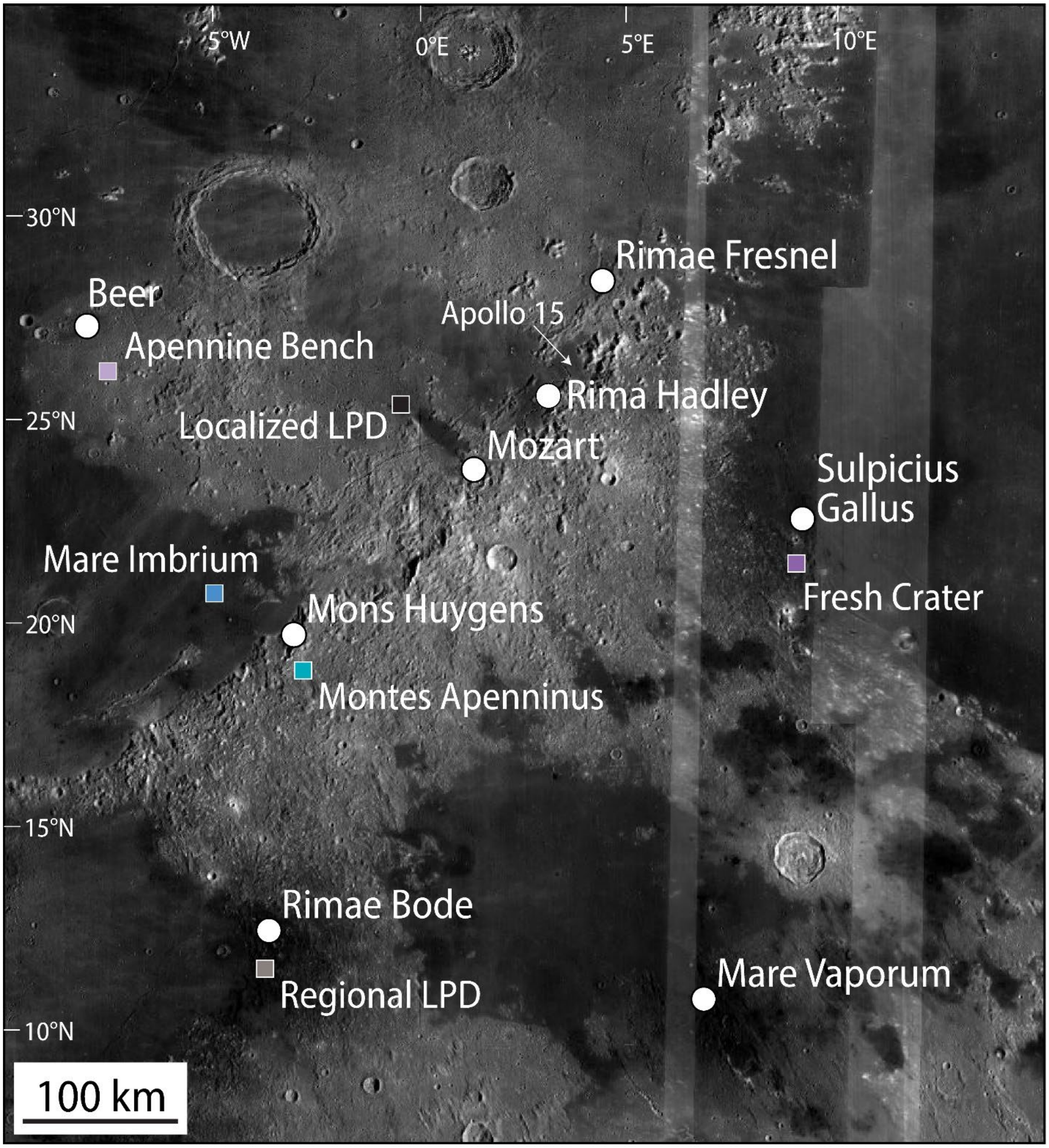

Figure 11: Moon Mineralogy Mapper mosaic of Montes Apenninus region (reflectance in Band 82, 2.98 µm). Lunar pyroclastic deposits are indicated as white circles. Squares are areas of averaged representative spectra presented in Figure 14, with coordinated colors. North is up in all figures. Note: data used to create all images in this manuscript are provided at the link referenced in the Data Availability Statement.

There are forty-six rilles within the Montes Apenninus study region (Hurwitz et al., 2013). Sinuous rilles are typically thought to be formed via lava incision into the lunar surface during an effusive eruption (Hurwitz et al., 2013b) or from the channelization of a flow in a constructed channel (Spudis et al., 1988). Although they are associated with effusive volcanic deposits and may include eruptive vents, their relationship to explosive volcanism and emplacement is not always clear. Three LPDs in the Montes Apenninus region are named for nearby fissures (Rimae Bode, Rimae Fresnel, and Rima Hadley). "Rima" (plural "Rimae)," means "fissure" or a long opening in the surface and does not imply a specific formation process. We investigate the relationship between the eruption that form fissures such as these and the pyroclastic deposits that are near them, observing stratigraphic relationships and differences in glass signature strength that appears in a variety of band parameters that we derive, with spectral and contextual confirmation.

LPD	**Area (km^2)**	**Geologic Setting**
Mons Huygens (Fig. 11)	10	Highlands margin
Fresnel (Fig. 6)	307	On a sinuous rille
Mozart DMD (Fig. 5)	589	On a sinuous rille
Beer (Fig. 10)	623	On the Apennine Bench
Rima Hadley (Fig. 7)	898	On a sinuous rille
Mare Vaporum (Fig. 12)	4129	Center of a mare, extending to mare margin
Sulpicius Gallus (Fig. 9)	4322	Mare margin
Rima Bode (Fig. 8)	6620	Mare margin

Table 2: Identified LPDs in the study area and geologic terrain that the LPD mantles. The areal extent is from (Gaddis et al., 2003).

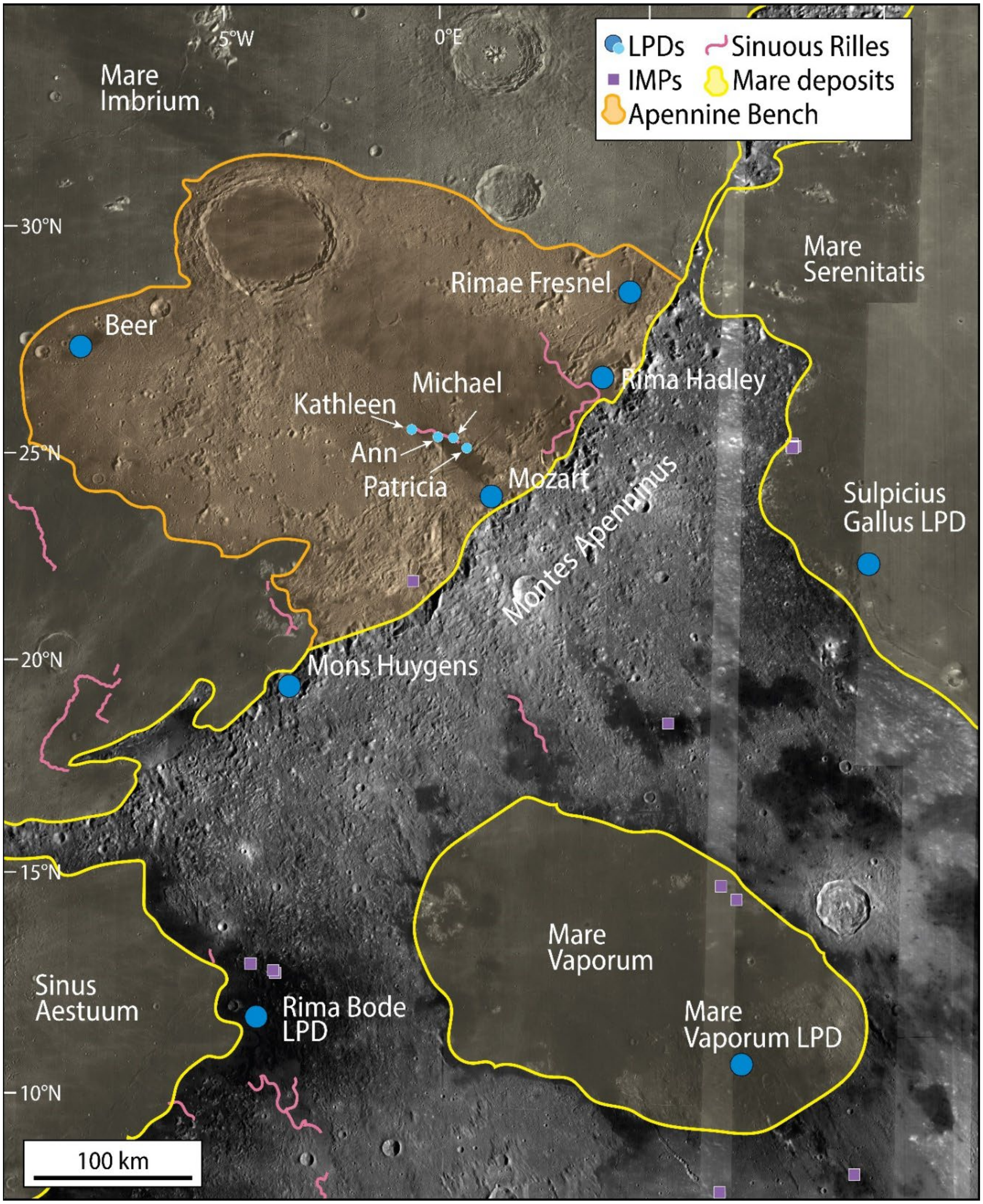

Figure 12: Lunar Pyroclastic Deposits (LPDs) and other volcanic features shown on the Moon Mineralogy Mapper mosaic from Figure 11. Labeled circles indicate locations of LPDs (dark blue for known LPDs, light blue circles with white outlines for newly-added LPDs); squares indicate Irregular Mare Patches (Braden et al., 2014a)*; pink lines indicate sinuous rilles (Hurwitz et al., 2013); peach irregular shapes outline major mare basins discussed in this work, and the yellow irregular shape outlines the Apennine Bench within Mare Imbrium.*

3.4 Methods

We conducted a compositional analysis of the Montes Apenninus study region, focusing on LPDs and features near LPDs (e.g., sinuous rilles, irregular mare patches, rocks exposed by fresh impact craters within mare). We used hyperspectral visible and near-infrared spectra from the Moon Mineralogy Mapper (M^3) imaging spectrometer which flew onboard the Indian Space Research Organization's Chandrayaan-1 spacecraft (e.g., Pieters et al., 2009). The high spectral resolution (10 nm spectral sampling) and broad wavelength range of M^3 (0.35–3.0 μm) is particularly well-suited to characterize the iron absorption features that are characteristic of iron-bearing minerals and glasses. Specifically, we investigate absorption bands near 1 μm and 2 μm, which are useful for characterizing mafic mineralogy of LPDs, mapping glass content variability between effusive and explosive volcanism, and identifying other volcanic and non-volcanic spectral diversity in the surrounding terrain. We explore the variability of these minerals within pyroclastic deposits, and use differences observed on the surface to infer the subsurface state at the time of eruption.

3.4.1 Spectral processing

We used hyperspectral M^3 data (spatial resolution of up to 140m/pixel in 82 spectral channels) to characterize the composition of LPDs at visible and near-infrared wavelengths. We used the publicly available data from the Planetary Data System (PDS; see Supplementary Materials for the list of images used and their optical periods, Boardman et al., 2011). We mosaicked thirty-seven hyperspectral image cubes covering the region from 0°N to 35°N and from 10°W to 15°E (Figure 11, see Data Availability Statement for data access). The Level 1B data includes resampled, scaled, calibrated spectral radiance data including the observation geometry and illumination on a pixel-by-pixel basis. The Level 2 reflectance data includes corrections for thermal emission, topographic, photometric, and instrumental effects (Boardman et al., 2011; Clark et al., 2011; Green et al., 2011). Both L1B and L2 data were processed in Interactive Data Language (IDL) to create final images following the methods of Horgan et al. (2014) to suppress the continuum contribution due to factors like space weathering and physical properties, and to smooth the spectra to better evaluate spectral variability. The continuum was modeled as a linear convex hull with two segments between 0.75 and 2.6 µm with a floating central tie point near 1.5 µm (Horgan et al., 2014). The images were mosaicked and then projected onto a cylindrical projection. Of the 37 images incorporated into the mosaic, only seven were from the later 2C optical period during which Chandrayaan-1 orbited at twice the altitude, resulting in reduced spatial resolution. Data were taken at the lower 100 km orbit in optical period 1 and the later 200 km orbit in optical period 2, resulting in resolutions of 140 m/pix and 280 m/pix, respectively. We did not downsample the greater mosaic to the lower resolution and retained the original spatial resolution and noise rate of the better images in the mosaic. The issues observed between optical periods can be observed in Figure 13 RGB composite of the Montes Apenninus region: spectra taken from the same pyroclastic deposit in two optical periods (e.g., Rima Hadley in this figure in a pinker image than what blends with the adjacent image where Rima Fresnel is located) have significant differences that cannot be accounted for through compositional or mineralogical factors. We further evaluate the raw and continuum removed but non-smoothed spectra for irregular features, significant noise, and features that do not have correlations to known lab spectra of minerals (e.g., Horgan et al., 2014). We determined that for the best fidelity of investigation, regions within the 2C optical period images were investigated separately from the other images and spectral sampling was not compared across obvious image boundaries to avoid potential processing discrepancies due to variations in photometric correction differences between different parts of the orbital campaign (e.g., Boardman et al., 2011). These spectra were not eliminated from evaluation but were not directly compared to spectra from images that did not appear consistent.

To evaluate how the mineralogy varies spatially across the study region, we produced band parameter maps that highlight specific iron-bearing mineral absorption bands in each mosaic (see below and Table 2). The band parameter maps were viewed individually (e.g., Figure 15) and in triplets as false color RGB composites (e.g., Figure 13). These maps were used to evaluate changes in mineralogy in our research area and to identify regions of interest (ROI) for collecting average spectra. We derive 1- µm and 2- µm band parameters to capture the absorption band near 1 and 2 µm due to crystal field effects in ferrous iron, which cause a split in energy levels of partially filled 3d orbitals (Horgan et al., 2014). These band parameters include the band depth to investigate the strength of the absorption bands, band center position to determine the effects of mineralogy on the composition and locations of those bands, band asymmetry to investigate contributions such as mineral mixing and amorphization (altering the crystalline structure of a material, specifically resulting in the broadening of spectral bands), and band area to evaluate the area under the curve for mineral mixing and signal strength (see Horgan et al., 2014 for a thorough description of band parameters).

Band parameter	**Target component**	**Evaluation**
GLA	Iron-bearing glass	$(R_{1.15} + R_{1.18} + R_{1.2})/3$
OPX	Orthopyroxene	$(R_{0.88} + R_{0.90} + R_{0.92})/3$
CPX	Clinopyroxene	$(R_{2.10} + R_{2.155} + R_{2.20})/3$
1bc	Band center at 1 µm	$q(\min[W_{0.8}, W_{1.4}])$
2bc	Band center at 2 µm	$q(\min[W_{1.6}, W_{2.5}])$

Table 3: Derivation of mineral band parameters for targeted pyroclastic indicator minerals. R_N is the reflectance at a specific wavelength, W_N is the wavelength at that location on the spectrum (in

μm). For example, the GLA band parameter is defined as the average band depth below the continuum at 1.15 μm, 1.18 μm and 1.2 μm. q(min[W_{N1},W_{N2}]) represents the wavelength position of the minimum of a fourth-order polynomial fit within the specified range (W_{N1} and W_{N2}). For example, the band center at 1 μm is the wavelength position of the minimum of a fourth-order polynomial fit between 0.8 μm and 1.4 μm.

3.4.2 Data Visualization

The parameter maps were analyzed in the Environment for Visualizing Images (ENVI) to assist with spectral retrieval, context, and for stratigraphic interpretation. We also exported the parameter maps and evaluated them in ESRI ArcGIS. The parameter maps were overlain onto the visible Lunar Reconnaissance Orbiter (LRO) Wide Angle Camera (WAC) global morphologic mosaic of the Moon (Speyerer et al., 2011; Wagner et al., 2015) for morphological context. Viewing compositional information in a morphologic context allows us to identify and characterize specific geomorphic features (e.g., craters, rilles, slope faces, mounds) that may be vents and/or substrates and gives us the ability to gain insight into emplacement history and distribution of the pyroclastic material on the lunar surface.

We target regions in the glass band parameter map that have strong signatures for spectral analysis, particularly near irregular depressions and potential vents where effusive features appear to originate, where explosive volcanism could be correlated. These indicators we call a high glass signature strength in the map, or in regions where we are able to confirm spectral indicators of glass, locations that have a high glass concentration. We interpret a trend in stronger glass signature to increased glass content, within the geologic context of the dispersal near an eruptive vent or a volcanic feature likely to produce an explosive eruption. The glass signature in the glass band parameter map targets the depth below the continuum between 1.15 μm and 1.20 μm, and is confirmed in spectra by an asymmetric 1 μm band. Some locations identified in the glass band parameter maps as having elevated glass signatures might have symmetrical bands shifted to longer wavelengths, thus increasing this band depth value, resulting in the stronger glass signal strength. These detections in the glass band parameter map are interpreted as not due to glass. This is why we conduct the spectral confirmation to evaluate whether the glass band parameter map is identifying glass or another compositional component in the lunar regolith. Where LPDs were thought to occur but did not contain significant glass, we used the locations of the LPD from literature and evaluated spectra from those areas directly. We use the boundary of the glass signature strength, RGB composite maps, and spectral confirmation to evaluate the extent of the pyroclastic deposits and their relationship to the extent of the effusive volcanic features. In this way, we derive information on stratigraphic and contextual relationships between the pyroclastic eruption and effusive eruption.

3.4.3 Mineralogy and spectral analysis

For each region of interest (identified in Table 1) we first use the band parameter maps overlain onto the WAC mosaic to characterize the area. We identified areas for spectral retrieval as laid out in Section 2.2, noting areas where surface components (e.g., slopes, fresh impact craters, shadows) may be affecting the spectra or increasing noise. We identified representative spectra from each feature of interest to validate the findings from the band parameter maps. We also investigated spectra of highland and mare regions near LPDs, and volcanic and non-volcanic features spatially correlated to pyroclastic deposits (e.g., sinuous rilles, fresh impact crater materials surrounding pyroclastic deposits). Spectra from the pyroclastic deposits were compared to these regions to evaluate the compositional differences of the pyroclastic deposits and nearby non-pyroclastic features. This includes constraining the mineralogy and identifying any stratigraphic relationships (i.e., identifying crosscutting relationships to identify relative timing of the emplacement of a mare or rille and a pyroclastic deposit). Band parameter analysis can provide targets to investigate endmember spectra and areas of mineral mixing. Variations in composition due to mixing can be evaluated using the 1 μm and 2 μm band centers, RGB composite maps thereof, and following with investigation of individual spectra. Although individual compositions may not be able to be determined from the band parameter maps, it has been shown that investigation of individual spectra can mitigate this uncertainty (Horgan et al., 2014).

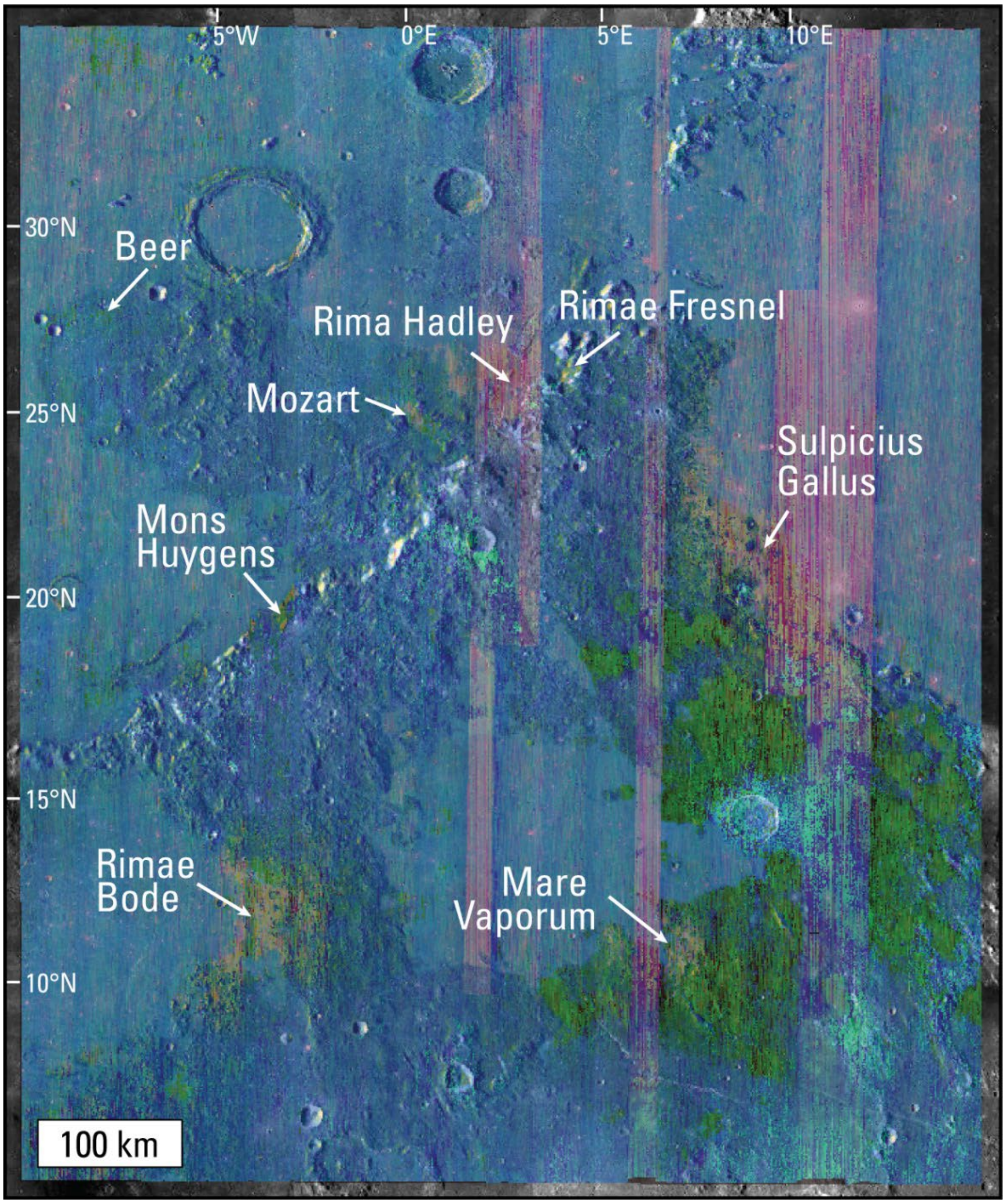

Figure 13: RGB of Montes Apenninus region where the red channel is the glass band parameter map, the green channel is the 1-μm band center and the blue channel is the 2-μm band center.

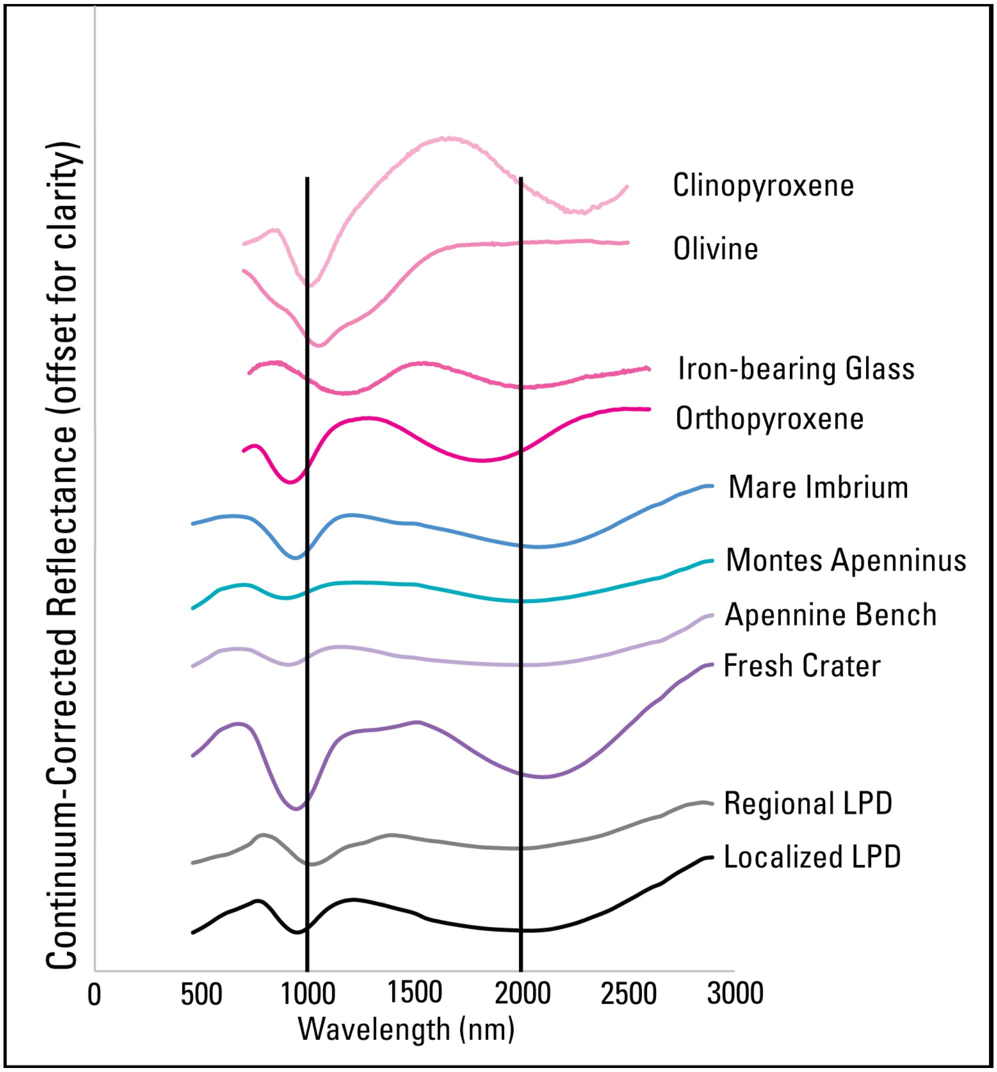

Figure 14 Sample spectra from the Montes Apenninus study region (bottom six spectra, this study), and example lab spectra from (top four spectra, Horgan et al., 2014). Locations for all six spectra from this study are indicated in Figure 11, by the same colors. See Data Availability Statement for data access.

Iron-bearing glass is a component of explosive volcanism, distinct from crystalline mare basalts and other types of effusive volcanic features (Gaddis et al., 2003). The reflectance spectra of iron-bearing glass is identified by a broad and symmetric absorption band between 1.07 µm and 1.20 µm and sometimes exhibits a weak absorption band centered near 2 µm (Figure 14, Horgan et al., 2014). The glass band parameter (see Table 2 for definition) highlights olivine or glass as both have an absorption in this region of the spectrum (Figure 14). Glass and olivine can be distinguished by the spectral behavior near 2 μm: glass has a 2-μm band while olivine does not. We therefore refer throughout this manuscript to this parameter as the glass band parameter, because olivine was not identified in any spectra investigated in the study area. Glass is a poor absorber with a complex shape compared to other iron-bearing minerals, so a significant glass content is required to change the shape of the spectrum of the 1 μm band for detection. This means that, although a signature may be identified in the glass band parameter map, the detection may not be due to glass, and for that reason, we use the asymmetry of the 1 μm band and can confirm glass by investigating the shift of the 2 μm band in instances with inconclusive results. These observed changes to the 1-μm and 2-μm bands are typically only present when the content of iron-bearing glass is at high abundances (50–80 wt% obtained from comparisons to lab spectra, Bennett et al., 2016; Horgan et al., 2014).

Basaltic rocks characteristically include other iron-bearing minerals like pyroxenes (Klima et al., 2011), which have strong absorptions at 1 μm and 2 μm. Two structural types, orthopyroxene and clinopyroxene, can be distinguished in their spectral characteristics and are present in different geomorphic features and landforms on the Moon (e.g., Table 2). These two structural forms of pyroxene are compositionally different with clinopyroxene containing calcium, and generally forms at lower temperatures than orthopyroxene. Orthopyroxene is characterized in spectra by a narrow, symmetrical absorption band near 0.9 μm and a broad absorption band near 1.9 μm. Clinopyroxene is a common component of juvenile pyroclastic material (i.e., original magma, and not erupted country rock), identified in spectra by a narrow 1 μm absorption band shifted to longer wavelengths than orthopyroxene to 1 μm or 1.05 μm, and an absorption band between 2 μm and 2.4 μm (Horgan et al., 2014). Fresh impact craters in mare have very strong spectral features as there is less continuum suppression by space weathering (Figure 14). Despite sometimes having a highlighted glass signature in the glass band parameter maps, the spectrum of a fresh impact crater in the mare usually has a 2-μm band center shifted to longer wavelengths, indicating the glass component is a minor contribution to the spectrum and the significant 1 μm band depth may be influencing the 1-μm spectral feature more than glass.

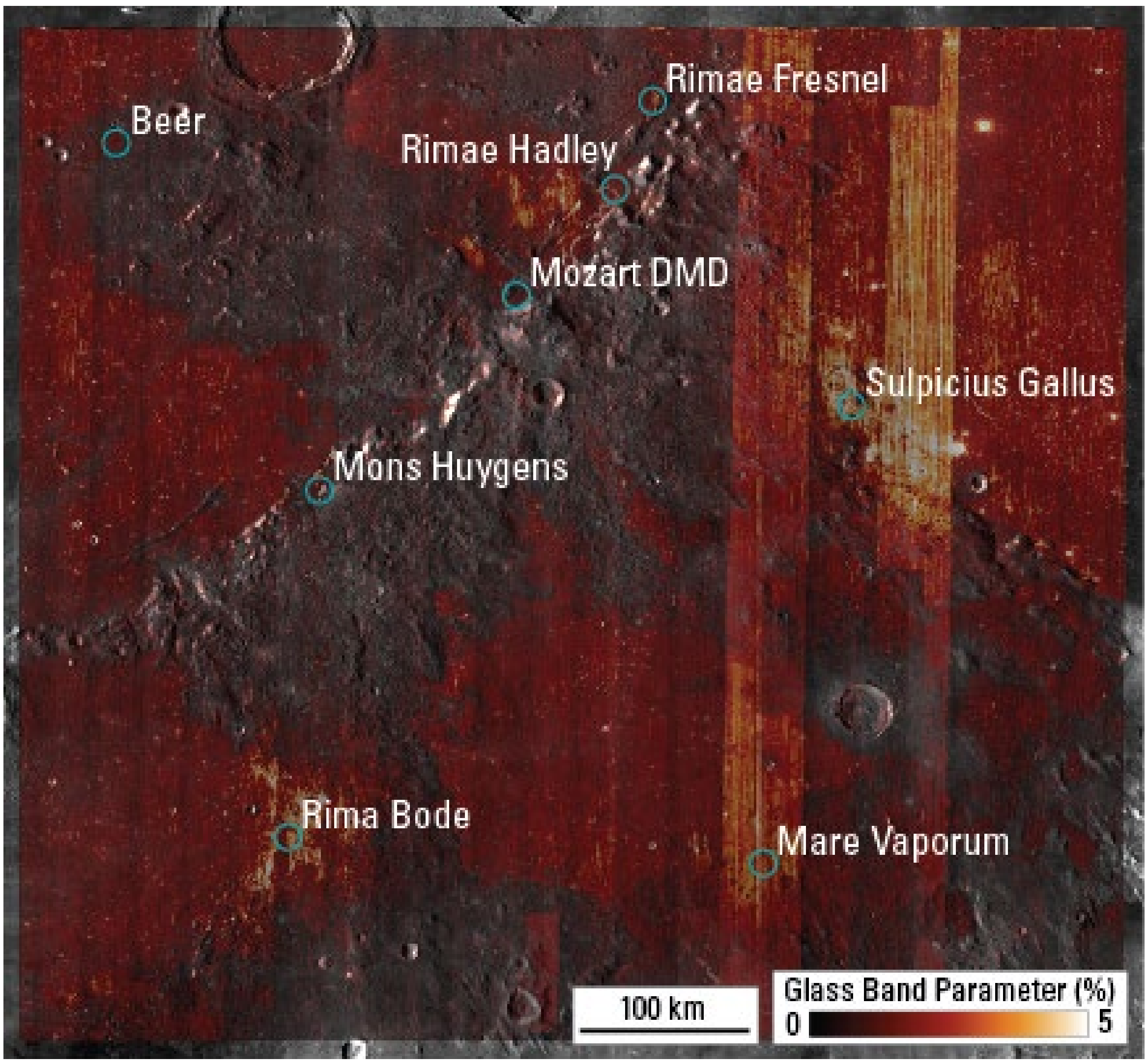

Figure 15: Glass/olivine band depth spectral parameter mapped mosaic of Montes Apenninus region with Lunar Reconnaissance Orbiter Camera Wide Angle Camera as background (see Supplementary materials for image names). Glass/olivine band parameter highlights enhanced absorption between 1.15 μm and 1.20 μm in continuum removed spectra, interpreted as a glass/olivine signature. For interpretation of the references to color in the figure legend, the reader is referred to the web version of this article.

3.5 Results and Interpretations

The M^3 derived glass band parameter map highlights the band signal strength at 1.15 μm, where glass has a strong signal (Bennett et al., 2016; Horgan et al., 2014). An enhanced glass signature (~3-5%, indicated by red in Figure 15) in the map indicates that there is likely glassy/olivine material, ~1 – 3%, indicated by yellow indicates that there is a potential that there is glassy/olivine material, and blue (0 – ~1%) indicate that the material in that pixel is not likely to be glassy or contain olivine. The glass band parameter map (Figure 15) shows that most Lunar Pyroclastic Deposits (LPDs, indicated blue circles) in our study area exhibit detectable glass signatures in the glass band parameter map, which we interpret as due to concentrated glass relative to other components of the spectrum at 1 μm. The signal strength between LPDs vary and specific interpretations for each deposit are discussed further below. Most effusive features in the glass band parameter map have very little or no glass signature, and highlands materials have no glass signature.

Several LPDs are located along the perimeter of mare basins, consistent with prior observations that explosive volcanism occurs with mare emplacement (Head, 1974; Gaddis et al., 1985). These deposits typically exhibit stronger glass signatures than other LPDs and tend to have a greater spatial extent than the other deposits identified in this region (all mare margin deposits are in the regional size classification of greater than 1000 km^2). Few deposits on the lunar surface are identified in the interior of mare basins as most "mare margin" deposits are on the perimeter instead of the interior. Additionally, few mare margin deposits are of a localized size classification and are instead typically much larger than 1,000 km^2 (Hawke et al., 1989). In the Montes Apenninus study region this is also true as Mare Vaporum LPD is the only pyroclastic deposit that is in the interior of a mare basin, and we have no mare margin deposits (including Mare Vaporum, if classified as a mare margin deposit) that are of the localized size classification of smaller than 1,000 km^2.

Here we describe the relationships between each of the explosive deposits investigated in this study and effusive features that they are most closely related to, spatially, or that they are named for. We categorize these LPDs by the effusive features to which they are related, and describe how each LPD relates stratigraphically, compositionally, and morphologically to that effusive feature.

3.5.1 Sinuous Rille LPDs

Four of the eight LPDs in the Montes Apenninus study region are near features categorized as rilles or Rima/Rimae, which means "fissure:" the pyroclastic deposits near Rimae Fresnel, Rima Hadley, Rimae Bode, and (unofficially named) Mozart Rille. In this section, we evaluate whether the eruption of LPDs occurred in connection with the eruption of the sinuous rilles, including whether LPDs near suspected vents relate to the effusive volcanism. Three identified LPDs in the Montes Apenninus are near fissure features previously classified as sinuous rilles (Mozart DMD near Mozart Rille (Figure 16), Rima Bode LPD near Rimae Bode, and Rima Hadley LPD near Rima Hadley; Hurwitz et al., 2013), which are interpreted as lava channels (i.e., effusive features) on the lunar surface. One additional fissure feature (Rimae Fresnel) appears to also be a lava channel due to its sinuosity, apparent "bathtub rings" marking high-flow of lava in the southern extent of the rille, and appearance of flow textures in the northern extent of the rille (Figure 17c Figure 17d). LPDs named after nearby Rima/Rimae may or may not be related to the same volcanic emplacement processes or events that formed the rilles.

Mozart rille is a sinuous rille west of the Montes Apenninus highlands structure (Figure 12), along which there are four irregularly shaped depressions (from west, the initiation of the fissure, to east, the outflow of the fissure): Kathleen, Ann, Michael, and Patricia (Figure 16). These four features were originally named in 1974 (Defense Mapping Agency, 1974), but they were not hypothesized to be of any specific origin was ascribed to them at the time (i.e., they were not identified as pyroclastic deposits or volcanic vents). All four irregular depressions along Mozart Rille exhibited an elevated signal in the glass band parameter map (Figure 16b), but only Michael had a noticeable glass signature in the more complete spectral analysis. Figure 16c shows that the M^3 spectrum exhibits a shoulder in the 1-µm band for Michael. The Ann depression also has a potential glass spectral signature with a small shoulder near the peak just long of 1 µm. Spectral analysis of the Kathleen depression, the apparent source vent of Mozart Rille (Coombs et al., 1988), does not have a recognized asymmetry or spectral shoulder at 1 µm that would be indicative of glass, nor is the band center at 1 µm shifted to longer wavelengths that could indicate a contribution to the spectrum from glassy or olivine material as previously reported. Coombs et al. (1988) reported pyroclastic material at Ann, potentially flowing into Michael as a collapse feature; however, Michael has a strong standalone glass signature on the downstream side of the vent, indicating the presence of a separate, somewhat isolated pyroclastic eruption at this location. The Patricia depression shows the weakest glass signature in the glass band parameter map, and overall weak spectral contrast, which would be consistent with tectonic emplacement of the Patricia depression rather than volcanic emplacement or from volcanic collapse (both of which would show stronger spectral indicators of volcanic minerals), consistent with Coombs et al. (1988). The outlet of the Mozart Rille structure flows into the Patricia depression and Lacus Mozart, the southern end of which is bound by a highlands mound. “Mozart DMD” in Figure 16 is a previously identified “dark mantling deposit” (Blewett and Hawke, 2001; Hawke et al., 1979a), here determined to have a weak 1-µm band depth and an average albedo characteristic of the surrounding terrain, which is not typical for a localized LPD. This feature is further described in the Discussion section below.

Spectra from this region do not demonstrate glassy material contributing to the spectrum at 1 µm, nor is there increased spectral contrast at characteristic iron-bearing absorption bands that would typically be indicative of volcanic minerals. This analysis was unable to confirm the presence of an LPD at the Mozart DMD location.

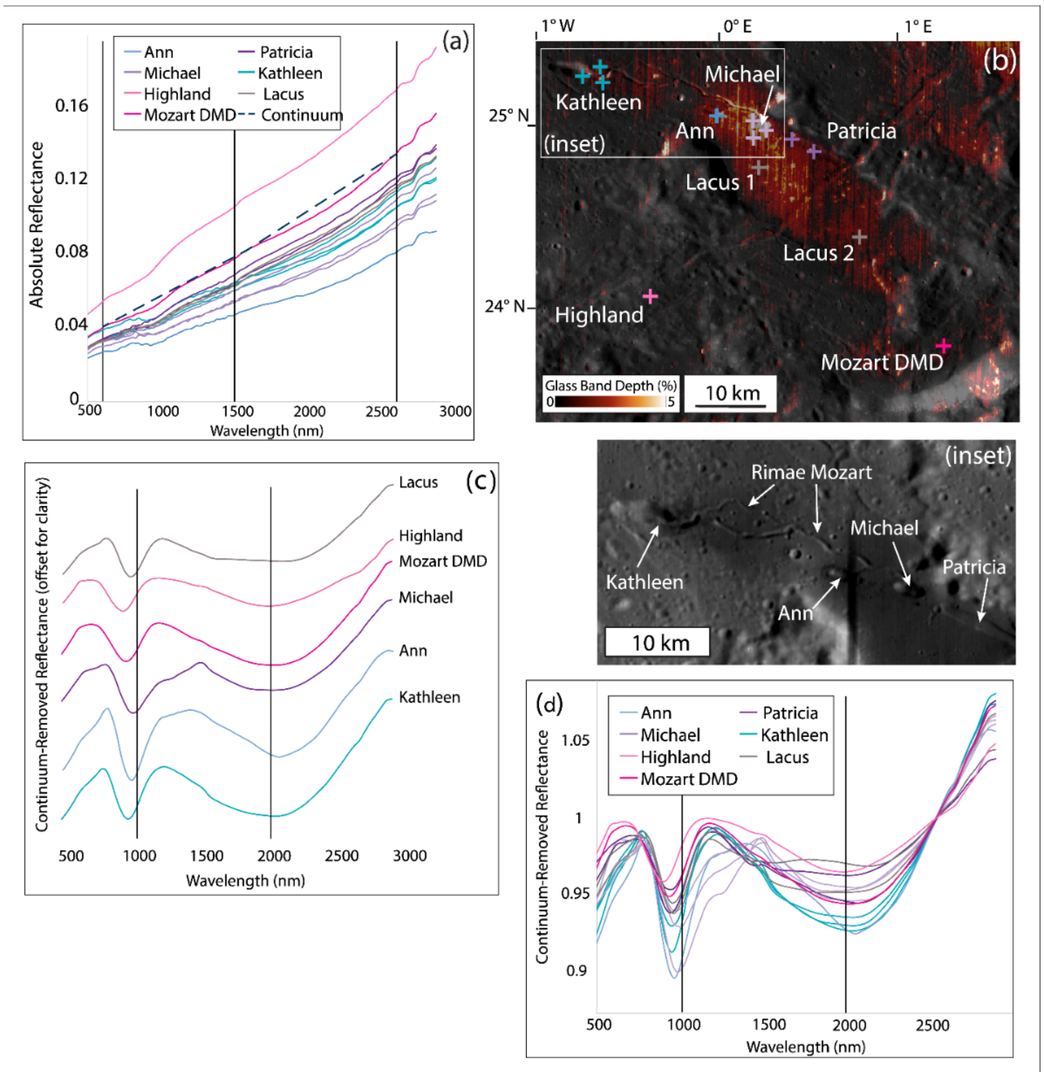

Figure 16: Results from Mozart region: (a) Raw reflectance spectra of regions of interest indicated in (b) used to create averaged spectra for a location – black vertical lines indicate the endpoints used for continuum removal; (b) Mozart region in glass band parameter map overlaid on WAC basemap with spectral points indicated (inset below showing irregular depression Kathleen, Michael, Ann, and part of Patricia); (c) Averaged spectra of each of regions in (c) – vertical lines indicate 1-µm and 2-µm wavelengths, spectra offset for clarity. (d) Spectra from (a) with continuum removal applied – vertical lines indicate 1-µm and 2-µm wavelengths

The Fresnel LPD is a localized pyroclastic deposit (307 km^2) that, in analysis of our glass band parameter map, mantles Rimae Fresnel (Figure 17). The Fresnel LPD as previously reported in literature was identified near the location of LPD 1 in Figure 17a (Gaddis et al., 2003b), which is where we would expect to find spectral signatures consistent with a pyroclastic deposit. Although the Fresnel LPD has a detectable and consistent color difference in the glass band parameter map, the signature is generally weaker than other LPDs (and at times weaker than mare basalts). If we interpret this as a glass signature, the distribution of glass would be generally homogenous: the signature strength does not get stronger or weaker within the proposed deposit boundary. No vent structure that could have sourced the Fresnel LPD was identified in the mare or surrounds based on the glass band parameter map or from visual inspection of the WAC morphology map. Therefore, there is not a clear spatial relationship between the LPD and a rille vent structure as had been observed in the Mozart Rille LPDs. We interpret the LPD mantling the rille (i.e., being stratigraphically on top of the rille) as having come after the rille flows. Additionally, no clear source vent or inferred vent as hypothesized for the Rima Bode LPD (see mare margin deposits below) was identified.

In spectral analysis of many areas within the Fresnel LPD region, we did not observe a clear indication that glass was a significant component of the spectra at 1 μm. The spectra of the LPDs had as much asymmetry as spectra of the Apennine Bench (an area expected to not be glassy) and Mare Imbrium, and the band centers at 1 μm were not shifted to longer wavelengths in the LPDs than non-pyroclastic materials. The boundary extent of this LPD could not be determined definitively using the glass band parameter map in combination with point spectra and spectral ROIs. We note, however, that the lack of a strong glass signature and a clear pattern of explosive eruption is more likely to indicate a diffuse, non-glassy, or heavily weathered deposit disbursed over the rille than it would indicate a concentrated deposit that was associated with the rille. There was no identified glass signature within the rille or nearer to the fissure than there was disbursed farther away from the fissure, indicating that the LPD previously identified may not be well-correlated with the formation of Rimae Fresnel.

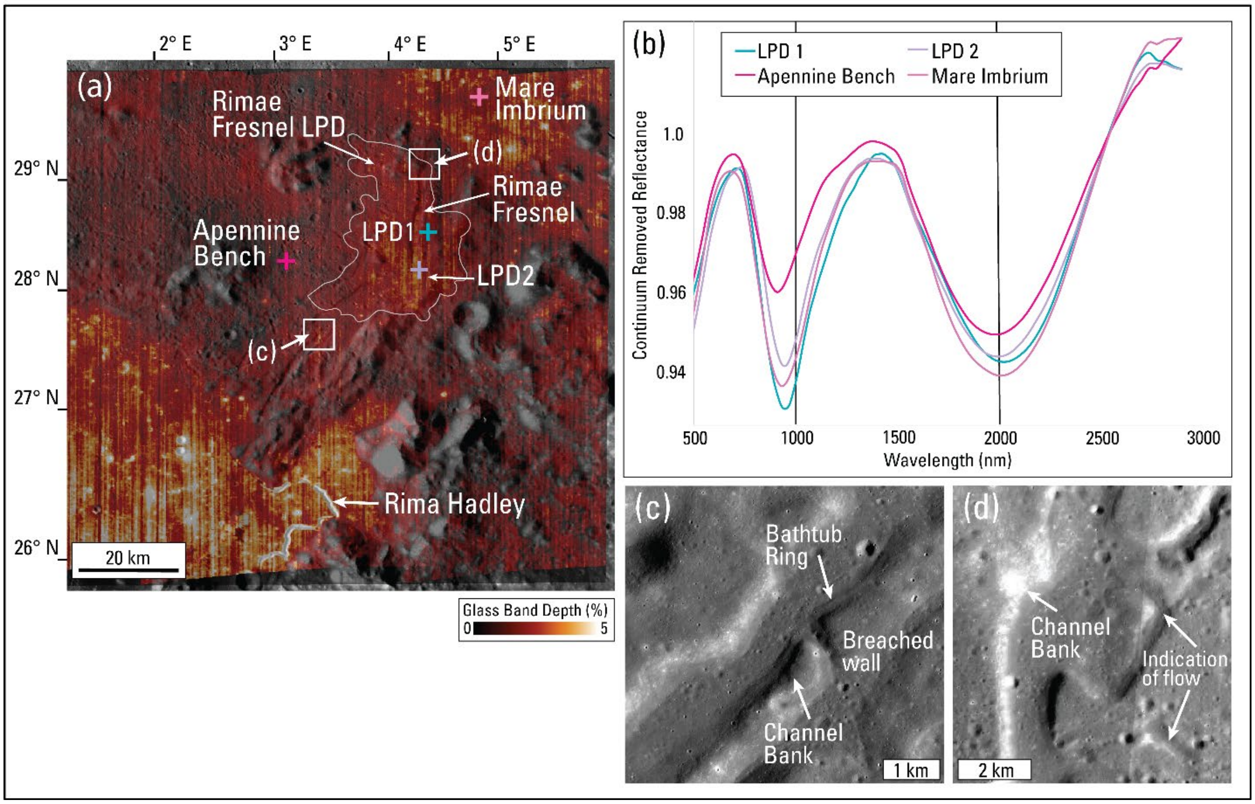

Figure 17: Results from Rimae Fresnel region (a) Rimae Fresnel region in glass band parameter map with indicated areas for each spectral ROI and insets for observations of lava flow features. (b) Spectra from 6a with continuum removal applied (vertical lines indicate 1-µm and 2-µm wavelengths); (c) inset from 6a demonstrating one area with observed "bathtub rings" indicative of receding lava flows in LROC Narrow Angle Camera; (d) inset from 6a demonstrating areas of sinuosity which would not be expected for a tectonic feature (arrows near "Indication of flow") from LROC NAC.

Rima Hadley LPD is a localized pyroclastic deposit (898 km^2, Figure 18) that was visited during the Apollo 15 mission as a site of importance for anorthositic materials from the Apennine Bench, rille materials and context for Rima Hadley, and mare lavas from Palus Putredinis. Samples collected include green pyroclastic glass beads of primitive origin, hypothesized to be derived from a mantle source with little magmatic evolution (Delano, 1986b; Steele et al., 1992). The spectra of the region where Apollo 15 activities occurred (labeled "LPD 1" which is the approximate location of the Lunar Roving Vehicle and ancillary sampling equipment) is similar to mare spectra within the Rima Hadley region (Figure 18b): there is noticeable asymmetry of the 1-μm band, but it does not have a recognizable shoulder, and the mare and LPD spectra both have broad 2-μm bands centered at or very near 2 μm. This broadening/asymmetry of the 1-μm band is consistent with a contribution of glass to the spectrum at that location. This asymmetry/shoulder is only slightly present within the Rima Hadley rille, which would indicate that the very strong glass signature visible in the parameter map within Rima Hadley is likely a slope effect from the steep sides of the rille.

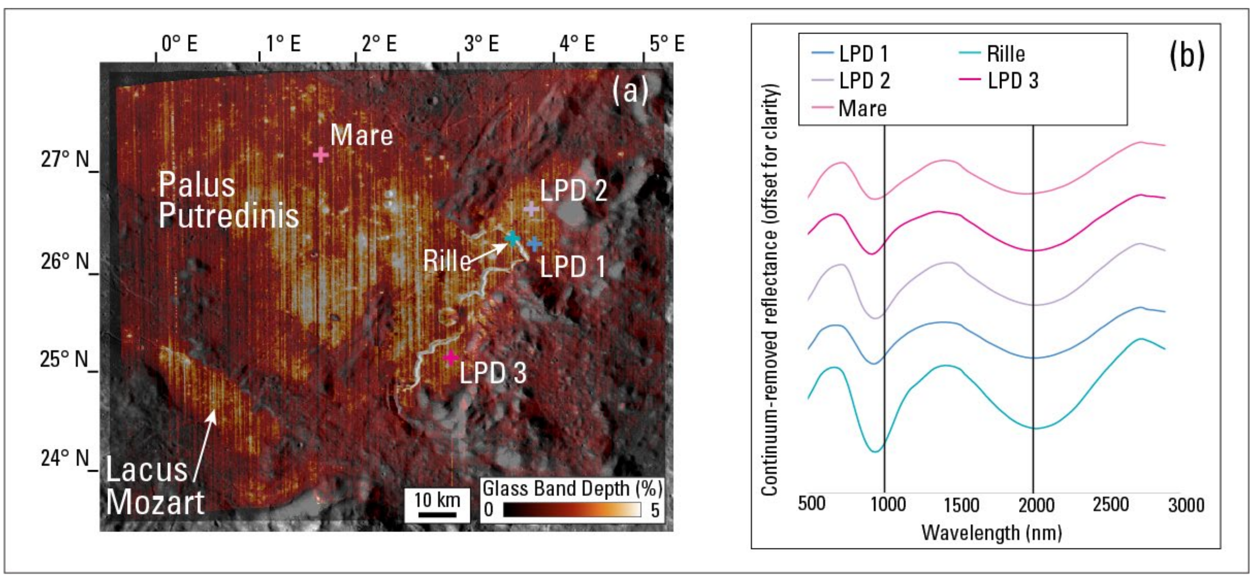

Figure 18: Results from Rima Hadley region (a) Rima Hadley region in glass band parameter map derived from M^3, overlain on WAC Basemap. (b) Stacked continuum removed reflectance spectra of the locations indicated in (a), black vertical lines indicate 1 μm and 2 μm wavelengths.

3.5.2 Mare Margin LPDs

Rima Bode LPD is a regional LPD (6,620 km^2) on the eastern margin of the Sinus Aestuum mare, visibly mantling both mare and highland terrains. The Rima Bode LPD has a strong glass signature (Figure 19a) and has areas in the center of the deposit where this signature is stronger than the distal parts of the deposit. It has been hypothesized that, due to the distribution of pyroclastic materials and shape of the Rimae Bode LPD (arcuate, with a core of concentration on the western margin and thinning mantle on the eastern margin), a possible vent structure from which the pyroclastic deposit was sourced may be located within the Sinus Aestuum basin that is now covered by mare lavas (Gaddis et al., 1985). Our results show a distribution of glass in the same arcuate pattern previously observed around the mare, becoming more diffuse into the highland regions, supporting this interpretation.

The Rimae Bode sinuous rille lies to the south of the Rima Bode LPD. The Rimae Bode sinuous rille and lava flows from the rille are separated from the Sinus Aestuum lavas to the west by a continuation of the highlands ridge / montes (mountains) from the north. This highlands area appears to be covered with a pyroclastic mantling (as indicated by the yellow coloration in the RGB composites in Figure 19a), but the Rimae Bode rille and lavas and do not demonstrate a strong glass signature, indicating that they are not mantled by pyroclastic material from the regional LPD. As the pyroclastic deposit does not mantle the rille or rille lavas, this indicates the Rimae Bode rille is stratigraphically younger than the Rima Bode LPD.

We present a composite of images from three band parameters – the glass, orthopyroxene, and clinopyroxene band parameters in the red, green, and blue channels, respectively. The majority of the LPD is yellow, indicating a mixture of glass and orthopyroxene. Distal parts of the LPD, especially regions on the western mare side, have more pink, indicating less pyroxene and a stronger glass signature. North of an unnamed fissure within the Rima Bode LPD (highlighted in the inset in Figure 19b) is a pyroclastic mantling region that is noticeably greener than the rest of the LPD. This greener area would indicate less glassy material and more orthopyroxene,

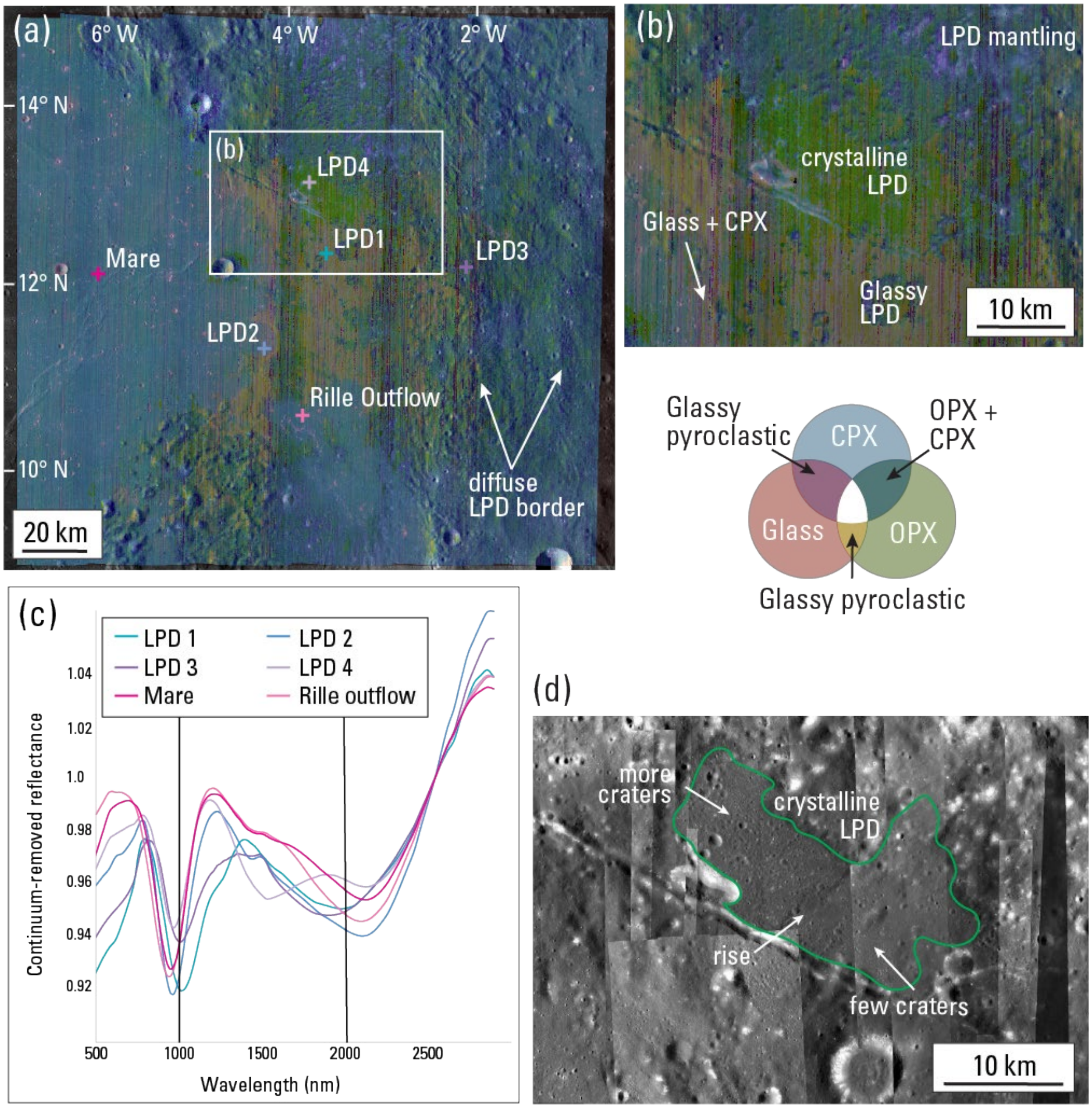

Figure 19: Results from Rimae Bode region (a) RGB composite of Rimae Bode region where the red channel is the glass band parameter map, the green channel is the 1 µm band center, and the blue channel is the 2 µm band center. (b) Inset of northern part of the Rima Bode LPD region in the M^3 mosaic with mineralogy labeled. Below (b) is a color interpretation of the RGB composite colors (c) Continuum removed spectra from sampling locations indicated in (a), vertical lines indicate 1µm and 2µm wavelengths. (d) Close-up of the green crystalline area showing the difference in cratering above a topographic rise and below from LROC NAC.

potentially comprising a more crystalline component than the rest of the LPD. Much of this green area is distinct in the number of apparent impact craters on the surface, and the eastern half of the green has fewer craters in the M^3 mosaic. This observation would be consistent with the eastern area being visible pyroclastic mantling, resulting in more loosely compacted regolith and lower crater retention properties and the western area being a more cohesive lava flow or consolidated spatter with mare-type crater retention rates (Lucchitta and Sanchez, 1975b). However, since both the eastern area with few craters and the western area with many craters are green in the RGB map, it appears that both have a compositional similarity, and these regions have a complex eruptive history.

Sulpicius Gallus LPD (4,322 km^2, Figure 20) is a regional LPD on the southwestern margin of Mare Serenitatis, previously identified as a “black spot” (Pieters et al., 1973). Orange and red soils were observed from the Apollo 17 Lunar Module around small craters and rimless depressions in the Sulpicius Gallus area (Cernan et al., 1972). One of the M^3 images in this region has an inconsistent signature, shown in Figure 20a. We interpret this behavior to be an instrument anomaly, and we do not use spectra from this image for any scientific interpretations or comparisons. We don’t include this instrument anomaly in the RGB composite in presented in Figure 20b but do show it in Figure 14. We present spectra from Figure 20a in Figure 20c to demonstrate the effect this has on comparing across inconsistent images. The unsmoothed spectra of LPD 2 (within the anomalous image) have greater noise rate than other spectra sampled in this region, and the unusually broad 1 μm absorption feature does not have a mineralogical or compositional cause.

The Sulpicius Gallus LPD has elevated signatures in the glass band parameter map, and in spectral analysis, LPD 1 (an area expected to have the most well-defined pyroclastic signatures) had a well-defined shoulder and had a 1-µm band center shifted to longer wavelengths, which would be indicative of pyroclastic material. The "Margin" spectral location in Figure 20c had decreased asymmetry at 1 µm (i.e., no shoulder) and the 1-µm band center was shifted to shorter wavelengths, demonstrating decreased pyroclastic signal and increased mixing. These locations were also distinct from mare materials, which was highlighted in the RGB composite map (Figure 20b). Two pyroclastic deposit types were highlighted in this area, each with distinctive two characteristics: a glassy component mantling the mare margin (LPD 1 in Figure 20a), and a crystalline/mixing component dispersed on the highlands above the mare (LPD 2 Figure 20a). These can be distinguished by their colors in the RGB composite maps – the glassy pyroclastic material is yellow, pink, or magenta, and the crystalline pyroclastic material or pyroclastic material that is mixing with highland regolith is green or teal. The LPD demonstrates a stronger glass signature when mantling the mafic mare lavas than when dispersed or mixed within the anorthositic highlands. This pattern was also observed with the Rima Bode LPD, both LPDs in each of these regions having a lower glass signature in the RGB composite when mantling highlands than when mantling mare.

The fresh impact crater sampled in the mare region had an RGB signature of a pyroclastic deposit (see Figure 19 for reference) with a strong glass signature and a small amount of clinopyroxene mixing. Based on the observations from the Apollo 17 crew that many of the small craters in this area were observed to have orange, tan, and red material around the rims, we could not exclude the possibility that these small craters may have exhumed pyroclastic glass from below during impact (Lucchitta & Schmitt, 1974).

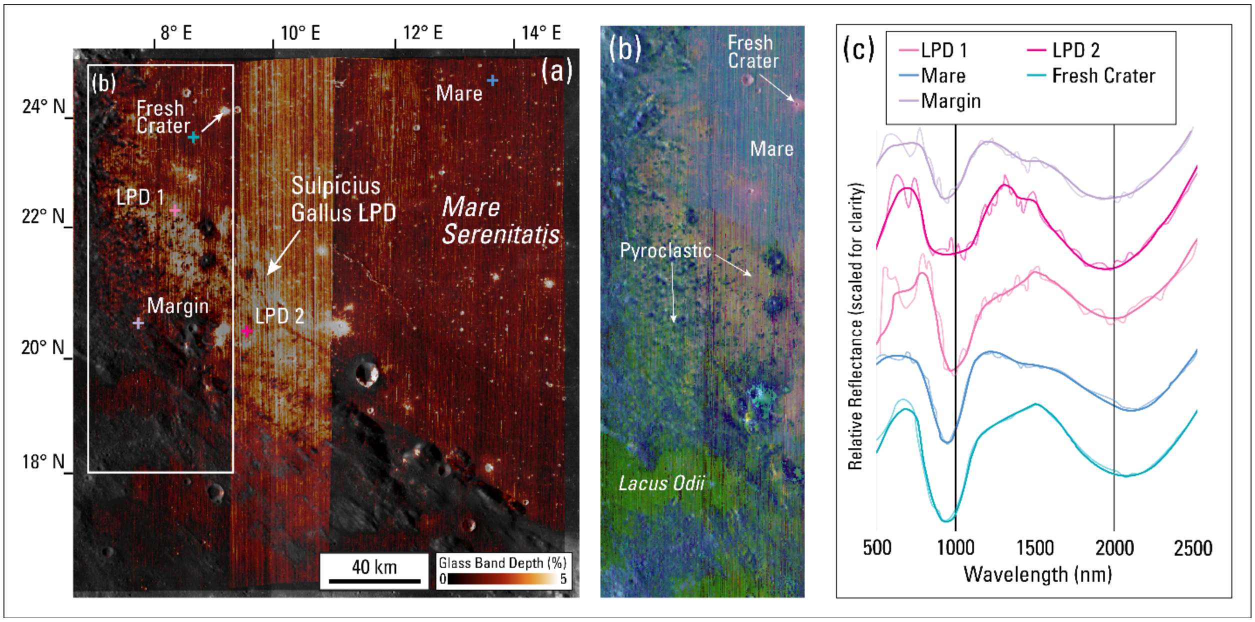

Figure 20: Results from Sulpicius Gallus region (a) Glass band parameter map for Sulpicius Gallus region with inset (b) further evaluated in RGB composite (b) RGB composite of western portion of Sulpicius Gallus deposit where the red channel is glass band parameter, the green channel is the 1-µm band center, and the blue channel is the 2-µm band center (c) Continuum removed reflectance (smoothed in foreground and unsmoothed in background) spectra of ROIs indicated in (a) and (b), offset to show clarity – black vertical lines mark the 1-µm and 2-µm locations. *LPD 2 was included to demonstrate spectral variation within images of different optical periods.*

3.5.3 Other LPDs in the Montes Apenninus Region

Beer LPD is a localized (623 km^2; Gaddis et al., 2003) pyroclastic deposit situated on the Apennine Bench (Figure 21). Relative to the background, there is little signal in the glass band parameter map (Figure 21b). This observation is also consistent with the spectral analysis as none of the spectra in these regions had significant asymmetry in the 1-µm band region and the spectral contrast was overall low. The strength of these absorptions, when compared to mare spectra near this LPD, is generally weak indicating that this could be a diffuse crystalline LPD or the spectral contrast is reduced due to significant space weathering and impact gardening. This LPD is situated on the Apennine Bench (the only LPD in the Montes Apenninus study region fully on the Apennine Bench), which comprises highland composition of weak 1-µm and 2-µm signatures characteristic of significant plagioclase contribution to the spectrum relative to other minerals (e.g., pyroxenes and magnesian minerals).

The Beer LPD has fewer small craters than the surrounding region, which is typical of the unconsolidated nature of LPDs (Lucchitta and Sanchez, 1975b), which would suggest less space weathering. The deposit appears to be smoother in texture than the highland materials of the Apennine Bench, but no source vent was identified by mineralogical distribution or by a search for a morphological vent structure. The darker material of the Beer LPD stands out on the lighter highlands of the Apennine Bench, but the LPD is higher in albedo than the regional deposits evaluated. No obvious effusive feature was identified near the regions with lower albedo and suppressed topography.

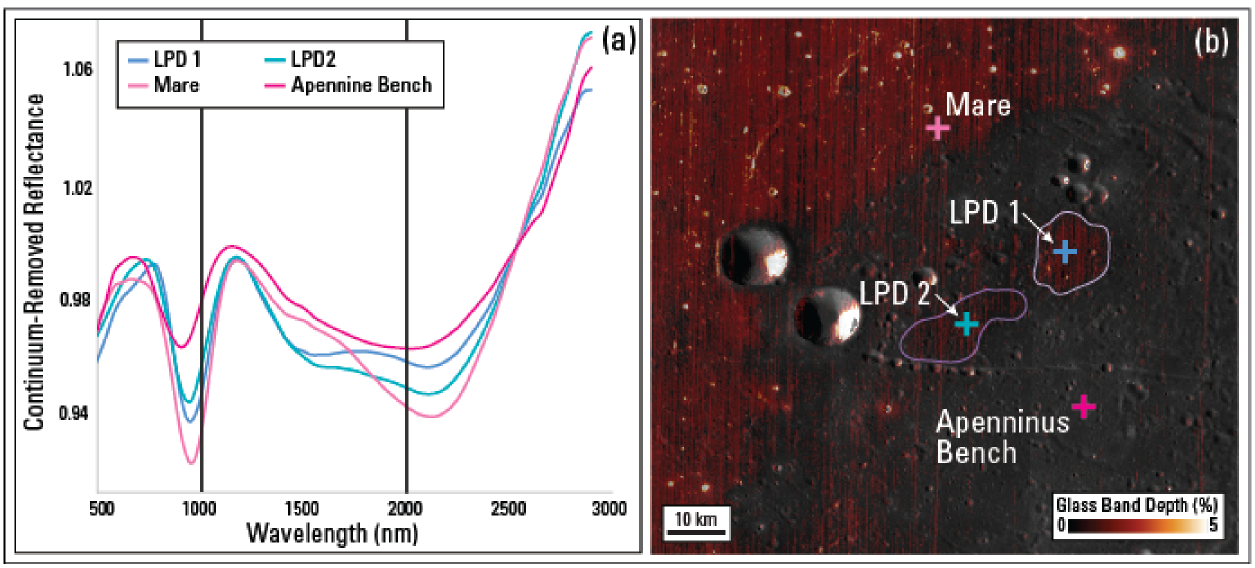

Figure 21: *Results from Beer region (a) Continuum removed reflectance spectra of the locations indicated in (b), black vertical lines indicate 1-µm and 2-µm wavelengths. (b) Beer region in glass band parameter map derived from M^3, overlain on WAC Basemap. Purple outlines indicate areas with highest signature of glass and outline the probable extent of the Beer LPD.*

Mons Huygens LPD is a very small localized (~10 km^2) pyroclastic deposit at the base of the Montes Apenninus (Hawke et al., 1979; Figure 22). Although many regions in this area have possible glass signatures in the map, spectral analysis of many of these regions reveals some of these are slope effects: the non-smoothed or continuum removed spectra have significant noise and smoothed/continuum removed spectra have absorption features that do not have correlations to minerals expected in these rocks. Our evaluation of the extent of the Mons Huygens LPD is consistent with the original estimates of the areal extent from literature (Hawke et al., 1979a). Similar to Mozart DMD, the Mons Huygens LPD deposit does not demonstrate the low albedo of most LPDs and spectra indicate that a strong observable asymmetry at 1 µm indicative of glassy material was not observed. No vent structure was readily apparent, but this area is characterized by uneven terrain, as demonstrated by the high frequency of false positives in the glass signature map (e.g., slopes greater than 30°, topographic shadowing, and noise effects; see Section 3.3 for additional information about identifying slope effects).

It is important to note that this deposit was identified to be on highlands in prior literature (Hawke et al., 1979a), which would be an area that would not have any observable signature in the glass band parameter map. As observed in this region, the only areas within the highlands that are not background colors are on high slopes, indicating that these glass detections are false positives due to slope effects (see Section 3.3 for additional information about identifying slope effects). As this LPD location does have a moderate signature in the glass band parameter map and is yellow in the RGB composite (similar to the Rima Bode LPD in the same RGB color composite), this could indicate that there is a pyroclastic deposit present that is masked by crystalline material or has been heavily impact gardened. The glass signature of the LPD is similar to that of the adjacent mare region but different in composition, so as it is situated on the elevated mons/montes, it is unlikely these materials were emplaced together. This is also supported by the spectra, as the mare and LPD spectra have distinct shapes and band center locations.

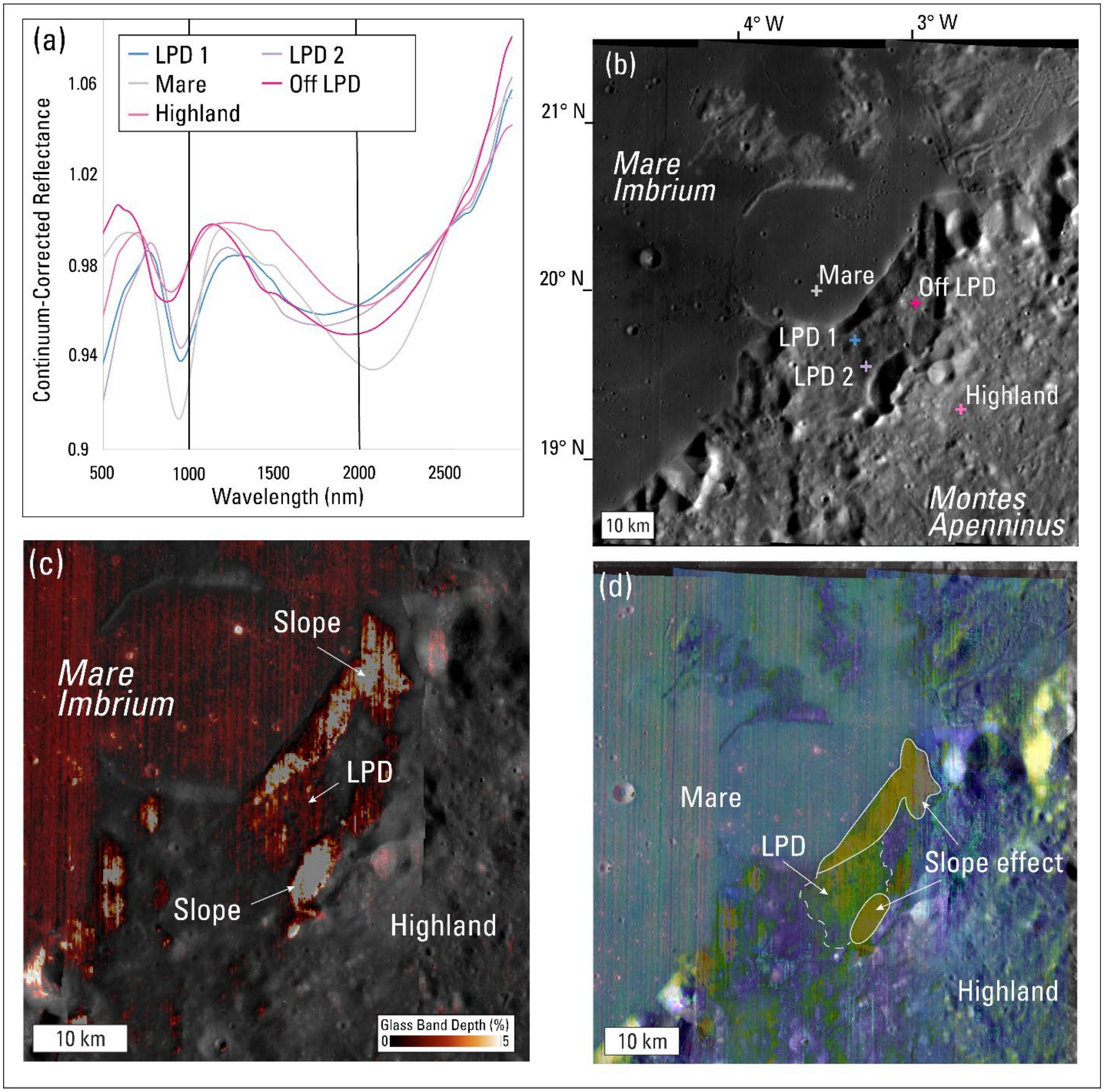

Figure 22: Results from Mons Huygens region (a) Continuum-corrected reflectance spectra of regions of interest indicated in (b) – black vertical lines mark the 1 µm and 2 µm locations; (b) Albedo mosaic (2856 µm, channel 82) from M^3 of the Mons Huygens region with spectral locations identified; (c) Mons Huygens region in glass band parameter map derived from M^3, overlain on WAC Basemap. Note some high glass signatures in this region are associated with steep slope faces. (d) RGB composite of Mons Huygens region where the red channel is the glass band parameter, the green channel is the 1µm band center, and the blue channel is the 2µm band center. Note saturation of yellow where slope faces are, and greener areas demonstrating mineralogical distinction of the LPD from the adjacent mare.

Mare Vaporum LPD is a regional LPD (4,129 km^2) located within the interior of Mare Vaporum. This LPD has been previously identified as a "black spot" (Pieters et al., 1973) and although the majority of the deposit is within the Mare Vaporum basin, it is observably lower in albedo than the surrounding mare (Figure 23). The Mare Vaporum LPD does not have an identified vent structure, but a portion of the northwest region of the deposit appears to be embayed by mare lavas. Similar to the Rima Bode inferred vent in Sinus Aestuum, due to the distribution of pyroclastic materials and shape of the Mare Vaporum LPD (somewhat arcuate, with a core of concentration in the center of the arc and thinning mantle on the outside of the arc on the east), a possible vent structure from which the pyroclastic deposit was sourced may be located within the Mare Vaporum basin. This could indicate the vent structure was covered by mare lavas in later stages of volcanic activity after degassing of the magma chamber during long-duration volcanic eruption. The strength of the signal in the mare in the glass band parameter is similar to that of the pyroclastic deposit. However, investigating these two regions in the RGB composite (Figure 23), there is a distinct difference between the yellow pyroclastic deposit (similar to Rima Bode LPD) and the pinkish-blue mare. The Mare Vaporum LPD sampling locations had an observed asymmetry at 1 μm that could indicate this increased glass signature is from glass in the pyroclastic deposit. The spectrum from the proximal part of the deposit has a well-defined shoulder near the 1 μm region, suggesting increased glass than at the distal portion of the pyroclastic deposit.

The spectra of the mare region has very little observable shoulder or asymmetry at 1 μm that would indicate glass, and this detection in the glass band parameter map is more likely due to deepening of the band depth due to the shift of the 1 μm band to longer wavelengths. Almost no asymmetry at the 1-μm spectral band was observed at the lava flow location where lava from a channel spills out onto the mare basin floor, indicating that although this feature has a low albedo even on the dark mare, it is unlikely to be of pyroclastic origin and is a lava flow.

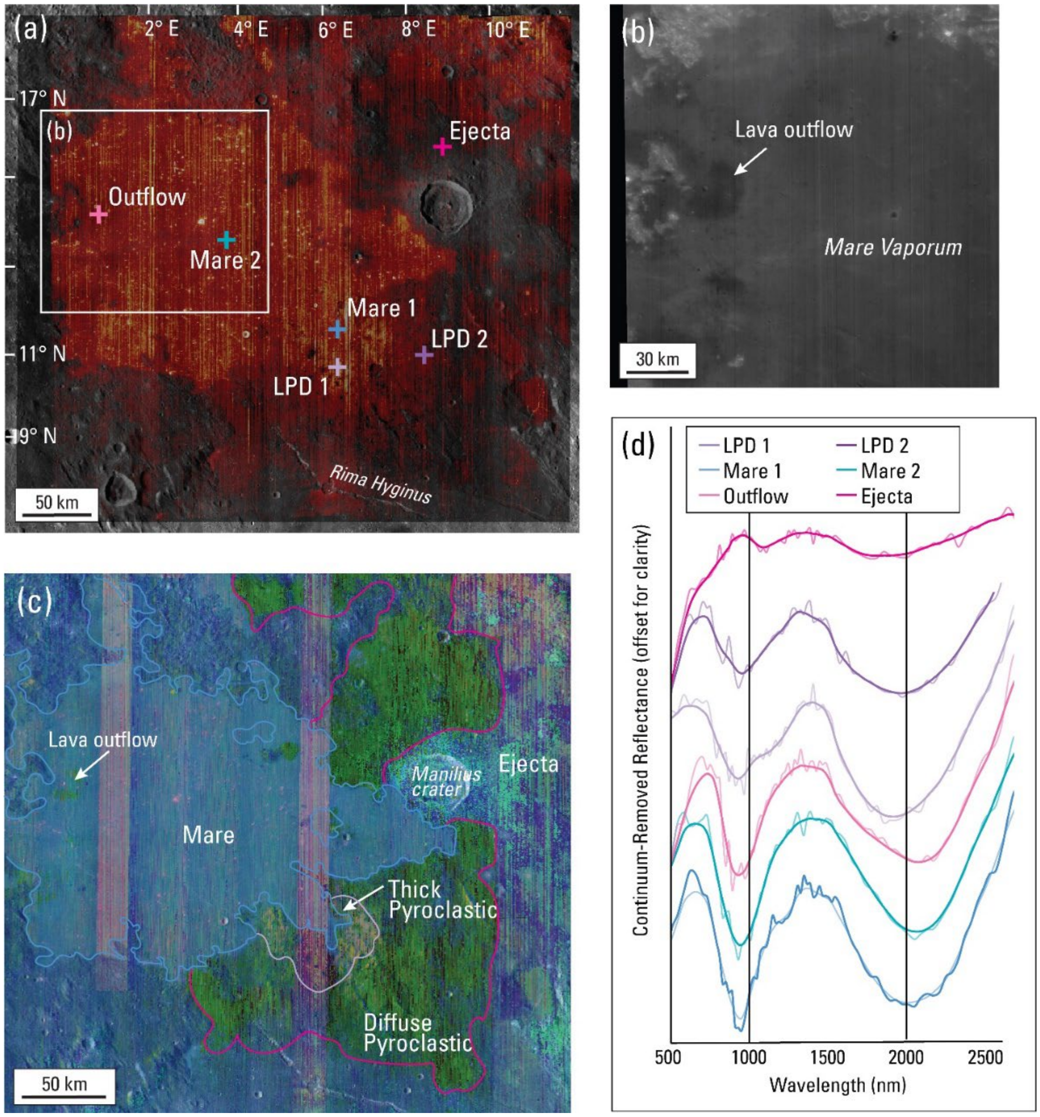

Figure 23: Results from Mare Vaporum region (a) Mare Vaporum region in glass band parameter map derived from M^3, overlain on WAC Basemap with spectral locations identified. (b) Albedo mosaic (2856 µm, channel 82) from M^3 of the lava flow region identified in (a); (c) RGB composite of Mons Huygens region where the red channel is the glass band parameter, the green channel is the 1µm band center, and the blue channel is the 2µm band center. Note saturation of yellow where slope faces are, and greener areas demonstrating mineralogical distinction of the LPD from the adjacent mare; (d) Smoothed and example of the unsmoothed, continuum-removed reflectance spectra of regions of interest indicated in (a) – black vertical lines mark the 1 µm and 2 µm locations.

3.6 Discussion

3.6.1 Previously unpublished LPDs

The spectral data suggest there are previously unidentified (or understudied) LPDs in the study area at several sites along Mozart Rille. Michael and Ann are identified as volcanic vents along Mozart Rille and exhibit characteristic asymmetry at 1 µm indicative of the presence of a mantle composed of glassy volcanic materials. These regions display strong contextual characteristics of explosive volcanism at a volcanic vent as the distribution of materials is mostly downstream of the lava channel and close to the vent. Kathleen is an irregular depression that appears to mark the initiation of the Mozart fissure (aka the "cobra head") and although has a signal in the glass signature map, spectra of this region do not show strong asymmetry at 1 µm indicative of glassy material. Ann is also an irregular shaped depression but is offset from Mozart Rille and is deeper than Kathleen, potentially representing a secondary vent in a buried fissure system. This mantling deposit appears to be pyroclastic in nature and has strong spatial relationships with Mozart Rille, suggesting contiguous eruption or eruption in phases along a fissure or linear vent system. This type of volcanism is commonly observed on Earth, such as the 2018 fissure eruption in Hawai‘i, with lava fountaining and lava flows occurring at multiple vents at different times along the 6.8 km fissure (Neal et al., 2019).

3.6.2 Mozart DMD

We find that that some LPDs do not exhibit the low albedo that was previously used to identify the LPD but still have spectral features characteristic of pyroclastic material. We observe this at Mons Huygens LPD but this has been noted elsewhere before (e.g., the Compton-Belkovich Volcanic Complex pyroclastics (Chauhan et al., 2015), SE Nectaris regional deposit, and Antoniadi pyroclastic cones (Sruthi and Senthil Kumar, 2014)). The Mozart "dark mantle deposit" was identified as a potential pyroclastic deposit in Hawke et al. (1979) and later as a "dark mantled valley" by Blewett and Hawke (2001) and was labeled as Mozart DMD for consistency in this work. This feature was not observed to have a low relative albedo in M^3 like the pyroclastic materials of the vents along Mozart Rille. In the glass band parameter map (Figure 16), this area had no 1 µm asymmetry and a very weak 1-µm absorption (which would be a combination of crystalline material and pyroxenes), indicating a very low chance of glassy pyroclastic material. M^3 spectra from this valley were also not consistent with spectra from other glassy pyroclastic deposits. The spectral signature at 1 µm is more consistent with highlands materials than pyroclastic emplacement, with a contribution from pyroxenes. This could indicate that if explosive volcanism was occurring at this location, the primary component was mostly crystalline and fragmented rock and a minor juvenile component.

3.6.3 Signature Strength and Mixing

The Beer LPD is another pyroclastic deposit that has a very weak glass signature compared to other LPDs in the study region, in addition to having spectral signatures similar to nearby mare. The Beer LPD is separated from the mare by the Apennine Bench formation and as the Beer LPD is not near a sinuous rille or other feature indicative of effusive volcanism. Weak glass signatures could indicate the presence of a thick eruption column, leading to the crystallization of minerals rather than quenching into glass; however, the Beer LPD also has weaker mafic signatures which would indicate that the deposit does not likely have a large component of pyroclastic material, glassy or crystalline.

Alternate explanations include a thin pyroclastic deposit, that the deposit has been heavily altered by space weathering or impact gardening, or that the eruption was Vulcanian with little juvenile material. If sourced from the same magma as the mare, then a crystalline deposit, from an optically thick eruption column that shields pyroclastic droplets from quenching would likely have a stronger mafic signature, similar to the adjacent mare. Without characteristic mineralogy of crystalline or glassy basaltic material in individual spectra, it does not appear that Beer is a crystalline deposit. In a study of the proportion of juvenile to non-juvenile components of 23 localized LPDs, Keske et al. (2020) found that the sampled LPDs can contain a range of juvenile proportion from 0% − 100%, depending on factors such as geologic context, vent morphometry, and volatile content. As no vent was identified, we are unable to calculate the juvenile proportion using these methods, but there would be the potential that this is an eruption with a low proportion of juvenile material.. Lastly, even well-characterized LPDs have reduced signature strength at the distal parts of the deposit as thinner parts are mixed with underlying substrate due to impact gardening and spectral contrast is reduced due to space weathering. Many of the spectral features of the LPD appear to be an average between the Bench materials and the adjacent mare (i.e., crystalline basaltic mineralogy), with higher contributions from basaltic signatures (e.g., 1-μm and 2-μm band centers shifted to higher wavelengths). As this deposit does not demonstrate strong absorptions, it is plausible that it is a thin pyroclastic deposit with a moderate to high non-juvenile component that has been heavily space weathered.

3.6.4 Relationships between effusive and explosive volcanic features on the Moon

Localized LPDs identified in the Mozart region demonstrate a strong connection between explosive and effusive eruptions. Multiple LPDs (Kathleen, Ann, and Michael) lie alongside Mozart Rille and each has a stronger glass signature on the downstream portion of the depression, demonstrating a structural connection between the erupting pyroclasts and the flow of the rille. These strongly indicate multiple vents alongside a main rille as an effusive fissure eruption with localized lava-fountaining from these vents resulting in relatively small deposits. Spectral analysis of the Ann and Michael depressions show that they are spectrally consistent with LPDs. The explosive eruption of these materials concurrently with the emplacement of Mozart Rille would be consistent with known fissure-type eruption mechanisms on Earth (Popa et al., 2021b). The three LPDs along a sinuous rille would be consistent with co-eruption of the rille with the pyroclastic eruption, indicating that explosive and effusive eruption was occurring in this location, likely at the same time.

The vent location of the Rima Bode LPD can be inferred from the distribution of glass and pyroclastic material, emanating from a central location within Sinus Aestuum (Gaddis et al., 1985). Given that lavas from Rimae Bode appear to embay the pyroclastic materials (Figure 19) and there may be a vent that sourced the LPD in the adjacent mare (Gaddis et al., 1985) on the opposite side of the LPD from the rille, it is unlikely that the rille is directly connected with the Rima Bode LPD. The Rimae Bode rille lavas to the southeast and the Sinus Aestuum mare lavas to the west (unrelated effusive volcanic events) both stratigraphically overlie the Rima Bode LPD. This suggests a complex stratigraphy of effusive and explosive volcanic emplacement in this region, as the Rima Bode LPD was emplaced prior to the Sinus Aestuum mare infill, but also prior to the emplacement of the Rimae Bode sinuous rille lava flows.

In contrast, the Fresnel LPD is evenly distributed and does not appear to have a concentrated glass region that could be used to indicate a vent location. As the Fresnel LPD mantles the central portion of Rimae Fresnel and the surrounding region, (and not where the flow originated), it is unlikely the explosive eruptive activity was occurring from the same vent as the effusive flow. If the explosive and effusive volcanism were happening concurrently, the LPD would be expected to mantle only a portion of the rille (as seen with the LPDs along Mozart rille) or would mantle the northern or southern extent of Rimae Fresnel, from which the rille lavas originated. Because the pyroclastic deposit is observed to mantle the rille and surrounding region with no structural relationship to the effusive flow, and there is no clear spatial relationship between a potential vent, the rille, and the LPD, these results suggest that the LPD was emplaced after the rille flow, and that they were likely not sourced from the same vent. Therefore, the eruption that resulted in the deposition of the Fresnel LPD is unlikely correlated to its namesake fissure.

The glass signatures around Rima Hadley extend into mare materials of Palus Putredinis with a similar strength to the areas around Rima Hadley. We hypothesize that either the explosive materials of around Rima Hadley and the effusive materials of Palus Putredinis are from the same eruption, or Palus Putredinis is mantled by pyroclastic material. The glassy signature is observed almost all the way around the base of the mounds to the west of Rima Hadley and does not appear to mantle low mounds between Rima Hadley and Palus Putredinis. This would be inconsistent with pyroclastic eruption, which would have likely mantled the low mounds because pyroclasts in this high volume of eruption would have been able to reach these elevations. Either spatter melt could have flowed around the mounds and into Palus Putredinis, or there could have been multiple eruptive events that contributed to the strong glass signatures in this area.

These data indicate that the compositional and stratigraphic relationships between explosive and effusive features cannot be generalized in the Montes Apenninus region. In some locations, there is evidence for both effusive and explosive activity from one vent (along Mozart Rille), as is often observed on Earth. In other locations, explosive and effusive activity are co-located but are shown not to be sourced from the same vent. Of these examples, sometimes the stratigraphically youngest deposit is the effusive deposit(s) (e.g., Rima Bode), and sometimes it is the explosive deposit (e.g., Rimae Fresnel). Each of these scenarios has unique implications for the volcanic history of the location, and therefore detailed analyses are required to interpret the volcanic history of the region, the volatile evolution of the local magma (and therefore potential trapped volatiles of the minerals and glasses), and the potential resource use of materials based on composition and physical properties.

3.7 Conclusion

We evaluated the presence, distribution, and composition of several regional and localized equatorial LPDs. We showed that the compositional and stratigraphic relationships between explosive and effusive volcanic features cannot be generalized in the Montes Apenninus region. Instead, the LPDs have a full diversity of temporal and spatial relationships with nearby effusive features. Pyroclastic deposits evaluated in this study demonstrate a range of glass distribution and stratigraphic relationships with effusive features. One previously identified pyroclastic deposit, Mozart DMD, did not demonstrate characteristic glass signatures or a low albedo using this dataset. However newly identified LPDs (e.g., along vents along Mozart Rille) can be recognized where previous studies using lower spectral and spatial resolution datasets could not confirm an LPD. We also observed explosive volcanic deposits around vents along Mozart Rille, demonstrating an instance where explosive and effusive volcanism was likely occurring at the same vent. The relationship between effusive and explosive volcanism is not commonly evaluated but is an essential component of the eruptive history of a locality.

3.8 Data Availability Statement

The M^3 L1B and L2 data are available on the Planetary Data System (PDS) Cartography and Imaging Node: https://pds-imaging.jpl.nasa.gov/portal/chandrayaan-1_mission.html. The LROC WAC Basemap is available at this link: https://astrogeology.usgs.gov/search/map/Moon/LRO/LROC_WAC/Lunar_LRO_LROC_WAC_Mosaic_global_100m_June2013. LROC NAC screenshots were obtained from the LROC

Quickmap at https://quickmap.lroc.asu.edu. The M^3 processed mosaics (raw, continuum-removed, and continuum-removed and smoothed spectral cubes) and associated metadata used for the analysis in this study are available at (Pigue et al., 2023). The mosaics include the Band 82 albedo image, 1-µm and 2-µm band parameter maps, glass band parameter map, and ASCII files of all spectra presented in this manuscript. For software, see Horgan et al., 2014 and Bennett et al., 2016.

3.9 Acknowledgements

This work was supported by funds from the NASA Lunar Data Analysis Program, via Inter-Agency Transfer to the USGS under the Grant Submission Number 18-LDAP18_2-0028. Any use of trade, firm, or product names is for descriptive purposes only and does not imply endorsement by the U.S. Government.

We would like to thank Schuyler Borges and Christian Tai Udovicic for very helpful reviews on early versions of this manuscript and members of the INF 604 class at NAU for providing thorough feedback. We also appreciate helpful reviews from Laszlo Kestay, Lillian Ostrach, Janet Richey, and Tenielle Gaither. Thank you also to Christopher Edwards and the PIXEL group for support.

3.10 Supplementary Materials

3.10.1 Table 4: M^3 images used in processing and their optical periods

Image ID	Optical Period
m3g20090106t152345	OP1A
m3g20090108t044645	OP1A

m3g20090109T022525	OP1A
m3g20090205t225833	OP1B
m3g20090205t211213	OP1B
m3g20090205t013151	OP1B
m3g20090204t234545	OP1B
m3g20090205t171614	OP1B
m3g20090205t190233	OP1B
m3g20090205t150614	OP1B
m3g20090206t010833	OP1B
m3g20090206t030351	OP1B
m3g20090206t050647	OP1B
m3g20090206t065053	OP1B
m3g20090206t084850	OP1B
m3g20090206t105850	OP1B
m3g20090206t124510	OP1B
m3g20090205t071411	OP1B
m3g20090202t064453	OP1B
m3g20090205t111013	OP1B
m3g20090205t131953	OP1B
m3g20090204t233457	OP1B
m3g20090205t074030	OP1B
m3g20090205t092400	OP1B
m3g20090205t113340	OP1B

m3g20090204t173931	OP1B
m3g20090204t152951	OP1B
m3g20090204t192552	OP1B
m3g20090204t134332	OP1B
m3g20090607t201038	OP2C
m3g20090607t153144	OP2C
m3g20090608t083142	OP2C
m3g20090608t042049	OP2C
m3g20090608t000122	OP2C
m3g20090607t193433	OP2C
m3g20090608t125102	OP2C
m3g20090608t083142	OP2C

3.10.2 Regions of interest (ROIs) that each spectral sampling point represents

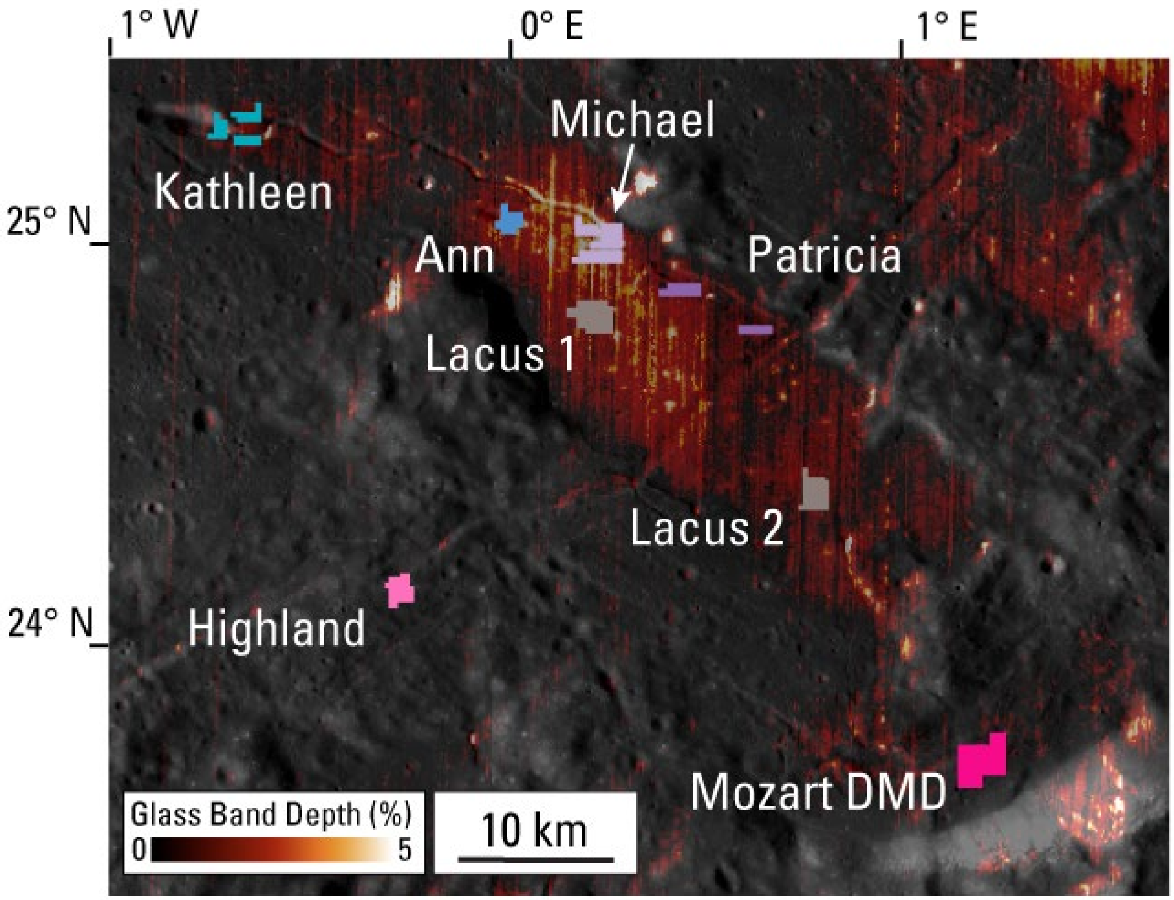

Figure 24 Supplementary Figure 1: True boundaries of the spectral regions of interest (ROIs) represented by the points in Figure 16.

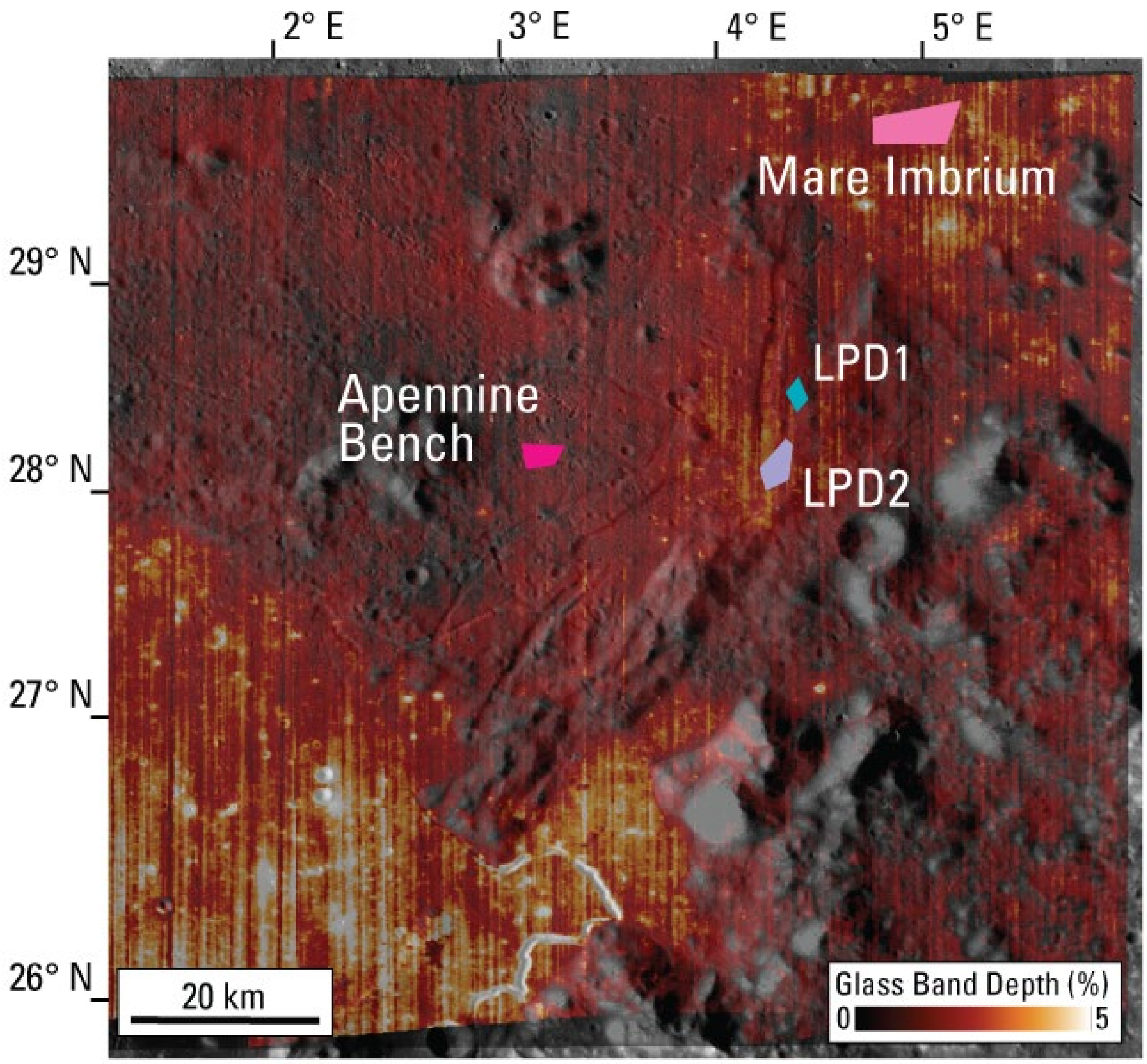

Figure 25: Supplementary Figure 2: True boundaries of the spectral regions of interest (ROIs) represented by the points in Figure 17.

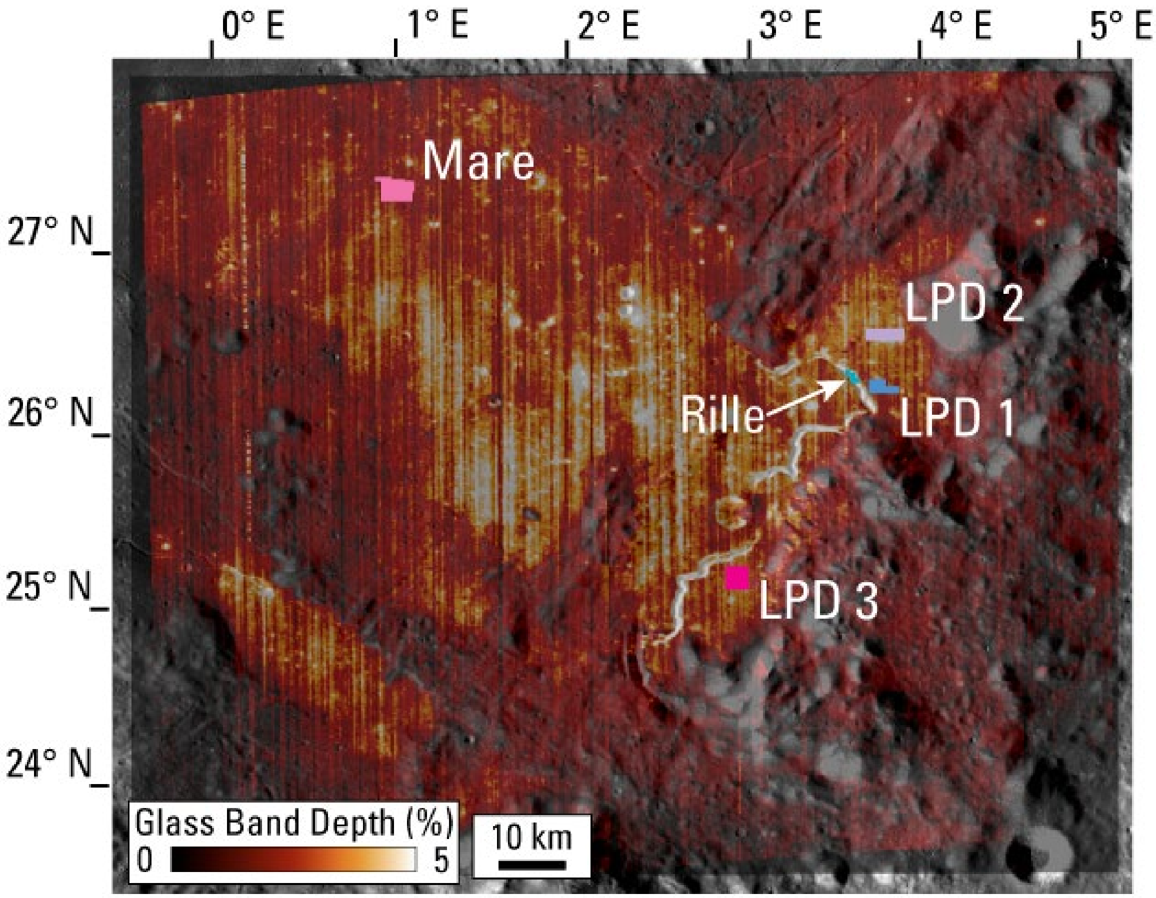

Figure 26: Supplementary Figure 3: True boundaries of the spectral regions of interest (ROIs) represented by the points in Figure 18.

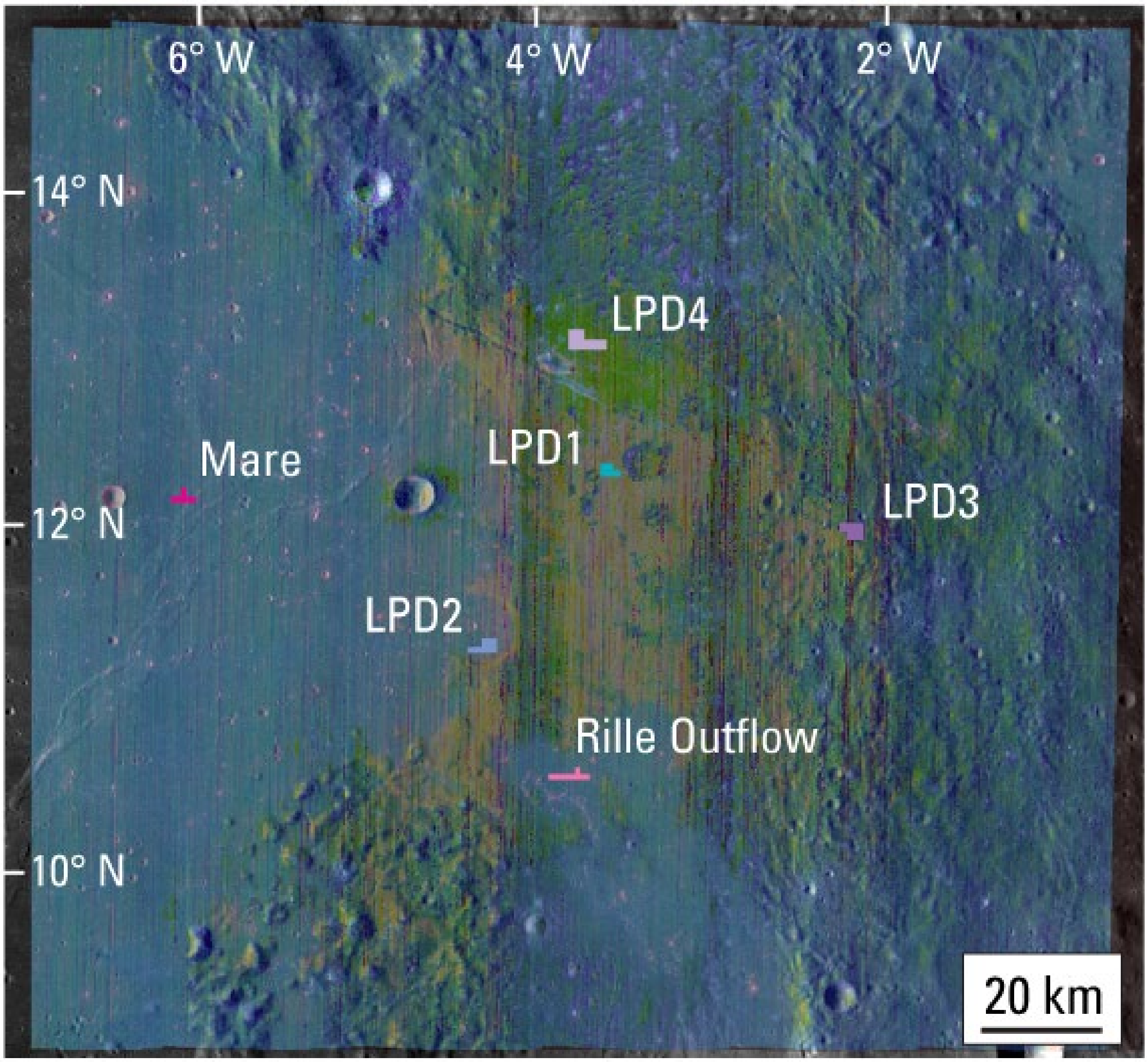

Figure 27: Supplementary Figure 4: True boundaries of the spectral regions of interest (ROIs) represented by the points in Figure 19.

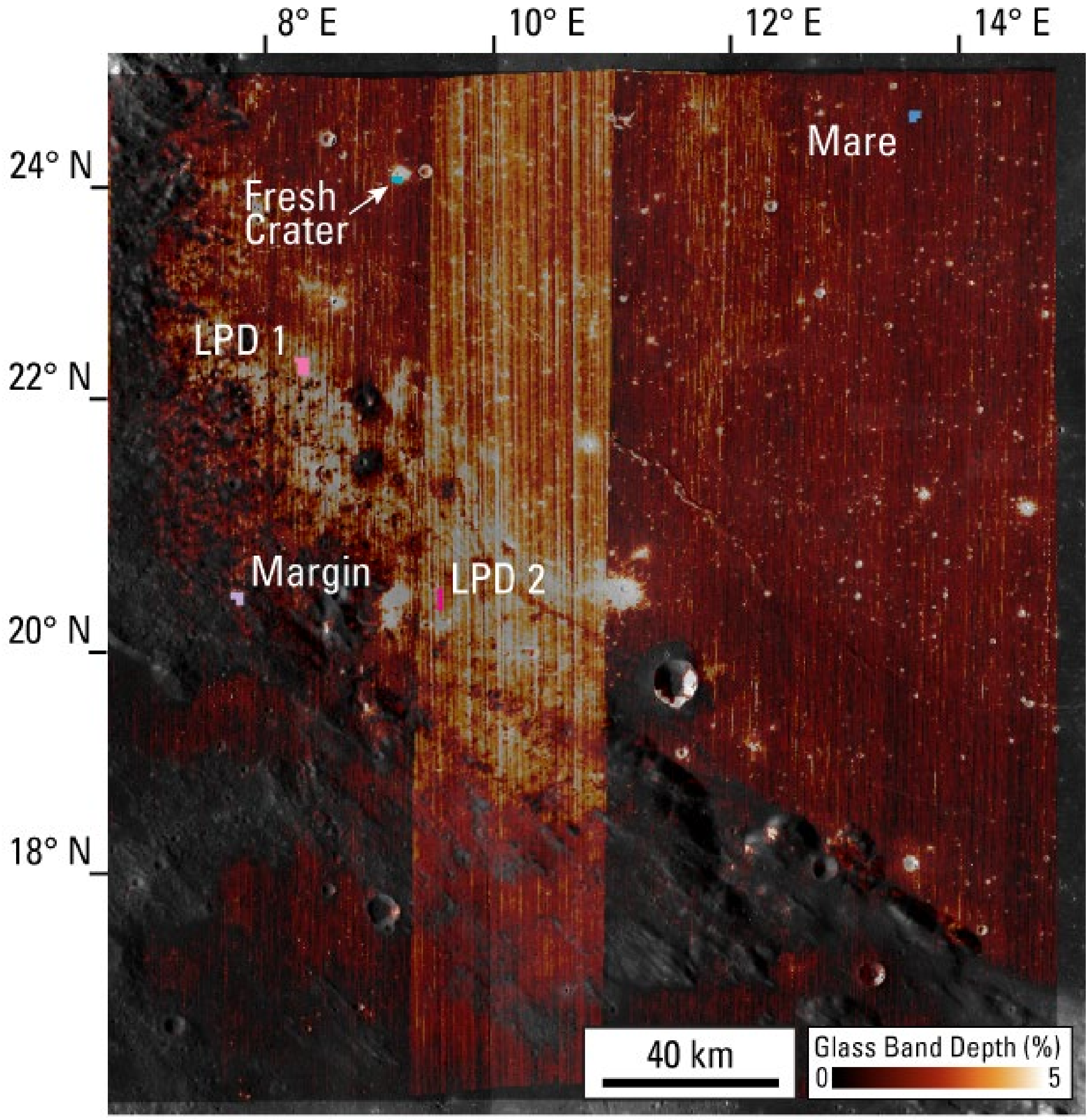

Figure 28: Supplementary Figure 5: True boundaries of the spectral regions of interest (ROIs) represented by the points in Figure 20.

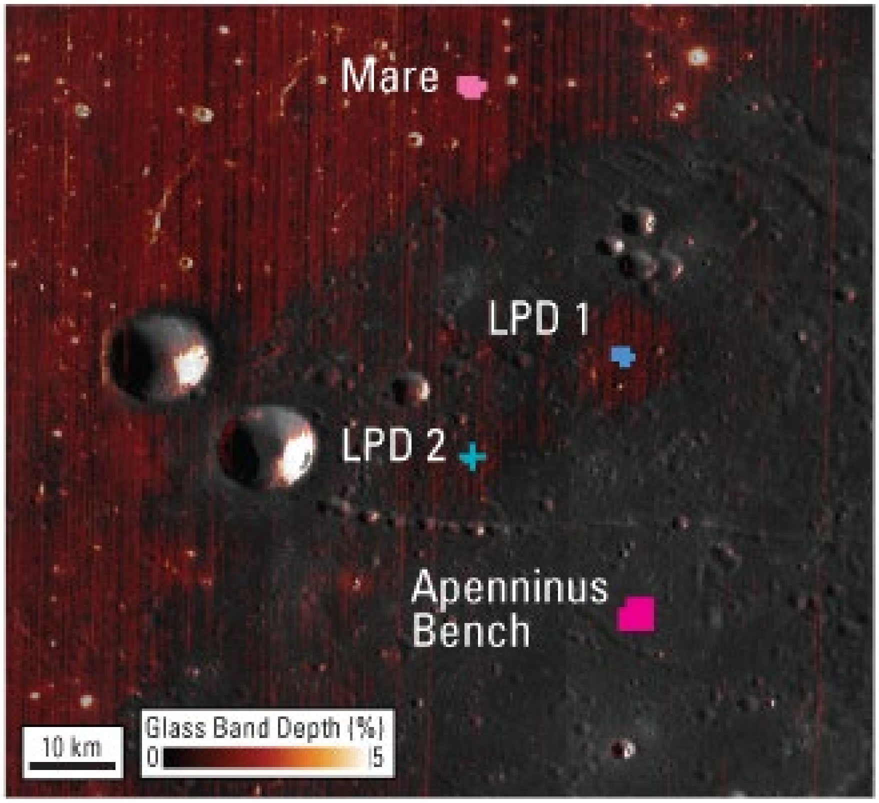

Figure 29: Supplementary Figure 6: True boundaries of the spectral regions of interest (ROIs) represented by the points in Figure 21.

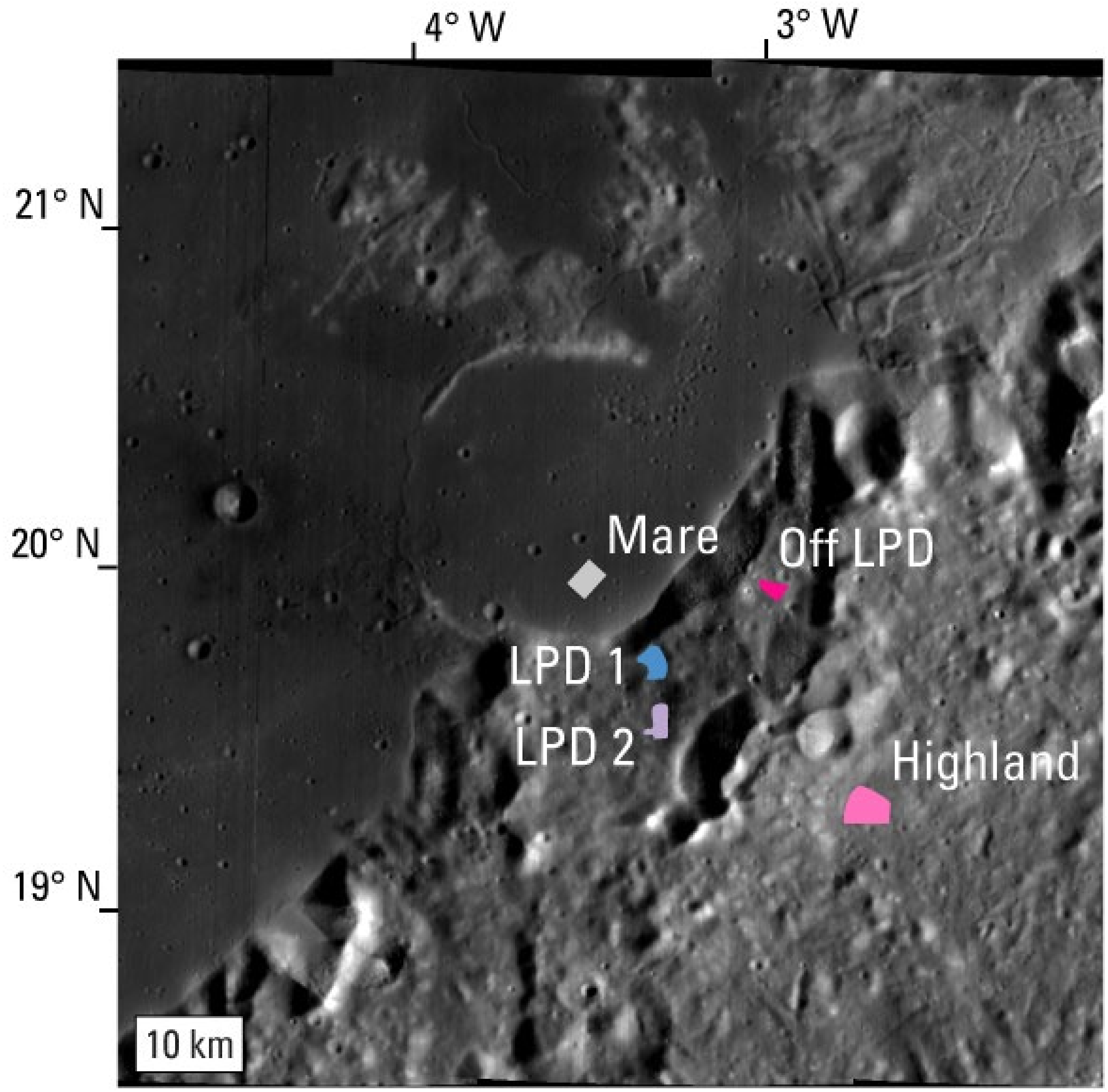

Figure 30: Supplementary Figure 7: True boundaries of the spectral regions of interest (ROIs) represented by the points in Figure 22.

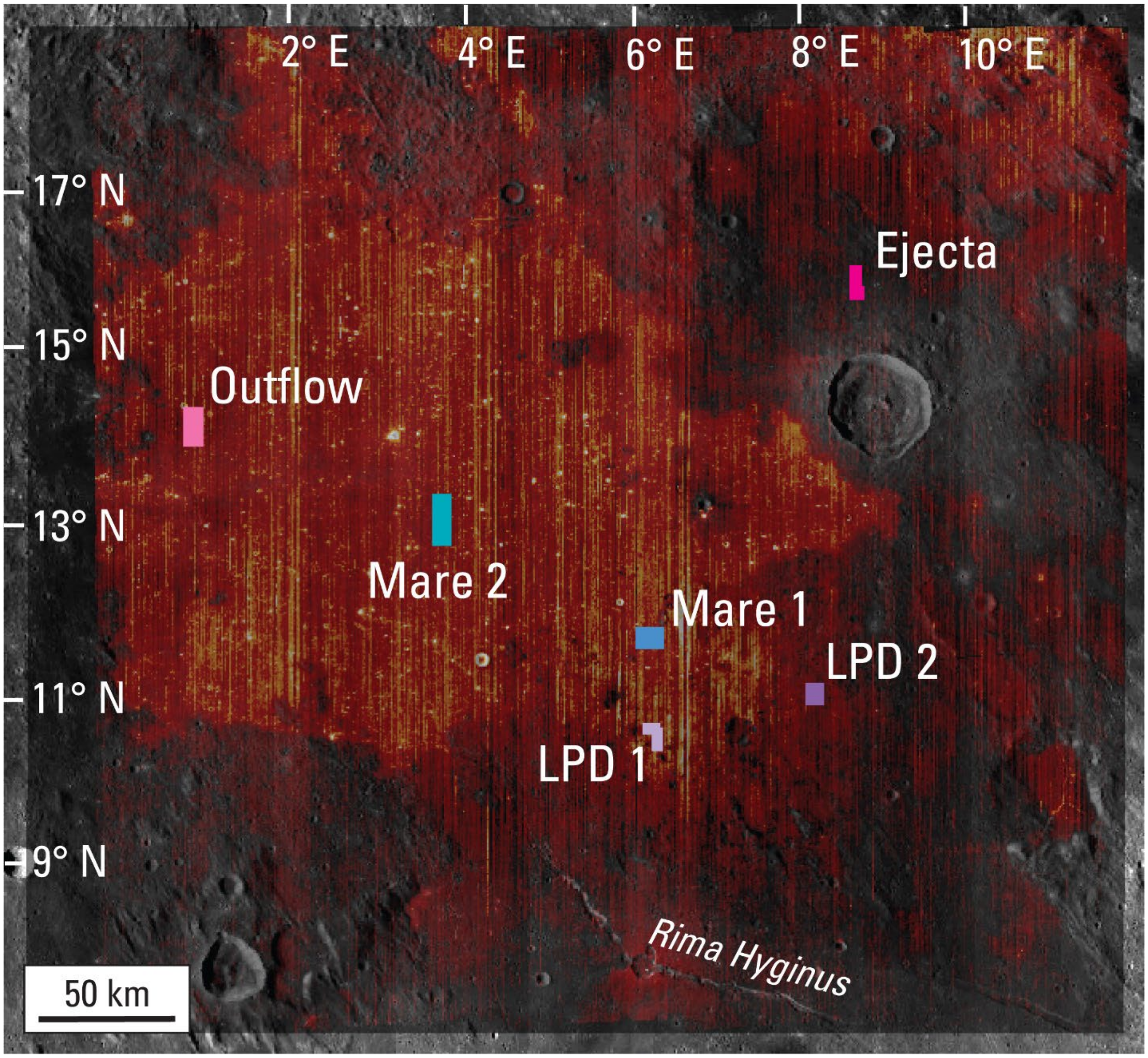

Figure 31: Supplementary Figure 8: True boundaries of the spectral regions of interest (ROIs) represented by the points in Figure 23.

Chapter 4: Varied volcanic history in Mare Vaporum revealed by thermal and thermophysical properties

Abstract

Volcanic features on the Moon often have variable thermophysical properties, owing to their emplacement style and volcanic textures. These volcanic features include lunar pyroclastic deposits which are remnants of explosive volcanism on the Moon, large basaltic plains called maria, channelized lavas within sinuous rilles, and the unusual volcanic irregular mare patches. The variability in physical properties can be tied to eruption styles and magmatic conditions, which can provide insight into the stratigraphic relationships and geologic history of a region. In investigation, we reveal thermophysical properties of volcanic features in the Mare Vaporum basin from the Diviner Lunar Radiometer Experiment (Diviner). Building on a hypothesis that volcanism on the lunar volcanism is similar to terrestrial volcanism (i.e., individual eruptive vents can have multiple eruptive phases and variable eruption types rather than following a linear progression or occurring separately), we create a geologic history of the Mare Vaporum volcanic deposits. We evaluate the complexities of relationships between various volcanic features in a region to understand lunar evolution and magmatic conditions more fully. We find that the pyroclastic deposit is partially covered by the mare lavas, as observed by the high contrast between the thermal and thermophysical properties between the mare and LPD. Further, the mare embays and covers the Manilius crater ejecta blanket, establishing a relative stratigraphic relationship within the basin. These stratigraphic relationships have revealed that Manilius crater must be older than a previously-reported Eratosthenian age, and that the Mare Vaporum LPD erupted prior to, or at the same time as the mare lavas.

4.1 Introduction

Surface temperatures of the Moon can provide an understanding of characteristic physical properties of materials (Bandfield et al., 2011; Hayne et al., 2017; Williams et al., 2017). These thermophysical properties can be used to evaluate the surface expression of volcanic deposits, which can be related to their eruption styles and eruption conditions. Lunar Pyroclastic Deposits (LPDs) are the products of explosive eruption that blanket the underlying features of the lunar surface (Gaddis et al., 2003; further developed in Chapter 2). Variability of block content of a pyroclastic deposit can reveal the eruption style of an LPD (e.g., Bennett et al., 2016; Carter et al., 2009). Contrasting explosive deposits are effusive volcanic features, those which flow out onto the surface. These have many manifestations on Moon, including mare flood basalts, channelized flows such as sinuous rilles, individual flow lobes often related to these features, and is one of the potential formation mechanisms of irregular mare patches (Elder et al., 2017). Compositional and visual datasets often only probe the top few microns of regolith and miss critical subsurface and near-subsurface physical properties that can reveal less space-weathered and reworked materials as well as properties such as block content. From the Diviner Lunar Radiometer Experiment (Diviner) dataset, we highlight several volcanic features in the Mare Vaporum region (Figure 32) that display variations in temperatures, rock abundance, relative thermal inertia, and albedo that result from varied emplacement styles and subsurface conditions (i.e., composition and volatile content Bennett et al., 2016; Elder and Hayne, 2017; Ghent et al., 2014; Williams et al., 2022). We use the varying thermophysical properties of lava flows, LPDs and other volcanic features that we observe to (1) identify different volcanic features in the Mare Vaporum region and describe their thermophysical properties, (2) interpret how the volcanic units were emplaced based on our observations and (3) interpret the stratigraphic relationships of the units to infer a geologic history of the Mare Vaporum region.

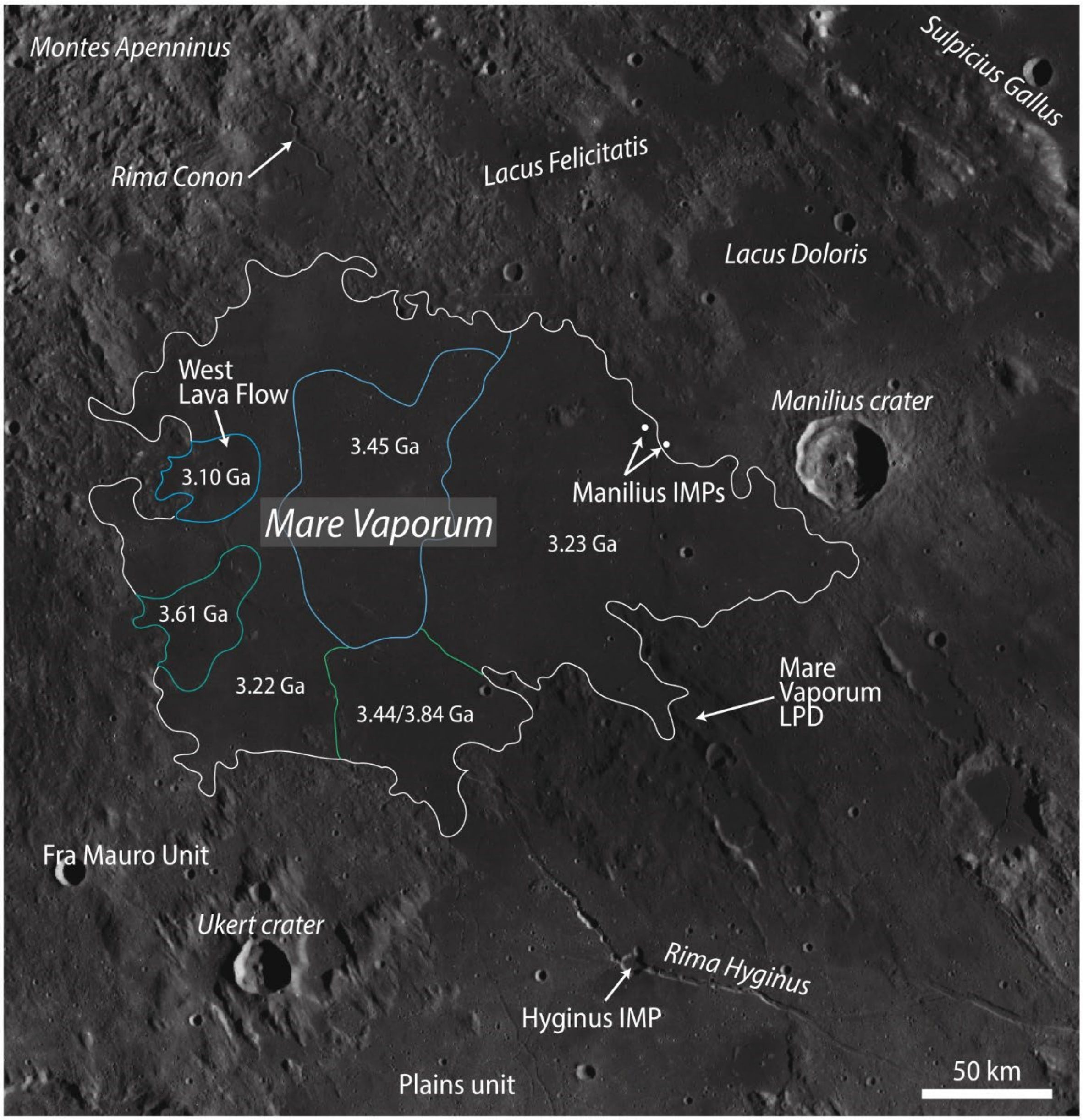

Figure 32: Mare Vaporum study region in WAC-big shadows. Features assigned formal names are italicized, features assigned informal names are not italicized. Mare age dates are from Hiesinger et al., (2011), unit formation names are from Fortezzo et al., (2020).

Although the lunar regolith demonstrates broad uniformity in terms of regolith characteristics (Hayne et al., 2017) and temperature cycles (particularly in this study region; Vasavada et al., 2012) at the global scale, subtle differences in temperatures between geologic features have been noted resulting from variations in albedo, grain packing, and rock abundance. These differences are targeted here for further investigation and comparison between features within the Mare Vaporum basin. Mare basalts are often low in albedo, but not as low as many pyroclastic deposits. Highlands plains are often high albedo, and this contrast can often be used to delineate compositional boundaries. Variable surface features such as these, especially on localized scales, can be broadly characterized by their maximum and minimum temperatures and by thermophysical properties derived from these, especially where factors like albedo and rock content contribute to anisothermality within a detector's field of view (Bandfield et al., 2015; Ghent et al., 2014). Daytime maximum temperatures are sensitive to the albedo of the surface and to the thermal inertia of the material (Williams et al., 2017). Higher minimum nighttime temperatures result from materials that retain their heat during the course of a cooling cycle such as darker rocks (e.g., mare), and lower minimum nighttime temperatures indicate materials that are unconsolidated and have a low thermal inertia such as pyroclastic deposits and fluffy regolith.

The Mare Vaporum basin was formed over 3.6 Ga from a large impact and a mare basin infill event (Hiesinger et al., 2010). Since this time, the basin has been active with a variety of volcanic and non-volcanic processes acting within the region including explosive volcanism (i.e., emplacement of the Mare Vaporum, Rima Conon, and Rima Hyginus LPDs), effusive volcanism (evidenced by several mare flood basalts, lava flow lobes, and sinuous rilles), formation of the Rima Hyginus and Manilius-1 and Manilius-2 irregular mare patches, and a range of impact craters including at least one cold spot crater and the ~35 km diameter Manilius crater. The formation of both explosive and effusive volcanism in this basin demonstrates a range of magma compositions and/or subsurface storage conditions, leading to the eruption of a variety of volcanic features. One of the main differences between effusive and explosive volcanism on the Moon is related to volatile content; explosive volcanism requires a relatively volatile-rich eruption whereas effusive activity is thought to be relatively volatile-poor (Wilson and Head, 2018). The complex relationships between explosive and effusive features at a site relate directly to subsurface volatile inventory and magmatic evolution. The degassing of explosive eruptions can transition the event to an effusive flow, indicating a change in the volatile inventory of the erupting magma chamber (e.g., Barnes et al., 2019; Popa et al., 2021b). Conversely, an infusion of new magma from the lunar interior or a change in magma properties via melt fractionation can transition an effusive flow into an explosive eruption (e.g., Cassidy et al., 2018).

Explosive volcanic deposits demonstrate a range of surface characteristics, related to the subsurface plumbing conditions at the time of eruption. The physical properties of volcanic deposits can be linked to eruption styles, used to identify stratigraphic relationships, and used to understand volcanic evolution. The eruption style of an explosive volcanic deposit is revealed in the blockiness of the erupted materials. Homogenous, fine-grained pyroclastic deposits likely formed from a lava fountain eruption style, which erupts small droplets of magma in a jet-like stream. Lava fountaining eruptions on the Moon typically have a higher glass content and lower proportion of blocks of country rock (Bennett et al., 2016c; Gaddis et al., 2003c). Pyroclastic deposits with increased block content (i.e., higher rock abundance) more likely erupted in a Vulcanian event, with the juvenile magmatic material expelling a cap of country rock. The cap of country rock fragments into larger blocks, distributing these blocks around the vent along with smaller magmatic fragments of juvenile material (Bennett et al., 2016; Gaddis et al., 2016).

Understanding lunar volcanic processes is an important scientific goal, especially on the Moon where the volatile inventory is becoming a topic of interest for *in situ* resource utilization (Committee on the Scientific Context for Exploration of the Moon et al., 2007; van der Bogert et al., 2021). Increased understanding of volatile-driven volcanic activity will become a critical component to recognizing high-priority targets for resource potential in addition to understanding the geologic evolution of the Moon and Earth. In this study, we evaluate the thermophysical properties of the Mare Vaporum region, which contains multiple types of volcanism that each exhibit different thermal properties/different physical properties, to constrain their geologic history. Despite many of the descriptions of volcanic features being based on observations of physical properties (e.g., low albedo pyroclastic deposits), a comprehensive evaluation of the physical properties of a wide variety of volcanic features in the same region has not been conducted. Here we evaluate in detail differences between regolith types focusing on an area with a regional pyroclastic deposit, multiple irregular mare patches, mare flows, and a complex lava outflow channel within a restricted latitude range near the equator. We hypothesize that the Mare Vaporum LPD has similar thermal properties to other regional LPDs and exhibits a low thermal inertia as compared to typical regolith and lava flows. This would be characteristic of low block content, ejecting mostly fine-grained material and less country rock, indicative of a fire fountaining eruption consistent with most regional LPDs. Further, we also predict that we will be able to use the variable thermal and thermophysical properties to construct a geologic history using the LPD and relative stratigraphy of features in the Mare Vaporum basin.

4.2 Background

The Mare Vaporum basin is a ~350 km diameter (by longitude) mare infilled basin centered near ~14°N, ~4°E on the near side of the Moon (Figure 32). The irregular-shaped basin is bound by the Montes Apenninus (and the Imbrium Apenninus Formation Unit) to the north and west, and the Imbrium Fra Mauro Formation Unit to the west, south, east, and north (Fortezzo et al., 2020). Hiesinger et al., (2010) and Fortezzo et al., (2020) have each mapped several mare basalt flows on the interior of the basin, age dated to 3.61 to 3.10 Ga (Hiesinger et al., 2010). Mapped mare units from crater counting in the Mare Vaporum basin are included in Figure 32 (Hiesinger et al., 2011). Manilius Crater is a major identifiable feature within the basin, a complex crater in the northeast of Mare Vaporum, that although has a bright appearance and a sharp crater rim that would potential indicate Copernican age, Manilius crater has older age dating: it's currently mapped as Eratosthenian (Fortezzo et al., 2020), but may have been formed earlier in the Late Imbrian (Kumaresan and Saravanavel, 2019). Several smaller features have been identified within and surrounding the Mare Vaporum basin, which are the focus of this study and discussed here. We evaluate the stratigraphic relationships between these features (e.g., lava flows, pyroclastic deposits, irregular mare patches and other geologic features) using thermophysical properties to elucidate a geologic history of the Mare Vaporum basin. Several of these features have been mapped and evaluated previously using a variety of datasets.

4.2.1 Pyroclastic deposits

Pyroclastic deposits are the result of explosive volcanism and at the time of eruption typically blanket the surrounding terrain in a layer of erupted material, suppressing the underlying local topography. This erupted material is a mix of juvenile magmatic minerals and glass beads, typically of ash/lapilli size and blocks of country rock expelled during the eruption. LPDs have been described as having generally low thermal inertia due to their eruptive dispersal of small particles and "fluffy" texture. They are also described as having a low albedo (e.g., the regional pyroclastic deposit highlighted in Figure 32 is darker than Mare Vaporum lava flows embaying it from the northwest) and have been given the descriptive name “dark mantling deposits.” Due to the homogenous, fine-grained nature of LPDs, thick deposits have also been observed to have low crater retention properties (Lucchitta and Sanchez, 1975).

There are three previously identified pyroclastic deposits in the Mare Vaporum basin, of varying magmatic source regions. The Mare Vaporum LPD (referred throughout as MV LPD to prevent confusion with the Mare Vaporum mare basin) is a regional pyroclastic deposit (i.e., pyroclastic deposits that are greater than 1000 km^2 in area; Gaddis et al., 2003) in the eastern interior of the Mare Vaporum basin. Many regional LPDs are on the margins of major mare basins and are thought to have erupted contemporaneously with the mare lavas, or immediately preceding mare emplacement and then were embayed by mare lavas (e.g., Chapter 3; Head, 1974). Regional LPDs are typically homogenous, fine-grained deposits resulting from lava fountaining eruptions of a large volume of juvenile material and a minimal portion of country rock (Adams et al., 1974; Gaddis et al., 2003; Weitz et al., 1998). This indicates this deposit is likely to have a lower thermal inertia than average surface materials or blocky regolith as the broad dispersal of homogenous, fine-grained material would result in regolith that has a lower heat retention through the lunar night than a consolidated or solid material.

The Rima Hyginus irregular mare patch (IMP) and graben to the south is also associated with a localized LPD (i.e., a pyroclastic deposit smaller than 1000 km^2; Gaddis et al., 2003) that mantles the region surrounding the IMP. This LPD has been hypothesized to have been emplaced with the irregular mare patch depression (Wilson et al., 2011). During the eruption of and emplacement of the IMP, it was hypothesized that a volatile-rich eruption with mostly juvenile material erupted contemporaneously with the IMP. Localized LPDs present with a wide variety of proportions of juvenile and country rock components, owing to a varied eruption style of each volcanic vent

(Bennett et al., 2016; Keske et al., 2020). This means that the thermophysical properties of the Hyginus LPD cannot be as easily predicted as with regional LPDs, which are typically associated with lava fountaining eruptions. Wilson et al., (2011) hypothesized that this LPD was formed from the expulsion primarily of volcanic gases at the top of a dike and a small proportion of juvenile material. In this case, the Hyginus LPD is situated in an area mapped as "Imbrium Plains" rather than the typical mare; however, if we infer that this unit has properties similar to mare, the Hyginus LPD would have a lower thermal inertia than the surrounding Imbrium plains unit with a very low rock abundance.

4.2.2 Mare units and lava flows

One mare unit is mapped in Fortezzo et al., (2020), an upper Imbrium mare unit (Im2) that comprises the majority of the basin floor. Various smaller mare flows (mapped as Em) around the outer rim of Mare Vaporum are also mapped, one to the west, one to the southwest, and one to the south. The assigned ages of these flows (I for Imbrian mare, E for Eratosthenian lava flows) contrast mapped units from Hiesinger et al., (2010), which found that only one flow occurred in the Eratosthenian era with the remaining flows being over 3.2 Ga in age. The western lava flow evaluated here (labeled as such in Figure 32) was mapped by Hiesinger et al., (2010) as a 3.10 Ga lava unit, the youngest in the Mare Vaporum basin. The majority of the Mare Vaporum lava flows were mapped as 3.22 – 3.23 Ga by Hiesinger et al., (2010), including the mare basalts that are observed to embay the MV LPD and the basalts bordering the western boundary. These younger flows are bisected by an older flow unit in the center of the Mare Vaporum basin, at 3.5 Ga (Hiesinger et al., 2010). In Figure 32 and other observed maps (e.g., WAC Morphology map, Figure 33, left), the western lava flow has noticeably lower albedo and appears to flow from the

Imbrium Apenninus formation to the west through a restricted channel, and then spreading into a lava fan onto the 3.2 Ga lava flows of the Mare Vaporum basin.

4.2.3 Crater materials

The largest crater in the Mare Vaporum basin is Manilius crater, a bright, 35 km complex crater in the northeast of the basin. The crater and its ~75 km diameter asymmetrical ejecta blanket are mapped in Fortezzo et al., (2020) as Eratosthenian. Hyginus N crater is an irregularly-shaped Copernican-aged crater in the center of the MV LPD. Hyginus N does not display a bright crater ejecta blanket or stand out against the dark mantling of the LPD, but its large size (8 – 10 km in diameter, with a depth of ~875 m) suggest it likely would've penetrated the mantling deposit to the substrate below. Additionally, its dark appearance suggests it could potentially be mantled by the pyroclastic deposit, which will be investigated further in this study. A cold spot crater was identified in the western lava flow and was one that had been identified by Bandfield et al., (2014). Cold spot craters are small, fresh craters that demonstrate thermophysical properties of having a very low block content (and therefore almost no excavation of rocks creating an ejecta blanket), but a very fluffy disturbed upper regolith layer (Bandfield et al., 2014). These craters are thought to be very recent as they have been shown to degrade fairly rapidly in the lunar environment (Bandfield et al., 2014; Williams et al., 2018).

4.2.4 Rima Hyginus Graben and IMP and Manilius IMPs

Unlike a sinuous rille, which are often interpreted to be interpreted as a remnant of the formation of a lava channel (e.g., Hurwitz et al., 2013 and references therein), Rima Hyginus has been interpreted to be a linear graben related to the emplacement of a shallow dike intrusion (Wilson et al., 2011). Rima Hyginus is also related to the Hyginus Irregular Mare Patch (IMP) as likely being sourced from the same dike system, forming as a result of the same eruption (Wilson et al., 2011). Surrounding the IMP is a mantling of pyroclastic material (Rima Hyginus LPD), discussed in Section 4.2.1. The Rima Hyginus fissure forming as a linear collapse feature in the surface, following above the space vacated by the retreat of a linear dike (Wilson et al., 2011). The Hyginus IMP was observed to have a low albedo, low circular polarization ratio terrain surrounding it (Carter et al., 2013; Elder et al., 2017), indicating relatively fine-grained, block-free material surrounding the IMP. IMPs are typically compositionally similar to surrounding mare, although this is an area of active research; albedo is often tied to composition and in most cases, IMPs have albedos that are similar to the mare in which they are emplaced, implying that their daytime maximum temperature should be similar to surrounding mare. Prior investigations into the thermophysical properties of IMPs has revealed that they typically have higher rock abundance than surrounding terrain, but often not as high as similarly-aged craters (Elder et al., 2017). Elder et al., 2017 also investigated the H-parameter of a selection of IMPs and determined that the three of the four IMPs investigated had a slightly lower H-parameter value than the surrounding mare regolith.

Two additional IMPs are present in the Mare Vaporum region: Manilius-1 and Manilius-2 (Braden et al., 2014). Manilius-1 is a ~3.55 km long, 0.35 km wide (at its widest point) irregular mare patch situated west of a northeastern wrinkle ridge in Mare Vaporum. Manilius-2 is east of this same wrinkle ridge and is smaller (0.55 km x 0.3 km). Neither of the Manilius IMPs demonstrate a pyroclastic mantling like the Hyginus IMP does, and neither appear to be associated with any other geologic feature as, other than the wrinkle ridges, there are no other geologic features in the vicinity (e.g., sinuous rilles, lobate scarps, other lava flows). In this study, we investigate the thermal properties of the Manilius IMPs and their relationships to nearby wrinkle ridges and mare lava flows with respect to their physical properties. Byron et al., (2022) determined that IMPs generally have a higher rock abundance than typical maria, but a lower rock abundance than rocky crater ejecta, using similar methods that we employ here.

4.3 Methods

We use the multispectral Diviner Lunar Radiometer Experiment (Diviner) instrument from the Lunar Reconnaissance Orbiter spacecraft (Paige, et al., 2010) to evaluate surface temperatures and thermophysical properties of the Mare Vaporum region of the Moon. Measurements are made in the visible through infrared parts of the electromagnetic spectrum in nine spectral bands covering 0.3 – 400 µm. Diviner channels 3 – 9 measure the thermal environment of the lunar surface over temperatures from ~20 – 400 K (Paige et al., 2010; Williams et al., 2021). Surface brightness temperatures of the Moon have been acquired globally, near-continuously since July of 2009 (Paige et al., 2010) The Diviner instrument obtains nadir-pointing temperature measurements at multiple local times (Keller et al., 2016; Williams et al., 2016). Over 13 years of data acquired by Diviner have been compiled into a set of surface temperatures in the Mare Vaporum region over a range of local times. Using daytime and nighttime surface brightness temperatures, we also obtained updated rock abundance maps from Powell et al., (2023) and relative thermal inertia (as H-parameter) from Hayne et al., (2017).

Diviner channels 3 – 9 Reduced Data Records (RDR) were used to generate a gridded dataset at 128 pixels per degree for the Mare Vaporum region (7°N – 20°N, -3°E – 13°E) following the methods of Williams et al., (2022, 2017). The RDR contains an Activity Flag, which we used to constrain the data for emission angle, noise, and calibration. The dataset was processed in 1° tiles of longitude and latitude, resulting in 108 tiles of binned radiances covering the Mare Vaporum basin. Binned radiances were then converted to brightness temperatures, and the bolometric temperature was calculated as described in Paige et al., (2010; Williams et al., 2022).

Thermal contrast between rocks and regolith fines causes multiple temperatures to be present within the detector's field of view. Highly conductive solid rock contributes higher temperatures to nighttime emissivity data than insulating regolith. Temperature measurements are sensitive to the thermal conductivity of the surface layer to a depth that scales with the energy input (Bandfield et al., 2011; Hayne et al., 2017; Vasavada et al., 2012). Differences in brightness temperatures between the Diviner infrared channels occur when a mixture of temperatures is detected by the instrument within a detector's field of view (Williams et al., 2022). The anisothermality observed with nighttime temperatures is indicative of surfaces of differing thermophysical properties (e.g., rocks and soils) radiating at different temperatures within a single Diviner pixel. Anomalously warm areas at night are characterized by high rock abundances (Bandfield et al., 2011), as rocks (in this case, those greater than ~50 cm) are capable of absorbing more heat and retaining the heat longer than unconsolidated regolith. The rock abundance (also often referred to as the rock concentration or rock areal fraction) is the proportion of the field of view comprising rocks over a pre-determined size (50 cm in this study). Regions dominated by larger rocks are expected to have a higher rock abundance (e.g., impact crater ejecta blankets, particularly of young, fresh craters and slopes where mass wasting has occurred), and regions associated with fine-grained material are expected to have lower rock abundance (e.g., older regions with increased boulder comminution, fine-grained pyroclastic deposits). The rock abundance of localized pyroclastic deposits have been measured to range from 0.0024–0.0054 with a mean of 0.0038 (Trang et al., 2017). Heavily space-weathered, impact gardened, and comminuted highlands have similar modal rock abundance to this at values of 0.005, contrasting younger basaltic maria at a modal rock abundance of 0.186 (Bandfield et al., 2011). Anomalously rocky areas and young craters have the highest modal rock abundance at 0.635 and 0.984, respectively (Bandfield et al., 2011).

The top ~1–2 meters of regolith is affected primarily by physical surface properties, including micro- and macro-meteorite bombardment, impact gardening, regolith overturn, and regolith compaction from overburden pressure. These processes affect the regolith layer's bulk density and grain size (e.g., boulder and rock breakdown), which are known to affect observed surface temperatures. Constraining soil properties like thermal conductivity and density using *in situ* and remote observations produce a parameter that describes regolith density with depth (H-parameter; Hayne et al. 2017, Vasavada et al. 2012, Williams et al. 2017). Hayne et al. (2017) fit the model to the global Diviner nighttime temperatures (Bandfield et al., 2017) with H as a free parameter, creating a global H-parameter map. H-parameter is a property of the upper ~10 cm of regolith that many interpret as "fluffiness" of the regolith but is more directly interpreted as the variable density of the upper regolith layers as a function of depth. Unconsolidated, fine-grained materials have a lower density on the surface, which is observed in the H-parameter map as an increase in the depth of the thermal response (e.g., 0.08 m – 0.09 m for typical "fluffy" pyroclastic-type material). More consolidated rocks closer to the surface or a more coherent near-surface layer increases the density and conductivity of rock and regolith layers, reducing the depth interpreted in the H-parameter map (e.g., 0.05 m – 0.06 m for older, consolidated mare or highlands).

For this analysis, we produce surface bolometric temperatures of Mare Vaporum following the methods of Williams et al., (2022). These methods include the production of rock abundance and H-parameter maps of the same gridded region from the maps of Bandfield et al., (2011) and Hayne et al., (2017), respectively. Using a combination of rock abundance (see section 4.3.1) and inferred thermophysical properties like density and soil thermal conductivity, we can infer regolith properties from surface temperatures. For data analysis of rock abundance, however, we use updated maps of Powell et al., (2023), which incorporates improved georeferencing and thermal modeling of existing rock abundance maps.

4.4 Results

The temperature of a surface varies throughout the lunar day and night (unmitigated by effects from an atmosphere) as a function of rock and regolith properties such as albedo, rock abundance, and regolith compaction. Temperature contrasts observed using Diviner were used to derive properties such as rock abundance and H-parameter, which we use to infer eruption conditions and relationships between volcanic units. Daytime maximum temperatures are most sensitive to the albedo of a surface (Williams et al., 2022), where lighter highlands will be lower in temperature and darker maria or pyroclastic deposits will be higher in temperature. Nighttime minimum temperatures are sensitive to regolith properties in the top ~10 – 20 cm and vary with the thermal inertia of materials (Williams et al., 2022).

4.4.1 Albedo and Temperature Contrasts

Regions around Mare Vaporum can be characterized by their albedo and surface texture. Mare Vaporum is visible in Figure 33a as a dark, smooth region speckled with many small, high albedo impact craters. The regional MV LPD is lower in albedo than the mare, and fewer bright craters are visible. A darker lava flow lobe is visible in the western part of Mare Vaporum (indicated in the LROC EMP map). This lava flow appears to flow from a lighter highlands outlet (west of the lava flow arrow), onto the mare basalt terrain.

Albedo has typically been used to differentiate a pyroclastic deposit from surrounding highland/mare materials and regolith, but regolith properties of pyroclastic deposits can also be used to distinguish the fine-grained LPDs from other lunar surfaces. Differences between Diviner channels occur when surfaces of different materials radiate at different temperatures, resulting in a mixture of temperatures within a detector's field of view (Williams et al., 2022). Figure 33b shows the difference in brightness temperatures between Diviner channels 6 and 8 over a 4-hour time window centered at midnight. Areas with higher temperature values in this map indicate locations where the temperature contrast is larger, with a mixture of materials that have highly contrasting thermal inertias (i.e., a mixture of rocks and regolith; Williams et al., 2022). Mare Vaporum has a relatively low $T_6 - T_8$ temperature contrast, punctuated by a large number of small craters with high $T_6 - T_8$ temperature contrasts. The lower $T_6 - T_8$ temperature contrast would be consistent with a more homogenized, lower inertia material.

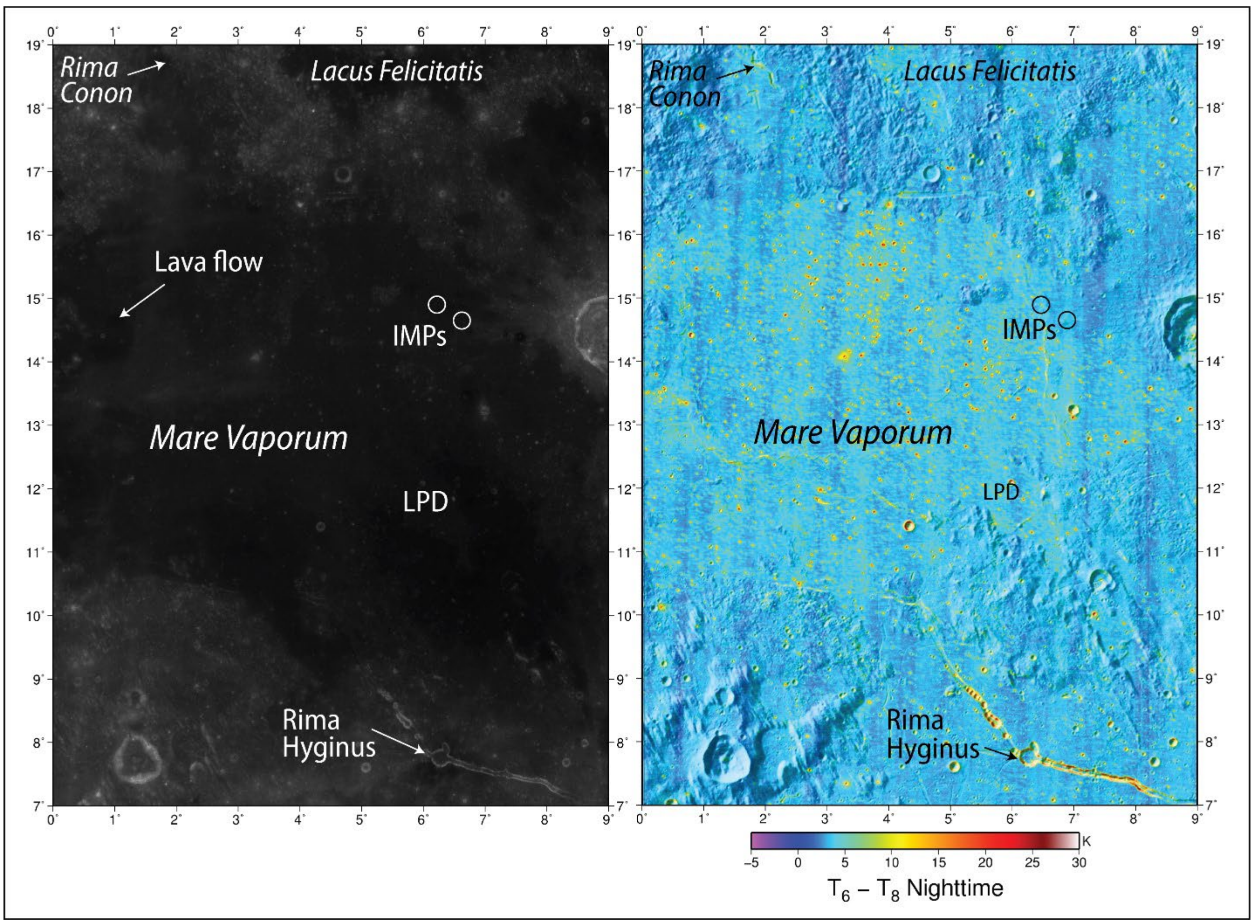

Figure 33: Surface features of the Mare Vaporum basin. Left: Lunar Reconnaissance Orbiter Camera (LROC) empirically normalized 643 nm single band mosaic, highlighting albedo

variations of the surface. Right: Band difference of Diviner temperature channels 6 and 8. Areas with higher values indicate regions that have a larger mixture of materials with contrasting thermal inertias (i.e., a heterogeneity of regolith fines and rocks).

4.4.2 Minimum and Maximum Temperatures

The minimum and maximum temperatures are shown in Figure 34a and Figure 34b, respectively. Minimum temperatures represent pre-sunrise values, whereas maximum temperatures occur at local noon, where coverage has been obtained (see figure caption for details). Maximum temperatures in the total image range from 369 K – 404 K, with an average of 391 K. Deviations in maximum and minimum nighttime temperatures are highlighted in Figure 34c and Figure 34d respectively, which shows normalized temperatures by latitude-dependent fit to the zonal mean temperatures of the data (additional details in Williams et al., 2022).

Mare Vaporum generally exhibits minimum temperature values ranging from 89 K – 111 K, which is near the mean minimum temperature for the region (or within a deviation of +/- 1 K – 2 K; Figure 33b). The maximum temperature in Mare Vaporum is 385 – 396 K (mean of ~ 393 K), with a deviation from normalized maximum temperatures of approximately +/- 5 K. Impact craters are less visible in maximum temperature deviations. Numerous small impact craters are obvious in Mare Vaporum, as they are marked by spots of higher minimum temperatures with deviations of more than 15 K higher than the normalized minimum temperature (the highest minimum temperature in this region being found near an impact crater at 137 K). Similar to these small impact craters, Rima Hyginus LPD exhibits low nighttime temperatures, ranging between 89 – 97 K, with maximum daytime temperatures ranging from 388 – 395 K (the average being similar to Mare Vaporum at 393 K). Minimum temperatures in the Rima Hyginus graben deviates from the normalized mean temperature by over 30 K in some pixels, but typically 15 – 20 K overall. The

IMP itself is opposite to these, however with a temperature range of 93 – 399 K, and minimum/maximum temperature averages of and 95 – 398 K, respectively.

The rille of Rima Conon is visible as a high minimum temperature value, with low discernable variation in the maximum temperature values. The mare surrounding Rima Conon is visible as a distinct unit, separate from the lower-temperature highlands to the east and west of the mare in minimum temperature map. No additional discernable structure was apparent to indicate pyroclastic mantling or other volcanic features other than the mare. The lava flow in the western part of Mare Vaporum has a lower minimum temperature than surrounding mare; however, there is a cold-spot crater in this region that may be mitigating the results in this location (discussed further in Section 4.5.2). MV LPD is a regional LPD (i.e., greater than 1,000 km^2), and is visible in the minimum nighttime temperature maps as having a lower temperature than surrounding highlands and mare. Minimum temperatures of the MV LPD are typically 88 – 104 K, typically lower than the normalized temperatures by 1 – 3 K. Maximum temperatures range from 386 K – 402 K, and have an average that is higher than Mare Vaporum at 397 K.

The normalized minimum (Figure 34c) and maximum (Figure 34d) temperature maps were combined into a composite RGB image with the LROC WAC empirically normalized 643 nm single band mosaic (Figure 33a) to evaluate large-scale changes in physical properties in the Mare Vaporum region (Figure 35). For this composite, the red channel is the LROC WAC mosaic which provides information about the brightness of the surface, the green channel is the normalized minimum temperature map, and the blue channel is the normalized maximum temperature map. Areas that are high in albedo have increased red content (e.g., red, orange, purple) and areas that are low albedo will lack red coloration.

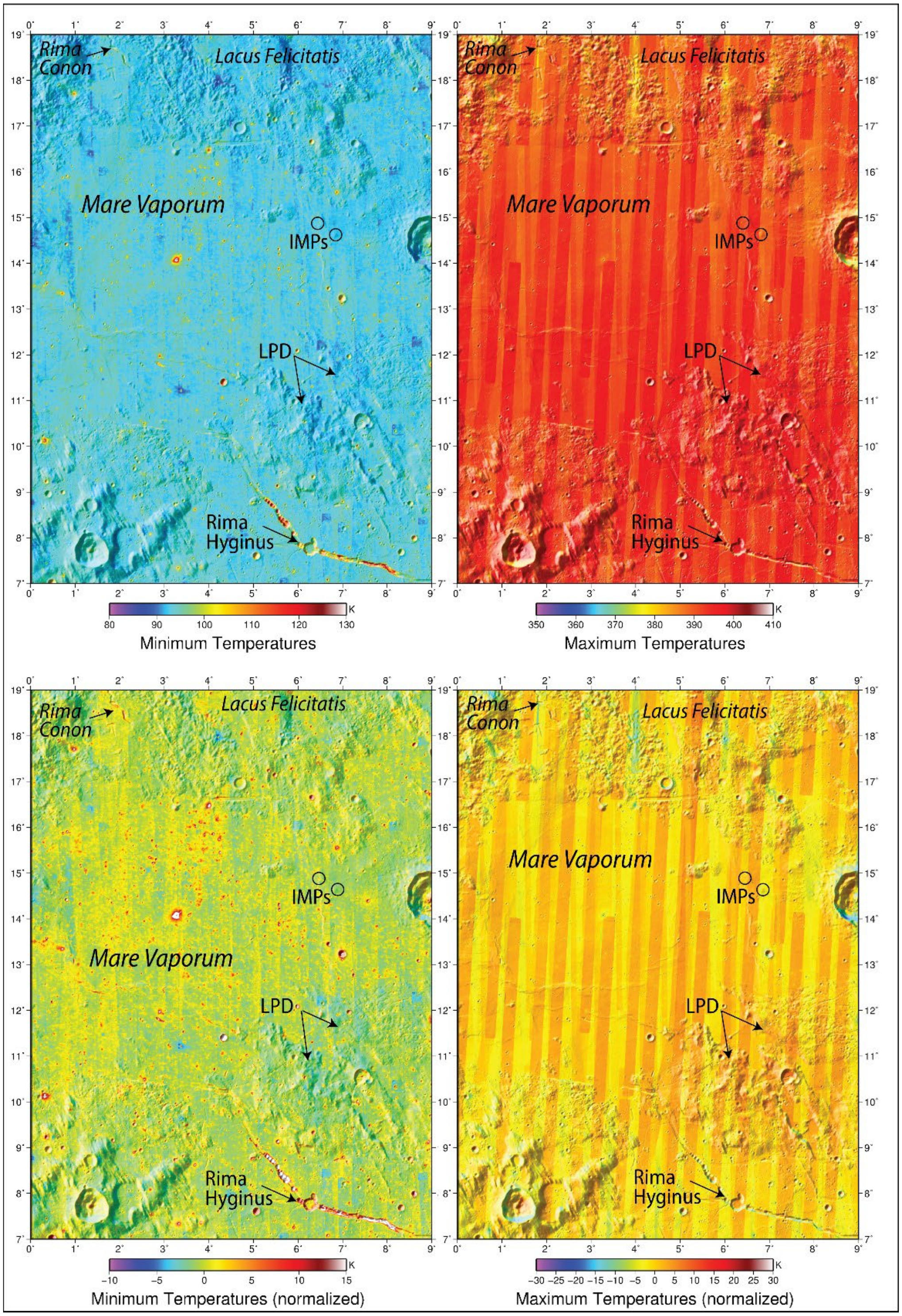

Figure 34: Minimum and maximum temperature maps of Mare Vaporum region. (a) Minimum bolometric temperature map, (b) Maximum bolometric temperature map, (c) Minimum temperatures normalized by a cosine function fit to the zonal mean temperature map, and (d) Maximum temperatures normalized by a cosine function fit to the zonal mean temperature map, Vertical striping in the maximum temperature maps is a result of the lack of coverage of the at the local noon time for that orbital ground track.

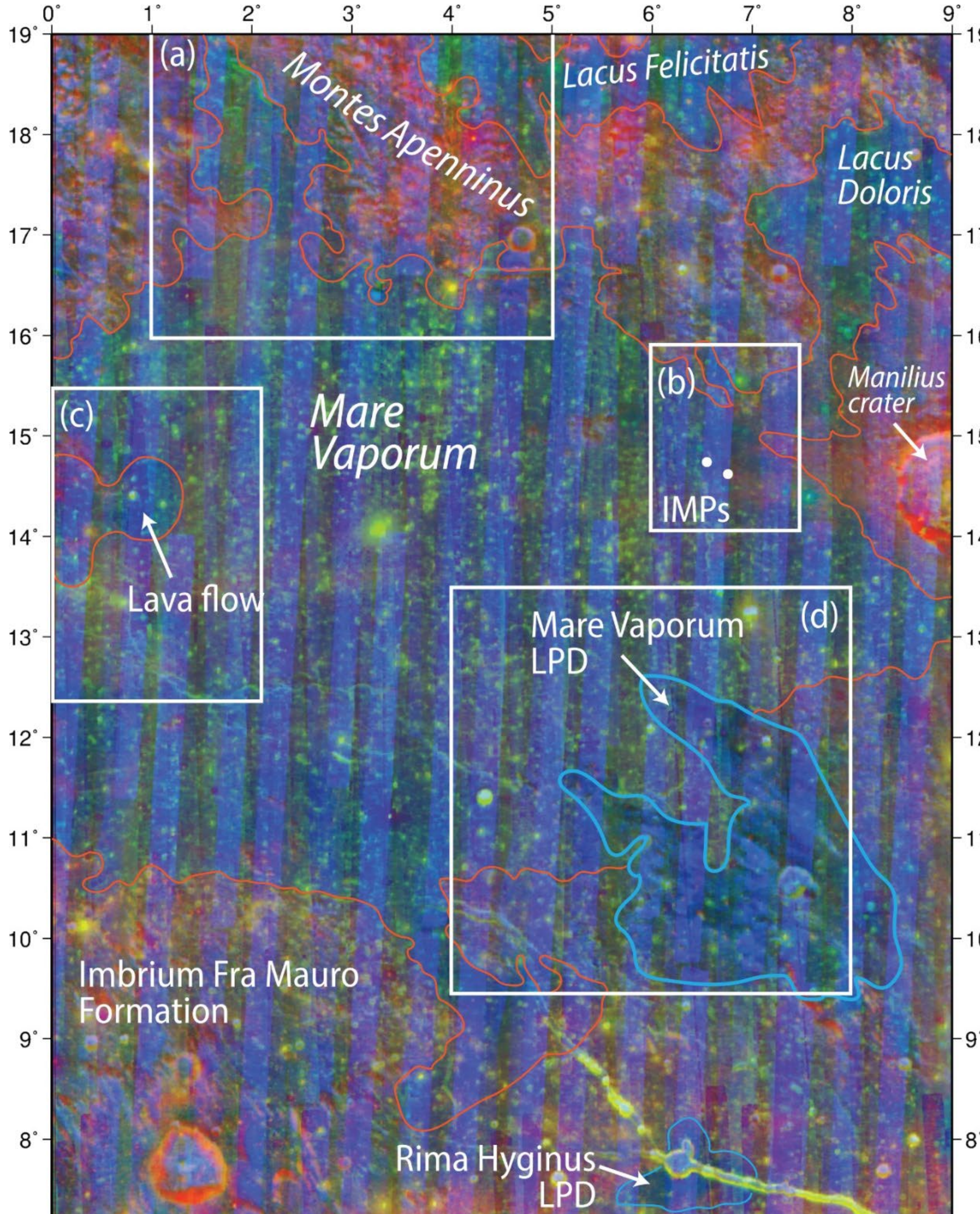

Figure 35: RGB color composite map of the Mare Vaporum basin. Red channel is the LROC WAC empirically normalized 643 nm single band mosaic and provides information about the brightness of the surface, green channel is the normalized minimum temperature map and can be used to infer the presence high thermal inertia materials, and blue channel is the normalized maximum temperature map and can be used to infer the presence of low thermal inertia materials. LPD boundaries were created from this study, mare boundaries were approximated from Nelson et al., (2014) as mapped in LROC Quickmap.

Mare Vaporum overall is dark blue to blue, indicating dark, low-thermal inertia material. As the blue channel is associated with maximum temperature, this indicates that the areas with the highest temperatures would be the MV LPD, followed by the Mare Vaporum mare, and then smaller volcanic deposits like Rima Hyginus LPD and Lacus Doloris. Highland and plains terrains in Figure 33 are marked by red and orange colors, indicating the composite is dominated by the red albedo channel. This reflects the higher albedo highlands standing out against the lower albedo mare and pyroclastic deposits. Manilius crater is bright orange with a yellow central peak (nearly out of frame), indicating contributions from the bright albedo channel in red and a minor contribution from the minimum temperature map. This contrasts many of the smaller craters, which are yellow or teal, indicating that the smaller craters have a higher thermal inertia.

Many fresh craters are observed to be yellow as they exhibit a very high albedo (and therefore have a strong contribution from the bright image in the red channel) and a contribution from the minimum temperature channel (Figure 34c). Some fresh craters, however, are teal in the RGB composite map, indicating that although they share a high contribution from the minimum temperature channel, they are dark. This is confirmed in a close inspection of Figure 36a – teal craters in the RGB composite correspond to dark halo craters in the albedo map and yellow craters in the RGB composite correspond to bright craters in the albedo map.

4.4.3 Rock abundance

An area with fewer rocks that are greater than 50 cm would appear dark blue or blue in Figure 37, and areas with a high abundance of rocks greater than 50 cm would appear yellow, orange, or red in Figure 37. Mare Vaporum had a generally low background rock abundance with regions with high rock abundance throughout (Figure 38). These regions of high rock abundance are associated with impact craters.

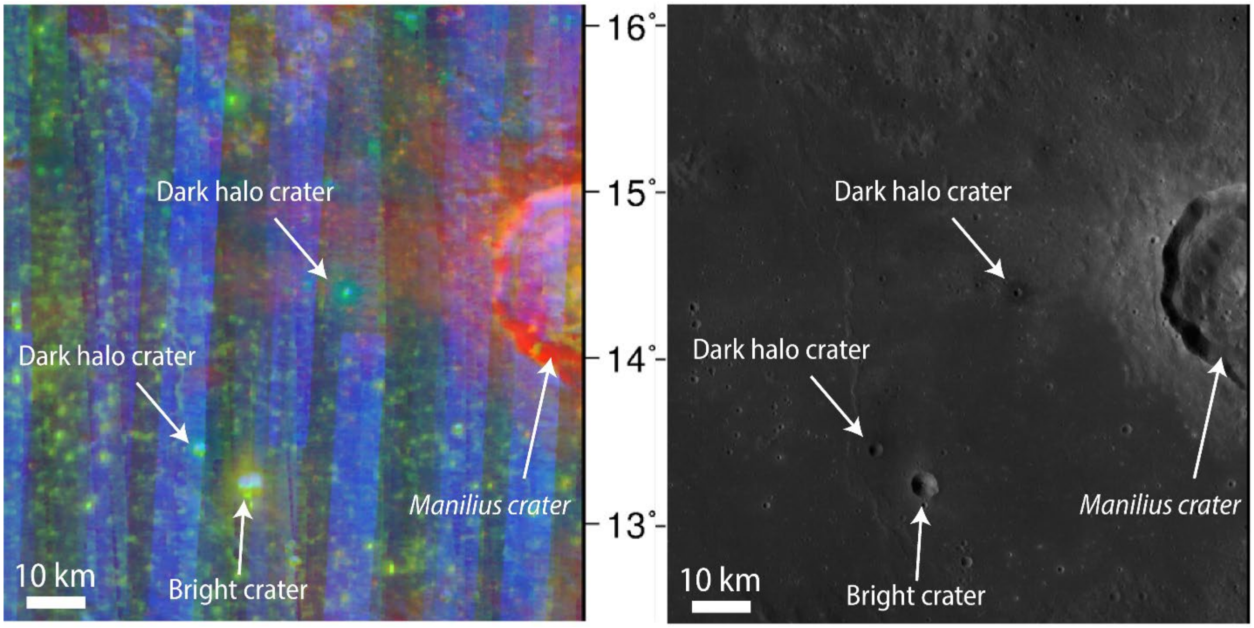

Figure 36: RGB composite (see Figure 35), left, of the eastern region of Mare Vaporum, showing select craters that appear teal and yellow in the RGB composite. Right shows this region in WAC morphology, showing that the teal craters are associated with dark halo craters and the yellow craters are associated with bright craters. Note Manilius crater, which appears red in the RGB composite.

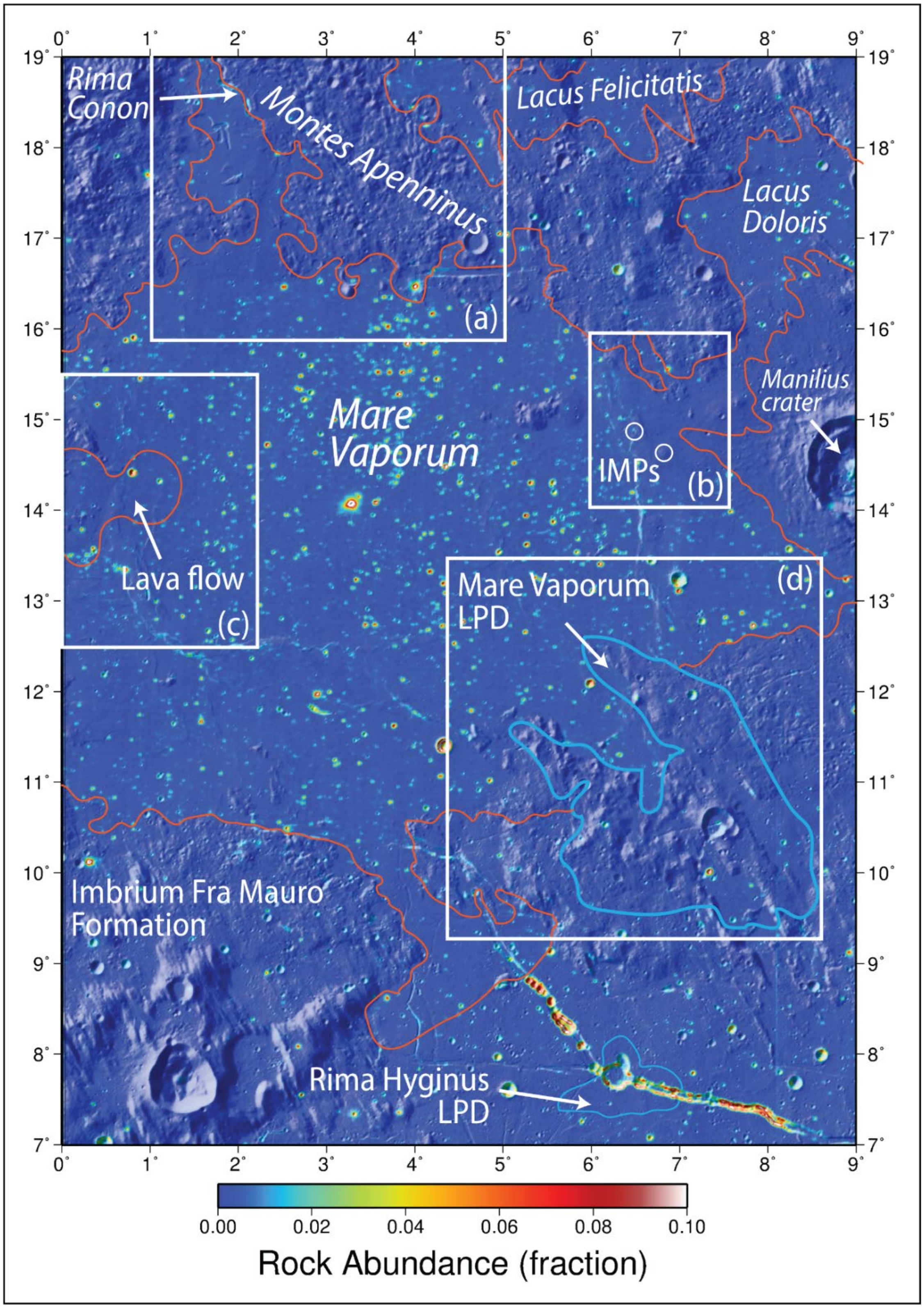

Figure 37: Rock abundance for the Mare Vaporum Basin. Regions in white boxes are highlighted in Figure 35 and discussed further in this section.

Mare Vaporum is marked with numerous small craters interspersed throughout an area with moderate rock abundance. These craters push the maximum rock abundance in areas to above 0.17 (not including clear outliers), but generally mare with minimal craters has an average rock abundance of ~0.0039 (stdev: 0.0037). More typical mare regions (i.e., regions selected regardless of high or low crater populations) range in rock abundance from 0.004 to 0.011. The MV LPD has very few impact craters, and a lower average rock abundance at ~0.0024 (stdev: 0.0010). Highlands terrains surrounding Mare Vaporum generally demonstrated a lower rock abundance than the mare basalts: ~0.0024 (stdev: 0.0012) near Rima Conon, and similar to the ejecta blanket of Manilius crater (~0.0024, stdev: 0.0011). The center of the crater floor of Manilius crater has a higher mean rock abundance of 0.009 (stdev: 0.0081).

4.4.4: H-parameter

Regolith properties have a greater effect on nighttime temperatures within the diurnal thermal skin depth (~10 – 20 cm). Areas with high rock abundance will demonstrate a low H-parameter, whereas regions with unconsolidated, "fluffy" regolith will demonstrate a high H-parameter. Mare Vaporum demonstrates a moderate H-parameter (0.070 – 0.072 m), speckled with many very low H-parameter small impact craters (Figure 39). The oldest mare flow demonstrates a slightly higher H-parameter value (0.071 m) than the west lava flow (0.070). Highlands terrains surrounding this region have a more variable H-parameter, with some regions having an H-parameter similar to mare basalts and other locations within the highlands having an intermediary H-parameter between rocky areas and basaltic areas. The Manilius IMPs both have a slightly lower H-parameter than the surrounding mare basalts, with Manilius-1 (the larger of the two) having a lower value than Manilius-1 (Figure 41 for increased detail).

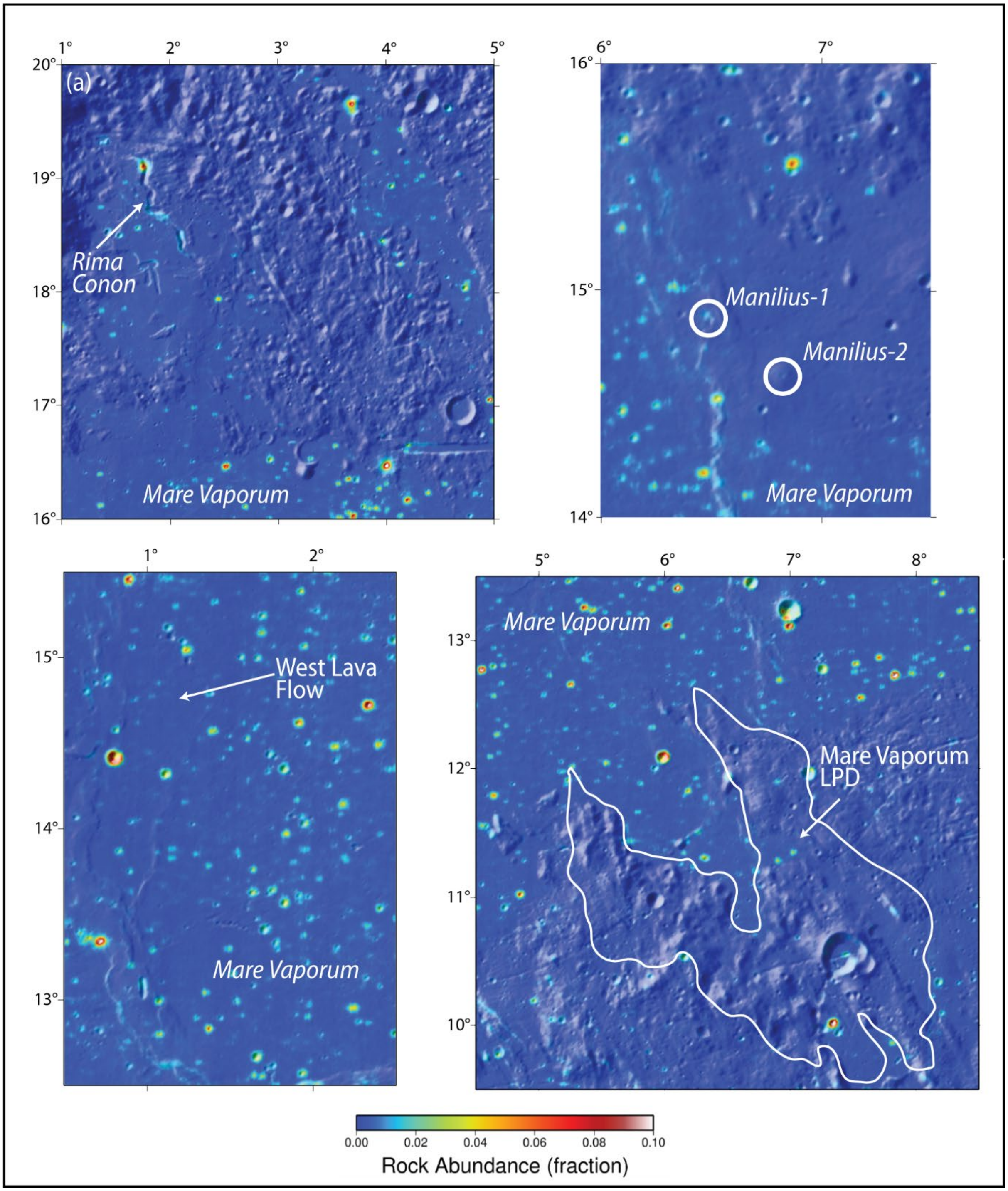

Figure 38: Rock abundance of four regions identified in Figure 35: (a) Rima Conon, (b) Manilius-1 and Manilius-2 IMPs, (c) West lava flow, and (d) MV LPD.

The MV LPD (Figure 40) has a higher H-parameter than the mare to the northwest and a much higher H-parameter than the highlands to the east and southwest at 0.080 m. The Rima Hyginus LPD was expected to have a comparable H-parameter value, as the eruption had previously been described as a volatile-rich eruption comprising very low rock content (Wilson et al., 2011). The H-parameter value was more comparable to typical mare materials, however, at 0.072 m on the northern side of the graben and 0.070 m in the southern portion of the LPD at Rima Hyginus. The Manilius crater ejecta blanket had a higher H-parameter value than this at 0.075 m, indicating that the ejecta of Manilius crater had a "fluffier," less consolidated regolith than the Rima Hyginus LPD.

4.5 Discussion

4.5.1 Geologic history of Mare Vaporum LPD

Mare Vaporum LPD (MV LPD) demonstrates a lower rock abundance and higher H-parameter than the surrounding mare flows and the mare flow labeled "west lava flow" in Figure 32. The dispersal of the pyroclasts onto the highlands plains indicates that the pyroclastic deposit was emplaced after the highlands plains had formed in this region, mantling the region. Colors in the RGB composite (Figure 35) can be interpreted for their thermophysical properties related to temperature and albedo. Comparing mapped units observed in Figure 32 with colors associated with these units, basaltic materials (i.e., mare basalts, lava flows, pyroclastic deposits) are generally blue, with the darker blue being observed on the regional LPD and the Mare Vaporum mare basalts including a mix of blue/purple. The darker blue of the LPD relative to the mare basalts indicate that the LPD has a lower albedo than the surrounding areas (including the dark mare) and has a lower thermal inertia than the mare basalts, which are somewhat brighter than the LPD (see Williams et al., 2022 for an in-depth interpretation of the RGB color trends). The mare basalt to the west demonstrates a higher rock abundance and lower H-parameter, particularly in the region between western limbs of the pyroclastic deposit. Not only does this indicate that the mare lavas flowed into and embayed the pyroclastic-mantled highlands, this helps further characterize the mantling nature of the pyroclastic deposit.

4.5.2 Geologic history of lava flows in Mare Vaporum

The lava flow in the west of the Mare Vaporum basin appears to flow from the Montes Apenninus highlands to the west into the Mare Vaporum basin. No vent structure was apparent to identify the source of this flow, and no nearby related pyroclastic deposits were identified. As the lava flow is visible in the LROC WAC map (Figure 33, left), we can interpret the west lava flow as being younger than the mare flows in this region. This is supported by a crater counting age of 3.10 Ga, younger than the surrounding Mare Vaporum lava age of 3.22 Ga (Hiesinger et al., 2011). The location and morphology of this flow lobe implies that it flowed from the direction of the highlands and that it does not appear to be related to the mare emplacement or general mare flows. There did not appear to be a sinuous rille feature that would indicate late-stage emplacement or lava drainage from back-flow of mare lavas from the highlands regions. A morphologic investigation of this lava flow would be necessary to determine how this lava flow relates to the mare basin formation and how the lava flow lobe relates to the highlands terrain from which it flows. “Bathtub rings” or remnant lava flow indicators in the highlands in high-resolution LROC NAC imagery could reveal mare lava overflow and storage, that was released during later stages of mare cooling, flowing back onto the mare basin as a younger flow. Alternatively, morphologic mapping in detail could reveal indications of a vent structure or fissure on the mare margin from which this flow originated.

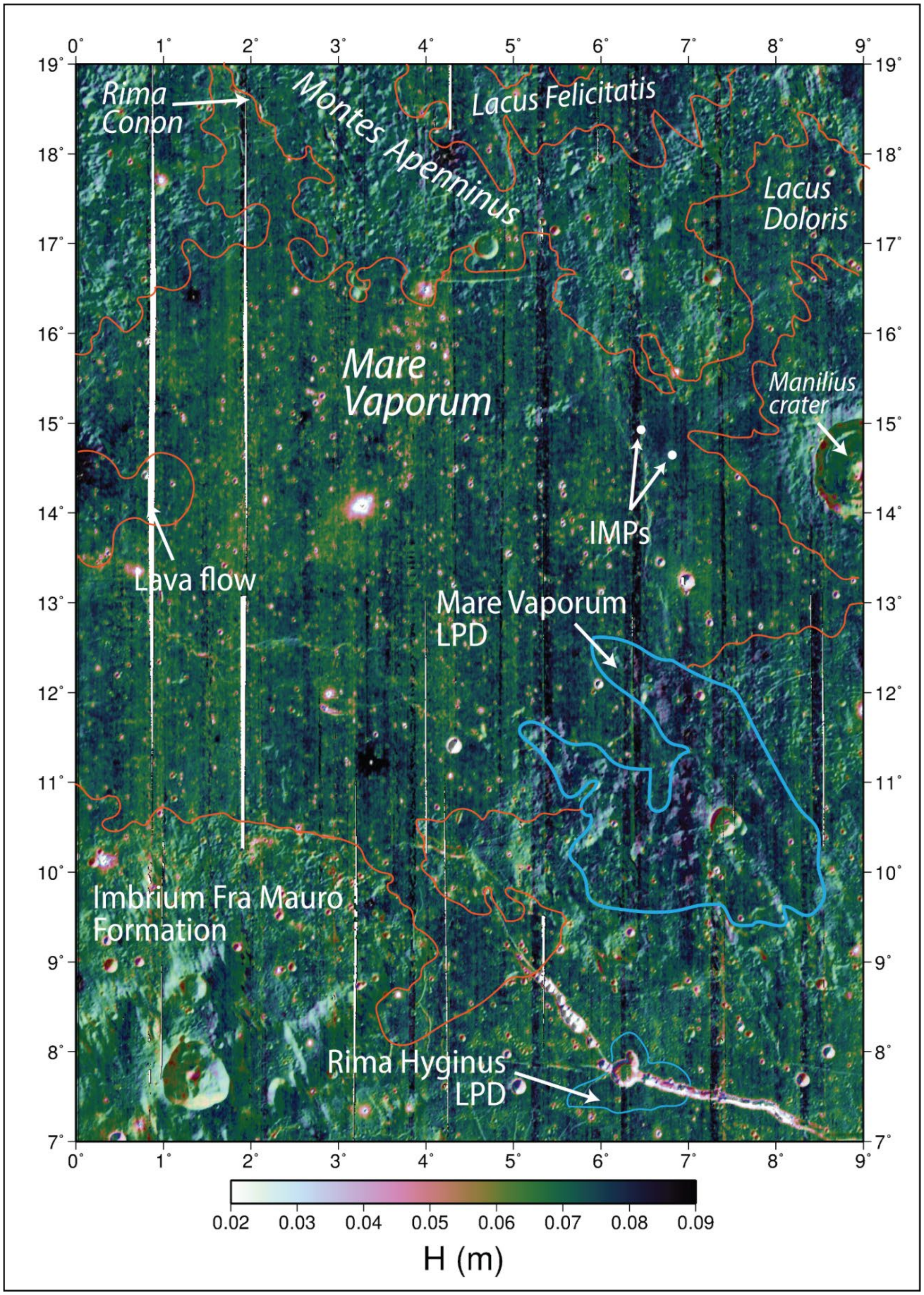

Figure 39: H-parameter for the Mare Vaporum Basin. Regions in white boxes are highlighted in Figure 35 and discussed further in this section.

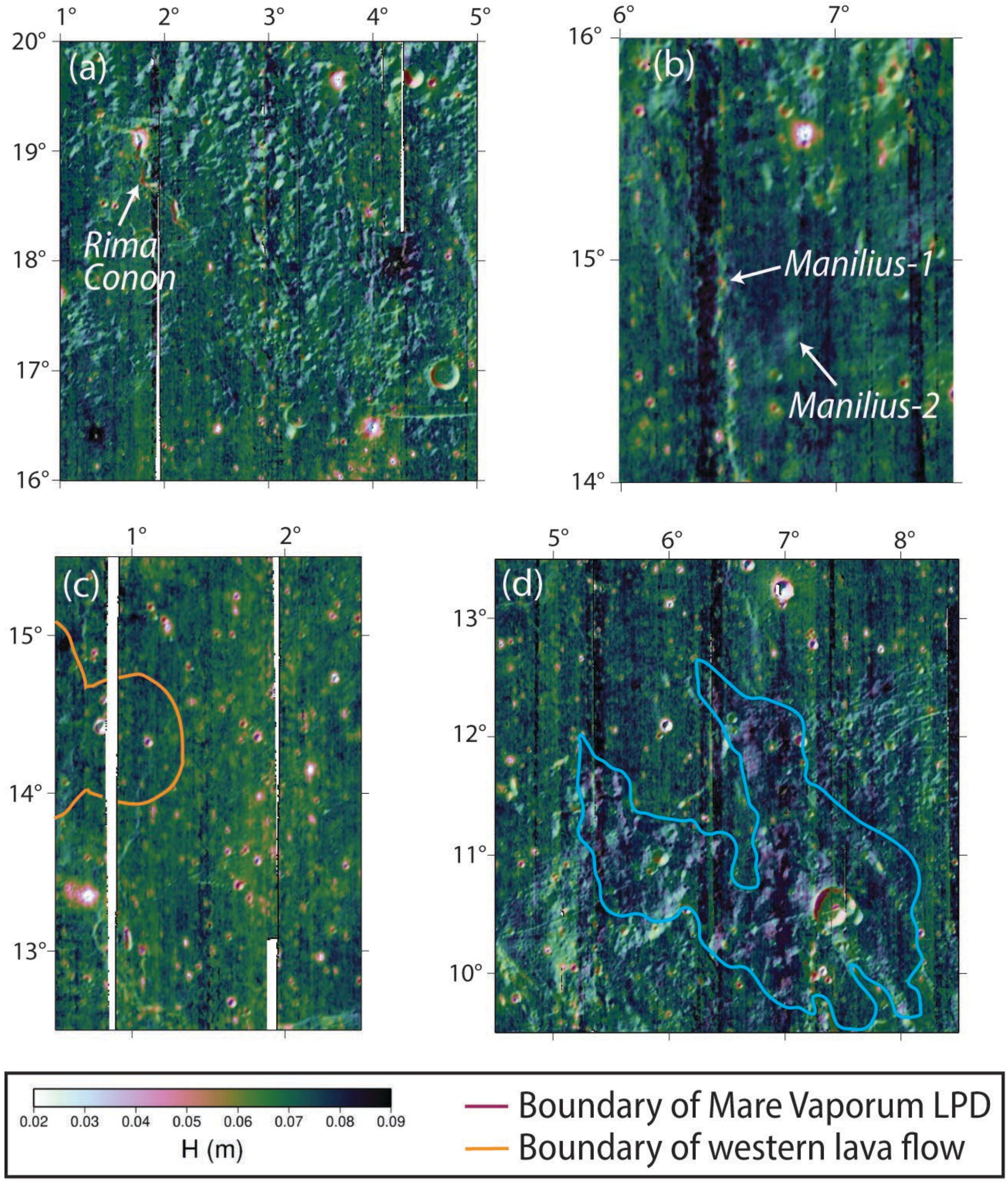

Figure 40: H-parameter of four regions identified in Figure 39: (a) Rima Conon, (b) Manilius-1 and Manilius-2 IMPs, (c) West lava flow, and (d) MV LPD.

4.5.3 Impact craters in and around Mare Vaporum Basin

Many impact craters are visible in the Mare Vaporum Basin, of varying ages, sizes, and with different albedos reflecting varying excavated compositions. Impact craters of variable ages, albedos, and excavation depths will have different physical properties that are revealed in the investigation of thermophysical and thermal properties. For example, multiple cold spot craters are visible in the H-parameter map as very high H-parameter values (i.e., “fluffy” regolith, where the regolith has a low density). Cold-spot craters excavate upper regolith indicating fairly recent resurfacing. The Manilius crater ejecta blanket has a low rock abundance and a high H-parameter. Impact craters typically excavate rocks, that are broken down mechanically over time at a rate that can be estimated (Ghent et al., 2014). The low rock abundance and high H-parameter of the Manilius crater ejecta blanket suggests the excavated rocks been broken down into a fine regolith, which implies that the impact occurred in the distant past, rather than the recent past. Small craters in the Mare Vaporum basin exhibit contrasting results in the RGB composite map of maximum and minimum temperatures and brightness. Craters that are yellow in the RGB composite are interpreted as being bright and having a high thermal inertia, whereas craters that are teal in the RGB composite are interpreted as being dark and having a high thermal inertia. These findings correspond to bright craters and dark halo craters, respectively, on the WAC morphology mosaic. We suggest that the dark halo craters in these areas are excavating dark material from below the mare. This material could potentially be pyroclastic material that had been buried by the mare flows and is being exhumed by the impact. The ejecta blankets of bright craters, conversely, contain less-weathered mare materials that have been excavated from under the top regolith layer. As these craters are similar in size and close in distance (i.e., in the same region of the mare basin), it is unlikely they could be used to determine mare lava thickness. Depth to excavated material may be inferred at single crater locations; however as there are indications that the depth to the darker pyroclastic material is variable, it is likely that this is a multi-layered volcanic feature.

4.5.4 Observations of Manilius-1 and Manilius-2 IMPs

The area surrounding Manilius-1 and Manilius-2 irregular mare patches (IMPs) has a generally high H-parameter, indicating consolidated materials (e.g., lava flows, mare basalts) and/or a low albedo (e.g., mare basalts, pyroclastic deposits with high rock abundance). Both IMPs demonstrate increased rock abundance from the surrounding mare, even when compared with the nearby wrinkle ridge and large and small impact craters, which would be expected to have slump or ejecta-related boulders. The rock abundance of Manilius-1 is similar only to nearby fresh craters that have a brighter appearance and sharper rim than the more degraded craters in the area immediately surrounding Manilius-1. Because these features are small, we investigated them further with NAC images (Klem et al., 2014; Robinson et al., 2010; Wagner et al., 2015), which confirmed that the change in H-parameter and rock abundance we observed was correlated to the locations of the IMPs and not another feature nearby (e.g., the nearby wrinkle ridge or a small impact crater; Figure 41). These observations demonstrate clear differences between the Irregular Mare Patches (IMPs) and the mare, supporting that there are differences in how IMPs and mare flows are emplaced.

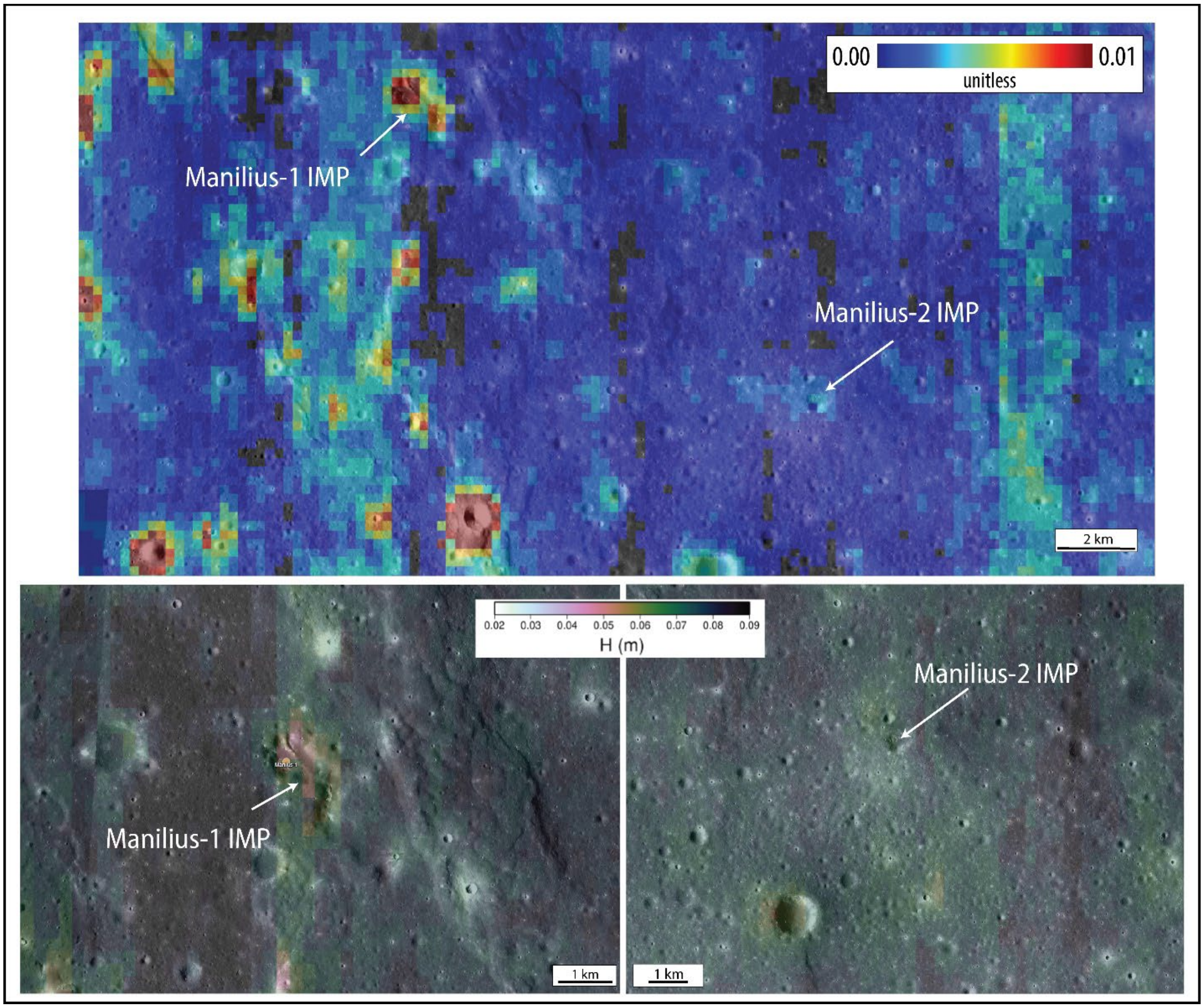

Figure 41: Rock abundance (top) and H-parameter overlayed onto high-resolution NAC Images of Manilius-1 (bottom left) and Manilius-2 (bottom right) IMPs.

4.5.5 Reconstructing a Geologic History

We can establish a relative stratigraphic history for the Mare Vaporum basin, supported in locations by crater counting ages and mapped geologic units. The west lava flow is relatively the youngest unit overlying the mare, as its shape can be delineated as separate from the remaining mare flows as a lobate flow in albedo maps. This is confirmed by the crater counting age as being the youngest of the lavas in the Mare Vaporum basin of 3.10 Ga (Hiesinger et al., 2011). The Rima Conon rille is also younger than the Mare Vaporum lava flows, as it incises into the mare basalts. The relative ages between the west lava flow and Rima Conon could not be determined as there are no cross-cutting relationships between these two features and the thermal observations between the features indicate typical mare properties. Small impact craters in Mare Vaporum increase the overall rock abundance of the mare slightly as the impact excavates rocks from the subsurface and as the impact craters are younger than the mare, these rocks are still comminuting into finer rocks and regolith (Hörz and Cintala, 1997). A large number of small craters are visible in the north-central part of Mare Vaporum, particularly in the rock abundance map (Figure 37). This part of the mare basin is mapped as one of the older mare units at 3.45 Ga by crater counting (Hiesinger et al., 2011). The high number of craters visible in our thermal and thermophysical maps is consistent with this older crater counting age.

The MV LPD is embayed by Mare Vaporum lavas, indicating that the pyroclastic deposit was emplaced prior to the lavas and were later, in part, covered. The pyroclastic deposit thins distally into the highland areas to the south and southeast and generally do not have areas that have sharp contacts that would indicate similar embayment. This is supported by compositional analysis in Chapter 3, where there is a core of pyroclastic material high in glass, and a distal portion of deposit that has a mix of glass and substrate material. This would indicate that the highlands in this area are older than the regional MV LPD, having been mantled by the pyroclastic deposit. The pyroclastic deposit appears to mantle knobby/rugged terrain that was potentially of highlands composition, with mare lavas rising to fill topography around the rising lava. In terms of the orientation and morphology of the pyroclastic deposit, most LPDs are typically circular to sub-circular with irregular boundaries (Gaddis et al., 1985). MV LPD, however has an appearance like an involuted arrow, with the mare lavas occupying the negative space. The original form of the LPD would've likely been somewhat circular to sub-circular with a vent in the center. This central region and the pyroclastic vent or fissure has been flooded with mare basalt, producing the shape of the pyroclastic deposit that is now observed. This suggests that, although the pyroclastic deposit has not been covered by the mare lavas stratigraphically, this is because the pyroclastic materials likely ejected ballistically onto the highlands regions above the mare, and the mare lavas did not reach a sufficiently high enough level to cover the pyroclastic deposit. Although it has previously been suggested that many volcanic relationships can be complex and have multiple phases of eruption (Chapter 3), this observation suggests that the Mare Vaporum pyroclastic deposit is a mare margin deposit that erupted prior to the mare lavas, sharing a magma source with the mare basin, and likely degassing the sourced magma.

The Manilius crater ejecta is truncated to the southwest, in the direction of the mare. This suggests that the Mare Vaporum lavas rose to cover parts of the ejecta blanket in this region, indicating that Manilius crater is older than Mare Vaporum. This would therefore rule out a Copernican or Eratosthenian age for Manilius crater, as the mapped age of Mare Vaporum is greater than 3.2 Ga (Hiesinger et al., 2011). Further investigation into the age dating of Manilius crater (e.g., through crater counting) or into the original evaluation of the age dating of the Manilius crater and what datasets were used to inform this age determination could be used to redefine the geologic age of this large crater.

The pyroclastics surrounding Rima Hyginus mantle the region surrounding the Rima Hyginus IMP, which is mapped in Fortezzo et al., (2020) as “Imbrium plains,” which is interpreted as being of “ambiguous origin, likely Orientale and other large impact ejecta.”. These features would be Imbrium in age or younger as they cut through and are emplaced on top of the Imbrium-dated features. There are no indications that the Rima Hyginus features relate to volcanic features in Mare Vaporum in terms of stratigraphic or volcanic relationships (e.g., no cross-cutting relationships could be identified, and the thermophysical properties appear to be distinct from the

IMPs, LPDs, and other features in the rest of the region). The mapped "Imbrium plains" terrain generally have similar physical properties to older mare features: lower albedo than typical highlands but not as dark as younger mare (which is also noted as a feature of the mapped unit: "intermediate albedo"), rock abundance relatively higher than highlands but not as observably high as Mare Vaporum, and an overall H-parameter that's lower than the moderate highlands terrains. This indicates that further investigation into the composition of the "Imbrium plains" is warranted to determine whether these are compositionally related to the Orientale basin or other crater ejecta as reported, or if the terrain represents an older volcanic terrain that pre-dates Mare Vaporum.

4.5.6: Investigation of previously identified features

In addition to the pyroclastic deposits investigated in this study (i.e., Mare Vaporum regional LPD and Rima Hyginus LPD), three others were mapped in the geologic map by Fortezzo et al., (2020) as "dark mantling units," which are interpreted as pyroclastic in origin. For this study, we named them Boscovich LPD-1, Boscovich LPD-2, and Rima Conon LPD (Figure 42), after the features most closely are located. The two LPDs near Boscovich crater are localized in size (i.e., smaller than 1000 km^2), and Rima Conon LPD is regional in size classification (greater than 1000 km^2). The Rima Conon LPD could be interpreted as being related to the magma source and eruption of the Rima Conon sinuous rille, either erupting simultaneously (similarly to Mozart rille of Chapter 3), or could be interpreted as only being related to the mare, and not being related to the rille at all (similarly to Rima Fresnel of Chapter 3). The Rima Conon region has a low rock abundance and high H-parameter, but this is expected for the highland region that it mantles, and no correlation to the mapped region of the LPD and trends in these thermophysical properties could be found. Similarly, the Bostovich crater LPDs were not discernable in the rock abundance or H-parameter maps as distinct from the crater ejecta or surrounding heavily-reworked highland terrain.

Preliminary investigation into these features in compositional datasets (e.g., Chapter 3) also did not reveal clear indications of pyroclastic features at these locations, or in patterns associated with the mapped dark mantling units. These dark mantling units were likely identified in older datasets (e.g., Clementine, Lunar Orbiter) and investigation into these methods of characterization could inform future investigations for confirming and delineating these pyroclastic deposits. Detailed morphologic mapping could also reveal finer detail not available in these maps, such as transintions between mantled areas and regions of decreased crater retention, identifications of volcanic vents, and/or flow textures visible in high spatial resolution datasets (e.g., LROC NAC).

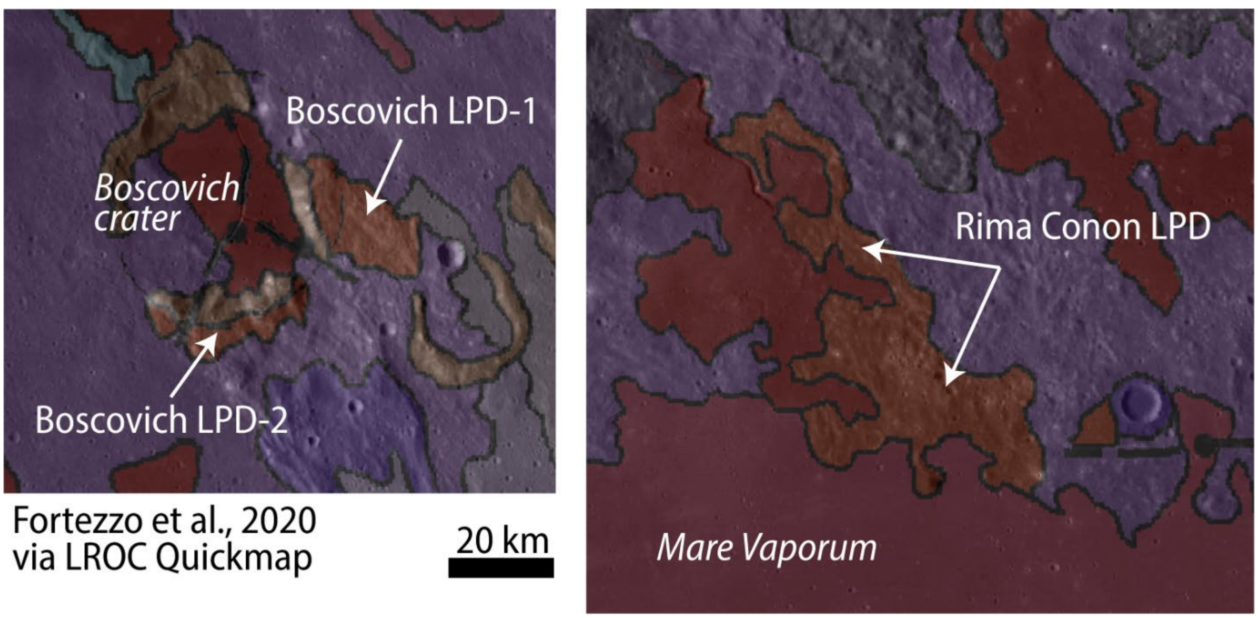

Figure 42: Boscovich Crater LPDs (left) and Rima Conon LPD (right) from Fortezzo et al., (2020) Unified Geologic Map of the Moon. Red-orange units are labeled "Imbrium dark mantled" units in the map, and are interpreted as "pyroclastic material" in the Description of Map Units. Red units are mare lavas and purple units are highland terrains.

4.6 Conclusion

In this work we use Diviner Lunar Radiometer Experiment data to evaluate temperatures and thermophysical properties of several volcanic features in the Mare Vaporum region. These volcanic features are diverse in eruption style therefore display variations in temperatures, rock abundance, relative thermal inertia, and albedo that result from variations that arise during volcanic emplacement (e.g., grain size, composition). We find that the regional Mare Vaporum LPD has a low rock abundance and high H-parameter, contrasting the mare flows which have a higher rock abundance and lower H-parameter. The mare appears to embay the pyroclastic deposit at all lower elevations as observed by the high contrast between the thermal and thermophysical properties between the mare and LPD and therefore represents an instance of volatile loss via pyroclastic eruption, followed by late-stage effusive mare infilling. Additionally, the mare lava embays and covers the Manilius crater ejecta blanket, establishing a relative stratigraphic relationship within the basin. These stratigraphic relationships have revealed that Manilius crater must be older than a previously-reported Eratosthenian age based on the crater counting age of the mare lavas as older than the established boundary of the Eratosthenian/Imbrium boundary. Variations in thermal and thermophysical properties are correlated to differences in geologic units, which we've used to establish stratigraphic relationships between observed features in the Mare Vaporum basin.

Chapter 5: Discussion and Conclusions

5.1 Discussion of Results

The research I have shown builds on past knowledge in explosive volcanism on the Moon, contributes new discoveries of sites of explosive volcanism, and makes new connections between the different types of volcanism on the Moon. I created a new inventory of pyroclastic deposits for the lunar community to evaluate in detail, and I use this inventory to connect these pyroclastic deposits to trends in lunar crustal structure and magma source regions. The trends I found relating explosive volcanism and magma sources, distribution, and other volcanic features have not been evaluated statistically. The work I've created also connects explosive volcanism to the subsurface volatile inventory as the distribution of explosive volcanism directly relates to regions of the lunar subsurface that are most volatile-rich. I take information from this inventory (i.e., connections of explosive volcanism to magma source regions) and investigate deeper into the relationships between these volatile-rich eruptions and other volcanic features, which could potentially be sourced from the same magma. Results from this analysis indicate that lunar volcanism can be as complex as terrestrial volcanism with different types of relationships between LPDs and co-located effusive features. I dive deeper into this conclusion and investigate the physical properties of features of geologic features using their thermal and thermophysical properties to develop a geologic history of a region. This study has revealed that we can use differences in physical properties to determine stratigraphic relationships about different geologic features. These combined analyses enhance what we know about the relationships between explosive and effusive volcanic features, and creates new datasets and lines of investigation for the lunar community to pursue further studies in the distribution of lunar volatiles, lunar geologic history, and lunar origins.

The evolution of lunar volcanic eruptions have been considered to follow a linear degassing phase from explosive to effusive eruption; I demonstrate in Chapter 3 that pyroclastic volcanism doesn't always follow this linear trend and can have complexities similar to terrestrial volcanism. These results open new lines of research into the evolution of volcanism on the Moon, which directly relates to the evolution of the lunar interior. Treating explosive volcanism as part of a complex system instead of a simple linear progression changes how subsurface volatiles are stored and magma evolves. Changes in volatile content and species, in addition to changes in composition due to melt fractionation can be recorded in the surface volcanic features. We can investigate this further using future sample return missions, investigating the diversity of pyroclastic deposits, which have been identified as high-priority scientific and exploration targets. For example, returning samples of "black spot" high-titanium deposits, pyroclastics associated with silicic volcanism, and by finding glassy and non-glassy deposits to evaluate volatile content and volatile species. These deposits represent the composition and volatile content of the lunar deep interior and can be related to the evolution of the Moon via compositional analysis. Connecting these returned samples to remote sensing observations, including those from new and future missions (e.g., Lunar Trailblazer, PRISM) can field-validate our understanding of remotely sensed observations and provide further constraints on how we use remote sensing observations to study the lunar surface. Follow-up studies using results from near-infrared and thermal-infrared remote observations from Trailblazer, which will be obtained simultaneously can reveal higher detail in volatile species and composition than previously evaluated.

Differences between explosive and effusive deposits are not restricted to composition and mineralogy, but also include differences in physical properties such as grain size, albedo, and grain packing. To expand the analyses conducted in Chapter 2 on relationships between explosive deposits to magma source regions and in Chapter 3 on compositional relationships between explosive and effusive deposits of shared magma source regions, I then study the thermal and thermophysical properties of explosive deposits to understand physical properties of explosive deposits. I characterize the temperatures, rock abundance, and H-parameter of features within the Mare Vaporum basin within the previously analyzed Montes Apenninus region to investigate the geologic history and context of these features.

The orientation and morphology of the pyroclastic deposit in the Mare Vaporum basin has an appearance like an involuted arrow, with the mare lavas occupying the negative space. The original form of the LPD would've likely been somewhat circular to sub-circular with a vent in the center, indicating that this central region that the likely vent occupied has been flooded with mare basalt, producing the shape of the pyroclastic deposit that is now observed. Small craters in the Mare

Vaporum basin exhibit variable results in an RGB composite map of maximum and minimum temperatures and brightness. Craters of similar size that are yellow in the RGB composite are interpreted as being bright, whereas craters that are teal in the RGB composite are interpreted as being dark. We subsequently correlate the yellow craters in the RGB map to bright craters in the WAC morphology mosaic, which we interpret as fresh ejecta of less-weathered mare that has been ejected from under the top regolith layer. We correlate the teal craters with dark halo craters in the WAC morphology mosaic which we interpret as excavating dark material from below the mare. This material could potentially be pyroclastic material that had been buried by the mare flows and is being exhumed by the impact. Additionally, we investigate the large Manilius crater ejecta, which has been truncated by mare in the thermophysical maps. This suggests that the Mare Vaporum lavas rose to cover parts of the ejecta blanket in this region, indicating that Manilius crater is older than Mare Vaporum. This would therefore rule out the previously-mapped Eratosthenian age for Manilius crater, as the mapped age of Mare Vaporum is greater than 3.2 Ga (Hiesinger et al., 2011).

Volcanically, the features in Mare Vaporum exhibit thermophysical properties that are distinct, and these can be traced to physical properties that can be used to delineate boundaries and infer relationships between these features. The Mare Vaporum regional pyroclastic deposit demonstrates a lower rock abundance and higher H-parameter than the surrounding mare flows, revealing its fine-grained nature. In an RGB color composite image evaluated, pyroclastic deposit had a darker blue color than the mare basalts, indicating that the LPD has a lower albedo and lower thermal inertia than the surrounding areas (including the dark mare). The fine-grained, low-albedo pyroclastic deposit appears to mantle knobby/rugged terrain that was potentially highlands material, with rockier mare lavas rising to fill topography around the rising lava. No pyroclastic material was observed mantling the mare lavas, suggesting an earlier volatile-rich explosive eruption, creating the pyroclastic deposit that mantled the surrounding highlands, followed by a volatile-depleted mare infilling phase.

5.2: Conclusion

In this work, I created a database of known pyroclastic deposits on the Moon as identified in literature and through additional observations. This inventory updates a database conducted in 2003 (Gaddis et al., 2003), providing additional information on these pyroclastic deposits, and adding new pyroclastic deposits to the global dataset. This also provides a consistent baseline for all pyroclastic deposits, as this analysis was conducted using the same methodology for the LPD inventory and provides a broad overview from which future studies can build. The analysis conducted in 2003 provides a comprehensive compositional analysis of an inventory of LPDs which are included in this dataset, providing an enhancement of the original results. As the inventory of deposits has now been evaluated in its entirety using two datasets, this starts a baseline that can grow to other datasets and increase the amount and types of information about LPDs globally. This database is being made public as a GIS shapefile of LPD extent boundaries, providing researchers a single, accessible source from which to the ability to compare the boundaries of with their own tools.

We use the new inventory of LPDs to understand the distribution of pyroclastic material on the surface of the Moon and the distribution of sites of known volatile-rich magma sources. We evaluated the areal extent of each identified pyroclastic deposit to collate a single source for known areal extents for identified LPDs. These areal extents are used by the lunar community to infer explosive eruption styles and are therefore critical to understanding and characterizing thoroughly. We evaluate the distribution of areal extents of LPDs and classify them using the Jenks Natural

Breaks methods to identify natural breaks in the dataset that might reveal changes in magma conditions that would result in different magma flux rates. This removes arbitrary classification and returns a statistical classification, whereby the data demonstrate where the gaps exist and how many gaps are present. The results indicate that, although sizes range from 2 km^2 to nearly 50,000 km^2, very small pyroclastic deposits are very common, with deposits 100 km^2 or smaller comprising 41.9% of all deposits and deposits 500 km^2 or smaller comprising 69% of all LPDs. As these size classifications are used by the lunar community to infer eruption conditions, further investigation into the clustering of the areal extents and the correlation to LPD physical and compositional properties is required. After LPDs have been fully evaluated by size in both the smaller size classification and large size classification, the composition, crystallinity, and physical properties of LPDs should be conducted to determine if there are trends within each size classification. Evaluating each size group and characterizing these as a set can reveal whether eruption conditions influence deposit size. Understanding trends within size groups also can be used to characterize magma conditions such as volatile flux (via crystallinity), compositional evolution between deposits, and lunar thermal evolution. Future work could also include expanding the compositional analysis of LPDs to evaluate mineralogy and composition of the deposits, connecting these compositional factors to the diverse magma source regions. Summarizing various mineral components of LPDs (e.g., glass content, ilmenite) in addition to pyroxene composition (i.e., clinopyroxene, orthopyroxene), and investigating how LPDs within magma source regions may be similar or different can provide insights into interior magma conditions, and elucidate reasons why differences between LPDs may exist.

Using this new inventory, I demonstrate that the majority of pyroclastic deposits are found on the near side of the Moon (82.1%), which is a figure that has been known but not previously quantified. Although this was expected as the majority of lunar basaltic volcanism is found on the near side of the Moon, and it is common that different types of volcanism are likely to occur in the same regions, if not from the same magma plumbing systems, this was not expected to have such a large difference to the far side of the Moon. Additionally, the crust is thickest on the far side of the Moon (with the exception of the South Pole Aitken Basin), which would create a limit on dike expansion and magma rise. LPDs are also mostly found closer to the equator than to the poles with 90.5% being within 50° N/S. This was a surprising finding, as the area with the thinnest crust, the South Pole Aitken Basin, is near the south pole and extends northward into latitudes high enough to fill in data points above 50°. This suggests that crustal thickness is not the only consideration for creating an eruption, but additional limits for eruption exist. Magma ascent must therefore be more influenced by intrinsic conditions such as volatile content/species, volatile exsolution, and magma fragmentation and not as restricted by crustal thickness than originally hypothesized.

In addition to evaluating LPDs by latitude and longitude, we also connect pyroclastic deposits with other types of magma source regions and find that the more LPDs occur in floor-fractured craters than are associated with any other type of magma source region (44.1%). Although it has been observed that LPDs are commonly found in floor-fractured craters in the past, it is significant that there is a high frequency of LPDs found only in floor-fractured craters as opposed to any of the other eleven magma source regions evaluated in this study. LPDs are also associated with other types of volcanic features such as sinuous rilles (i.e., lava channels) and mare basins. Evaluating how effusive and explosive volcanism relate is an important component to understanding the geologic evolution of the Moon. Pyroclastic deposits related to other effusive features can be used to characterize the volatile and compositional evolution of the magma system. It has been hypothesized that lunar volcanic features evolve from a volatile-rich degassing phase to a volatile-depleted effusive phase. To evaluate whether this is true for all lunar volcanic systems, we must conduct a more focused evaluation of a selection of pyroclastic features related to a variety of co-located effusive features.

By studying a region of the near side of the Moon near the equator, I further investigate the relationships between explosive deposits and magma source regions. To evaluate magma source regions and explosive deposits, we characterized the diversity of the mineralogy of pyroclastic deposits within the Montes Apenninus region, within the context of relating these to nearby effusive features. We evaluated mineralogical and compositional differences between pyroclastic deposits and effusive features to develop an eruptive relationship between each LPD in the region and nearby effusive features. Using compositional and spatial relationships between the effusive and explosive volcanic mineralogy, we evaluated the timing and potential co-occurrence of these eruptions.

We showed that the compositional and stratigraphic relationships between explosive and effusive volcanic features cannot be generalized in the Montes Apenninus region and that the LPDs have a full diversity of temporal and spatial relationships with nearby effusive features. The relationship between effusive and explosive volcanism is not commonly evaluated but is an essential component of the eruptive history of a locality. The LPDs evaluated in the Montes Apenninus region demonstrated a range of glass distribution and stratigraphic relationships with nearby effusive features. Newly identified LPDs in the region (e.g., along vents along Mozart rille) can be recognized using this methodology where previous studies using lower spectral and spatial resolution datasets could not confirm an LPD. We observed explosive volcanic deposits around vents along Mozart rille, demonstrating an instance where explosive and effusive volcanism was likely occurring at the same vent.

Contrasting the Mozart rille LPDs, the Fresnel LPD in the Montes Apenninus region mantles the central portion of Rimae Fresnel and the surrounding region. It is unlikely the explosive volcanism was occurring from the same vent as the effusive flow as if this were the case, the LPD would be expected to mantle only a portion of the rille (as seen with the LPDs along Mozart rille) or would mantle the northern or southern extent of Rimae Fresnel, from which the rille lavas originated. There is no clear spatial relationship between a potential volcanic vent, the lava channel, and the LPD so these results suggest that the LPD was emplaced after the rille flow, and that they were likely not sourced from the same vent. Therefore, the eruption that resulted in the deposition of the Fresnel LPD is unlikely correlated to its namesake fissure. The differences between the Mozart rille and Rimae Fresnel LPDs demonstrate that there isn't a single eruptive model that can describe the relationships between explosive and effusive volcanism.

Future work in this sector can include expanding the mineralogical dataset to include volcanically-relevant minerals and compositions (e.g., clinopyroxene and orthopyroxene) and connecting magma source regions through index minerals (e.g., shared ilmenite from the deep interior). Although not indicative of explosive eruption, ilmenite has been identified in pyroclastic deposits, and can be used to connect to effusive features, indicating a potential shared magma source. Additional morphologic studies can be used to further define stratigraphic relationships and identify complex geologic histories in regions where there are many different volcanic and non-volcanic features. Additionally, explosive volcanic features can erupt from a variety of eruption styles with a range of crystallinities. Combining the relationships between explosive and effusive volcanism and expanding the eruption styles to include explosive volcanic styles (e.g., Vulcanian, Strombolian, lava fountaining) using crystallinity and composition would provide enhanced insights into the volcanic plumbing systems and evolution of the magma bodies. The lunar surface has endured billions of years of reworking by impacts and space weathering, homogenizing surface layers of volcanic features and making differences between effusive and explosive features more difficult to discern. *In situ* measurements and observations from landed missions (e.g., Artemis, PRISM, other CLPS landers and rovers) can provide additional detail not available to lower spatial resolution of orbital spacecraft. Additionally, returned samples can also provide insights into magmatic conditions of explosive and effusive features not directly available from remote sensing, such as magma cooling rates, absolute ages, and complex compositions.

After evaluating composition of the Montes Apenninus region, I then focused on a smaller region within the Montes Apenninus for Chapter 3, relating explosive and effusive features in Mare Vaporum by investigating their thermophysical properties. This enhances what was learned from the compositional analysis by factoring in the relative thermal inertia (a property indicating how "fluffy" the regolith is, reported as H-parameter) and rock abundance of explosive and effusive features within the Mare Vaporum basin. In addition to these thermophysical properties, I also evaluate thermal properties, which are tied to the physical properties of the different materials in the Mare Vaporum region. These physical properties can be used to connect surface materials to volcanic eruption styles (e.g., effusive lava flows, blocky Vulcanian pyroclastic deposits, fine-grained lava-fountain pyroclastic deposits). This expands on the composition of volcanic features found in Chapter 3, which can often be similar for deposits that have erupted from the same magma source.

I find thermal and thermophysical properties of a selection of volcanic and non-volcanic features in the Mare Vaporum basin. In addition to minimum nighttime temperature and maximum daytime temperatures, I also evaluate the rock abundance and H-parameter (a regolith property interpreted as the change in density with depth) of features to relate their geologic histories. The variety of volcanic and non-volcanic features in the Mare Vaporum basin demonstrate a range of temperatures, which relate to their physical properties including albedo, rock content, and homogeneity. I was able to establish relative geologic histories between large impact craters, mare lavas, and other geologic feaures within the Mare Vaporum basin. The large Manilius crater had previously been identified as younger than the emplacement of the mare lavas in Mare Vaporum, but based on how Mare Vaporum embays the Manilius crater ejecta blanket, Manilius crater must be older than Mare Vaporum. The regional Mare Vaporum LPD is also embayed by the Mare Vaporum lavas, establishing that the LPD erupted prior to the emplacement of the lavas or was contiguous with their eruption.

Three pyroclastic deposits that had been previously mapped in this region were not easily identified using thermal and thermophysical observations during the course of this study. Future work will include investigating these further using additional morphological and compositional datasets, and at higher resolutions to understand whether these would be reasonably expected to have been identified, and understanding what datasets were used to identify these deposits previously. Additionally, we will investigate the thermal properties of the irregular mare patches and surrounding areas in more detail to determine if there are any conclusions that we can make about the age of these controversial features.

This combined work spans the entire lunar surface, investigating explosive volcanism with a wide lens. This breadth of information allows for a wide variety of trends including global distributions of explosive volcanism, relationships to other types of volcanism, and the investigation of these as potential resources in regions that may be targeted for future exploration. These combined chapters also go into fine detail into a single location, investigating that location with all datasets and all methodologies used in this work. This narrow focus is required to elucidate the fine detail needed to understand the complexity of the relationships between the various types of volcanism on the Moon. These relationships are important to understand as they relate directly to the evolution of the deep interior, and to the origins of the Moon.

6 References

Adams, J.B., Pieters, C., McCord, T., 1974. Orange glass: Evidence for regional deposits of pyroclastic origin on the Moon. Proc. 5th Lunar Planet. Sci. Conf.

Allen, C.C., Morris, R.V., McKay, D.S., 1996. Oxygen extraction from lunar soils and pyroclastic glass. J. Geophys. Res. Planets 101, 26085–26095. https://doi.org/10.1029/96JE02726

Bandfield, J.L., Ghent, R.R., Vasavada, A.R., Paige, D.A., Lawrence, S.J., Robinson, M.S., 2011. Lunar surface rock abundance and regolith fines temperatures derived from LRO Diviner Radiometer data. J. Geophys. Res. 116, E00H02. https://doi.org/10.1029/2011JE003866

Bandfield, J.L., Hayne, P.O., Williams, J.-P., Greenhagen, B.T., Paige, D.A., 2015. Lunar surface roughness derived from LRO Diviner Radiometer observations. Icarus 248, 357–372. https://doi.org/10.1016/j.icarus.2014.11.009

Bandfield, J.L., Song, E., Hayne, P.O., Brand, B.D., Ghent, R.R., Vasavada, A.R., Paige, D.A., 2014. Lunar cold spots: Granular flow features and extensive insulating materials surrounding young craters. Icarus 231, 221–231. https://doi.org/10.1016/j.icarus.2013.12.017

Barnes, J.J., Franchi, I.A., McCubbin, F.M., Anand, M., 2019. Multiple reservoirs of volatiles in the Moon revealed by the isotopic composition of chlorine in lunar basalts. Geochim. Cosmochim. Acta 266, 144–162. https://doi.org/10.1016/j.gca.2018.12.032

Bennett, K.A., Horgan, B.H.N., Gaddis, L.R., Greenhagen, B.T., Allen, C.C., Hayne, P.O., Bell, J.F., Paige, D.A., 2016. Complex explosive volcanic activity on the Moon within Oppenheimer crater. Icarus 273, 296–314. https://doi.org/10.1016/j.icarus.2016.02.007

Besse, S., Sunshine, J.M., Gaddis, L.R., 2014. Volcanic glass signatures in spectroscopic survey of newly proposed lunar pyroclastic deposits: LUNAR VOLCANIC GLASS. J. Geophys. Res. Planets 119, 355–372. https://doi.org/10.1002/2013JE004537

Blewett, D.T., Hawke, B.R., 2001. Remote sensing and geological studies of the Hadley-Apennine region of the Moon. Meteorit. Planet. Sci. 36, 701–730. https://doi.org/10.1111/j.1945-5100.2001.tb01909.x

Boardman, J.W., Pieters, C.M., Green, R.O., Lundeen, S.R., Varanasi, P., Nettles, J., Petro, N., Isaacson, P., Besse, S., Taylor, L.A., 2011. Measuring moonlight: An overview of the spatial properties, lunar coverage, selenolocation, and related Level 1B products of the Moon Mineralogy Mapper. J. Geophys. Res. 116, E00G14. https://doi.org/10.1029/2010JE003730

Braden, S.E., Stopar, J.D., Robinson, M.S., Lawrence, S.J., van der Bogert, C.H., Hiesinger, H., 2014. Evidence for basaltic volcanism on the Moon within the past 100 million years. Nat. Geosci. 7, 787–791. https://doi.org/10.1038/ngeo2252

Byron, B.D., Elder, C.M., Williams, J. -P., Ghent, R.R., Gallinger, C.L., Hayne, P.O., Paige, D.A., 2022. Thermophysical Properties of Lunar Irregular Mare Patches From LRO Diviner Radiometer Data. J. Geophys. Res. Planets 127. https://doi.org/10.1029/2022JE007214

Carter, L.M., Campbell, B.A., Hawke, B.R., Campbell, D.B., Nolan, M.C., 2009. Radar remote sensing of pyroclastic deposits in the southern Mare Serenitatis and Mare Vaporum regions of the Moon. J. Geophys. Res. 114, E11004. https://doi.org/10.1029/2009JE003406

Carter, L.M., Hawke, B.R., Garry, W.B., Campbell, B.A., Giguere, T.A., Bussey, D.B.J., 2013. Radar Observations of Lunar Hollow Terrain. LPSC 44th.
Cassidy, M., Manga, M., Cashman, K., Bachmann, O., 2018. Controls on explosive-effusive volcanic eruption styles. Nat. Commun. 9, 2839. https://doi.org/10.1038/s41467-018-05293-3
Cernan, E.A., Evans, R.E., Schmitt, H.H., 1972. Apollo 17 Technical air-to-ground voice transcription.
Chauhan, M., Bhattacharya, S., Saran, S., Chauhan, P., Dagar, A., 2015. Compton–Belkovich Volcanic Complex (CBVC): An ash flow caldera on the Moon. Icarus 253, 115–129. https://doi.org/10.1016/j.icarus.2015.02.024
Circular (Circular), 2023. , Circular.
Clark, R.N., Pieters, C.M., Green, R.O., Boardman, J.W., Petro, N.E., 2011. Thermal removal from near-infrared imaging spectroscopy data of the Moon. J. Geophys. Res. 116, E00G16. https://doi.org/10.1029/2010JE003751
Clegg-Watkins, R.N., Jolliff, B.L., Watkins, M.J., Coman, E., Giguere, T.A., Stopar, J.D., Lawrence, S.J., 2017. Nonmare volcanism on the Moon: Photometric evidence for the presence of evolved silicic materials. Icarus 285, 169–184. https://doi.org/10.1016/j.icarus.2016.12.004
Committee on the Scientific Context for Exploration of the Moon, Space Studies Board, Division on Engineering and Physical Sciences, National Research Council, 2007. The Scientific Context for Exploration of the Moon. National Academies Press, Washington, D.C. https://doi.org/10.17226/11954
Coombs, C.R., Hawke, B.R., 1991. Pyroclastic deposits on the western limb of the Moon.
Coombs, C.R., Hawke, B.R., Wilson, L., 1988. Geologic and Remote Sensing Studies of Rima Mozart. Proc. 18th Lunar Planet. Sci. Conf.
Crawford, I.A., 2015. Lunar resources: A review. Prog. Phys. Geogr. Earth Environ. 39, 137–167. https://doi.org/10.1177/0309133314567585
Defense Mapping Agency, 1974. Rima Mozart. 41A3S1(50).
Delano, J.W., 1986. Pristine Lunar Glasses: Criteria, data, and implications. Proc. 16th Lunar Planet. Sci. Conf.
Elder, C.M., Hayne, P.O., 2017. Thermophysical properties of Lunar Volcanic Deposits. LPSC 58th.
Elder, C.M., Hayne, P.O., Bandfield, J.L., Ghent, R.R., Williams, J.-P., Donaldson Hanna, K.L., Paige, D.A., 2017. Young lunar volcanic features: Thermophysical properties and formation. Icarus 290, 224–237. https://doi.org/10.1016/j.icarus.2017.03.004
Fegley, B., 1993. Resources of near-Earth space. University of Arizona Press, Tucson.
Fogel, R.A., Rutherford, M.J., 1995. Magmatic volatiles in primitive lunar glasses: I. FTIR and EPMA analyses of Apollo 15 green and yellow glasses and revision of the volatile-assisted fire-fountain theory. Geochim. Cosmochim. Acta 59, 201–215. https://doi.org/10.1016/0016-7037(94)00377-X
Gaddis, L.R., Hawke, B.R., Robinson, M.S., Coombs, C., 2000. Compositional analyses of small lunar pyroclastic deposits using Clementine multispectral data. J. Geophys. Res. Planets 105, 4245–4262. https://doi.org/10.1029/1999JE001070
Gaddis, L.R., Horgan, B.N.H., McBride, M., Bennett, K.A., Stopar, J., Gustafson, J.O., 2016. Alphonsus Crater: Compositional Clues to Eruptions Styles of Lunar Small Volcanoes.

Gaddis, Lisa R, Pieters, C.M., Ray Hawke, B., 1985. Remote sensing of lunar pyroclastic mantling deposits. Icarus 61, 461–489. https://doi.org/10.1016/0019-1035(85)90136-8
Gaddis, L.R., Staid, M.I., Tyburczy, J.A., Hawke, B.R., Petro, N.E., 2003. Compositional analyses of lunar pyroclastic deposits. Icarus 161, 262–280. https://doi.org/10.1016/S0019-1035(02)00036-2
Garrick-Bethell, I., Nimmo, F., Wieczorek, M.A., 2010. Structure and Formation of the Lunar Farside Highlands. Science 330, 949–951. https://doi.org/10.1126/science.1193424
Ghent, R.R., Hayne, P.O., Bandfield, J.L., Campbell, B.A., Allen, C.C., Carter, L.M., Paige, D.A., 2014. Constraints on the recent rate of lunar ejecta breakdown and implications for crater ages. Geology 42, 1059–1062. https://doi.org/10.1130/G35926.1
Green, R.O., Pieters, C., Mouroulis, P., Eastwood, M., Boardman, J., Glavich, T., Isaacson, P., Annadurai, M., Besse, S., Barr, D., Buratti, B., Cate, D., Chatterjee, A., Clark, R., Cheek, L., Combe, J., Dhingra, D., Essandoh, V., Geier, S., Goswami, J.N., Green, R., Haemmerle, V., Head, J., Hovland, L., Hyman, S., Klima, R., Koch, T., Kramer, G., Kumar, A.S.K., Lee, K., Lundeen, S., Malaret, E., McCord, T., McLaughlin, S., Mustard, J., Nettles, J., Petro, N., Plourde, K., Racho, C., Rodriquez, J., Runyon, C., Sellar, G., Smith, C., Sobel, H., Staid, M., Sunshine, J., Taylor, L., Thaisen, K., Tompkins, S., Tseng, H., Vane, G., Varanasi, P., White, M., Wilson, D., 2011. The Moon Mineralogy Mapper (M^3) imaging spectrometer for lunar science: Instrument description, calibration, on-orbit measurements, science data calibration and on-orbit validation. J. Geophys. Res. 116, E00G19. https://doi.org/10.1029/2011JE003797
Gustafson, J.O., Bell III, J.F., Gaddis, L.R., Hawke, B.R., Giguere, T.A., 2012. Characterization of previously unidentified lunar pyroclastic deposits using Lunar Reconnaissance Orbiter Camera data. J. Geophys. Res. Planets 117. https://doi.org/10.1029/2011JE003893
Hauri, E.H., Weinreich, T., Saal, A.E., Rutherford, M.C., Van Orman, J.A., 2011. High Pre-Eruptive Water Contents Preserved in Lunar Melt Inclusions. Science 333, 213–215. https://doi.org/10.1126/science.1204626
Hawke, B.R., Coombs, C.R., Gaddis, L.R., Lucey, P.G., Owensby, P.D., 1989. Remote sensing and geologic studies of localized dark mantle deposits on the moon. Lunar Planet. Sci. Conf. Proc. 19, 255–268.
Hawke, B.R., MacLaskey, D., McCord, T.B., Adams, J.B., Head, J.W., Pieters, C.M., Zisk, S.H., 1979. Multispectral mapping of the Apollo 15–Apennine region: The identification and distribution of regional pyroclastic deposits. Proc. 10th Lunar Planet. Sci. Conf. 2995–3015.
Hayne, P.O., Bandfield, J.L., Siegler, M.A., Vasavada, A.R., Ghent, R.R., Williams, J.-P., Greenhagen, B.T., Aharonson, O., Elder, C.M., Lucey, P.G., Paige, D.A., 2017. Global Regolith Thermophysical Properties of the Moon From the Diviner Lunar Radiometer Experiment: Lunar Regolith Thermophysical Properties. J. Geophys. Res. Planets 122, 2371–2400. https://doi.org/10.1002/2017JE005387
Head, J.W., 1974. Lunar dark-mantle deposits: possible clues to the distribution of early mare deposits. Proc. 5th Lunar Planet. Sci. Conf.
Head, J.W., Wilson, L., 2017. Generation, ascent and eruption of magma on the Moon: New insights into source depths, magma supply, intrusions and effusive/explosive eruptions (Part 2: Predicted emplacement processes and observations). Icarus 283, 176–223. https://doi.org/10.1016/j.icarus.2016.05.031

Head, J.W., Wilson, L., 1979. Alphonsus-type dark-halo craters - Morphology, morphometry and eruption conditions.

Heiken, G.H., McKay, D.S., Brown, R.W., 1974. Lunar deposits of possible pyroclastic origin. Geochim. Cosmochim. Acta 38, 1703–1718. https://doi.org/10.1016/0016-7037(74)90187-2

Henderson, M.J.B., Horgan, B.H.N., Rowe, M.C., Wall, K.T., Scudder, N.A., 2021. Determining the Volcanic Eruption Style of Tephra Deposits From Infrared Spectroscopy. Earth Space Sci. 8. https://doi.org/10.1029/2019EA001013

Hiesinger, H., Head, J.W., Wolf, U., Jaumann, R., Neukum, G., 2011. Ages and stratigraphy of lunar mare basalts: A synthesis, in: Recent Advances and Current Research Issues in Lunar Stratigraphy. Geological Society of America. https://doi.org/10.1130/2011.2477(01)

Horgan, B.H.N., Cloutis, E.A., Mann, P., Bell, J.F., 2014. Near-infrared spectra of ferrous mineral mixtures and methods for their identification in planetary surface spectra. Icarus 234, 132–154. https://doi.org/10.1016/j.icarus.2014.02.031

Hörz, F., Cintala, M., 1997. The Barringer Award Address Presented 1996 July 25, Berlin, Germany: Impact experiments related to the evolution of planetary regoliths. Meteorit. Planet. Sci. 32, 179–209. https://doi.org/10.1111/j.1945-5100.1997.tb01259.x

Hurwitz, D.M., Head, J.W., Hiesinger, H., 2013. Lunar sinuous rilles: Distribution, characteristics, and implications for their origin. Planet. Space Sci. 79–80, 1–38. https://doi.org/10.1016/j.pss.2012.10.019

International Astronomical Union, n.d. Gazetteer of Planetary Nomenclature. URL https://planetarynames.wr.usgs.gov/

Jawin, E.R., Besse, S., Gaddis, L.R., Sunshine, J.M., Head, J.W., Mazrouei, S., 2015. Examining spectral variations in localized lunar dark mantle deposits: SPECTRAL VARIATIONS IN LUNAR LDMDS. J. Geophys. Res. Planets 120, 1310–1331. https://doi.org/10.1002/2014JE004759

Jawin, E.R., Valencia, S.N., Watkins, R.N., Crowell, J.M., Neal, C.R., Schmidt, G., 2019. Lunar Science for Landed Missions Workshop Findings Report. Earth Space Sci. 6, 2–40. https://doi.org/10.1029/2018EA000490

Jenks, G.F., 1967. The Data Model Concept in Statistical Mapping, in: International Yearbook of Cartography. pp. 186–190.

Jozwiak, L.M., Head, J.W., Wilson, L., 2015. Lunar floor-fractured craters as magmatic intrusions: Geometry, modes of emplacement, associated tectonic and volcanic features, and implications for gravity anomalies. Icarus 248, 424–447. https://doi.org/10.1016/j.icarus.2014.10.052

Jozwiak, L.M., Head, J.W., Zuber, M.T., Smith, D.E., Neumann, G.A., 2012. Lunar floor-fractured craters: Classification, distribution, origin and implications for magmatism and shallow crustal structure: FLOOR-FRACTURED CRATER DISTRIBUTION AND ORIGIN. J. Geophys. Res. Planets 117, n/a-n/a. https://doi.org/10.1029/2012JE004134

Keske, A.L., Clarke, A.B., Robinson, M.S., 2020. On the eruptive origins of lunar localized pyroclastic deposits. Earth Planet. Sci. Lett. 547, 116426. https://doi.org/10.1016/j.epsl.2020.116426

Klem, S.M., Henriksen, M.R., Stopar, J., Boyd, A., Robinson, M.S., The LROC Science Team, 2014. Controlled LROC Narrow Angle Camera High Resolution Mosaics. LPSC 45th.

Klima, R.L., Pieters, C.M., Boardman, J.W., Green, R.O., Head, J.W., Isaacson, P.J., Mustard, J.F., Nettles, J.W., Petro, N.E., Staid, M.I., Sunshine, J.M., Taylor, L.A., Tompkins, S., 2011. New insights into lunar petrology: Distribution and composition of prominent low-Ca pyroxene exposures as observed by the Moon Mineralogy Mapper (M^3). J. Geophys. Res. 116, E00G06. https://doi.org/10.1029/2010JE003719

Kumaresan, P.R., Saravanavel, J., 2019. Morphological and Chronological Mapping of Manilius Crater Region Using Chandrayaan-1 Data Sets. J. Indian Soc. Remote Sens. 47, 839–851. https://doi.org/10.1007/s12524-019-00967-x

Lawrence, S.J., Hawke, B.R., 2008. Lunar Pyroclastic Deposits: an accessible and quantifiable lunar resource. LPSC 39th.

Li, S., Milliken, R.E., 2017. Water on the surface of the Moon as seen by the Moon Mineralogy Mapper: Distribution, abundance, and origins. Sci. Adv. 3, e1701471. https://doi.org/10.1126/sciadv.1701471

Lo, M., La Spina, G., Joy, K.H., Polacci, M., Burton, M., 2021. Determining the Effect of Varying Magmatic Volatile Content on Lunar Magma Ascent Dynamics. J. Geophys. Res. Planets 126. https://doi.org/10.1029/2021JE006939

Lucchitta, B.K., Sanchez, A.G., 1975. Crater studies in the Apollo 17 region. Proc. 6th Lunar Planet. Sci. Conf.

Lucchitta, B.K., Schmitt, H.H., 1974. Orange material in the Sulpicius Gallus formation at the southwestern edge of Mare Serenitatis. Proc. 5th Lunar Planet. Sci. Conf.

Luo, B., Wang, Z., Song, J., Qian, Y., He, Q., Li, Y., Head, J.W., Moynier, F., Xiao, L., Becker, H., Huang, B., Ruan, B., Hu, Y., Pan, F., Xu, C., Liu, W., Zong, K., Zhao, J., Zhang, W., Hu, Z., She, Z., Wu, X., Zhang, H., 2023. The magmatic architecture and evolution of the Chang'e-5 lunar basalts. Nat. Geosci. 16, 301–308. https://doi.org/10.1038/s41561-023-01146-x

Mackin, J.H., 1969. Origin of Lunar Maria. GSA Bull. 80, 735–748. https://doi.org/10.1130/0016-7606(1969)80[735:OOLM]2.0.CO;2

McCord, T.B., Clark, R.N., Hawke, B.R., McFadden, L.A., Owensby, P.D., Pieters, C.M., Adams, J.B., 1981. Moon: Near-infrared spectral reflectance, A first good look. J. Geophys. Res. Solid Earth 86, 10883–10892. https://doi.org/10.1029/JB086iB11p10883

McGetchin, T.R., Head, J.W., 1973. Lunar Cinder Cones. Science 180, 68–71. https://doi.org/10.1126/science.180.4081.68

Morgan, C., Wilson, L., Head, J.W., 2021. Formation and dispersal of pyroclasts on the Moon: Indicators of lunar magma volatile contents. J. Volcanol. Geotherm. Res. 413, 107217. https://doi.org/10.1016/j.jvolgeores.2021.107217

Mustard, J.F., Murchie, S., Erard, S., Sunshine, J., 1997. In situ compositions of Martian volcanics: Implications for the mantle. J. Geophys. Res. Planets 102, 25605–25615. https://doi.org/10.1029/97JE02354

Neal, C.A., Brantley, S.R., Antolik, L., Babb, J.L., Burgess, M., Calles, K., Cappos, M., Chang, J.C., Conway, S., Desmither, L., Dotray, P., Elias, T., Fukunaga, P., Fuke, S., Johanson, I.A., Kamibayashi, K., Kauahikaua, J., Lee, R.L., Pekalib, S., Miklius, A., Million, W., Moniz, C.J., Nadeau, P.A., Okubo, P., Parcheta, C., Patrick, M.R., Shiro, B., Swanson, D.A., Tollett, W., Trusdell, F., Younger, E.F., Zoeller, M.H., Montgomery-Brown, E.K., Anderson, K.R., Poland, M.P., Ball, J.L., Bard, J., Coombs, M., Dietterich, H.R., Kern, C., Thelen, W.A., Cervelli, P.F., Orr, T., Houghton, B.F., Gansecki, C., Hazlett, R., Lundgren, P., Diefenbach, A.K., Lerner, A.H., Waite, G., Kelly, P., Clor, L., Werner, C.,

Mulliken, K., Fisher, G., Damby, D., 2019. The 2018 rift eruption and summit collapse of Kīlauea Volcano. Science 363, 367–374. https://doi.org/10.1126/science.aav7046
Paige, D. A., Foote, M.C., Greenhagen, B.T., Schofield, J.T., Calcutt, S., Vasavada, A.R., Preston, D.J., Taylor, F.W., Allen, C.C., Snook, K.J., Jakosky, B.M., Murray, B.C., Soderblom, L.A., Jau, B., Loring, S., Bulharowski, J., Bowles, N.E., Thomas, I.R., Sullivan, M.T., Avis, C., De Jong, E.M., Hartford, W., McCleese, D.J., 2010. The Lunar Reconnaissance Orbiter Diviner Lunar Radiometer Experiment. Space Sci. Rev. 150, 125–160. https://doi.org/10.1007/s11214-009-9529-2
Paige, David A., Siegler, M.A., Zhang, J.A., Hayne, P.O., Foote, E.J., Bennett, K.A., Vasavada, A.R., Greenhagen, B.T., Schofield, J.T., McCleese, D.J., Foote, M.C., DeJong, E., Bills, B.G., Hartford, W., Murray, B.C., Allen, C.C., Snook, K., Soderblom, L.A., Calcutt, S., Taylor, F.W., Bowles, N.E., Bandfield, J.L., Elphic, R., Ghent, R., Glotch, T.D., Wyatt, M.B., Lucey, P.G., 2010. Diviner Lunar Radiometer Observations of Cold Traps in the Moon's South Polar Region. Science 330, 479–482. https://doi.org/10.1126/science.1187726
Pieters, C., McCord, T.B., Zisk, S., Adams, J.B., 1973. Lunar black spots and nature of the Apollo 17 landing area. J. Geophys. Res. 78, 5867–5875. https://doi.org/10.1029/JB078i026p05867
Pieters, C.M., Boardman, J., Buratti, B., Chatterjee, A., Clark, R., Glavich, T., Green, R., Head III, J.W., Isaacson, P., Malaret, E., McCord, T., Mustard, J., Petro, N., Runyon, C., Staid, M., Sunshine, J., Taylor, L., Tompkins, S., Varanasi, P., White, M., 2009. The Moon Mineralogy Mapper (M^3) on Chandrayaan-1. Curr. Sci. 96, 500–505.
Pigue, L.M., Bennett, K.A., Horgan, B.H.N., Gaddis, L.R., 2023. Data for Relationship between explosive and effusive volcanism in the Montes Apenninus region of the Moon. https://doi.org/10.5281/zenodo.7757418
Popa, R.-G., Bachmann, O., Huber, C., 2021. Explosive or effusive style of volcanic eruption determined by magma storage conditions. Nat. Geosci. 14, 781–786. https://doi.org/10.1038/s41561-021-00827-9
Popa, R.-G., Tollan, P., Bachmann, O., Schenker, V., Ellis, B., Allaz, J.M., 2021c. Water exsolution in the magma chamber favors effusive eruptions: Application of Cl-F partitioning behavior at the Nisyros-Yali volcanic area. Chem. Geol. 570, 120170. https://doi.org/10.1016/j.chemgeo.2021.120170
Powell, T.M., Horvath, T., Robles, V.L., Williams, J. -P., Hayne, P.O., Gallinger, C.L., Greenhagen, B.T., McDougall, D.S., Paige, D.A., 2023. High-Resolution Nighttime Temperature and Rock Abundance Mapping of the Moon Using the Diviner Lunar Radiometer Experiment With a Model for Topographic Removal. J. Geophys. Res. Planets 128. https://doi.org/10.1029/2022JE007532
Qiao, L., Head, J., Wilson, L., Xiao, L., Kreslavsky, M., Dufek, J., 2017. Ina pit crater on the Moon: Extrusion of waning-stage lava lake magmatic foam results in extremely young crater retention ages. Geology 45, 455–458. https://doi.org/10.1130/G38594.1
Reid, A., Ridley, W., Donaldson, C., Brown, R.W., 1974. GLASS COMPOSITIONS IN THE ORANGE AND GREY SOILS FROM SHORTY CRATER, APOLLO 17. Eos Trans. Am. Geophys. Union 54, 607–608.
Renggli, C.J., King, P.L., Henley, R.W., Norman, M.D., 2017. Volcanic gas composition, metal dispersion and deposition during explosive volcanic eruptions on the Moon. Geochim. Cosmochim. Acta 206, 296–311. https://doi.org/10.1016/j.gca.2017.03.012

Robinson, M.S., Brylow, S.M., Tschimmel, M., Humm, D., Lawrence, S.J., Thomas, P.C., Denevi, B.W., Bowman-Cisneros, E., Zerr, J., Ravine, M.A., Caplinger, M.A., Ghaemi, F.T., Schaffner, J.A., Malin, M.C., Mahanti, P., Bartels, A., Anderson, J., Tran, T.N., Eliason, E.M., McEwen, A.S., Turtle, E., Jolliff, B.L., Hiesinger, H., 2010. Lunar Reconnaissance Orbiter Camera (LROC) Instrument Overview. Space Sci. Rev. 150, 81–124. https://doi.org/10.1007/s11214-010-9634-2

Saal, A.E., Hauri, E.H., Cascio, M.L., Van Orman, J.A., Rutherford, M.C., Cooper, R.F., 2008. Volatile content of lunar volcanic glasses and the presence of water in the Moon's interior. Nature 454, 192–195. https://doi.org/10.1038/nature07047

Sato, H., Robinson, M.S., Lawrence, S.J., Denevi, B.W., Hapke, B., Jolliff, B.L., Hiesinger, H., 2017. Lunar mare TiO 2 abundances estimated from UV/Vis reflectance. Icarus 296, 216–238. https://doi.org/10.1016/j.icarus.2017.06.013

Scudder, N.A., Horgan, B.H.N., Rampe, E.B., Smith, R.J., Rutledge, A.M., 2021. The effects of magmatic evolution, crystallinity, and microtexture on the visible/near-infrared and thermal-infrared spectra of volcanic rocks. Icarus 359, 114344. https://doi.org/10.1016/j.icarus.2021.114344

Shearer, C.K., Papike, J.J., 1993. Basaltic magmatism on the Moon: A perspective from volcanic picritic glass beads. Geochim. Cosmochim. Acta 57, 4785–4812. https://doi.org/10.1016/0016-7037(93)90200-G

Souchon, A.L., Besse, S., Pinet, P.C., Chevrel, S.D., Daydou, Y.H., Josset, J.-L., D'Uston, L., Haruyama, J., 2013. Local spectrophotometric properties of pyroclastic deposits at the Lavoisier lunar crater. Icarus 225, 1–14. https://doi.org/10.1016/j.icarus.2013.03.004

Speyerer, E.J., Robinson, M.S., Denevi, B.W., the LROC Team, 2011. Lunar Reconnaissance Orbiter Camera Global Morphological Map of the Moon. 42nd Lunar Planet. Sci. Conf.

Spudis, P.D., Swann, G.A., Greeley, R., 1988. The formation of Hadley Rille and implications for the geology of theApollo 15 region. Lunar Planet. Sci. Conf. Proc. 18, 243–254.

Sruthi, U., Senthil Kumar, P., 2014. Volcanism on farside of the Moon: New evidence from Antoniadi in South Pole Aitken basin. Icarus 242, 249–268. https://doi.org/10.1016/j.icarus.2014.07.030

Staid, M.I., Pieters, C.M., Besse, S., Boardman, J., Dhingra, D., Green, R., Head, J.W., Isaacson, P., Klima, R., Kramer, G., Mustard, J.M., Runyon, C., Sunshine, J., Taylor, L.A., 2011. The mineralogy of late stage lunar volcanism as observed by the Moon Mineralogy Mapper on Chandrayaan-1. J. Geophys. Res. 116, E00G10. https://doi.org/10.1029/2010JE003735

Steele, A.M., Colson, R.O., Korotev, R.L., Haskin, L.A., 1992. Apollo 15 green glass: Compositional distribution and petrogenesis. Geochim. Cosmochim. Acta 56, 4075–4090. https://doi.org/10.1016/0016-7037(92)90017-D

Surkov, Y., Shkuratov, Y., Kaydash, V., Korokhin, V., Videen, G., 2020. Lunar ilmenite content as assessed by improved Chandrayaan-1 M3 data. Icarus 341, 113661. https://doi.org/10.1016/j.icarus.2020.113661

Trang, D., Gillis-Davis, J.J., Lemelin, M., Cahill, J.T.S., Hawke, B.R., Giguere, T.A., 2017. The compositional and physical properties of localized lunar pyroclastic deposits. Icarus 283, 232–253. https://doi.org/10.1016/j.icarus.2016.09.025

Trang, D., Tonkham, T., Filiberto, J., Li, S., Lemelin, M., Elder, C.M., 2022. Eruption characteristics of lunar localized pyroclastic deposits as evidenced by remotely sensed

water, mineralogy, and regolith. Icarus 375, 114837. https://doi.org/10.1016/j.icarus.2021.114837
van der Bogert, C.H., Hiesinger, H., Pretto, I., Venditti, F., Lewang, A., Richter, L., Binns, D., Gläser, P., 2021. Science-rich Sites for In Situ Resource Utilization Characterization and End-to-end Demonstration Missions. Planet. Sci. J. 2, 84. https://doi.org/10.3847/PSJ/abedbb
Vasavada, A.R., Bandfield, J.L., Greenhagen, B.T., Hayne, P.O., Siegler, M.A., Williams, J.-P., Paige, D.A., 2012. Lunar equatorial surface temperatures and regolith properties from the Diviner Lunar Radiometer Experiment: LUNAR EQUATORIAL REGOLITH PROPERTIES. J. Geophys. Res. Planets 117, n/a-n/a. https://doi.org/10.1029/2011JE003987
Wadsworth, F.B., Llewellin, E.W., Vasseur, J., Gardner, J.E., Tuffen, H., 2020. Explosive-effusive volcanic eruption transitions caused by sintering. Sci. Adv. 6, eaba7940. https://doi.org/10.1126/sciadv.aba7940
Wagner, R.V., Speyerer, E.J., Robinson, M.S., the LROC Team, 2015. New Mosaicked Data Products from the LROC Team. 46th Lunar Planet. Sci. Conf.
Weitz, C.M., Head, J.W., Pieters, C.M., 1998. Lunar regional dark mantle deposits: Geologic, multispectral, and modeling studies. J. Geophys. Res. Planets 103, 22725–22759. https://doi.org/10.1029/98JE02027
Wieczorek, M.A., Neumann, G.A., Nimmo, F., Kiefer, W.S., Taylor, G.J., Melosh, H.J., Phillips, R.J., Solomon, S.C., Andrews-Hanna, J.C., Asmar, S.W., Konopliv, A.S., Lemoine, F.G., Smith, D.E., Watkins, M.M., Williams, J.G., Zuber, M.T., 2013. The Crust of the Moon as Seen by GRAIL. Science 339, 671–675. https://doi.org/10.1126/science.1231530
Williams, J., Greenhagen, B.T., Bennett, K.A., Paige, D.A., Kumari, N., Ahrens, C.J., Rubanenko, L., Powell, T.M., Prem, P., Blewett, D.T., Russell, P.S., Hayne, P.O., Sullivan, M.T., 2022. Temperatures of the Lacus Mortis Region of the Moon. Earth Space Sci. 9. https://doi.org/10.1029/2021EA001966
Williams, J.-P., Bandfield, J.L., Paige, D.A., Powell, T.M., Greenhagen, B.T., Taylor, S., Hayne, P.O., Speyerer, E.J., Ghent, R.R., Costello, E.S., 2018. Lunar Cold Spots and Crater Production on the Moon. J. Geophys. Res. Planets 123, 2380–2392. https://doi.org/10.1029/2018JE005652
Williams, J.-P., Paige, D.A., Greenhagen, B.T., Sefton-Nash, E., 2017. The global surface temperatures of the Moon as measured by the Diviner Lunar Radiometer Experiment. Icarus 283, 300–325. https://doi.org/10.1016/j.icarus.2016.08.012
Wilson, L., Hawke, B.R., Giguere, T.A., Petrycki, E.R., 2011. An igneous origin for Rima Hyginus and Hyginus crater on the Moon. Icarus 215, 584–595. https://doi.org/10.1016/j.icarus.2011.07.003
Wilson, L., Head, J.W., 2018. Controls on Lunar Basaltic Volcanic Eruption Structure and Morphology: Gas Release Patterns in Sequential Eruption Phases. Geophys. Res. Lett. https://doi.org/10.1029/2018GL078327
Wilson, L., Head, J.W., 2017. Generation, ascent and eruption of magma on the Moon: New insights into source depths, magma supply, intrusions and effusive/explosive eruptions (Part 1: Theory). Icarus 283, 146–175. https://doi.org/10.1016/j.icarus.2015.12.039
Wilson, L., Head, J.W., 1981. Ascent and eruption of basaltic magma on the Earth and Moon. J. Geophys. Res. Solid Earth 86, 2971–3001. https://doi.org/10.1029/JB086iB04p02971

Wood, J.A., 1973. Bombardment as a cause of the lunar asymmetry. The Moon 8, 73–103. https://doi.org/10.1007/BF00562751
Zhu, M., Wünnemann, K., Potter, R.W.K., Kleine, T., Morbidelli, A., 2019. Are the Moon's Nearside-Farside Asymmetries the Result of a Giant Impact? J. Geophys. Res. Planets 124, 2117–2140. https://doi.org/10.1029/2018JE005826

Appendix I: *In situ* resource utilization potential of LPDs in the Montes Apenninus region of the Moon

Abstract

Lunar Pyroclastic Deposits (LPDs, sites of explosive volcanism on the Moon) have been targeted for *in situ* resource utilization because they are rich in metals, yield more oxygen when processed than other regolith materials, and are easier to process due to their generally uniform grain size. We evaluate the ISRU potential of identified LPDs in the Montes Apenninus region of the Moon - an equatorial region on the nearside that has been visited by multiple Apollo missions and has a wide variety of explosive deposits. Differences in explosivity can result in deposits that have varied volatile species, volatile content, and eruptive flux, resulting in a different ISRU potential for each deposit. As a result of these complexities, a case-by-case consideration for *in situ* resource utilization is warranted and we present a preliminary resource assessment for 9 LPDs in our study area.

AI.1 Introduction

Volcanic products are sourced from mantle materials or shallow magma reservoirs and provide information about the magma from which the eruptive products were sourced. Lunar Pyroclastic Deposits (LPDs) are the surface materials left on the Moon by explosive eruptions and have a generally unconsolidated and homogenous nature owing to their emplacement. Pyroclastic deposits preserve information about magma cooling rates, compositional evolution through partial differentiation and fractional crystallization, and the structure of the lunar subsurface (Keske et al., 2020; Wilson and Head, 1981). In addition to this high scientific value, LPDs are important resource targets as demonstrated by Artemis III Science Definition Team Report, (2020) due to their generally uniform grain size ideal for processing (Hawke et al., 1990), above-average metal oxide content on grain surfaces, and volatile entrapment (Hauri et al., 2011; Saal et al., 2008). In this study, we evaluate the ISRU potential of identified pyroclastic deposits in the Montes Apenninus region of the Moon. The Montes Apenninus region was selected for this study because it includes a variety of volcanic deposits including regional LPDs, localized LPDs associated with sinuous rilles, and effusive volcanic features including volcanic rilles, irregular mare patches, and major and minor mare infilled basins. Additionally, samples were collected during Apollo 15 sampling activities in Rima Hadley, which is within this study region, providing a wealth of detailed *in situ* information on this study site.

A pyroclastic eruption is driven by volatiles such as water (Gaddis et al., 2003; Renggli et al., 2017), carbon monoxide (Fogel and Rutherford, 1995; Wilson and Head, 1981), or H_2 (Lo et al., 2021). These volatiles can be captured in melt inclusions within crystals, some of which have been investigated from Apollo samples to have high water and carbon dioxide content (Hauri et al., 2011; Saal et al., 2008). Many explosive deposits have a high content of glass-rich juvenile pyroclastic material, a critical lunar resource that can be used to enable future human exploration of the Solar System ("Artemis III Science Definition Team Report," 2020). Pyroclastic glass has the highest oxygen yield of any other lunar material when broken down and is a primary component of the homogenous, fine grained deposits that are easier to process than rocky and crystalline materials.

In this abbreviated study, we characterize the composition, trafficability, and areal extent of materials within a selection of explosive volcanic features and categorize them based on their potential for use as a resource. We investigate each deposit's mineralogy in detail, specifically targeting effective glass proportion (relative to non-glass component) and ilmenite content. We detail each deposit's geologic context and determine its ISRU potential by (1) characterizing the glass and ilmenite content of pyroclastic deposits within the Montes Apenninus region, (2) evaluating the rock abundance, H-parameter, and slope of a deposit for trafficability, and (3) delineate the areal extent using multiple datasets (i.e., visible, near-infrared, and thermal infrared).

AI.1 Background

Recent research in lunar exploration has indicated the importance of in situ resource utilization as a priority in advancing space exploration, but much is still unknown about future needs (Jawin et al., 2019) and much has yet to be evaluated and quantified (*Circular*, 2023). Many locations have been identified as potential landed mission targets, that each address specific scientific goals and ISRU objectives, and some of which include various types of pyroclastic deposits (Jawin et al., 2019). Pyroclastic deposits are often targeted due to their homogeneity, ilmenite and metal content, volatile content, and to study the shielding effects of the fine-grained pyroclastic materials (Jawin et al., 2019; Lawrence and Hawke, 2008).

Explosive lunar volcanism often results in homogenous, fine-grained, loosely-compacted deposits targeted for oxygen processing production, as the feedstock for these processes is most efficient in the absence of blocks and large ranges of grain sizes. The fine, uniform grain size also means that pyroclastic material can be more easily collected and transported, and used as a cover material for lunar bases (Lawrence and Hawke, 2008). The primary component of many of the regional pyroclastic deposits is thought to be volcanic glass beads in the tens of microns in diameter size fraction. In addition to generally being broken down more easily by extraction processes, pyroclastic glasses were observed to have the highest oxygen yield of any other type of lunar regolith material (Allen et al., 1996).

Many pyroclastic deposits contain ilmenite (Fe_2TiO_3) as a primary compositional component or titanium oxide (TiO_2) as a surface grain coating. Not only are the iron and titanium valuable as resource metals, ilmenite has special priority as a feedstock for various volatile entrapment. ^{3}He is a component of a nuclear fusion process for energy production, and potentially exists on the Moon, in a non-uniform spatial distribution (Crawford, 2015). The spatial distribution of ^{3}He and the preferential retention of isotopes of He indicate that ^{3}He may be most abundant in Ti-rich materials, including pyroclastic deposits, if present (Fegley, 1993).

We target these primary resource uses from nine pyroclastic deposits in the Montes Apenninus region to evaluate the resource potential of a variety of types locations with pyroclastic material feedstock. We evaluate the glass content of each deposit as a function of the signal strength, confirmed by spectra in the Vis-NIR, to determine how probable the LPD has a large supply (in terms of areal extent, deposit thickness, and signal strength of glassy material) of pyroclastic glass. We include the same analysis of ilmenite using the band parameter we created (see Chapter 2), comparing this to TiO_2 from WAC. We also include a discussion of the total deposit extent based off of albedo from the methods of Chapter 2. This includes portions of the deposit with less value than having glass-rich material (and therefore lower oxygen yield) and ilmenite-rich material (and therefore lower metal and ^{3}He yield), but homogenous, fine-grained material for general use and processing efficiency. We also include a discussion of the trafficability of the deposit, as roving and maneuvering on thick, unconsolidated pyroclastic deposits may provide a challenge to future explorers (Jawin et al., 2019).

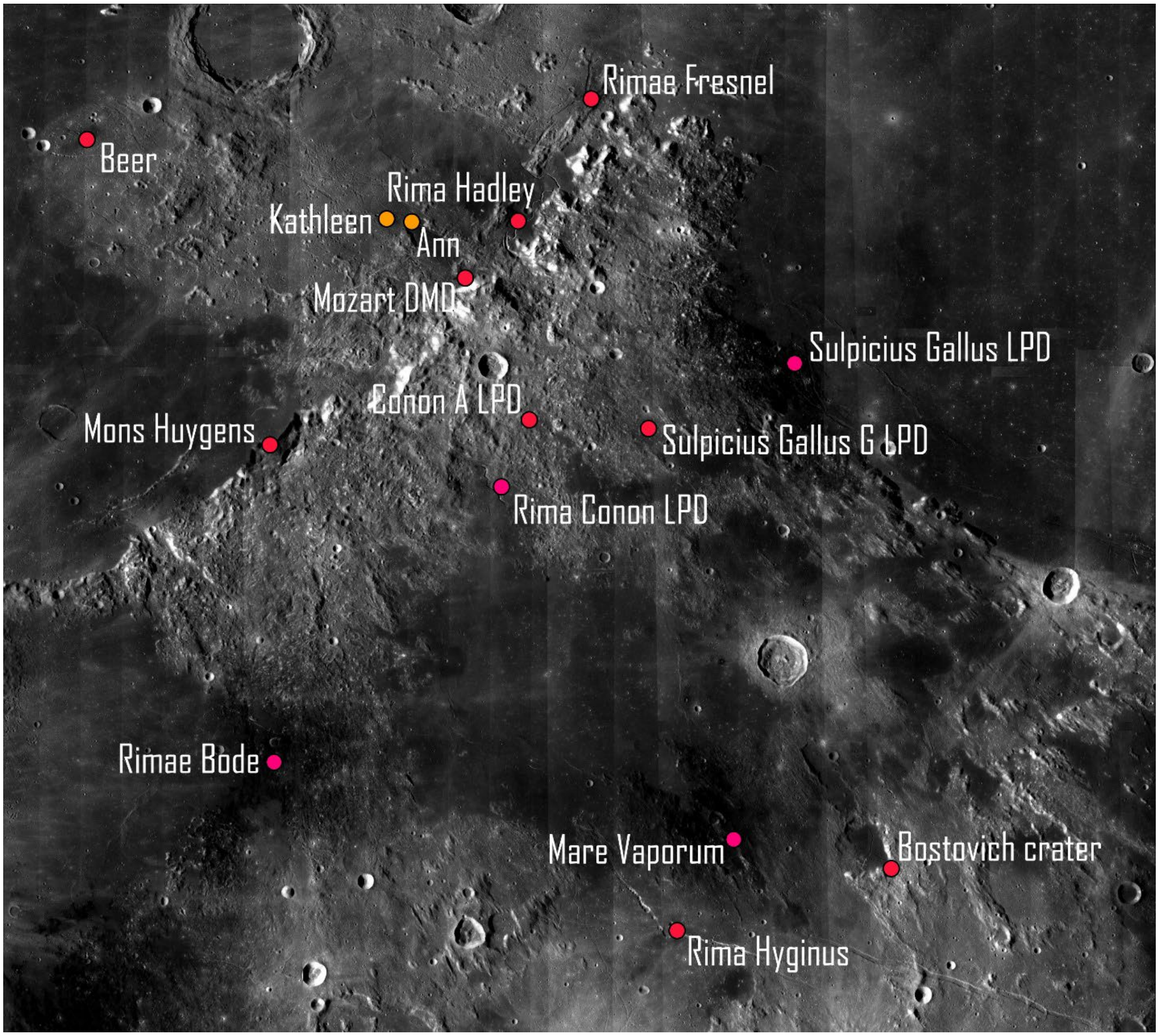

Figure A1: M^3 mosaic of Montes Apenninus region. Lunar pyroclastic deposits are indicated as circles of varying color representing their areal extent, indicated in the legend.

AI.1.2 Description of Study Region

Montes Apenninus is a northeast-southwest trending chain of highland-type mountainous terrain that are part of the eastern rim of the Imbrium basin. There are thirteen previously identified LPDs in the Montes Apenninus study region (Chapter 3 and Chapter 4). In this analysis, we evaluate nine of these, eliminating four that were not easily identified by glass distribution, albedo, thermal, or thermophysical properties in previous studies (i.e., Bostovich crater LPD, Rima Conon LPD, Sulpicius Gallus G LPD, and Mozart DMD; Chapter 3 and Chapter 4). The Montes

Apenninus region is on the lunar nearside and is an equatorial region, ideally positioning it for continuous Earth communication.

AI.2 Methods

We conducted a compositional analysis of the Montes Apenninus study region, focusing on previously identified LPDs (Figure A1). We used the hyperspectral visible and near-infrared data from the Moon Mineralogy Mapper (M^3) instrument (Pieters et al., 2009) for high spectral resolution and for evaluating iron-bearing glass and minerals. Specifically, we highlight absorptions near 1 µm and 2 µm, which are useful for characterizing targeted mineralogy of LPDs, mapping iron-bearing glass content variability between deposits, and identifying critical resource minerals such as ilmenite. We explore these minerals within pyroclastic deposits (e.g., clinopyroxene, ilmenite, and orthopyroxene), and use differences observed on the surface to understand the resource potential of different types of pyroclastic deposits. Iron-bearing glass is a component of explosive volcanism, distinct from crystalline mare basalts and typically absent in other types of effusive volcanic features (Gaddis et al., 2003).

AI.2.1 Spectroscopic analysis in the Vis-NIR

The hyperspectral M^3 data (spatial resolution of up to 280 m/pixel in 82 spectral channels) were used to characterize the mineralogy of LPDs at visible and near-infrared (0.43 – 3.0 µm) wavelengths. We use the publicly available data from the Planetary Data System (PDS, see Supplementary Materials for images used and their optical periods). We used M^3 image mosaics produced in Chapter 2 and archived on Zenodo. M^3 data were processed following the methods of Horgan et al. (2014) to remove continuum contribution due to space weathering and to smooth the continuum to better evaluate spectral variability. The spectral continuum removal comprised a linear convex hull with end tie points at 0.6 and 2.6 µm with a central tie point at 1.5 µm. After processing, we derived band parameter maps identified in Table 2 and other products to evaluate the composition of the region.

To evaluate how the mineralogy varies spatially across the study region, we produced band parameter maps that highlight specific mineral abundances in each mosaic. The parameters we used include the 1 µm and 2 µm band depths and centers, as well as parameters that can identify glass/olivine, pyroxenes, and ilmenite (see Table 1). The band parameter maps were viewed individually and the boundary extents of the LPDs were evaluated following methods below. We also derive band parameters for targeted band parameter space (e.g., 1 and 2 µm band depth and band center) and for targeted mineral components following the methods of Horgan et al., (2014; Pigue et al., 2023). Specifically, the 1 µm and 2 µm band parameters to capture glass and mineral absorptions due to spectroscopic effects from iron (e.g., band depth, band center, and band asymmetry). We also use clinopyroxene, orthopyroxene, and glass parameters that have been derived previously to investigate the distribution of LPDs and to distinguish LPDs from non-explosive volcanic feature and other geologic features (Bennett et al., 2016; Horgan et al., 2014). For this study we created an ilmenite band parameter based on observations in RELAB spectra of ilmenite (Surkov et al., 2020).

Band parameter	Target component	Evaluation
GLA	Iron-bearing glass*	$(R_{1.15} + R_{1.18} + R_{1.2})/3$
OPX	Orthopyroxene	$(R_{0.88} + R_{0.90} + R_{0.92})/3$
CPX	Clinopyroxene	$(R_{2.10} + R_{2.155} + R_{2.20})/3$
ILM	Ilmenite	$((R_{1.29} + R_{1.70})/2) - R_{1.49}$

Table A1: Derivation of mineral band parameters for targeted pyroclastic indicator minerals. R_N is the reflectance at a specific wavelength. For example, the GLA band parameter is defined as the average band depth below the continuum at 1.15 µm, 1.18 µm and 1.2 µm.

**bdgla targets a spectral region that can indicate glass or olivine, and therefore in areas where a strong bdgla signature is identified, spectra are evaluated to determine if the contribution to the spectrum is likely glass or olivine.*

AI.2.2 Spectral analysis

For each pyroclastic deposit identified in Table 1, we first used the band parameter maps viewed in ENVI to evaluate areas of concentrated signal for each parameter. We identified areas where there are strong, homogenous signatures in the maps and evaluated the spectra of these regions, noting areas where surface components (e.g., slopes, craters, shadows) may be affecting the spectra, increasing noise. This includes constraining the mineralogy and identifying any stratigraphic relationships that may affect the distribution of pyroclastic materials (e.g., ejecta from a nearby crater or mare embayment. Once we compiled all these results, we compared the mineralogy of each pyroclastic deposit to determine the *in situ* resource potential.

The glass band parameter will identify olivine or glass as both have an absorption in a similar location at 1 µm. Glass and olivine can be distinguished by the spectral behavior near 2 µm: glass has a 2 µm band while olivine does not. The reflectance spectrum of iron-bearing glass is typically characterized by a broad and symmetric absorption band between 1.07 µm and 1.20 µm, although some spectra sometime exhibit a weak absorption band centered near 2 µm (Horgan et al., 2014). In individual spectra, we can distinguish this from olivine as the 1 µm band center of olivine is shifted to shorter wavelengths at 1.05 µm and olivine does not exhibit a 2 µm band absorption. Ilmenite has two absorptions, one at the extreme end of the spectral range of M^3 at ~0.45 µm and another within the M^3 spectral range at ~1.5 µm (Staid et al., 2011). The ilmenite spectral parameter developed in this work targets the absorption band at ~1.5 µm (see Chapter 2 for details).

AI.2.3 Data interpretation

Spectra of Lunar Pyroclastic Deposits (LPDs) in our study area typically show increased absorption between 1.15 µm and 1.20 µm, creating a wide absorption band at 1 µm that is indicative of increased glass content (Horgan et al., 2014). To determine whether the signature strength is due to glass (explosive volcanism) or olivine, individual spectra from these areas were examined (see Chapter 4 for a description of spectral interpretations). An enhanced glass signature indicates that there is a high confidence of glassy/olivine material; a weak glass signature (red/orange) indicates there is a moderate confidence of glassy/olivine material. Dark red and background (gray) colors indicate that there is a high confidence that the material in that pixel is not likely to be glassy or contain olivine.

We generate boundaries of the LPDs using band parameter thresholds, outlined in the methods section of Chapter 2. These boundaries are taken from the albedo image from M^3, evaluating the distribution of pyroclasts relative to the substrate as a function of albedo. The deposits in the Montes Apenninus study region are all lower in albedo than the surrounding terrain, providing the ability to evaluate the areal extent of the LPDs.

AI.3 Results

In regional maps of the Montes Apenninus area, many pyroclastic deposits stand out as low-albedo features and as having a generally high glass content. This is demonstrated in the glass spectral parameter map (see Chapter 3) as the LPDs having a strong glass signature (indicated by light red/white color), although the strength of the absorption varies between LPDs. Mare margin deposits typically exhibit stronger glass signatures than other LPDs and tend to be larger than the other deposits identified in this region (Chapter 3).

AI.3.1 Relative Albedo

The Beer LPD is a localized pyroclastic deposit on the light plains of the Apennine Bench. The darker material of the Beer LPD stands out on the lighter highlands of the Apennine Bench, but the LPD appears higher in albedo by visual inspection than the regional deposits evaluated in this study. Band thresholding confirms the visual inspection, and the areal extent by albedo was determined to be 242.6 km^2, significantly lower than the previously reported 623 km^2 (Gaddis et al., 2003). Previous studies show Beer LPD to be split into two distinct regions, but the band threshold shows material with similar albedo connecting the two lobes (see Chapter 2).

Rima Hadley is an LPD that was visited during Apollo 15 as a site of importance for a variety of geologic factors. The albedo of the area around the Apollo 15 landing site (north of Hadley Rille / Hadley Cleft) is lower than Palus Putredinis to the west. The threshold values for the lowest threshold confirm that the area within Palus Putredinis has a lower albedo than the areas within and around Hadley Rille. For the average albedo threshold, the area in and around Rima Hadley and within Palus Putredinis are consistent with the mapped single mare unit in Fortezzo (2020). Previously in the localized LPD category (LPDs below 1000 km^2), if the areas within Palus Putredinis are included as this work suggests, the new areal extent is 2713.2 km^2.

Rima Mozart is a sinuous rille west of Montes Apenninus (Figure A2), along which there are four irregularly-shaped depressions (from west to east): Kathleen, Ann, Michael, and Patricia that lead into Lacus Mozart. The Lacus Mozart basalt has a low albedo relative to the surrounding light plains unit of the Apennine Bench between Montes Apenninus and Montes Archimedes. As a result of low albedo of the lacus, the boundary extent of Ann, Michael, and Patricia based on albedo were not able to be discerned using the thresholding methods. The Kathleen depression stands out against the light plains and the boundary was able to be distinguished in albedo thresholding. The areal extent of the region of interest created by the albedo threshold for Kathleen was 69.4 km^2.

The Rimae Fresnel LPD is a localized pyroclastic deposit associated with a fissure structure to the west of the northern extent of the Montes Apenninus. The LPD has an irregular shape in the albedo threshold method. There is a visible low-albedo portion of the deposit around the central bend in the fissure, and this is confirmed by the albedo thresholding. An expanded threshold was created to evaluate a wider distribution of materials. This expanded threshold did not significantly modify other evaluated LPDs on highland substrates (e.g., Beer), but provided additional clarity on the shape of the deposit. The boundary extent of the Rimae Fresnel LPD from these methods was determined to be 460.3 km^2.

Mons Huygens LPD is a very small localized pyroclastic deposit at the base of the Montes Apenninus (Hawke et al., 1979b). Although the albedo band threshold was able to identify material at the location of the Mons Huygens LPD as distinct from the highlands of the Montes Apenninus, the albedo of the adjacent mare is lower than the LPD. Additionally, the albedo of the LPD was high enough that the expanded threshold previously created was used to determine the confidence of this finding. The expanded threshold filled in gaps between regions of low albedo creating a more complete shape. The boundary extent of the Rimae Fresnel LPD from these methods was determined to be 172.8 km^2.

Mare Vaporum LPD is located within the Mare Vaporum basin, but is not considered one of the regional deposits on a mare margin. Similar to regional mare margin deposits, however, the Mare Vaporum LPD does not have an identified vent structure. The regional LPD has a very low albedo that could be distinguished from the low albedo of the mare, but as there are two orbits over the Mare Vaporum LPD that are from different orbital periods, the resampling of these images in the mosaic alters the band thresholding (see Methods for a full description of this). The boundary extent could be estimated using moving thresholds for each image of the mosaic, however, and was determined to be 9684.6 km^2. This is significantly larger than the previous estimate of 4129 km^2 (Gaddis et al., 2003c), which indicates that the albedo threshold may be overestimating the boundary in this case.

The Sulpicius Gallus LPD also has four orbits over the pyroclastic deposit that are from different orbital periods, resulting in the alteration of the band thresholding as with Mare Vaporum LPD. The boundary extent could be estimated using moving thresholds for each image of the mosaic, however. As one of the “black spot” LPDs, much of the Sulpicius Gallus LPD is within the lowest albedo “shadow” threshold (see section 4.2 for additional information about the black spot LPDs), especially in the images in the mosaic that are in orbital periods that are consistent with each other (i.e., not in the “bad” image). The boundary extent could be estimated using moving thresholds for each image of the mosaic, however, and was significantly larger than the previous estimate of 4322 km^2 (Gaddis et al., 2003), which indicates that the albedo threshold may again be overestimating the boundary in this case.

Rima Bode LPD is a regional mare margin LPD visibly mantling both the Sinus Aestuum mare and Montes Apenninus highland terrains. As another of the “black spot” LPDs, much of the central portion of the Rima Bode LPD is within the lowest albedo “shadow” threshold. The shadow threshold straddles the mare margin near the center of the LPD. The remaining deposit is distributed fairly symmetrically around this lowest albedo region, over the mare and highland.

AI.3.2 Glass content

The Beer LPD has little glass signature relative to the background (Pigue et al., 2023). This is also consistent with spectral analysis as spectra evaluated from this region did not have significant asymmetry in the 1-μm band and the spectral contrast was overall low. As the signal was so low, a boundary was not able to be delineated for an areal extent.

The Rimae Fresnel LPD appears to have a very weak glass signature in the glass band parameter map. However, spectral analysis of many areas within the Rimae Fresnel LPD did not confirm a clear indication that glass was a significant component of the spectra at 1 μm (Pigue et al., 2023). As this signature was not confirmed by spectral analysis and the delineation of the on-deposit and off-deposit regions could not be confirmed in the band parameter map, we were not able to find an areal extent of glass for Rimae Fresnel LPD.

The Rima Mozart region has a sinuous rille (Rima Mozart) that initiates at a vent known as Kathleen, flows east-southeast and terminates at Rima Bradley within Lacus Mozart. Lacus Mozart is divided into a northern and southern region by Rima Bradley, a graben type fissure. The northern half of Lacus Mozart has an elevated glass signature in the glass band parameter map, but the southern half does not have this elevated signature. All four depressions along Mozart rille exhibited an elevated signal in the glass band parameter map, but only Michael had a noticeable glass signature in the more complete spectral analysis (Pigue et al., 2023). Although it has one of the stronger glass signatures in the glass band parameter map, spectral analysis of the Kathleen depression does not have a recognized asymmetry. The spectra of Kathleen also does not have a spectral shoulder at 1 μm that would be indicative of glass, nor is the band center at 1 μm shifted to longer wavelengths that could indicate a contribution to the spectrum from glassy or olivine-rich material. Although the remaining vent depressions had an elevated glass signature in the glass band parameter map, spectral analysis revealed that these regions did not have a recognized asymmetry or spectral shoulder at 1 μm that would be indicative of glass, nor is the band center at

1 µm shifted to longer wavelengths that could indicate a contribution to the spectrum from glassy or olivine material.

Rima Hadley is a localized LPD that was visited during Apollo 15 (known as Hadley Cleft) as a site of importance for a variety of geologic factors. Samples collected from the Apollo 15 mission sampling locations include green pyroclastic glass beads of primitive origin (Delano, 1986; Steele et al., 1992). The area around which Apollo landing and sampling locations occurred (north of the Rima Hadley channel) has a relatively weak glass signature in the glass band parameter map, compared with glass signatures in Palus Putredinis to the west. Spectra observed is comparable to typical LPDs: various locations sampled within this region (including the immediate surrounds of Rima Hadley) have an asymmetric 1 µm band, and a broad 2 µm band centered at 2 µm. The glassy signatures around Rima Hadley extend into Palus Putredinis around some topographically high features/mounds, but the glass does not appear to mantle the mounds . The areas that have the strongest glass signatures around Rima Hadley and within Palus Putredinis are both mapped as a single mare unit in Fortezzo (2020). The areal extent of glass-rich material in the Rima Hadley region (including the low-signature area around Rima Hadley) is 3226.0 km^2.

Rimae Bode is a regional LPD on the eastern margin of the Sinus Aestuum mare, visibly covering both mare and highland terrains with a low-albedo mantle. The Rimae Bode LPD has a strong glass signature with variability observed throughout the deposit. There is a strong signature in the center of the deposit and thins towards the distal parts of the deposit. It has been hypothesized that, due to the distribution of pyroclastic materials (strong signature towards the center and thinning distally) and arcuate shape of the Rimae Bode LPD with a core of concentration on the western margin, a possible vent structure from which the pyroclastic deposit was sourced may be located within the Sinus Aestuum basin that is now covered by mare lavas (Gaddis et al., 1985).

Sulpicius Gallus LPD is a regional LPD on the southwestern margin of Mare Serenitatis. The Sulpicius Gallus LPD has elevated signatures in the glass band parameter map, and in spectral analysis, portions of the LPD a well-defined shoulder and had a 1-µm band center shifted to longer wavelengths, which would be indicative of pyroclastic material. Portions of the LPD that appear to be mixed with highland material beyond the margin of the mare basin had spectra that were less indicative of pyroclastic glass, and would be considered to have a more crystalline or diffuse glass signature.

Beer LPD is a localized pyroclastic deposit situated on the Apennine Bench. The darker material of the Beer LPD stands out on the lighter highlands of the Apennine Bench, but the LPD is higher in albedo than typical LPDs. Relative to other LPDs, it also has a low, but detectable, glass signature in the glass band parameter map. The potentially low glass content that was observed in the glass band parameter map (indicating a small band depth around 1.2 µm) can also be seen in the spectra from the Beer LPD. The strength of the absorption around 1 µm, when compared to mare spectra near this LPD, is generally weak indicating that this could be a diffuse LPD or has reduced spectral contrast due to space weathering and impact gardening. The mapped boundary of the Beer LPD in this work was significantly smaller than 623 km^2, which could be due to differences in instrumentation between previous studies and M^3. Although it is unclear what was used to determine the area of the Beer LPD in literature (for which the referenced area is taken), it has been observed that maps produced using albedo tend to result in larger deposit boundaries, resulting from differences in skin depth and spectral contrast between instruments (Glaspie et al., 2018). Beer LPD does not have a significant ilmenite signature in the M^3 derived ilmenite parameter map, although there are indications in spectra that there is a minor absorption at 1.5 um.

Mons Huygens LPD is a very small localized pyroclastic deposit at the base of the Montes Apenninus (Hawke et al., 1979; Figure A1). Although many regions in this area have strong glass signatures, spectral analysis of many of these locations reveals some of these are slope effects (see Methods for a description of this effect). Spectra indicate there is a pyroclastic signature with strong absorptions at 1 μm and 2 μm and a strong glass signature.

AI.3.2 Ilmenite content

The Beer LPD, Mons Huygens, Bostovitch Crater, and Conon A LPDs did not have ilmenite signature in the ilmenite band parameter map, and were generally close to background values. These observations were also consistent with the LROC WAC-derived TiO_2 abundance map.

The Rimae Fresnel LPD has a low ilmenite signature, but may have been somewhat elevated from background values. This is consistent with the LROC WAC-derived TiO_2 abundance map, which shows 0.2 wt% titanium content (Sato et al., 2017) which is very low. Although a signature was detected in the ilmenite map, a boundary could not be delineated in the Montes Apenninus mosaic. The Rima Conon LPD also had a detectable ilmenite signature but may have been generally close to background values. The LROC WAC-derived TiO_2 abundance map shows a 1.2 wt% titanium content (Sato et al., 2017). Although a signature was detected in the ilmenite map, a boundary could not be delineated in the Montes Apenninus mosaic. The boundary in the LROC WAC-derived TiO2 mosaic was only moderately correlated to the LPD, and was generally more consistent with the presence of mare basalts in this region.

The Kathleen LPD also had a low ilmenite signature in the ilmenite band parameter map, corresponding to the location of the albedo and glass signatures. The Kathleen depression also had an increased signature, but it is unclear whether this is a slope effect. The areal extent of the ilmenite of the Kathleen LPD is 11.2 km^2. Lacus Mozart also had increased ilmenite signature, indicating a potential ilmenite mineralogy in the mare.

The Rima Hadley region has a moderate ilmenite signature in the ilmenite band parameter map, increasing in the Palus Putredinis region. The area of the Apollo 15 sampling has a very weak ilmenite signature except for within the rille, which is likely a slope effect. The areal extent of the ilmenite region in Palus Putredinis is 1541.3 km^2. This region is also encompassed by the albedo and glass regions previously identified.

The Mare Vaporum LPD is mostly obscured by the images in the different orbital periods and the ilmenite signature could not be determined from the Montes Apenninus mosaic. This was also the case for the Hyginus LPD, although within the over-sampled image, there was a pattern of increased ilmenite that matched the boundary of the Hyginus LPD in albedo and glass. The Sulpicius Gallus G LPD is split into two different orbital periods. The part of the LPD in the images that are consistent with the rest of the mosaic has no ilmenite signature.

The Sulpicius Gallus LPD is partly obscured by the images in the different orbital periods and the ilmenite signature was uncertain from the Montes Apenninus mosaic. In areas where the ilmenite signature could be observed, it was clear that the LPD had an elevated signature from the mare. A small absorption feature in the LPD at 1.5 µm in spectral analysis could be indicative of ilmenite, which is consistent with our ilmenite abundance map: the LPD demonstrates stronger signatures of ilmenite than the mare. This was also consistent with the The LROC WAC-derived TiO_2 abundance map, which shows higher TiO^2 in the area of the LPD than in the mare. The areal extent of the ilmenite could not be determined as a result of the changes in orbital periods of the images.

The Rima Bode LPD has a strong ilmenite signature, mostly correlating with the center of the deposit where the glass signature is the strongest. This is consistent with the “black spot” nature of this LPD – LPDs with high glass and ilmenite content. The areal extent of the ilmenite-rich region is 3472.3 km^2, which is more consistent with previous estimates.

AI.3.3 In Situ Resource Potential

LPDs have been targeted as potential resources as they are a rich source of metals, hydrogen, and oxygen and have a generally uniform grain size, resulting in regolith that is relatively easy to process . However, we determined that not all LPDs in the study region have high glass content, and their usability may be limited by accessibility, deposit volume, and resource concentration. The “black beads” type of glass is associated with high titanium (i.e., Rima Bode, Mare Vaporum, Pieters et al., 1973) and would be a richer deposit of metals than typical lunar regolith. Few of the pyroclastic deposits in the study region are of this type of deposit, and LPDs that are not in this category also did not exhibit high ilmenite signatures.

We evaluate the resource potential of pyroclastic deposits confirmed within our study region by four high-priority ISRU considerations for LPDs: glass content, areal extent, ilmenite content, and ease of accessibility (see Table 3). These nine equatorial LPDs are well-positioned to provide communications access to Earth and many have already been targeted for potential resource use.

Pyroclastic deposit characteristics	High resource potential	Moderate resource potential	Low resource potential
Relative glass abundance	Primarily glass	Glass/crystalline mixture	No glass
Areal extent (albedo)	Large extent of glass-rich material	Large extent of glass/crystalline mixture or moderate extent of glass-rich material	Limited areal extent
Ease of accessibility	Located in a smooth, flat area	Moderate topography or mixed smooth and rugged terrain	Located in a rugged terrain
Relative ilmenite abundance	Strong ilmenite signature	Moderate ilmenite signature	Background ilmenite signature

Table A2: Characteristics of pyroclastic deposits that describe a deposit's resource potential

Deposits that are observed as having an overall strong glass signature are in the "primarily glass" category, whereas those which have a mix of glass and crystalline or have a weaker glass signature are in the moderate or low glass abundance categories. Deposits that have no glass signature but also do not have a well-characterized crystalline component (i.e., they do not display characteristic mafic mineralogy, iron-bearing mineral signatures indicative of volcanic eruption, or iron-bearing glass/olivine) are given a white background as having no resource potential with respect to glass. Similarly for glass, the ilmenite resource potential was determined using the ilmenite band parameter maps and the signal strength – strong signal was assigned a "high" result, detected signal was assigned "moderate," and background signal was assigned "low" to account for the potential that ilmenite could be present at the level of the signal to noise of this analysis. The areal extents are based off the largest of each of these band parameters (i.e., glass, albedo, ilmenite) as measured from Chapter 2 of this work. Ease of accessibility accounts for the rock abundance of terrain (Chapter 2), number of craters, type of substrate (e.g., highland has more obstacles than mare), and abundance of flat surfaces for potential landing sites. For this study, accessibility also assumes that a potential landing site would not include landing on a pyroclastic deposit due to the unpredictable and unconsolidated nature of a mantled.

LPD Cumulative ISRU potential was derived by combining the unweighted rating for all categories (dark green assigned a value of 3, medium green assigned a value of 2, and light green assigned a value of 1, white contributed no values to the total), and taking the average of the values to get the cumulative.

LPD Cumulative ISRU potential	Relative glass abundance	Relative ilmenite abundance	Areal extent	Ease of accessibility
Beer	Low glass, but not crystalline	Low	100 – 1000 km^2	High accessibility
Rima Hadley	Primarily Glass	Moderate	100 – 1000 km^2	Moderate accessibility
Mare Vaporum	Primarily Glass	High	>1000 km^2	High accessibility
Rimae Bode	Primarily Glass	High	>1000 km^2	Low accessibility
Rimae Fresnel	Low glass	Low	100 – 1000 km^2	Moderate accessibility
Sulpicius Gallus	Primarily Glass	High	>1000 km^2	Moderate accessibility
Mons Huygens	Low glass	None	<100 km^2	Low accessibility
Kathleen	Low glass	Low	<100 km^2	High accessibility
Hyginus	Low glass	Moderate	<100 km^2	High accessibility

Table A3: ISRU value of confirmed LPDs in the Montes Apenninus study region, listed in order of ISRU potential. Glass abundance and areal extent were determined using the glass band parameter map. Ease of accessibility is determined using the LROC WAC global basemap and M^3 albedo mosaic for smooth and rough terrain, craters, fissures, and other topographic features.

LPD spectra in Rimae Fresnel are similar to the nearby mare. Although LPDs are expected to exhibit mafic mineralogy and the glassines of the Rima Fresnel LPD is low, indicating that the spectra would be anticipated to be similar to a general mafic mare signature, other explanations can be considered which would have ISRU implications. As this deposit was previously noted in literature using different instruments and a signature could be present in the albedo map, the lack of a strong glass signature and spectral confirmation of glass is more likely to indicate a diffuse or heavily weathered deposit dispersed over the area. Rimae Fresnel pyroclastic material mantles a region with a generally basaltic composition and this mantling could be so thin that we are seeing through the pyroclastic material to the underlying basalts. This is common for diffuse LPDs or at the most distal regions of LPDs (e.g., Rimae Bode into Sinus Aestuum mare) where the glassy materials are less concentrated than they are near the vent. Another hypothesis is that this LPD contains basaltic fragments. This would also support the conclusion that Rima Fresnel has a lower ISRU potential as it has a lower glass content and the heterogeneity would be higher than other LPDs, reducing the capacity of its use as easily-processed regolith.

The Rimae Bode LPD has a high ISRU potential overall given its high glass content, high ilmenite signature and large areal extent. However, the distribution of the materials is not homogenous and there is an observed change in the distribution of glass content within the deposit. The richest portions of the deposit in terms of glass and ilmenite are in the proximal part of the deposit, straddling the mare and highland boundary. Access to this part of the deposit would be more difficult from surface mobile operations (especially from the highland/Montes Apenninus side to the east) due to the unpredictability of unconsolidated pyroclastic materials, as would landing in this area as the depth of the mantling is likely to be highly variable. Access could be provided from the Rimae Bode outflow lava areas as these are relatively flat and consolidated and located close to the richest parts of the LPD. As the accessibility to the regions of the deposit with the higher ISRU potential are restricted by topography or large distance, the accessibility score for the usable region would be reduced to "low," thereby reducing the overall score to "moderate" ISRU potential.

AI.4 Conclusion

We evaluate the *in situ* resource potential of thirteen equatorial LPDs. The relative glass content (as signature strength in the glass band parameter map), in combination with other factors such as areal extent and ease of accessibility are taken into consideration when evaluating a deposit's ISRU potential. Pyroclastic deposits evaluated in this study demonstrate a range of glass signature strength and mineralogy, indicating that each would not have equal consideration for ISRU potential. The LPDs with the lowest ISRU potential were Mons Huygens and Rima Fresnel as they had the lowest combined glass content, ilmenite content, and smallest areal extents. The LPDs with the highest ISRU potential was Mare Vaporum as it scored high in glass content, strong ilmenite signature, and a large areal extents. We found that the regional LPDs had highest overall potential, but that the ability to access the richest portions of the deposit (such that the ISRU potential of a regional deposit outweighs that of a localized deposit) can lower the accessibility rating enough to de-rank its overall total score below that of a localized deposit. Even with deposits with low *in situ* resource potential, there is a high value of scientific return from studying explosive volcanism such as elucidating volcanic history of the Moon, investigating planetary volatiles of the Earth and Moon, and evaluating the evolution of the solar system.